SYNTHESIS AND APPLICATION OF NATURAL POLYMER BASED HYDROGELS

A Thesis Submitted
in Partial Fulfillment of the Requirements
for the Degree of

DOCTOR OF PHILOSOPHY

in

Applied Chemistry

by

Manu

(2K20/PHDAC/01)

Under the supervision of

Prof. D. Kumar & Prof. Rajinder K. Gupta

Department of Applied Chemistry
DELHI TECHNOLOGICAL UNIVERSITY
(Formerly Delhi College of Engineering)
Shahbad Daulatpur, Main Bawana Road,
Delhi-110042 India

November, 2025

Dedicated
to
My
Family

ACKNOWLEDGEMENT

I would like to begin by thanking the Almighty God for blessing me with the strength, perseverance, and opportunity to complete this journey. Without His grace, the successful completion of my research work would not have been possible.

First and foremost, I owe my deepest gratitude to my supervisors, **Prof. D. Kumar** and **Prof. Rajinder K. Gupta**. They have been far more than academic guides to me; they have been mentors, role models, and sources of encouragement. I am truly blessed to have supervisors who not only guided me with patience and generosity but also believed in me even when I doubted myself. Their constant reassurance, encouragement, and big-picture perspective helped me see beyond immediate obstacles and stay focused on the larger goal. For their patience, faith, and unwavering support, I will remain forever grateful.

I am thankful to **Prof. Prateek Sharma**, Honorable Vice-Chancellor of Delhi Technological University, **Prof. Anil. Kumar**, Head of the Department, and **Prof. Ram Singh,** DRC Chairman, Department of Applied Chemistry, for providing the necessary research facilities and an excellent working environment in the department. I am also deeply appreciative of my SRC and DRC committee members, whose expertise and thoughtful suggestions greatly enhanced the quality of this work. I also express my gratitude to all faculty members and non-teaching staff of the Department of Applied Chemistry at DTU for their valuable support.

Beyond academia, I have been blessed with a circle of family and friends who never stopped believing in me, even when I struggled to believe in myself. To my parents, **Mr. Surender Nandal** and **Mrs. Sunil Mati**, their love has been my anchor. This achievement is not mine alone; it is the fruit of the sacrifices made by them to give me the opportunity to be here. To my siblings, **Anu** and **Sahil**, I am grateful for their constant encouragement. They have been my pillars of strength, standing by me through every challenge and supporting me in achieving my goals. A special mention goes to our family's little bundles of joy, **Nayra, Samayra** and **Shivansh**.

And to my friends, especially **Jyoti Malik** and **Vaishali Parashar**, I am thankful for their patience, for listening to my endless rambling about research, and for celebrating even the tiniest milestones with me. Both of them made this journey so much lighter and brighter. To my colleagues and peers in the Department, as well as my labmates (**Meenakshi Di, Divya Goel, Jitendra, Sweety, Tanvi, Nishtha, Divya Hooda, Tanushee, and Majeed**), I extend my warmest thanks. Whether it was sharing equipment and resources or simply exchanging smiles across lab benches, they made the lab feel like a second home. I also gratefully acknowledge **Delhi Technological University** for providing me with research facilities, resources, and an academic community that supported my growth. I am especially grateful to the UGC for awarding me the UGC-JRF, without which this research would not have been possible.

As I close this chapter, I want to thank every single person — whether mentioned here or not — who has walked with me on this journey. I will carry your kindness, encouragement, and love with me always.

Manu

DELHI TECHNOLOGICAL UNIVERSITY
(Formerly Delhi College of Engineering)
Shahbad Daulatpur, Main Bawana Road, Delhi-42

CANDIDATE'S DECLARATION

I **Manu** hereby certify that the work which is being presented in the thesis entitled **Synthesis And Application of Natural Polymer Based Hydrogels** in partial fulfillment of the requirements for the award of the Degree of Doctor of Philosophy, submitted in the **Department of Applied Chemistry**, Delhi Technological University is an authentic record of my own work carried out during the period from **26th August 2020** to **30th August 2025** under the supervision of **Prof. D. Kumar** and **Prof. Rajinder K. Gupta**. The matter presented in the thesis has not been submitted by me for the award of any other degree of this or any other Institute.

Place: Delhi
Date:

Manu
Research Scholar
Department of Applied Chemistry
Delhi Technological University,
Delhi-110042

DELHI TECHNOLOGICAL UNIVERSITY

(Formerly Delhi College of Engineering)
Shahbad Daulatpur, Main Bawana Road, Delhi-42

CERTIFICATE BY THE SUPERVISOR(s)

Certified that **Manu (2K20/PHDAC/01**) has carried out her research work presented in this thesis entitled **"Synthesis and Application of Natural Polymer Based Hydrogels"** for the award of **Doctor of Philosophy** in the Department of Applied Chemistry, Delhi Technological University, Delhi, under our supervision. The thesis embodies results of original work, and studies are carried out by the student herself and the contents of the thesis do not form the basis for the award of any other degree to the candidate or to anybody else from this or any other University/Institution.

Prof. D. Kumar	**Prof. Rajinder K. Gupta**
Department of Applied Chemistry,	Department of Applied Chemistry,
Delhi Technological University,	Delhi Technological University,
Delhi	Delhi

Prof. Anil Kumar
Head, Department of Applied Chemistry
Delhi Technological University
Delhi-110042

ABSTRACT

The depletion of fossil-based resources and increasing environmental concerns have intensified the search for sustainable, biodegradable, and eco-friendly materials. Natural polymer-based hydrogels derived from humic acid (HA), lignin, and lignite have emerged as promising candidates due to their multifunctional properties, including their ability to enhance soil moisture retention, control agrochemical release, adsorb pollutants, and contribute to energy storage applications. This research focuses on the synthesis, characterization, and application of these bio-based hydrogels, systematically investigating their structural, thermal, rheological, and morphological properties to optimize their performance for various applications.

The study begins with a comprehensive literature review exploring the significance of humic acid, lignin, and lignite in hydrogel synthesis and their applications in agriculture, and environmental remediation and energy storage. Key research gaps were identified, highlighting the need for more extensive studies on the multifunctionality of these natural polymers in hydrogel systems. The first experimental phase involved the synthesis and application of a lignosulfonate-grafted sodium acrylate hydrogel (LS-g-SAH) for controlled urea release. This hydrogel demonstrated 60% release of urea from LS-g-SAH in 24 h, significantly reducing nutrient leaching and improving soil fertility. The soil's water-holding capacity remarkably raised from 21.27 to 77.3 g using synthesized hydrogel. Also, the water evaporation rate reduced from 99 to 76.69% of the total added water. Enhanced water retention further contributed to increase in plant growth efficiency, making it a potential alternative to conventional fertilizers.

Following this, a humic acid-grafted sodium acrylate hydrogel (HA-g-SH) hydrogel was developed for controlled pesticide release, taking dinotefuran as model pesticide. The hydrogel enabled sustained pesticide release over 49 h 78.45%, improving bioavailability and increasing pest control efficiency of dinotefuran. This approach minimized environmental toxicity by reducing pesticide leaching in soil and water. To further enhance the stability of pesticides, a lignite- sodium acrylate hydrogel (Lt-g-SAH) was synthesized for UV protection of dinotefuran. The study revealed that after 30 days of UV irradiation, Lt-g-SAH group exhibited remarkable stability, with only a marginal decrease of 1.58% in Dinotefuran release, resulting in a final concentration of 41.73 mg. In stark contrast, the Ctrl group experienced a substantial reduction of 28.11% in Dinotefuran release, with the final concentration diminishing to 25.42 mg. This marked disparity in pesticide release profiles can be attributed to the differential susceptibility of the formulations to UV-induced degradation over time.

Based on the controlled-release capabilities, HA-g-SAH, LS-g-SAH, and Lt-g-SAH hydrogels were explored for comparative delivery of thiamethoxam. These hydrogels facilitated a controlled pesticide release for 49 h, reducing pesticide's application frequency, and minimizing environmental contamination. The release pattern followed the Fickian release mechanism as stated by the Korsmeyer-Peppas model and the Weibull model**.** The swelling index revealed a distinct order, with HA-g-SAH exhibiting the highest absorbency, followed by LS-g-SAH, Lt-g-SAH, and the control group. Moreover, the synthesized hydrogels demonstrated a significant impact on reducing soil water evaporation rates from 99 to 72.85% (HA-g-SAH), 74.79% (LS-g-SAH), 78.23% (Lt-g-SAH), and 85.23% (Ctrl) of the total added water on the 54th day.

Beyond their agricultural applications, these hydrogels were investigated for their potential in textile wastewater treatment. The comparative study demonstrated that HA-g-SAH, LS-g-SAH, and Lt-g-SAH hydrogels exhibited high adsorption capacities for methylene blue (MB), a common industrial dye, Under optimized conditions, HA-g-SAH achieved a maximum removal efficiency of 93.7 ±1.1% at 323.15 K, significantly outperforming LS-g-SAH (92.4 ±1.3%), Lt-g-SAH (82.4 ±1.4%), and the control (Ctrl) hydrogel (67.9 ±0.9%). The presence of functional groups in humic acid and lignin enhanced their binding affinity, making these hydrogels promising candidates for large-scale wastewater treatment applications.

This thesis provides a comprehensive analysis of natural polymer-based hydrogels and their potential to address critical challenges in agriculture, and environmental management. The findings suggest that humic acid, lignin and lignite based hydrogels can significantly reduce environmental pollution, enhance soil fertility, improve plant growth, and remove contaminants from water. Further research should focus on optimizing the scalability, durability, and biodegradability of these hydrogels to maximize their practical benefits and commercial viability.

LIST OF PUBLICATIONS

1. Manu, Kumar D, Gupta RK (2025) Harnessing lignite-based hydrogel for enhanced UV protection and delivery of dinotefuran in agriculture. Chemistry Select 10:e05884. https://doi.org/ 10.1002/slct.202405884. (IF=2)
2. Manu, Kumar D, Gupta RK (2024) Natural polymers-humic acid and lignin-based hydrogels: In agriculture, environment and energy storage. Ind Crops Prod 219:119029. https://doi.org/10.1016/j.indcrop.2024.119029. (IF=6.2)
3. Manu, Kumar D, Gupta RK (2024) Novel formulations of humic acid, lignin, and lignite grafted hydrogels for the slow release of thiamethoxam. Chemistry Select 9:e202304939. https://doi.org/10.1002/slct.202304939. (IF=2)
4. Manu, Kumar D, Gupta RK (2023) Synthesis, characterization and application of Lignosulphonate-g-poly(sodium acrylate) hydrogel. Indian J Chem Technol 30:753–764. https://doi.org/10.56042/ijct.v30i6.1325. (IF=1)
5. Manu, Kumar D, Gupta RK (2025) Comparative analysis of humic acid, lignin and lignite-based hydrogels for methylene blue dye removal. Indian J Chem Technol (under review). (IF=1)
6. Manu, Kumar D, Gupta RK (2025) Humic acid-integrated polymeric hydrogel: A dual strategy for sustained pesticide delivery and soil water retention. Eur. Polym. J. (under review) (IF=6.3)

TABLE OF CONTENTS

Acknowledgement .... *i*

Candidate's Declaration ....*iv*

Certificate by the Supervisor(s) ....*v*

Abstract ....*v*

List of Publications .... *viii*

Table of Contents .... *ix*

List of Tables ....*xiv*

List of Figures ....*xvi*

List of Symbols, Abbreviations and Nomenclature .... *xix*

CHAPTER-1 Introduction and literature review...1

1.1 Humic acid...2

1.2 Lignin..4

  1.2.1 Structural characteristics and types of lignin 4

1.3 Lignite...7

1.4 Hydrogels..9

  1.4.1 Swelling mechanism and thermodynamic potential of hydrogels.................... 11

  1.4.2 Functions of humic acid in hydrogels 12

  1.4.3 Functions of lignin in hydrogels... 14

1.5 Applications of nature-based hydrogels in agriculture 16

  1.5.1 Hydrogels in the soil-water-plant system.. 18

  1.5.2 Enhancing the water retention capability of the soil....................................... 19

  1.5.3 Controlled release of pesticides and fertilizers by hydrogels........................... 25

  1.5.4 Effects of hydrogel on vegetative plant growth 28

  1.5.5 Bio degradation 34

1.6 Applications of hydrogels in the environment..35

  1.6.1 Adsorption of soil and water pollutants 36

1.7. Applications of nature-based hydrogels in energy storage 39

1.8 Research gap 43

1.9 Aim and research objectives 44

CHAPTER-2:Synthesis, characterization and application of Lignosulphonate-g-poly (sodium acrylate) hydrogel......................49

2.1 Introduction..50

2.2 Experimental...52

- 2.2.1 Materials...52
- 2.2.2 Synthesis of LS-g-SAH...53

2.3 Results and discussion 58

- 2.3.1 Mechanism of the formation of lignosulfonate-g-sodium acrylate hydrogels..58
- 2.3.2 Characterization of hydrogel...59
- 2.3.3 Gel content (%) 65
- 2.3.4 Effect of variation of different parameters on the swelling index.....................66
- 2.3.5 Swelling studies 68
- 2.3.6 Agricultural applications of LS-g-SAH 69

2.4 Conclusion 73

CHAPTER-3: Humic acid-integrated polymeric hydrogel: a dual strategy for sustained pesticide delivery and soil water retention 74

3.1 Introduction 75

3.2 Material and methods 79

- 3.2.1 Materials..79
- 3.2.2 Preparation of ammonium humate 79
- 3.2.3 Ex situ preparation of HA-g-SAH...79
- 3.2.4 Characterization 80
  - 3.2.4.1 ^{13}C CPMAS NMR...80
  - 3.2.4.2 FT-IR 80
  - 3.2.4.3 Wide-angle X-ray diffraction (XRD) 81
  - 3.2.4.4 Thermogravimetric analysis (TGA) 81
  - 3.2.4.5 Scanning electron microscopy (SEM)...81
- 3.2.5 Swelling study of HA-g-SAH in distilled water 81
- 3.2.6 Network parameters 82
  - 3.2.6.1 Solvent interaction parameter...82
  - 3.2.6.2 Volume fraction 82
  - 3.2.6.3 Molecular weight between crosslinks 83
  - 3.2.6.4 Crosslinking density 83
- 3.2.7 Release of dinotefuran in water...83
  - 3.2.7.1 Preparation of the dinotefuran standard curve 83
  - 3.2.7.2 The loading efficiency and in vitro release of dinotefuran....................84
  - 3.2.7.3 Kinetics of model pesticide release...85

3.2.8 Water retention capacity 86
3.2.9 Statistical analysis 87
3.3. Results and discussion 87
3.3.1 Synthesis of HA-g-SAH 87
3.3.2 Swelling index and effect of parameters 89
3.3.2.1 Impact of biopolymer on swelling of hydrogel 89
3.3.2.2 Impact of initiator on swelling of hydrogel 90
3.3.2.3 Impact of crosslinker on swelling of hydrogel 90
3.3.3 Characterization 91
3.3.3.1 ^{13}C CPMAS NMR 91
3.3.3.2 FT-IR 93
3.3.3.3 SEM 94
3.3.3.4 XRD 95
3.3.3.5 TGA 96
3.3.4 Network parameters 97
3.3.5 Efficacy of loading efficiency 98
3.3.6 In vitro release of pesticide 98
3.3.7 Pesticide release kinetics 99
3.3.8 Non-fickian diffusion 101
3.3.9 Water retention capacity 102
3.4. Conclusion 103
3.5. Future directions 104

CHAPTER-4: Harnessing lignite-based hydrogel for enhanced UV protection and delivery of dinotefuran in agriculture 105

4.1 Introduction 106
4.2 Experimental 110
4.2.1 Materials 110
4.2.2 Preparation of ammonium lignite 110
4.2.3 *In situ* preparation of dinotefuran loaded Lt-g-SAH 111
4.2.4 Gel content analysis 111
4.2.5 Pesticide encapsulation efficiency and pesticide loading 111
4.2.6 Characterization 112
4.2.7 Swelling of Lt-g-SAH and ctrl in distilled water 113
4.2.8 Agricultural applications of Lt-g-SAH 113
4.3 Results and discussion 116
4.3.1 Synthesis of Lt-g-SAH 116
4.3.2 Characterization of hydrogels 116

4.3.2.1 ^{13}C CPMAS NMR 118
4.3.2.2 FT-IR 119
4.3.2.3 SEM 121
4.3.2.4 XRD 121
4.3.2.5 TGA 123
4.3.3 Swelling Index, and of Lt-g-SAH and Ctrl in distilled water 122
4.3.4 Effect of variation in concentration of different parameters on the swelling index of Lt-g-SAH 123
4.3.5 Effect of variation in concentration of biopolymer on SI 124
4.3.6 Effect of variation in concentration of initiator on SI 125
4.3.7 Effect of variation in concentration of crosslinker on SI 126
4.3.8 Agricultural application of Lt-g-SAH 127
4.4 Conclusion 132
CHAPTER-5: Novel formulations of humic acid, lignin, and lignite grafted hydrogels for the slow release of thiamethoxam 133
5.1 Introduction 134
5.2 Experimental 138
5.2.1 Materials 138
5.2.2 Preparation of ammonium humate and ammonium lignite 139
5.2.3 Characterization of synthesized hydrogels 139
5.2.4 Swelling experiment 140
5.2.5 Water evaporation study 140
5.2.6 Determination of loading efficiency of thiamethoxam in the synthesized hydrogels 141
5.2.7 *In vitro* loading and release of thiamethoxam by HA-g-SAH, LS-g-SAH, and Lt-g-SAH 142
5.3 Results and discussion 142
5.3.1 Mechanism for the formation of HA-g-SAH, LS-g-SAH, and Lt-g-SAH 142
5.3.2 Characterization of hydrogels 143
5.3.3 Swelling study of HA-g-SAH, LS-g-SAH, Lt-g-SAH and ctrl 152
5.3.3.1 Swelling study 152
5.3.3.2 Loading efficiency of HA-g-SAH, LS-g-SAH, Lt-g-SAH, and ctrl 153
5.3.4 Agricultural application of HA-g-SAH, LS-g-SAH, and Lt-g-SAH 154
5.4 Conclusion 159
CHAPTER- 6: Comparative analysis of humic acid, lignin and lignite-based hydrogels for methylene blue dye removal 160
6.1 Introduction 161

6.2 Experimental 164
    6.2.1 Swelling study 164
    6.2.2 MB adsorption experiment mechanism 165
6.3 Results and discussion 166
    6.3.1 Swelling study 166
    6.3.2 MB adsorption and isotherm study 167
6.4 Conclusion 177
Chapter-7: Conclusion, future scope and social impact 179
    7.1 Conclusion 182
    7.2 Future scope 182
    7.3 Social impact 183
References 182
Publications 227
Plagiarism Verification 233
Curriculum Vitae 234

LIST OF TABLES

Table No. *Page No.*

Table 1.1 : Different kinds of technical lignin...6

Table 1.2 : Literature overview of HA and lignin-hydrogels in various applications...10

Table 1.3 : A literature survey of HA and lignin-based hydrogels in agriculture...31

Table 1.4 : A literature survey of nature-based hydrogels for absorbing environmental toxic substances...38

Table 1.5 : Literature survey of nature-based hydrogels for energy storage application. 42

Table 2.1 : Various compositions used in synthesis with their swelling index. 53

Table 2.2 : Frequency sweep data of LS-g-SAH and ctrl hydrogels......................65

Table 2.3 : Mathematical models used for the study of release kinetics from LS-g-SAH..71

Table 2.4 : Wheatgrass growth parameters on the 14th day. a) only urea, b) control hydrogel-loaded urea, and c) LS-g-SAH loaded with urea. 72

Table 3.1 : Various formulations of HA-g-SAH..88

Table 3.2 : Calculated value of network parameter...97

Table 3.3 : Release kinetics data of dinotefuran from HA-g-SAH and ctrl using different mathematical models..102

Table 3.4 : ANOVA table for water retention capacity 102

Table 4.1 : XRD data of Lt-g-SAH and ctrl 120

Table 4.2 : ANOVA data of different studies. 129

Table 4.3 : Release kinetics data of dinotefuran using different mathematical models. 131

Table 5.1 : Frequency sweep rheological analysis data of HA-g-SAH, LS-g-SAH, Lt-g-SAH, and ctrl hydrogels..152

Table 5.2 : Swelling study analysis of various compositions of HA-g-SAH, LS-g-SAH, Lt-g-SAH and ctrl hydrogels (KPS = 0.0098 mol·L^{-1}, MBA = 0.021 mol·L^{-1})...152

Table No. ***Page No.***

Table 5.3 : ANOVA table for water evaporation ratio. 155

Table 5.4 : Mathematical models used for the study of release kinetics of thiamethoxam. 158

Table 6.1 : Swelling study analysis of various compositions of HA-g-SAH, LS-g-SAH, Lt-g-SAH and ctrl hydrogels (KPS = 0.0098 mol·L^{-1}, MBA = 0.021 mol·L^{-1}). 166

Table 6.2 : Taguchi L16 design table for HA-g-SAH, LS-g-SAH, Lt-g-SAH and ctrl hydrogel. 167

Table 6.3 : Thermodynamic parameters: ΔG°, ΔH°, and ΔS° of MB adsorbed on the HA-g-SAH, LS-g-SAH, Lt-g-SAH and ctrl. 170

Table 6.4 : Isotherms data for Langmuir adsorption isotherm. 175

Table 6.5 : Isotherms data for Freundlich adsorption isotherm 176

LIST OF FIGURES

Figure No. *Page No.*

Figure 1.1 : Model structure of humic acid. 3

Figure 1.2 : Lignin structure. Inset- lignin precursors. i)- p-coumaryl alcohol, ii) - coniferyl alcohol, iii) - sinapyl alcohol 5

Figure 1.3 : Molecular model of lignite coal. 7

Figure 1.4 : Effectiveness of hydrogels in soil amendment. 17

Figure 2.1 : Visual representation of the synthesis of LS-g-SAH. 54

Figure 2.2 : The FT-IR spectra of a) LS, b) Ctrl, and c) LS-g-SAH. 59

Figure 2.3 : SS ^{13}C CP-MAS NMR spectrum of a) ctrl, b) LS-g-SAH, and c) LS. 60

Figure 2.4 : SEM images of a) LS and b) LS-g-SAH. 61

Figure 2.5 : TGA analysis of a) LS-g-SAH, b) LS, and c) Ctrl. 62

Figure 2.6 : XRD analysis of a) LS, b) Ctrl, and c) LS-g-SAH. 63

Figure 2.7 : Rheological analysis a) amplitude sweep b) frequency sweep of LS-g-SAH, and c) frequency sweep of ctrl hydrogel 64

Figure 2.8 : Effect of variation of framework parameters on the swelling index a) biopolymer, b) initiator, and c) crosslinker. 66

Figure 2.9 : Swelling study of hydrogel 68

Figure 2.10 : Water retention capacity plot of soil amended with LS-g-SAH. 69

Figure 2.11 : Water evaporation study of soil amended with different concentrations of LS-g-SAH...69

Figure 2.12 : Urea release kinetics a) first order, b) Korsmeyer–Peppas, and c) Higuchi model in distilled water. 71

Figure 2.13 : Effect of hydrogel treatment on wheatgrass after 14 days. a) only urea, b) control hydrogel-loaded urea, and c) LS-g-SAH loaded with urea. 72

Figure 3.1 : Molecular structure of dinotefuran 77

Figure 3.2 : Molecular structure of humic acid 78

Figure 3.3 : Effect of variation in amount of a) biopolymer, b) initiator, and c) crosslinker on the swelling index of HA-g-SAH 14. 91

Figure 3.4 : The plot of ^{13}C CPMAS NMR of a) ammonium humate, b) HA-g-SAH and c) ctrl 92

Figure No. ***Page No.***

Figure 3.5 : The plot of FT-IR of a) HA, b) HA-g-SAH and, c) ctrl 93

Figure 3.6 : SEM micrographs of a) HA-g-SAH and b) ctrl 94

Figure 3.7 : The plot of XRD of a) ctrl, and b) HA-g-SAH 95

Figure 3.8 : The plot of TGA of a) HA-g-SAH and b) ctrl 96

Figure 3.9 : Kinetic modelling profiles: Korsmeyer Peppas model of a) HA-g-SAH, and b) ctrl ; Weibull model of c) HA-g-SAH and d) ctrl 100

Figure 3.10 : Water retention capacity plot of soil amended with HA-g-SAH and ctrl.. 102

Figure 4.1 : Molecular structure of dinotefuran. 107

Figure 4.2 : Molecular structure of lignite..108

Figure 4.3 : Solid-state ^{13}C-NMR of ammoniated lignite, b) dinotefuran, c) ctrl (without dinotefuran), and d) Lt-g-SAH..................................116

Figure 4.4 : FT-IR spectra of a) dinotefuran, b) ctrl, c) Lt-g-SAH, d) ammoniated lignite, and e) raw lignite. 117

Figure 4.5 : SEM images of a) Lt-g-SAH and b) ctrl..119

Figure 4.6 : XRD patterns of a) ammoniated lignite, b) dinotefuran, c) Lt-g-SAH, and d) ctrl...121

Figure 4.7 : TGA plots of a) dinotefuran, b) ctrl, and c) Lt-g-SAH. 121

Figure 4.8 : Effect of variation in swelling index of Lt-g-SAH against: a) biopolymer, b) initiator, c) crosslinker...124

Figure 4.9 : Water retention capacity plot of soil amended with Lt-g-SAH and ctrl. 127

Figure 4.10 : Amount of dinotefuran released from Lt-g-SAH and Ctrl after UV irradiation 128

Figure 4.11 : a) Korsmeyer Peppas model of Lt-g-SAH, b) Higuchi model of Lt-g-SAH c) first order model of Lt-g-SAH d) Korsmeyer Peppas model of ctrl e) Higuchi model of ctrl f) first order model of ctrl 130

Figure 5.1 : Chemical structures of a) humic acid, b) lignin, and c) lignite.......137

Figure No. ***Page No.***

Figure 5.2 : FT-IR of a) HA-g-SAH, b) LS-g-SAH, c) Lt-g-SAH and, d) ctrl hydrogels. 144

Figure 5.3 : SS ^{13}C CP-MAS NMR spectrum of a) ammonium humate, b) HA-g-SAH, c) lignosulfonic acid sodium salt, d) LS-g-SAH, e) ammonium lignite, f) Lt-g-SAH and g) ctrl. 145

Figure 5.4 : SEM images of a) HA-g-SAH, b) LS-g-SAH, c) Lt-g-SAH and d) ctrl 146

Figure 5.5 : TGA analysis of HA-g-SAH, LS-g-SAH, Lt-g-SAH, and ctrl. 148

Figure 5.6 : XRD analysis of HA-g-SAH, LS-g-SAH, Lt-g-SAH, and ctrl. 149

Figure 5.7 : Rheological analysis - amplitude sweep of a) HA-g-SAH, b) LS-g-SAH, c) Lt-g-SAH, and d) ctrl. 151

Figure 5.8 : Rheological analysis - frequency sweep of a) HA-g-SAH, b) LS-g-SAH, c) Lt-g-SAH, and d) ctrl. 151

Figure 5.9 : a) Comparative swelling, b) SI concerning time. 153

Figure 5.10 : Water evaporation study of soil amended with HA-g-SAH, LS-g-SAH, Lt-g-SAH, and ctrl hydrogels. 155

Figure 5.11 : Korsmeyer Peppas release kinetics of thiamethoxam from a) HA-g-SAH, b) LS-g-SAH, c) Lt-g-SAH, and d) ctrl. 157

Figure 5.12 : Weibull release kinetics of thiamethoxam from a) HA-g-SAH, b) LS-g-SAH, c) Lt-g-SAH, and d) ctrl. 157

Figure 6.1 : a) ANOVA box plots for Table 1, b) effect of the contact time on %R by HA-g-SAH, LS-g-SAH, Lt-g-SAH, and ctrl hydrogels at adsorbent conc.= 0.3 g, T= 323.15K, dye conc.= 20 mg·L^{-1} 168

Figure 6.2 : Effect of the variation in a) adsorbent dosage (T = 323.15 K, dye conc.= 20 mg·L^{-1}), b) temperature (adsorbent conc.= 0.3 g, dye conc.= 20 mg·L^{-1}), c) Van't Hoff plots of ln K_d against 1/T and d) initial dye concentration (adsorbent conc.= 0.3 g, T= 323.15K), on %R by HA-g-SAH, LS-g-SAH, Lt-g-SAH, and ctrl hydrogels 168

Figure 6.3 : Langmuir isotherm graph of a) HA-g-SAH, b) LS-g-SAH, c) Lt-g-SAH, and d) ctrl. 175

Figure 6.4 : Freundlich isotherm graph of a) HA-g-SAH, b) LS-g-SAH, c) Lt-g-SAH, and d) ctrl. 176

LIST OF SYMBOLS, ABBREVIATIONS AND NOMENCLATURE

ATR-FTIR : Attenuated Total Reflectance-Fourier Transform Infrared

cm : Centimeter

COO^- : Carboxylate

CP MAS : Cross Polarization Magic Angle Spin

DSC : Differential Scanning Calorimetry

DTGA : Differential Thermogravimetric Analysis

G' : Storage Modulus

G'' : Loss Modulus

HA-g-SAH : Humic acid Grafted Polysodiumacrylate Hydrogel

KPS : Potassium Persulfate

LS : Lignosulfonic Acid Sodium Salt

LS-g-SAH : Lignosulfonate Grafted Polysodiumacrylate Hydrogel

Lt-g-SAH : Lignite Grafted Polysodiumacrylate Hydrogel

MBA : N,N’ Methylenebisacrylamide

mL : Milliliter

NaOH : Sodium Hydroxide

nm : Nanometer

NMR : Nuclear Magnetic Resonance

SEM : Scanning Electron Microscopy

SI : Swelling Index

TGA : Thermogravimetric Analysis

XRD : X-ray Diffraction

WRC : Water Retention Capacity

$\boldsymbol{\theta}$: Diffraction Angle

χ : Solvent Interaction Parameter

M_c : Molecular Weight between Crosslinks

ρ : Crosslinking Density

CHAPTER-1

INTRODUCTION AND LITERATURE REVIEW

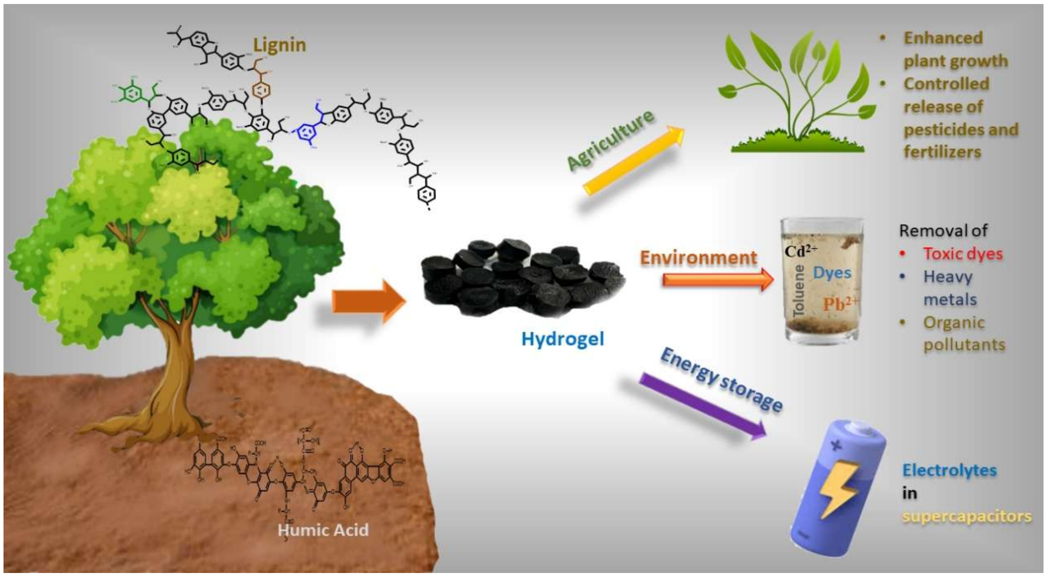
Lignin
Humic Acid
Hydrogel
Agriculture
Environment
Energy storage
Enhanced plant growth
Controlled release of pesticides and fertilizers
Removal of
Toxic dyes
Heavy metals
Organic pollutants
Cd^{2+}
Dyes
Toluene
Pb^{2+}
Electrolytes in supercapacitors

The gradual depletion of fossil resources has intensified the search for sustainable alternatives to petroleum-based polymers. Among the remarkable natural polymers, humic acid (HA), lignin and lignite stand out due to their versatile applications. This chapter addresses this gap by systematically exploring the roles of HA, lignin and lignite- based hydrogels in diverse fields.

1.1 Humic Acid

Most organic matter in soil is made up of humic compounds (humic and fulvic acids), which is frequently used interchangeably with soil organic matter [1]. The presence of carboxyl groups and the mild acidity of the phenolic groups in humic compounds contribute to their ability to exchange ions and form complexes. Due to their high pH-dependent charge, the filling of cation exchange sites, primarily with hydrogen (H) ions, makes the material an acid called Humic Acid (HA). The dominance of cations other than H on the exchange sites makes it a salt of HA, technically termed humate [2].

HA is readily soluble under alkaline conditions but insoluble in strong acids and has a pH below 2. The molecular weight of HA ranges from 5,000 to 100,000 Da, indicating a medium molecular size. Oxygen makes up 33–36% of the total mass in this material, whereas nitrogen makes up 4% [3]. Figure 1.1 shows HA's elemental composition, which typically contains carboxylic, phenolic, alcoholic, and carbonyl fractions [4]. The main sources of HA are soil, water, and leonardite [5].

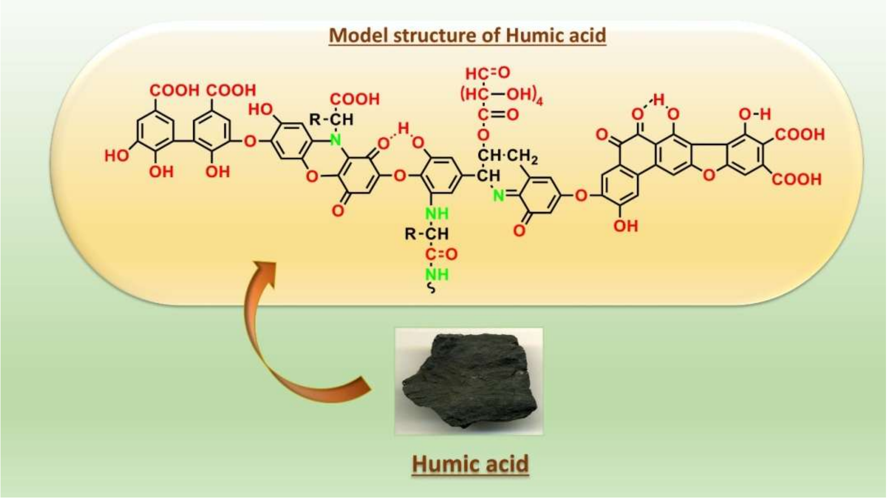

Figure 1. 1: Model structure of Humic acid.

The molecular structure of HA is made up of intricate organic combinations that are randomly connected to form incredibly complex substances. According to the widely accepted view, HAs are made up of relatively small molecules that self-organize into supramolecular structures stabilized by various interactions, including Van der Waals, π–π, CH–π interactions, and hydrogen bonding [6].

Yang et al. provided the first technical method for hydrothermal humification-based HA synthesis. This method relies on oxygen exclusion and hydrothermal condensation of wet biomass at autogenous pressure. Compared to flame processes, where a substantial amount of the carbon in the biomass is oxidized and released as greenhouse gases, this technique is very different. For instance, hydrothermal humification can be considered a modest chemical engineering process that resembles natural humification but with an acceleration factor of up to nine orders of magnitude when reactions are conducted at 200°C and 16 bar pressure. Additionally, hydrothermal processing is free of metabolization because it is an abiotic process and often produces great carbon yield. The humified product contains which is most of the carbon linked to biomass [7].

1.2 Lignin

F. Schulze was the first to use the term "lignin" in 1865. It comes from the Latin word ‘lignum’, which is a synonym for "wood ". Following cellulose, it is the most common aromatic polymer on the planet. It can be defined as a complex amorphous networked natural polymer consisting of heterogeneous phenyl propane units. It provides stiffness and strength to the cell walls and helps the internal fibres and cell wall to transport nutrients [8, 9]. It has a high calorific value, high thermal stability, good hardness, biodegradability, and oxidation resistance [10]. Lignin demonstrates that it can serve as an inexpensive and environmentally responsible feedstock for minerals, chemicals, and fuels [11]. The paper and pulp industries are primary global sources of lignin. Currently, the global paper and pulp industry produces between 50 to 70 million tons of lignin annually [12].

1.2.1 Structural characteristics and types of lignin

Lignin is a complex heteropolymer biosynthesized from phenylpropane units linked by various carbon-carbon bonds and ether bonds [13]. Lignin structure naturally incorporates 35 monomeric units [12]. The most primary(phenylpropanoid) subunits are p-hydroxyphenyl (H), guaiacyl (G) and syringyl (S), formed from p-hydroxycinnamyl (coumaryl), coniferyl and sinapyl alcohols (shown in Figure 1.2) are interlinked through C-O-C ether linkages (α-O-4, β-O-4, 4-O-4) and C-C linkages (β-β, β-1, β-5, 5–5) [14–16]. Novel monolignols are still being discovered, including caffeyl alcohol, tricin, monolignol benzoate, and piceatannol [12]. However, the structural features of lignin vary across the plant species along with the stage and growing environment of the plant [17]. In general, hardwood lignin contains an equal amount of coniferyl and sinapyl alcohols, whereas softwood lignin contains 90-95 wt % of coniferyl alcohol and remaining is the sinapyl alcohol. Grasses majorly contains coniferyl alcohol (75 wt%), sinapyl alcohol (20–25 wt%) and only 0–5 wt% of the coumaryl alcohol [15].

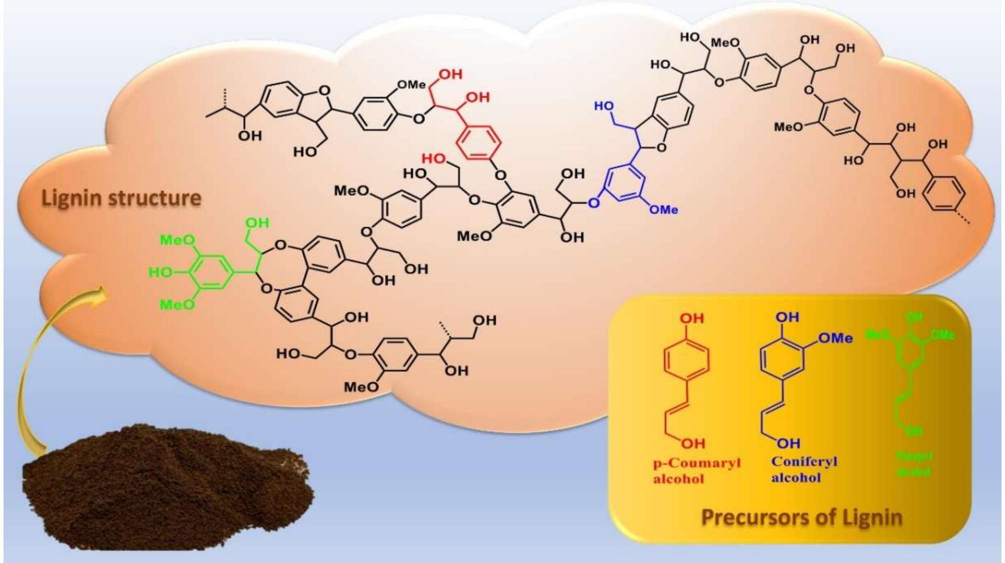

Figure 1. 2: Lignin structure. Inset- Lignin precursors. i)- p-coumaryl alcohol, ii) - coniferyl alcohol, iii) - sinapyl alcohol

Various kinds of lignins are obtained through different fractionation/isolation methods. Kraft process results in alkali lignin, lignosulfonates are obtained from the sulfite process, and organosolv lignin and hydrolytic lignin are products of the organosolv process and enzymatic hydrolysis. The sulfur-free pulping process gives soda lignin, and another sulfur-free lignin is achieved as a byproduct of the lignocellulosic biorefineries.

A brief explanation of these processes, along with other fractionation/ isolation methods, is given below in Table 1.1.

Table 1. 1: Different kinds of technical lignin

Types of Technical lignin			
S. No	**Type of technical lignin [18][19]**	**Molecular wt. (g·mol^{-1}) [19, 20]**	**Characteristics [21]**
1.	Kraft lignin	2000-7000	High purity (less amount of carbohydrate and inorganic residues) High content of industrial lignin Good solubility in alkaline conditions Poor water solubility
2.	Lignosulfonate	1000-150000	Common groups present are- sulfonic, carboxyl, and phenolic hydroxyl Considered as anionic surfactant Good water solubility
3.	Soda lignin	1000-3000	High content of carboxylic acid Obtained by soda pulping process No sulfur contents
4.	Ethanol Organosolv lignin	1000-4000	Free of sulfur content Easily soluble in polar and basic solutions
5.	Milled Wood Lignin (MWL)	5500-20000	Poor water solubility Low sulphur content
6.	Steam Explosion Lignin (SEL)	3500-15000	High-quality sulfur-free lignin
7.	Enzymatic lignin/ Hydrolysis lignin	5000-10000	Similar structure to pristine lignin No sulfur contents Low water and organic solvent solubility
8.	Hot-water extracted lignin	5000-10000	Lignin is 10-40 % recovered depending on reaction conditions
9.	Ammonia lignin	~4000	The process has lower basicity and milder cooking temperatures compared to hydrothermal pre-treatments
10.	Co-solvent enhanced lignocellulosic fractionation lignin (CELF)	1500-3000	Exhibited properties similar to that of ethanol organosolv lignin Results in high lignin purity and yield [22]
11.	γ-valerolactone Lignin (GVL)	~5500	High-purity lignin obtained GVL treated lignin retained more than half of their β−O−4 linkages [23]

Types of Technical lignin			
S. No	**Type of technical lignin [18][19]**	**Molecular wt. (g·mol^{-1}) [19, 20]**	**Characteristics [21]**
12.	Cyrene lignin	4000-6300	Obtained lignin has a high content of β−O−4 linkages and syringyl units [24]
13.	Ionic liquid lignin	~3200-3400	Low carbohydrate and sulfur content High recovery and purity of lignin
14.	Deep Eutectic Solvents (DES) Lignin	500-2600	Moderate to high purity lignin obtained with an abundance of β−O−4 linkages DES can be recovered after lignin fractionation and reused in subsequent pre-treatment processes [18, 25]

1.3 Lignite

Low-rank coals, including lignite, leonardite (highly oxidized lignite), and peat coals, are produced during the coalification process. These fossil fuels, which have a 500 billion tons worldwide reserve, are mainly employed as the burning fuel in power plants.[26] Figure 1.3 shows the molecular model of lignite coal.

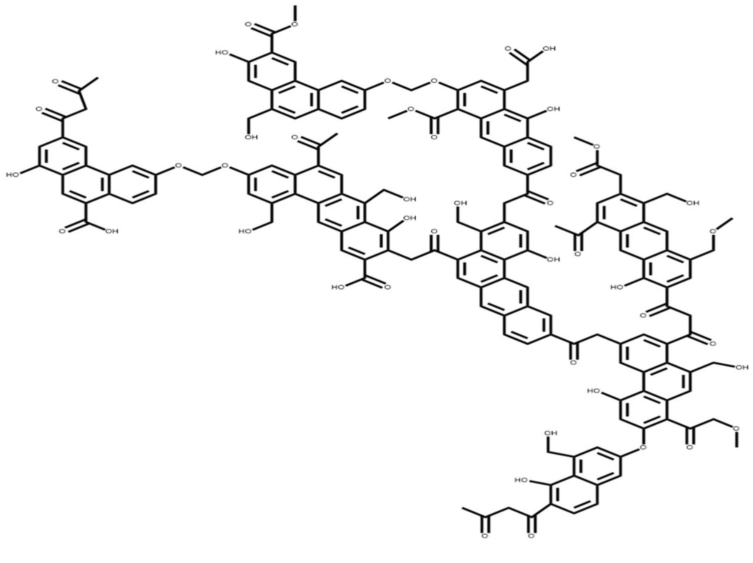

Figure 1. 3: Molecular model of lignite coal.

The following categories of lignite can be distinguished based on the degree of coalification and their physical-chemical characteristics, such as moisture content and exterior appearance.

Soft lignite - Low levels of coalification, 70–40% moisture content, pale-brown or brown-black color, and an unconcise structure.

Hard lignite - Strong levels of coalification, 40–20 weight percent moisture, brown to black color, compact structure, high mechanical strength.

Xylite lignite- a soft variety of lignite that still has its original wood structure.[27]

Peat and bituminous coal have intermediary products called lignite. The ineffective power production, higher CO_2 emissions, and increased coal consumption of lignite-fueled power plants are all caused by low heating values (typically less than 19.3 kJ $\cdot kg^{-1}$), low coalification (lowest ranking), high carbon dioxide emission factor (greater than 0.365 kg CO_2-eq/ MWh), high ash content (up to 25%), high volatile matter (greater than 24%), and significant moisture content (more than 30%). [26] Thus, direct burning of lignite is inappropriate due to the high concentration of organic oxygen, appropriate to be developed as a feed-stock for value-added chemicals. [28] Lignite is an important precursor of humic acid. Lignite carbon may remain in soil due to a low decomposition rate and have an impact on the quantity and composition of the Soil Organic Matter. [29] Humic acid is extracted from lignite by various treatments like a) alkaline extraction [30], b) acid liquid extraction [31], c) microbial conversion [32], d) hydrothermal method.[33] Although acid extraction is more efficient, the extracted sample still contains contaminants. While microbial conversion can provide a desirable pure HA, the procedure is time-consuming and has modest yields. The hydrothermal technique can produce yields of up to 90.2%. As a result of the alkalis' safety and lack of toxicity, previous treatment and alkaline extraction is seen to be better options for industrial scale-up.[34]

The best lignite for agricultural use is that with a low degree of coalification. A logical way to handle it is to use it as a rich supply of humic chemicals.[35] Conventional techniques of lignite HA extraction have been shown to improve crop yield and quality, tissue nutritional balance, and seed germination. They preserve the rhizosphere's chemical, physical, and biological features along with its diverse functions in the growth of the soil and crops.[34]

1.4 Hydrogels

Super-absorbent polymers, also known as hydrogels, may expand to absorb significant amounts of water or aqueous solutions. These can be synthesized through various chemical and physical techniques [36]. Chemical methods involve chemical cross-linking [37–39], grafting and irradiation [40, 41], and enzymatic reaction [42, 43]. Physical methods are heating/cooling [36], complex coacervation [44, 45], ionic interaction [46, 47], hydrogen bonding [48, 49], freeze-thawing [50, 51], and heat-induced aggregation [48, 49]. Hydrogels have been successfully employed in various fields, from biomedical to agriculture.

Some of these applications are listed below in Table 1. 2. In addition to surface adsorption, capillary and osmotic pressure are additional mechanisms that cause hydrogels to swell. Osmotic pressure is the primary motivating factor behind the water adsorption phenomenon the gels exhibit.

Temperature-sensitive hydrogels have the lowest critical solution temperature (LCST). The hydrophilic groups on the hydrogel's polymer chains form hydrogen bonds with the water molecules to cause swelling when the surrounding temperature is lower than the LCST of the hydrogel. The connection between hydrophobic groups in the polymeric chain is reinforced due to the weakening of the hydrogen bond caused by a rise in temperature, which causes the hydrogel to contract gradually. As the temperature rises above the LCST, the hydrophobic connection between polymeric chains becomes the dominant interaction. As a result, the swelling rate is dramatically reduced [52].

Table 1.2: Literature overview of HA and Lignin-hydrogels in various applications

Different applications of HA and Lignin based hydrogels				
S. No.	**Property**		**Components**	**Ref.**
1.	**Therapeutic action**			
	a)	Controlled drug release	- Hemicellulose, lignin, and pectin	[53]
			- Microcrystalline cellulose, lignin	[54]
				[55]
	b)	Antioxidant and antibacterial properties	- Polyvinyl alcohol/chitosan, lignin	[56]
				[57]
			- Alginate, lignin	[58]
	c)	Antimicrobial agent	- Humic substance, gelatin	
	d)	Wound dressing	- Humic acid, alginate	
2.	**Stimuli-responsive capability**			
	a)	Temperature, pH-responsive	- Methacrylated lignosulfonate Carboxylated lignin	[59]
			- Humic acid, chitosan, poly (vinyl alcohol)	[60][61]
	b)	Mechanically responsive	- Poly(ethylene glycol) methyl ether Methacrylate, kraft lignin	[62]
3.	**Biosensors and Bioelectrodes**			
	a)	Biosensors, electrode	- Lignin, cellulose -electrodes	[63]
				[64]
	b)	Metal-free supercapacitor	- Graphene and lignosulfonate hydrogels	
				[65]
	c)	Anti-freezing, anti-swelling, and anti-creep sensor	- Methacryloyl chloride, lignin	

4.	**Water purification**		
	a) Absorption of Cu(II) and Pb(II), Cd(II)	– Sulphonated humic acid resin	[66]
	b) Dye absorption	– Montmorillonite-Lignin Lignosulfonate	[67]
	Methylene Blue	– Poly (acrylic acid-*r*-acrylamide)	
	Methylene Blue		[69]
	Malachite green		[70]
	Malachite Green, Methylene Blue, and Crystal Violet	– Lignin Sulfonate, Tween 80, Formaldehyde, liquid paraffin – Humic acid, bentonite	[71]
5.	**Agriculture**		
	a) Controlled, slow-release fertilizer	– Lignin, agrochemical- IAC, herbicide-DCP – Humic acid, Urea	[72]
	b) Coating of fertilizer	– Lignin, acrylic acid, Cyfluthrin, Paraquat, Cyhalofop-butyl	[73]
		– Potassium salt of Humic Acid, Sodium Alginate, $CaCl_2$	[74]
	c) Enhanced water retention		[75]
6.	**UV Shielding**	- Lignin, polyacrylamide, polyacrylic acid	[76, 77]

1.4.1 Swelling mechanism and thermodynamic potential of hydrogels

Water can be present in the hydrogel in four different types:

(a) Free water in the hydrogel structure's outer layer may be easily removed.

(b) Interstitial water- physically confined within the network's interstices

(c) Water chemically bonded by functional groups and directly linked to the network cannot be withdrawn normally.

(d) Semi-bound water – is positioned between interstitial and chemically bound forms of water and is neither free nor bound [78].

The free mobility of water-water vibrations contributes to the solubility power of water. The water molecules attempt to destroy the hydrogel by altering its vibrational modes and eventually succeed in cleaving hydrogen bonds. The mobility process occurs when hydrogels containing hydrophilic functional groups like [COONa] contact water molecules, converting the kinetic energy of water-water vibrations into water-ion vibrations. The water vibration breaks down [COONa] into COO^- and Na^+, a process known as dissociation. The water molecules then neutralize the negative charges due to the negative charges repelling one another, hydrating the Na^+ ions as part of the hydration process. This is a sign that the hydrogen bonding has changed. It traps the water molecules inside the hydrogel's network structure's pores and causes swelling. Therefore, the presence of osmotically active mobile polar molecules is the driving force behind the swelling of a hydrogel [79].

The hydrogel's water potential may be used to predict how it would behave in the soil. According to osmotic principles, this thermodynamic potential controls the processes of water redistribution in the soil, transportation to plant roots, and absorption. The energy characteristics of soil water are often used to classify gravitational, hygroscopic, and capillary soil water. Only the capillary fraction of water, which falls within the pF (picofarad) range below 4.2-4.5, may be utilized by plants. As a result, there should be a considerable correlation between these conditions and the potential of water trapped in hydrogels [80].

1.4.2 Functions of humic acid in hydrogels

1.4.2.1 Humic acid as cross-linkers

Humic acids can be effective crosslinkers in hydrogel systems by aggregating polymer chains to form three-dimensional networks. For instance, Denis Miroshnichenko et al. synthesized hydrogels from hydroxypropyl methylcellulose modified with humic acids.

The crosslinking occurred through multipoint interactions between the carboxyl groups of humic acids and the polymer chains, resulting in stable hydrogel matrices [81]

1.4.2.2 Humic acid as a complexation agent/metal absorbent

Humic acids exhibit a high affinity for metal ions, making them effective agents for metal adsorption. Studies have demonstrated that the presence of humic acids enhances the adsorption of heavy metal ions and dyes. Baker and Khalili identified four distinct binding sites on humic acids for metal ion interactions, while Shaker and Albishri described three types of binding sites with varying adsorption capacities [82, 83] Martina Klučáková et al. synthesized hydrogels incorporating humic acids as active complexation agents, suggesting their potential for addressing specific environmental issues related to metal ion contamination.[84]

1.4.2.3 Humic acid as a grafted agent

Humic acids, specifically sodium humate, can be utilized in hydrogel synthesis due to their multifunctional aliphatic and aromatic components. These components contain numerous hydrophilic functional groups, such as carboxylates and phenolic hydroxyl groups. Singh and Singhal reported the grafting of humic acid onto acrylic acid, leading to the formation of superabsorbent hydrogels based on polyacrylic acid/acrylamide/sodium humate. These hydrogels, synthesized using ammonium persulfate as an initiator and N, N'-methylene bisacrylamide as a crosslinker, demonstrated impressive water absorbency, reaching up to 724 $g \cdot g^{-1}$. [85]

1.4.2.4 Humic acid as filled biomolecules

Humic acids can enhance the activity of protein enzymes, improve soil structure, and promote the absorption of nutrients such as nitrogen, phosphorus, and potassium in plants, ultimately increasing crop yields. [86, 87]

Hua et al. fabricated a semi-interpenetrating network (semi-IPN) hydrogel by free radical polymerization, utilizing N-isopropyl acrylamide and 2-acrylamido-2-methylpropanesulfonic acid as monomers. The hydrogel incorporated sodium alginate and humic acid as biomolecular fillers, resulting in a robust and functional hydrogel system.[73]

1.4.3 Functions of lignin in hydrogels

1.4.3.1 Lignin as self -polymerizing agent and initiator in hydrogels

Lignin and its derivatives are rich in phenolic hydroxyl and methoxy groups. These can be converted into the benzoquinone radicals in the redox process. A double network polymeric hydrogel was developed by Zhang et al., employing a rapid gelling process at room temperature initiated by a novel redox system comprising lignin sulfonate (LS), ferric ions (Fe^{3+}), and ammonium persulfate (APS). This system facilitates quick gelation, showcasing the potential of lignin derivatives in hydrogel synthesis. [88] Gan et al. demonstrated that a solution containing silver-lignin nanoparticles (Ag-Lignin NPs) and APS could produce sufficient radicals to initiate the self-polymerization of hydrogels under ambient conditions.

Furthermore, this solution could initiate the polymerization of various free-radical monomers, such as acrylic acid (AA), acrylamide, and poly(ethylene glycol), indicating its versatility in hydrogel formation. [89] Afewerki et al. engineered a lignin-based hydrogel using oxidative decarboxylation and quinone-catechol redox catalysis to generate free radicals. These radicals effectively triggered the self-gelation of the hydrogel at room temperature, further illustrating the utility of lignin in creating self-polymerizing hydrogels. [90]

1.4.3.2 Lignin as a reinforcing nanofiller

Cui et al. developed durable hydrogels featuring dynamic cross-links using Ag-decorated functionalized lignin nanoparticles, designated as LNP@Ag–Fe-PAA. In this design, the lignin nanoparticles decorated with silver serve dual roles: they act as reinforcing fillers and provide numerous sacrificial bonds. These bonds contribute to the formation of mechanically robust hydrogels and possess excellent self-healing properties. LNP@Ag as reinforcing nanofillers enhances the hydrogel's rigidity in aqueous environments, thereby significantly boosting its mechanical strength [91].

In another study, Huang et al. incorporated lignin nanorods into hydrogels to create reinforced nanocomposite hydrogels. These lignin nanorods acted as reinforcing fillers and connecting bridges within the polyacrylamide/poly(acrylic acid) (PAM/PAA) network through reversible hydrogen bonds. This incorporation endowed the hydrogels with outstanding tensile strength, showcasing the potential of lignin nanorods in improving the mechanical properties of hydrogel systems [76].

1.4.3.3 Lignin as a reducing agent

Phenolic OH groups in lignin nanoparticles (LNPs) can reduce Ag^+ ions to metallic Ag nanoparticles (Ag NPs) without additional reducing agents or external stimuli. [91] Similarly, Parajuli et al. developed hydrogels based on lignocatechol, lignophenol, and lignopyrogallol, which efficiently reduced Au(III) to elemental gold, demonstrating the potent reducing capability of lignin-derived compounds in hydrogel systems [92]

1.4.3.4 Lignin as a cross-linker

The hydroxyl groups in lignin act as crosslinking sites through hydrogen bonds.[93] Lignin's hydroxyl groups serve as crosslinking sites through hydrogen bonds. The abundant polar sites on lignin’s backbone can facilitate the physical crosslinking of hydrophilic polymers via hydrogen bonding. For instance, Oveissi et al. utilized lignin as a crosslinker to develop hydrophilic polyether-based polyurethane (HPU) hydrogels, which were then fabricated into flexible films for wearable electronics. [94] Ravishankar et al. synthesized biocompatible hydrogels by mixing an aqueous-acidic chitosan solution with alkali lignin. Ionotropic gelation occurred between the alkaline lignin and chitosan, producing physical hydrogels through simple mixing. Electrostatic interactions between phenoxide anions of lignin and the protonated cationic amine groups of chitosan drove this gelation. This method offers an inexpensive and sustainable alternative to traditional ionotropic crosslinkers for chitosan.[95] Huang et al. employed lignin molecules as extended crosslinkers, alongside epichlorohydrin as a short crosslinker, to prepare a cellulose derivative framework for a highly stretchable, self-healing hydroxyethyl cellulose hydrogel. [96]

1.4.3.5 Lignin as a UV blocking agent

Incorporating lignin nanoparticles into hydrogels imparts excellent UV-blocking performance due to lignin's natural UV-shielding properties, making the hydrogels suitable for applications in visual medical fields.[67, 76]

Wang et al. produced sulfonated lignin-Fe^{3+} chelates to create dynamically crosslinked hydrogels with UV-blocking properties. These chelates significantly enhanced the UV-blocking ability of the Fe-SL-g-PAA hydrogel. When applied as a polyethylene (PE) substrate coating, the hydrogel effectively blocked UV light, preventing fluorescence emission from a UV-sensitive area on a 100-CNY bill beneath it. [97]

1.5 Applications of nature-based hydrogels in Agriculture

In addition to air and soil, water plays a well-known role in the life of plants. This function involves transporting the necessary minerals for feeding, preserving the intracellular pressure for the cell's vertical growth, and taking part in photosynthesis

[80]. However, the shortage of water resources, excessive use of fertilizers, and desertification of the soil led to the degradation of cultivated land [98]. As per recent studies, the efficiency of water used in agricultural soil can be improved by using polymer hydrogels, reducing water loss and helping restore soil quality [99].

Using water-absorbent lignin-based hydrogels to increase soil water retention for plant uptake is a potential approach to improve water use effectiveness. Hydrogels made of lignin have already been used to coat seeds, deliver drugs, and absorb trace metal ions [100].

Thus, hydrogels made of HA and lignin can primarily enhance the soil's ability to retain water and support the slow release of agrochemicals. These enhance the physical and chemical characteristics of the soil while promoting plant development.

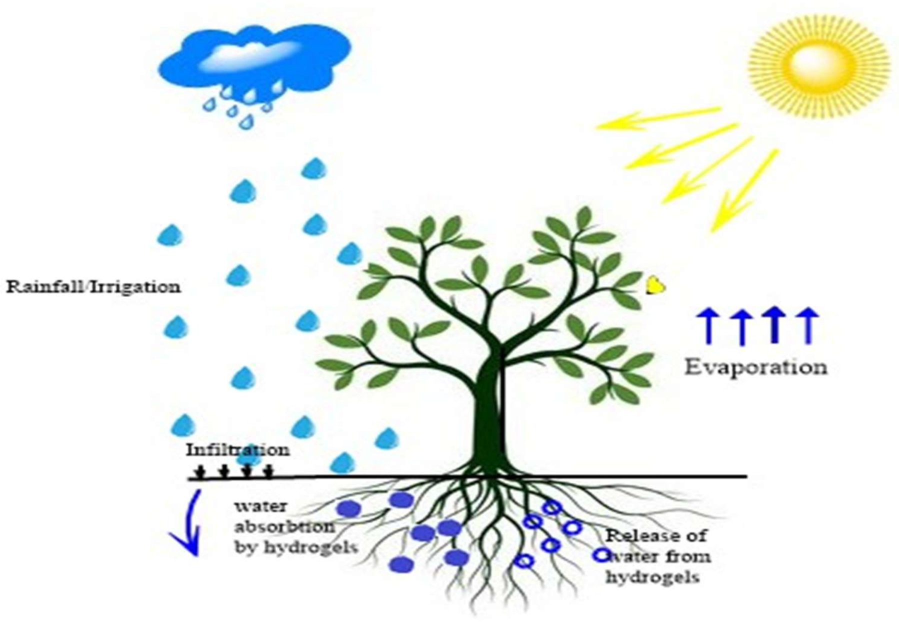
Rainfall/Irrigation
Evaporation
Infiltration
water absorbtion by hydrogels
Release of water from hydrogels

Figure 1.4: Effectiveness of hydrogels in soil amendment.

1.5.1 Hydrogels in the soil-water-plant system.

Usually, plants can efficiently produce biomass through photosynthesis using a small amount of soil water. Most of the soil's water evaporates through ineffective channels, particularly in sandy soils. Adding hydrogels to the soil increases the air and water infiltration area. Additionally, when the soil is dry, the hydrogel will quickly release water from its internal polymer network (Figure 1.4) [79]. Water redistribution processes result in this release of water stored in a hydrogel network over time into the surrounding soil matrix via the capillary forces. The swollen hydrogel brought interactions between soil and water, which also stabilizes the soil's structure [101].

An experiment conducted by soil experts explained the mechanism that shows the impact of hydrogel on soil parameters. The large capillaries in sandy soil could hold water when the hydrogel particles were inserted into the soil pores. However, the same capillaries in the control soil lacked this capacity. This pattern showed an increase in tiny capillaries and a decrease in the pores' average diameter. Another consequence was the blocking of the water evaporation routes from the soil layer. These channels arise as a result of physical evaporation as well as the hydraulic conductivity that promotes gravitational flow. All of these effects increase the soil's ability to hold onto water.

Apart from water holding hydrogels can be added to soil to enhance its physical properties, such as its structure and porosity [102].

1.5.2 Enhancing the water retention capability of the soil.

Water-absorbent hydrogels increase soil water retention for plant uptake. It is a potential method to improve the water use efficiency of plants. The swelling mechanism of hydrogels has already been discussed in the previous section.

The network chains' osmotic driving force toward infinite dilution comes next. The porosity of a hydrogel and its attraction to the aqueous solution are the main variables that affect its ability to swell [78]. Previous research suggests that hydrogels can improve soil moisture retention, particularly in areas of water constraint and drought.

Sodium humate (SH) based super-absorbent hydrogel synthesized by Agnihotri et al. was studied for use in agriculture as a soil conditioner to help sandy soil retain water. The addition of SH improved the resultant super-absorbent hydrogel's surface area and surface structure, which facilitated the diffusion of water into the polymeric web, increasing the swelling rate. The study discovered that the artificial super-absorbent hydrogels, with a swelling ratio of 906 $g \cdot g^{-1}$, could serve as an effective water-saving substance for agricultural applications. The concentration of SH affected the swelling kinetics of synthesized super-absorbent hydrogels. The swelling rate increases to 9.09 wt % of SH [103]. A new poly(acrylic acid-co-acrylamide) $AlZnFe_2O_4$/potassium humate super-absorbent hydrogel (PHNC) nanocomposite was synthesized by Shahid et al. The soil was treated with PHNC and air-dried. Comparing the amended soils to the unamended soils, the soils with 0.1 to 0.4 w/w% of synthesized PHNC significantly improved the moisture retention at field capacity. At various PHNC concentrations, the hydraulic conductivity and soil bulk density were also reduced compared to the control [104].

The soil's capacity to store more water was increased by potassium humate, which also boosted the plant’s growth, nutrient absorption, yield, and fruit quality, as shown in a study conducted by Sayed et al. under water stress conditions in Egypt for two successive seasons, 2015 and 2016, on Egazy olive trees (*Oleaeuropaea* L.). Potassium-humate treatment may improve soil's capacity to hold much more absorbed water, maintain soil temperature conducive to plant development, and increase soil aeration and soil workability by improving topsoil structure, all of which contribute to the observed enhancement impact [105].

Starch and SH were used as raw materials to create the starch-g-poly(acrylic acid)/sodium humate into a poly acrylic acid-co-acrylamide super-absorbent by graft copolymerization of starch and acrylic acid in the presence of SH in aqueous solution. Under optimal conditions, the super-absorbent hydrogels absorbed 86 and 1100 $g \cdot g^{-1}$ samples in 0.9 wt% NaCl solution and distilled water, respectively. This novel super-absorbent displayed remarkable water absorption, swelling, and reswelling capabilities and may be particularly helpful in the domains of agriculture and horticulture [106].

The research by Zheng et al. revealed that the combination incorporation of organomontmorilonite (O-MMT) and SH into a PAA-AM network increased the water absorbency of a super-absorbent composite when compared to the integration of only O-MMT or SH. The super-absorbent demonstrated a solid ability to hold onto water. A suitable amount of O-MMT might enhance the synthesized composites concerning their water absorbency, salt resistance, and ability to retain water in sandy soil, as shown by the sand soil's ability to conserve 24.4 wt% of water even after 30 days and contain 1.0 wt% super-absorbent composite [107]. A new potassium humate-acrylic acid-acrylamide (KHA-AA-AM) super-absorbent polymer was developed using leonardite potassium humate. The non-potassium humate super-absorbent polymer has lower water absorbency than the KHA-AA-AM super-absorbent polymer, which uses less than 40% potassium humate. [108] The capacity of the soil to hold water was also enhanced by the poly(acrylic acid), attapulgite, and SH super-absorbent composite. According to the results of its water-retention experiment, the soil retained more than 27% more water compared to the control after 30 days under the same conditions. The super-absorbent composite may be a suitable water-management material for horticulture and agriculture in arid and drought-prone locations [109].

A lignin-based hydrogel has been reported by Mazloom et al. as a naturally occurring plant-based water absorbent. The cross-linker poly(ethylene glycol) diglycidyl ether (PEGDGE) and alkali lignin polymers were used in this synthesis. Physicochemical properties, phytotoxicity, and biodegradability are key factors that determine hydrogel's potential to be used as a soil conditioner in arid soils [110].

The density of the cross-linkages and the kind of solvent impact how much a cross-linked polymer swells, following Flory and Rehner's equilibrium swelling theory [111]. Therefore, a hydrogel's ability to swell is significantly impacted by the cross-linker concentration in the hydrogel [112, 113]. The hydrogel's swelling ratio increases initially and declines as the cross-linker concentration is raised [114]. It was discovered that this is consistent with the way the PEGDGE cross-linker ratio affected the hydrogel's ability to swell. Despite being less than the currently available acrylate-based hydrogels, which have a swelling capacity of more than 100 $g \cdot g^{-1}$ hydrogel, the lignin-based hydrogel was reported to have a swelling capacity of 34 $g{\cdot}g^{-1}$ hydrogel. Despite the lower swelling index, it has a number of benefits.

-It is produced using a low-cost, renewable feed-stock, i.e., lignin alkali using non-toxic chemicals- NaOH and PEGDGE g that too in a small amount.

-It is consistent with the principles of green synthesis given by Prof. Paul T Anastas and John C Warner.

-It is biodegradable and non-toxic, posing no threat to soil health or crop growth.

-It functions in non-saline, saline conditions and sodic soils, so it is suitable for use in drought-impacted areas for better water retention [110].

By using konjac flour to cross-link sodium lignosulfonate and sodium alginate (L/KJ/SA), Song et al. synthesized green hydrogel. They investigated its agricultural utility by putting tobacco plants through drought stress tests [99]. The existence of hydrogen bonds between the ether oxygen atom of the lignin sulfonate, the alcohol hydroxyl group, and the hydroxyl group of alginate was established by Dumitriu et al. To a certain extent, this has determined the structure of the macromolecular chains present in hydrogel [115].

Synthesized hydrogels exhibited the potential to absorb large quantities of water. It decreased the water loss due to water infiltration by increasing the friction between hydrogel, soil particles, and water and blocking the soil pores. These hydrogels also reduced the leaching of fertilizer and the wilting time of tobacco, extending its growth time. The research conducted by Yang and Banedjschafie et al. supports these findings, which likewise concluded that adding hydrogels could prolong the growth of woody and herbaceous plants by up to 9–10 days [116, 117].

Morales et al. prepared physically cross-linked lignin polyvinyl alcohol (PVA) hydrogels using a green approach [118]. The hydrogel blends were treated using three different cross-linking procedures with a variation in freeze-thawing cycles and under a vacuum hood for a week to evaluate the influence of the synthesis processes. According to the study, lignin addition favoured the PVA hydrogels' ability to swell in every instance [119].

The size of the linked lignin molecules may have contributed to this action, which resulted in a swelling index of these materials that nearly exceeded 350%. Due to the high molecular weight of lignin, larger holes may develop. More water molecules may be able to enter through these pores [118]. Ciolacu et al. also described the identical behaviour for their chemically cross-linked PVA lignin hydrogels [120]. Yang et al. also showed that lignin enhanced the swelling properties of chitosan/PVA hydrogels [55].

The type of lignin used also affects the hydrogel's capacity to swell. Wu et al. validated this and reported that the hydrogels synthesized utilizing the three forms of lignin had highly varying swelling capabilities [114].

Mazloom et al. investigated how lignin-based hydrogels affected the development of maize plants under drought stress. The results showed that in comparison to synthetic hydrogel, lignin hydrogel was better at retaining water in arid environments, which was evident by the reduced production of proline, which is a water stress biomarker, in maize leaves [121].

Without any pretreatment, Meng et al. directly made hydrogels using red liquor. Lignosulphonates and polysaccharides, two of red liquor's major constituents, produced super-swelling bio-polymer hydrogels with excellent long-term water retention capabilities. These constituents are frequently thought of as fertilizers to enrich the soil. The hydrogels were categorized as super-swelling hydrogels with a swelling ratio of about 280 $g{\cdot}g^{-1}$ [102]. These hydrogels with extreme swelling had a slow water release capability. After 24 hours at 50 °C, it was discovered that hydrogels containing 0.4 g red liquor had an 80% water retention ratio. Regarding swelling and water retention in agriculture, red liquor-containing hydrogels thus proved to be good options for plants and vegetables.

The traditional PVA composite hydrogel had poor mechanical and swelling characteristics. To overcome this limitation, Wu et al. created super-absorbent hydrogels using biomass lignin as the raw material, PVA as the template for the matrix, and epichlorohydrin as the cross-linker. Surprisingly, a swelling ratio of up to 456 $g{\cdot}g^{-1}$ was found in modest conditions. When the alkali lignin concentration was 5%, the hydrogel's swelling index reached 570 $g{\cdot}g^{-1}$. For the lignin concentration of 10% in the enzymatically hydrolyzed lignin- PVA hydrogels, the swelling ratio of the hydrogel was as high as 554 $g{\cdot}g^{-1}$, and the yield was 45%. After ten days, the retention ratio of hydrogels with Lignin concentrations of 5%, 7.5%, and 10% named LP-5%, LP-7.5%, and LP-10%, respectively, remained at 134, 107, and 59 $g{\cdot}g^{-1}$. In hydrogels with lignin concentrations of 5%, 7.5%, and 10%, referred to as LP-5%, LP-7.5%, and LP-10%, respectively, the retention ratio remained at 134, 107, and 59 $g{\cdot}g^{-1}$ after 10 days. Consequently, the Lignin-PVA hydrogel proved to be a viable option for indoor pot culture and soil water conservation. It could swell swiftly and dehydrate gradually [114].

1.5.3 Controlled release of pesticides and fertilizers by hydrogels

Hydrogel-based pesticides act as release devices. They consist of a micro-capsuled or granular form of pesticide in a polymer network. Its main benefit is that the main active ingredient is released gradually or under control. This results in an extension of the application period, a decrease in dosage, and stabilization of the primary active ingredient against environmental degrading agents like light, air, humidity, and microorganisms. It lessens environmental contamination, phytotoxicity, aquatic toxicity, and irritation of human mucous membranes. The process of evaporation and leaching slows. It increases the number of target organisms and the ease of handling toxic materials.

Hydrogel is incorporated into fertilizers during preparation to lessen fertilizer leaching. As a result, the crop output increases while the need for fertilizer decreases. Fertilizers loaded into hydrogel release at a rate that is half of the fertilizer applied in water alone [79].

To create a pH-responsively controlled-release fertilizer, sodium alginate (SA), nano-silica aqueous dispersion, and HA hydrogel were used [75]. The sustained release of HA resulted from the swelling action of SA under alkaline conditions. This process confirmed that the environment suitable for the HA fertilizer is alkaline soil. The HA gel fertilizer contains many hydrophilic groups that retain the soil's moisture through hydrogen bonding. Thus, this fertilizer is capable of slowly releasing HA while retaining soil moisture.

Xianglin et al. successfully prepared a SH-modified super-absorbent resin (SAR), having high water absorbency and slow-release properties for fertilizer employing inverse suspension polymerization to study the release of SH in distilled water. The release of SH was observed to be faster in the initial 12 days. A similar release pattern was observed by Wang et al., where the maximum release became flat after 16 days [122]. The trend in the SH release can be attributed to the fact that the initial diffused SH out of the SAR was mostly filled physically, allowing it to diffuse into the water more quickly. It was followed by a decline in the release rate of SH, chemically bonded to acrylic acid and chitosan. This release could be attributed to a complex "swelling dissolution-diffusion" process from the SAR [123].

Another SH-based acrylic acid and acrylamide (PAA-AM) super-absorbent composite by Zhang et al. also enhanced water absorbency, salt resistance, and reswelling capacity. This improvement is due to the introduction of SH in the aqueous solution polymerization that culminated in the PAA-AM polymeric network. The release of SH's functionality was investigated experimentally by testing the water-retention capability of the composite in sand soil. These results indicated that the super-absorbent composite's efficiency of SH utilization and water-retention capability is greatly enhanced by introducing SH [124]. Wang et al. focused on a natural vegetable gum, i.e., Guar Gum-based super-absorbent employing partially neutralized acrylic acid and SH as other raw materials for improved water-absorption and water-retention capabilities [125].

Peng et al. created a lignin hydrogel-coated slow-release ammonium sulfate fertilizer. The outcomes show that the gel-coating layer efficiently limits water when it comes into contact with $(NH_4)_2SO_4$. Due to the concentration gradient between the hydrogel's interior and exterior, the hydrogel dissolved $(NH_4)_2SO_4$ when submerged in water and then exuded through the hydrogel along with water. It was discovered that the swelling ratio of $(NH_4)_2SO_4$ coated hydrogel directly correlated to the amount of $(NH_4)_2SO_4$ released in water. More $(NH_4)_2SO_4$ permeated the covering material due to hydrogels with higher swelling indices [126].

Ma et al. created iron fertilizer by polyacrylic acid grafted alkali lignin (ALS-G-P (AA)) via grafting amorphous alkali lignin with acrylic monomer, which boosted the cumulative release rate of iron. The effective release of ALS-G-P (AA) iron fertilizer was found to be 22 days. The study offered guidance for effectively applying iron fertilizer and alkali lignin in agricultural fields for controlled release application [127]. The same formulations were subsequently examined to add pesticides through an adsorption technique to various lignin-based polyacrylic acid (LBPAA) materials with variable lignin concentrations. This study investigated the possibility of using lignin with a hydrophobic backbone to alter the transfer properties of lignin-based polyacrylic acid. It also paved the way for the design of a new controlled-release formulation for pesticides. Model pesticides for this purpose were 1,1′-dimethyl-4,4′-bipyridinium dichloride (Paraquat), β-cyfluthrin (cyfluthrin), and cyhalofop-butyl. LBPAA's structure was relaxed by grafting, which made the gels sensitive to pH, temperature, and ionic strength changes. High loading and prolonged release of pesticides from LBPAA hydrogels suggest a potential use for controlled-release pesticides in the future [74].

A mixture of hydrogels and fertilizers can reduce the leaching and infiltration of nutrients in the soil by encapsulating them in the polymeric network of hydrogels before being released. Additionally, it lessens nutritional loss. For instance, L/KJ/SA hydrogel can lower N, P, and K soil nutrient loss. Also, the nutrient retention capacity is enhanced with an increase in L/KJ/SA hydrogel dose [99].

1.5.4 Effects of hydrogel on vegetative plant growth

As per the study by Mazloom et al., the maize plant was observed in drought stress subjected to the presence of lignin-based hydrogels in soil. Several observed parameters concluded many exciting results, such as the hydrogel treatments, which reduced the impact of drought stress on biomass synthesis and maize growth. Regardless of the soil water present, pot plants containing lignin hydrogel supplements grew higher than those in the no-hydrogel control. Montesano et al. reported a similar pattern of behavior in 2015 as well [121].

- 86% less proline (water stress biomarker) production in maize leaves
- The maize Phosphorous content was consistently greater in plants with lignin hydrogel than synthetic hydrogel.
- More leaf water content and 10% less electrolyte leakage

Lignin hydrogel buffered the soil pH and slightly increased the sodium concentration in the plant's shoots and the soil solution. However, this concentration was lower than synthetic hydrogel [121]. The use of lignosulfonate grafted sodium acrylate hydrogel for the soil treatment significantly improved the seed germination and average height of wheatgrass as well as served as a slow-release vehicle for urea [128].

Potassium humate-acrylic acid-acrylamide super-absorbent polymer is anticipated to have inherent advantages in supporting plant growth and improving the soil’s chemical and physical qualities since HA has remarkable properties in the field of agriculture and horticulture [108]. Agnihotri et al. synthesized a super-absorbent polymer using SH and studied its effect on corn and white gourd growth. Sets containing super-absorbent polymer showed good growth because the super-absorbent utilized the excess water, and the water was sufficient for forty-five days, making it clear that super-absorbent affects the plant growth of white gourd and corn [103].

Compared to control conditions, the poly (acrylic acid-co-acrylamide) $AlZnFe_2O_4$/potassium humate super-absorbent hydrogel nanocomposite (PHNC) amendment significantly delayed the wilting of seedling growth. The enhancement in soil moisture retention was made possible by adding PHNC to the soil. Wheat seed germination and seedling growth were significantly enhanced, and the wilting of seedlings was delayed by 6–9 days in the soil that had been supplemented with PHNC. These improvements led to better wheat plant establishment and growth. These findings suggested that soil type, moisture content, and nutrient availability all significantly influenced plant establishment and crop output [104].

Different potassium humate hydrogel application treatments on Egazy olive trees significantly increased the studied vegetative growth parameters, fruit physio-chemical properties, yield, and leaf mineral contents in the order: interaction of hydrogel + K-humate>hydrogel > K-humate. As the soil remained moist for a prolonged period of time, the hydrogel polymer improved the fruit's chemical qualities, improving microbial activity and nutrient availability as well as all fruit quality measures, such as fruit weight, length, breadth, and volume [105].

Chu et al. studied the effect of super-absorbent composite on the growth of corn. The plant in the pot began to wilt depending on the presence of PAA super-absorbents. However, even after 30 days, the plants in soil containing PAA/SH were still fresh [129]. The 3D network structure of the multifunctional super-absorbent composites created by Wang et al. with semicoke (SC) and HA allows for high water retention and favours slow-release performance. According to the study's soil column leaching experiment, the most significant quantity of HA released after nine days was 222.14 $mg{\cdot}L^{-1}$. Studying the growth performance of Qingan cabbage seedlings using PAA/HA/SC revealed that these seedlings exhibit greater growth vigour when PAA/HA/SC is added than when PAA/SC and a blank control group are used. In particular, fresh weight, root length, plant height, and dry weight of cabbage seedlings all benefited from applying the PAA/HA/SC. Compared to the blank control group, these metrics rose by 31.25, 31.07, 107.61, and 153.18%, respectively. The seedling height of Qingan cabbage still had a more significant growth capability when the HA-integrated hydrogel was added compared to PAA/SC and the blank control group [122].

The use of nature-based hydrogels in agriculture is listed in Table 1. 3.

Table 1. 3: A literature survey of HA and lignin-based hydrogels in agriculture

Agricultural applications of HA and Lignin based hydrogels					
S. No	Major components	Method of fabrication	Application	Swelling index	Ref.
1.	Sodium Alginate, Poly Acrylic Acid, and Sodium Humate	Free radical solution copolymerization.	Soil conditioner for water retention in sandy soil	906 ($g{\cdot}g^{-1}$)	[103]
2.	N-isopropylacrylamide and 2-acrylamide-2-methylpropanesulfonic acid, poly(ethylene glycol) dimethacrylate, humic acid	Free radical polymerization	excellent water absorption capacity and pH/temperature dual responsiveness.	31,388%	[73]
3.	Potassium humate (KHA), sodium alginate (SA), and acrylic acid (AA)	Graft copolymerization	favored crop growth and improved crop quality	621.46%	[130]
4.	Ammonium humate, Acrylic acid, NaOH, Ammonium persulfate, N,N' - Methylenebisacrylamide	Graft copolymerization	Moisture retention capacity, excellent water absorption capacity, Controlled-release device for pesticides	280.9 ($g{\cdot}g^{-1}$)	[131]
5.	Acrylic acid, Acrylamide, AlZnFe2O4, Potassium humate, diethylene glycol	Chemical cross-linking	Moisture retention and increased soil porosity, improved wheat seed germination and seedling growth	-	[104]
6.	Hydrogel, Potassium humate	Physical mixing	Improved yield, all vegetative growth parameters, leaf mineral content, and fruit physio-chemical properties	-	[105]
7.	Potassium humate, Sodium Alginate, $CaCl_2$	Freeze-drying	Controlled-release fertilizer, reduced soil bulk density and pH value, and increased total porosity and field water holding capacity.	-	[75]
8.	Starch and sodium	Graft	Excellent water	110 ($g{\cdot}g^{-1}$)	[106]

Agricultural applications of HA and Lignin based hydrogels					
S. No	**Major components**	**Method of fabrication**	**Application**	**Swelling index**	**Ref.**
	humate, Acrylic acid, NaOH, Ammonium persulfate, N,N' -Methylenebisacrylamide	copolymerization	absorption, swelling rate, and ability to reswell		
9.	Sodium humate, chitosan, acrylic acid, 2-acrylamide-2-methyl propyl sulfonic acid	Inverse suspension polymerization	Slow-release fertilizer of sodium humate	1097 ($g{\cdot}g^{-1}$)	[123]
10.	Sodium humate, acrylic acid, Ammonium persulfate, N,N' -Methylenebisacrylamide	Aqueous solution polymerization	Enhanced salt tolerance, the ability for swelling, and slow-release sodium humate fertilizer	1184 ($g{\cdot}g^{-1}$)	[124]
11.	Semicoke, Polyacrylic acid, Humic acid	Free radical polymerization	Enhanced water absorbency, slow-release fertilizer, and increased plant growth.	824 ($g{\cdot}g^{-1}$)	[122]
12.	Acrylic acid, acrylamide, organomontmorillonite, sodium humate	Graft copolymerization	Sand soil's capacity for retaining water while being salt-resistant and water-absorbent	591 ($g{\cdot}g^{-1}$)	[107]
13.	Acrylamide, acrylic acid, and potassium humate of leonardite	Free radical polymerization	Super-absorbent polymer is believed to provide inherent benefits for promoting plant development	756 ($g{\cdot}g^{-1}$)	[108]
14.	Attapulgite, poly(acrylic acid) sodium humate	Graft copolymerization	Good water retention, slow-release property of SH.	583 ($g{\cdot}g^{-1}$)	[109]
15.	Sodium humate micropowder, poly(acrylic acid)	Graft copolymerization	Agricultural water management tools for desert and drought-prone regions	684 ($g{\cdot}g^{-1}$)	[129]
16.	Sodium humate, guar gum, and partially neutralized acrylic acid	Solution polymerization	Fertilizer as well as an effective water-saving material for agriculture	532 ($g{\cdot}g^{-1}$)	[125]

Agricultural applications of HA and Lignin based hydrogels					
S. No	**Major components**	**Method of fabrication**	**Application**	**Swelling index**	**Ref.**
17.	Alkali lignin, polyacrylic acid, iron fertilizer	Graft copolymerization,	Efficient and slow-release iron fertilizer	1017 ($g{\cdot}g^{-1}$)	[127]
18.	Alkali lignin, polyacrylic acid, pesticide	Graft copolymerization,	High loading and sustained release of pesticides	465 ($g{\cdot}g^{-1}$)	[74]
19.	Sodium lignosulfonate, sodium alginate, Konjac flour	Chemical cross-linking	Improved water retention and photosynthetic capability of plants under drought stress, enhanced nutrition retention	41.13 ($g{\cdot}g^{-1}$)	[99]
20.	Lignin alkali, poly(ethylene glycol) diglycidyl ether, NaOH	Chemical cross-linking	Environmentally friendly additive to help dry, saline soils retain water	34 ($g{\cdot}g^{-1}$)	[110]
21.	Lignin alkali, poly(ethylene glycol) diglycidyl ether, NaOH	Graft copolymerization	Buffered the soil pH, slightly increased Na, P, the leaf water concentration in plant's shoots, and soil solution	-	[121]
22.	Sodium lignosulphonate, acrylic acid,	Chemical cross-linking	Reduced water evaporation, improved seed germination, slow release of urea	560 ($g{\cdot}g^{-1}$)	[128]
23.	Red liquor, Acrylic acid, APS, N,N′-Methylenebisacrylamide	Chemical cross-linking	High swelling and water retention in agriculture	280 ($g{\cdot}g^{-1}$)	[102]
24.	Lignin, PVA, NaOH	One pot synthesis	Agricultural practices such as seed planting and soil water retention	456 ($g{\cdot}g^{-1}$)	[114]
25.	Lignin and poly (vinyl alcohol)	Physical cross-linking- freeze-thaw	Improved water absorption	890%	[119]
26.	Nano-ferrous sulfide, lignin	Chemical cross-linking	Restoration of soil microbial community	-	[132]

Agricultural applications of HA and Lignin based hydrogels					
S. No	**Major components**	**Method of fabrication**	**Application**	**Swelling index**	**Ref.**
27.	Sodium lignosulphonate, Acrylic acid, NaOH, Ammonium persulfate, N,N' - Methylenebisacrylamide	Graft copolymerization	Moisture retention capacity, excellent water absorption capacity, Controlled-release device for pesticides	280.9 ($g{\cdot}g^{-1}$)	[131]

1.5.5 Bio degradation

Any soil additive used in agricultural soils shouldn't be toxic to seeds or plants. Since degraded products will be released into the soil, this can further cause soil pollution and harm the health of living beings through biological enrichment processes [133–135].

The biodegradability of lignin-based hydrogels relies on both the crosslinking density and the phenolics content within the hydrogels. A higher degree of crosslinking results in a more compact pore structure of the gel, thus limiting the access of ligninolytic fungi and actinomycetes. Consequently, hydrogels with strong crosslinking are less susceptible to microbial degradation than those with lower degrees of crosslinking.[136]

When placed in a solution with soil microbial inoculum, lignin-based PEGDGE hydrogel weighed 6.5% less after 40 days of incubation, demonstrating the microbial breakdown of the polymers [110]. According to Yamamoto et al., after 11 months, the fungus *Flammulinavelutipes* destroyed lignin gels created from lignin-phenol-resorcinol resin that had been dissolved in methanol [137].

Burkhard et al. investigated the rate at which hydrogel composed only of polyacrylate degraded. After 24 weeks of soil burial in loamy sand and loam, it was discovered to be just 0.45% and 0.82%, respectively [133].

The L/KJ/SA hydrogel comprises three natural biopolymers [99]. Long-time burial of L/KJ/SA hydrogels showed destruction in their network by microorganisms or water erosion. A comparison of acrylamide-based and Lignin/Konjac flour/Sodium Alginate hydrogel reported that the former degraded only 2% in the 120 days, while the latter showed a degradation of 6% of the weight in the first 60 days and 14% in the next 60 days. The degradation of organic hydrogel components increased the soil's absorption and desorption of oxygen [99].

A super-absorbent resin treated with SH reportedly deteriorated by 31.9% after 100 days, according to Xianglin et al. Under the effect of soil microbes and enzymes, the molecular chain of SAR ruptured, indicating strong soil degradation performance that was principally made possible by the degradable natural components [123].

1.6 Applications of hydrogels in the environment

The growing industrialization incorporated toxic metals into natural systems. Also, the practices, including burning fossil fuels, atmospheric deposition, metal mining, smelting, refining, and applying sewage sludge and industrial byproducts to the soil, seriously threaten the environment and human health. Heavy metals can accumulate in soils and harm the ecological community. Such metals can accumulate in the food chain and leak out of soils to contaminate ground water sources [138, 139]. Similarly, from a toxicological and aesthetic point of view, the movement of organic dyes in nature is a cause for concern [140]. Therefore, several researchers have studied soil and water pollutants' sorption, as summarized in Table 1. 4.

1.6.1 Adsorption of soil and water pollutants

Electrodialysis, chemical deposition, adsorption, membrane filtration, and ion exchange are a few techniques to remove metals from water. However, membrane filtration has poor selectivity, making materials susceptible to bacterial contamination. It is challenging to regenerate and is quickly oxidized, degraded, mechanically ruptured, and employed in ion exchange. Electrodialysis and phytoremediation require a lot of labour and are expensive for their selectivity. Chemical precipitation often results in precipitation that will break down and pollute the environment. Adsorption has been used extensively to remove metals from wastewater due to its low cost, ease of use, and high removal effectiveness compared to other approaches [139].

Metal ions and soil exhibit a complex formation behaviour in a natural system. The complexation of metal ions with dissolved organic materials can happen via one of three methods: a) the metal ion solubilization onto solid particles, b) the metal ion immobilization in the solid phase, and c) the metal ion complexation with dissolved organic matter. The distribution coefficient, often referred to as the partitioning between the soil and solution phase, relates to the mobility of metal ions in soils [141, 142].

Hydrogels made of lignin and HA have reportedly been used in water treatment to remove various pollutants [79, 102].

The adsorption of HAs on mineral particles is significantly influenced by the presence of divalent metal ions in aqueous solutions. In the presence of heavy metals, HAs may coagulate as a result of metal interactions with humic functional groups [143, 144]. It is widely acknowledged that the mobility of ionic compounds in soils and waterways is affected by their interactions with negatively charged (precipitated or dissolved) HAs. The fate of the ions in HA cannot be predicted or explained because of the wide range of structural complexity [140].

Sedláček et al. investigated the absorption behavior of Methylene blue and Rhodamine 6G by using agarose and HA-based hydrogel. At pH 11 and temperature 30°C, the diffusion coefficient was found to be 9.64 x 10^{10} $m^2 \cdot s^{-1}$ and 6.90 x 10^{10} $m^2 \cdot s^{-1}$ [145]. Fernandes et al. investigated the removal of Methylene blue (MB) from aqueous solutions at varying initial MB concentrations and at three different temperatures using peat, another humic-rich substance. The sorption process quickly reached equilibrium after 4 h and 30 min [146].

Lignin is a high-ideal material for this application because of its natural abundance and polyphenol-type structure. By interacting with aromatic contaminants, the phenolic rings found in lignin derivatives could improve the retention of these organic pollutants. Additionally, the pH sensitivity of lignin monomers may facilitate the hydrogel uptake of contaminants [147]. Lignin hydrogel can function as an amphoteric absorbent with the potential to absorb ions and toxic dyes, according to a paper by Thakur et al [148]. According to specific reviews, lignin and its derivatives effectively absorb heavy metals. Inorganic ions such Ni(II), Zn(II), As(II), Cr(III), Cr(VI), Co(II), Cd(II), Pb(II), Hg(II) and Cu(II) were successfully absorbed, according to these reviews [8, 78].

Table 1.4: A literature survey of nature-based hydrogels for absorbing environmental toxic substances

Environmental applications of HA and Lignin based hydrogels						
S. No	**Absorbent**	**Absorbed substance**	**Adsorption capacity/removal efficiency (%) ($mg{\cdot}g^{-1}$)**	**pH**	**Temperature (°C)**	**Ref.**
1.	Sodium humate/polyacrylamide/clay	Methylene blue	800	-	37	[149]
2.	Sodium alginate/sodium humate@Polyacrylamide hydrogel	Cu^{2+}	~134.65	3–6	20	[150]
3.	Sodium-humate /polyacrylamide double network hydrogel	Pb^{2+} Cu^{2+}	93.4 98.79	2-6	29.85	[151]
4.	Montmorillonite/humic acid/polyvinyl alcohol@polypyrrole hydrogel	Cr^{6+}	106.29	2-10	44.85	[152]
5.	Starch-humic acid composite	Pb^{2+} Methylene blue	50 90	4-6 4-9	24.8	[153]
6.	Sodium-humate, polyacrylamide	Pb^{2+} Cu^{2+}	93.4 98.79	-	-	[151]
7.	Humic acid/starch composite microspheres	Cr^{3+} Pb^{2+} Cu^{2+}	211.12 154.03 165.49	5	34.8	[139]
8.	Humic acid particles	Phenol	180	6	40	[142]
9.	Humic acid, modified titanium dioxide (TiO_2) nanoparticles	Methylene blue	1490	-	-	[154]
10.	Humic substance double network hydrogel	Pb^{2+} Cu^{2+} Cd^{2+}	360.50 151.00 412.76	5	24.8	[155]
11.	Alginate, humic acid, and iron aminoclay	Sr^{2+}	45.65	7	RT	[156]
12.	Lignosulfonate-g-acrylic acid hydrogel	Methylene blue	2013 93.45	3-8	30	[69] [157]
13.	Alkali lignin/montmorillonite	Toluene	90.14	6	25	[158]
14.	Lignin sulfonate-g-poly (acrylic acid-r-acrylamide) copolymer adsorbent	Malachite green	97	3-7	15-35	[70]

Environmental applications of HA and Lignin based hydrogels

S. No	Absorbent	Absorbed substance	Adsorption capacity/removal efficiency (%) ($mg{\cdot}g^{-1}$)	pH	Temperature (°C)	Ref.
15.	Sulfonate lignin-based hydrogels	Methylene blue	495	2-8.3	30	[159]
16.	Kraft lignin-N-isopropyl acrylamide hydrogel	Methylene blue	30	10	20	[160]
17.	Lignin, sodium alginate	Methylene blue	388.8	-	-	[161]
18.	Chitosan/sodium lignosulphonate	Co^{2+} Cu^{2+}	385 290	6	-	[162]
19.	cellulose nanofibers/carbon dots/alkali lignin	Cr^{6+}	599.9	-	-	[163]
20.	Alkaline lignin	Zn^{2+}	0.073	5	30	[147]
21.	Kraft lignin (Eucalyptus)	Cu^{2+} Cd^{2+}	87.05 137.14	4.5	25	[147]
22.	Alkaline lignin (wood)	Pb^{2+} Cd^{2+}	9.0 7.5	5	17	[147]
23.	Nano-ferrous sulfide@lignin hydrogel	Cd^{2+}	37.6 ; 34.5	-	-	[132]
24.	Sodium lignosulfonate, methacrylate anhydride, triethylamine	Cu^{2+}, CrO_4^{2-}, Co^{2+}	-	1-14	59.5	[164]
25.	Ferrous sulfide nanoparticle@lignin hydrogel composites	Cd^{2+}	22.4-49.6%	5.15, 5.34	-	[165]
26.	Lignin, montmorillonite	Cu^{2+}	1.17 mmol/g	1-5	-	[166]
27.	Xanthan gum, Sodium Lignosulfonate	Methylene Blue	91	-	25	[157]

1.7. Applications of nature-based hydrogels in Energy storage

Researchers are looking into renewable energy sources and developing novel energy storage technologies in response to the global energy issue brought on by rising fossil fuel usage [167]. Natural biopolymer-based gel made from renewable resources boosts the sustainability of finished products while reducing dependency on fossil fuels for energy storage [168]. Additionally, the growing use of electric vehicles, wearable electronics, and portable electronic devices is fueling demand for safe, low-cost, and lightweight energy storage devices with strong mechanical characteristics and superior electrochemical performance to further increase energy density and longevity compared to conventional devices [169].

A primary application for hydrogels in energy-storage devices is as an ionically conducting electrolyte. While the ions must be conveyed in substrate or solutions, the polymer networks can be employed as a solid, liquid, or swollen substrate. The disadvantages of the constrained contact area between the solid-state electrolyte and the electrode material are solved by hydrogel electrolytes. It also possesses the benefits of liquid electrolytes because of ion mobility [170]. Commercial separators (such as polyethylene (PE) or polypropylene (PP)) had poor ionic conductivity before the development of hydrogel-based electrolytes [171]. Thus, a variety of energy storage technologies, including supercapacitors and batteries, have used hydrogel electrolytes because of their high ionic conductivity and dimensional stability [172–174].

Lignin and HA might be viewed as perfect, sustainable substitutes for fossil fuels. Natural-source HA displays the fundamental traits of materials that resemble graphene oxide in shape, carbon-oxygen ratio, and structure [175]. HA is a naturally occurring polymer abundant in functional groups, including carboxyl, hydroxyl, and carbonyl. It also has strong redox and ionic adsorption characteristics [176]. According to recent research, HA may serve as an anode for lithium and sodium-ion batteries [177]. A graphene oxide-like substance known as "graphenol" was produced when HA was treated in reducing circumstances with pressurized hydrogen at low temperatures (150–250°C), according to groundbreaking research by Beall and colleagues [175]. To the best of our knowledge, no information regarding HA-based hydrogel as an electrode for energy storage applications is available in the open literature. However, an ample amount of data is present that proves its usefulness in this field [175, 178, 187, 188, 179–186].

Lignin is also a viable starting substrate for producing carbonaceous materials for energy storage [189]. As an aromatic polymer, lignin contains a significant amount of carbonyls and phenolic or phenolate structures, enabling it for strong crosslinking. Because of these unique physiochemical characteristics, lignin is viewed as a prospective contender for creating high-performance electrodes and electrolytes [190]. Several kinds of research have been carried out to utilize lignin as a feedstock for energy storage applications in the past half-decade, such as mesoporous carbon, fibre matrix, and flexible thin films for mechanical energy harvesters, photovoltaic devices, catalytic components, and energy storage systems [191].

Research has focused on creating high-performance flexible supercapacitors using hydrogel electrolytes made of biopolymers to fulfil the above practical requirements. In addition to having high energy storage capacity, multifunctional supercapacitors with hydrogel electrolytes made of this biopolymer have also been produced. A novel three-dimensional graphene hydrogel was created by Cui et al. using nitrogen-doped carbon dots made of lignin. Furthermore, they said that the cycle stability (cycle life after 5000 cycles is 92.3%) and rate performance of the all-lignin-based supercapacitor built with a lignin hydrogel as the electrolyte is excellent [192].

A biomass-based flexible supercapacitor with a pressure-sensitive lignin-based hydrogel electrode and cellulose/Li_2SO_4 hydrogel electrolyte was also synthesized [193]. The created flexible biomass-based supercapacitor demonstrated excellent rate capability, superior energy density (17.1 Wh·kg^{-1}), and high specific capacitance (292 F·g^{-1}).

Wang et al. prepared a multifunctional Ca^{2+}-tannic acid@ sulfonated lignin-polyacrylamide hydrogel via polyacrylamide system and Ca^{2+}-TA@SL composites. Here, Ca^{2+}-TA@SL composite was synthesized by doping tannic acid with sulfonated lignin, followed by the subsequent adsorption of Ca^{2+}. The addition of Ca^{2+}-TA@SL composites gave the hydrogel better antioxidant and antibacterial characteristics as well as superior conductivity, adhesion, and UV resistance [194]. Lignin hydrogels can also serve in the synthesis of a textile supercapacitor. For instance, the latest research combines polyaniline@carbon cloth as a flexible electrode and lignin hydrogel as a semi-solid electrolyte to form a flexible textile supercapacitor [63].

In the past decade, several kinds of research have been carried out to utilize lignin as a feedstock for energy storage applications. These researches have been summarized in Table 1. 5.

Table 1.5: Literature survey of nature-based hydrogels for energy storage application

Energy Storage applications of HA and Lignin based hydrogels					
S. No	**Major components**	**Ionic conductivity**	**Potential/ Specific Capacitance (SC)**	**Characteristics**	**Ref.**
1.	Lignin-H_2SO_4 hydrogel	80 mS cm^{-1}	Polyaniline//polyaniline SC (0.8 V)	Excellent shape recovery, mechanical strength, and high ionic conductivity	[195]
2.	Lignin, cellulose/Li_2SO_4 based supercapacitor	-	SC-292 F g^{-1}	High specific capacitance, superior energy density, and excellent rate capability	[193]
3.	Polyaniline lignosulfonate hydrogel	0.17 S cm^{-1}	SC- 505 and 558 Mf cm^{-2}	High capacitance retention rate	[196]
4.	Li_2SO_4-based neutral hydrogel electrolyte with	16 mS cm^{-1}	138.4 F g^{-1}	Ultra-high porosity	[197]

Energy Storage applications of HA and Lignin based hydrogels

S. No	Major components	Ionic conductivity	Potential/ Specific Capacitance (SC)	Characteristics	Ref.
	lignocellulose				
5.	Lignosulfonate, Al^{3+}, poly acrylic acid hydrogel	7.38 S m^{-1}	150.5 mV, SC- 245.4 F·g^{-1}	High capacitance retention rate	[198]
6.	Lignosulfonate poly (ethylene glycol) diglycidyl ether hydrogel	5.4 S m^{-1}	181 mV, SC- 236.9 F·g^{-1}	High capacitance retention rate	[199]
7.	Lignosulfonate/single-walled carbon nanotube hydrogels as electrodes, cellulose hydrogels	0.08 S cm^{-1}	SC- 292 F g^{-1}	Excellent flexibility, stability, and electrochemical performance	[200]
8.	Lignosulfonate/polypyrrole (Lig/PPy) hydrogel all-in-wood supercapacitor	-	SC- 1062 mF cm^{-2}	Good electrochemical performance even under high pressure	[201]
9.	Ca^{2+}-tannic acid@ sulfonated lignin-polyacrylamide hydrogel	0.91 S m^{-1}	-	Excellent conductivity, adhesion, UV resistance, antibacterial and antioxidant properties	[194]
10.	Lignin/polyacrylonitrile nanofiber electrode, hydrogel	10.35 mS cm^{-1}	129.23 F g^{-1}	High ionic conductivity and mechanical integrity, outstanding charge storage capability	[202]
11.	Ag-lignin nanoparticles, polyacrylamide hydrogel matrix	84.71 mS cm^{-1}	298.6 F g^{-1}	Adhesive and tough hydrogel matrix, high specific capacitance	[203]
12.	Lignin, gelatin	0.06 S cm^{-1}	145.14F/g	High ionic conductivity, robust adhesiveness and anti-freezing properties, flexible	[204]

1.8 Research Gap

The literature survey encompasses different polyphenolic biopolymers (Humic acid, lignin and lignite) exploring advancement in their hydrogels and applications. Nonetheless there's a notable gap in research regarding the potential application of humic acid, lignin and lignite based hydrogels in fields like agriculture and environment. This research aims to address this gap by creating hydrogels using different kinds of natural polymers, such as lignin, humic acid and and lignite, as a beginning material and explores their potential agricultural and environment applications.

1.9 Aim and Research Objectives

The aim of this research is “Synthesis and application of natural polymer based hydrogels”. To achieve this objective, the specific objectives are as follows:

- Synthesis of natural polymer based hydrogels.
- Characterization of hydrogels (qualitative and quantitative)

  Morphological

  Rheological

  Thermal

  Spectral
- Application of synthesized hydrogels

Overview of the research work

The thesis has been summarized into seven chapters which are being described briefly as below. The **chapter 1** describes natural polymers - humic acid, lignin and lignite. It presents an overview of the classification of the hydrogels based on source, crosslinking, composition, structure, physical properties, ionic charges, response and degradability. It also includes the applications of these polymer-based hydrogels in multiple fields such as biomedical, environment, agricultural and food industry.

Chapter 2 aims to synthesize lignosulfonate grafted sodium acrylate hydrogel (LS-g-SAH) and investigate its application in urea release behavior. The hydrogel has been characterized by different techniques. The release kinetics have been analyzed by using a UV-Visible spectrophotometer. The optimized composition of lignosulfonate, KPS, and N, N’-MBA has shown the highest water absorbency of 560 $g.g^{-1}$ in distilled water. The equilibrium swollen LS-g-SAH 12 hydrogel has slowly released 60% of loaded urea in 24 h and followed first-order release kinetics. Soil treatment with hydrogel has shown a significant effect in reducing the water evaporation rate. It also improved the seed germination and average height of wheatgrass. The synthesized LS-g-SAH is, thus, expected to have potential applications in modern sustainable agriculture.

The **chapter 3** introduces humic acid-based poly(sodium acrylate) hydrogel for slow release of pesticides, having dinotefuran as a model pesticide. The synthesis of humic acid grafted poly(sodium acrylate) hydrogel (HA-g-SAH) and control (Ctrl) through the graft co-polymerization method is detailed, with comprehensive characterization using ^{13}C NMR, FT-IR, XRD, SEM, and TGA techniques. Additionally, the release kinetics of dinotefuran are investigated via UV-Vis spectrophotometry to elucidate the controlled release. This study underscores the potential of humic acid-based hydrogels as versatile platforms for sustainable agricultural practices, offering enhanced environmental performance in pesticide delivery mechanisms. Incorporating humic acid improves soil's water retention capability and offers potential as a nitrogen fertilizer carrier, addressing critical challenges in sustainable crop production. Through a comprehensive evaluation, this study demonstrates the viability of humic acid-based hydrogel as a cost-effective and eco-friendly solution for advancing agricultural sustainability.

Chapter 4 addresses the UV degradation of pesticides and introduces dinotefuran-loaded, lignite-based poly(sodium acrylate) hydrogel (Lt-g-SAH) as a protective shield against UV radiation for dinotefuran. The synthesis of Lt-g-SAH and control hydrogel (Ctrl) through the graft co-polymerization method is detailed, with comprehensive characterization using ^{13}C CPMAS NMR, FT-IR, XRD, SEM, and TGA techniques. The release kinetics of dinotefuran are investigated via UV-Vis spectrophotometry to elucidate the controlled release. This study highlights the potential of lignite-based hydrogels as versatile platforms in pesticide protection, where dinotefuran was found to have a marginal decrease of 1.58% in Lt-g-SAH compared to 28.11% decrease of ctrl hydrogel and delivery mechanisms with the Lt-g-SAH demonstrating 62.46% pesticide release in 39 h in contrast to 56.22% release from ctrl in 33 h. The pesticide loading increased from 64.36 % in Ctrl to 70.12 % in Lt-g-SAH. Incorporating lignite in Lt-g-SAH also improves the soil's water retention capacity and offers potential as a nitrogen fertilizer carrier. Through a comprehensive evaluation, this study demonstrates the viability of lignite-based hydrogel as a cost-effective and eco-friendly solution for safeguarding pesticides for agricultural sustainability.

In **Chapter 5**, the novel use of natural polymers like humic acid, lignin, and lignite-based hydrogels has been explored for the formulation of pesticides and fertilizers that would reduce the residues in soil and runoff water that pose a threat to human health and the environment. Here, humic acid, lignin, and lignite grafted were analyzed for the ex-situ loading and release of thiamethoxam, a common pesticide. Various characterization techniques were employed, including ^{13}C-NMR, FT-IR, TGA, SEM, XRD and rheology. The release kinetics of thiamethoxam in water from the developed formulations were analyzed using the Korsmeyer-Peppas model and the Weibull model. Humic acid and lignin-based hydrogels exhibited a long-sustained release for 49 h, followed by lignite-based hydrogels (38 h). According to ANOVA results, the change of biopolymer proved to be an effective factor in reducing the water evaporation rate, which decreased from 99 to 72.85% in the soil amended with synthesized hydrogels. Thus, the novel formulations of humic acid, lignin, and lignite exhibit potential as slow-release vehicles for pesticides and fertilizers. This study provides valuable insights for the research community, addressing the need to develop effective strategies for mitigating pesticide residues in soil and water bodies.

Chapter 6 investigates the application of hydrogels incorporating natural polymers – humic acid, lignin, and lignite – to adsorb methylene blue (MB) dye from aqueous solutions. The hydrogels were synthesized via free radical polymerization and characterized using FT-IR, ^{13}C-NMR, SEM, TGA, and XRD. The synthesized hydrogels demonstrated exceptional swelling capabilities. The influence of various parameters, including adsorbent dosage (0.1-0.4 g), temperature (293.15-323.15 K), and initial dye concentration (5-20 $mg{\cdot}L^{-1}$) on MB removal efficiency was systematically evaluated using the Taguchi method. Under optimized conditions, HA-g-SAH achieved a maximum removal efficiency of 93.7±1.1% at 323.15 K, significantly outperforming LS-g-SAH (92.4±1.3%), Lt-g-SAH (82.4±1.4%), and the control (ctrl) hydrogel (67.9±0.9%). According to ANOVA results, the change of biopolymer proved to be an effective factor in the improved dye removal efficiency of hydrogels. Taking into account the enhanced dye removal efficiency of the hydrogels, the thermodynamic parameters ($\Delta G°$, $\Delta H°$, and $\Delta S°$) were evaluated to clarify the adsorption mechanisms under varying temperatures. The equilibrium adsorption data were interpreted using both the Langmuir and Freundlich isotherm models. Overall, the findings highlight the promise of natural polymer-derived hydrogels as sustainable and highly effective adsorbents for eliminating dyes from wastewater. Lastly, the

chapter 7 highlights the significance of developing hydrogels from natural polymers such as humic acid, lignin, and lignite as sustainable, biodegradable, and affordable alternatives to fossil fuel–based polymers. These hydrogels exhibit great potential in diverse applications, including controlled pesticide release, enhanced soil water retention, dye pollution treatment, and livestock nutrition, thereby supporting agricultural sustainability and food security. Furthermore, their prospective use in crop protection products, textile dye dispersants, and even energy storage systems underscores their versatility and relevance to multiple industries. By addressing environmental concerns, promoting cleaner technologies, and improving rural livelihoods, these biopolymer-based hydrogels offer a pathway toward both scientific innovation and societal well-being, positioning them as promising materials for a sustainable future.

CHAPTER-2

SYNTHESIS, CHARACTERIZATION AND APPLICATION OF LIGNOSULPHONATE-g-POLY (SODIUM ACRYLATE) HYDROGEL.

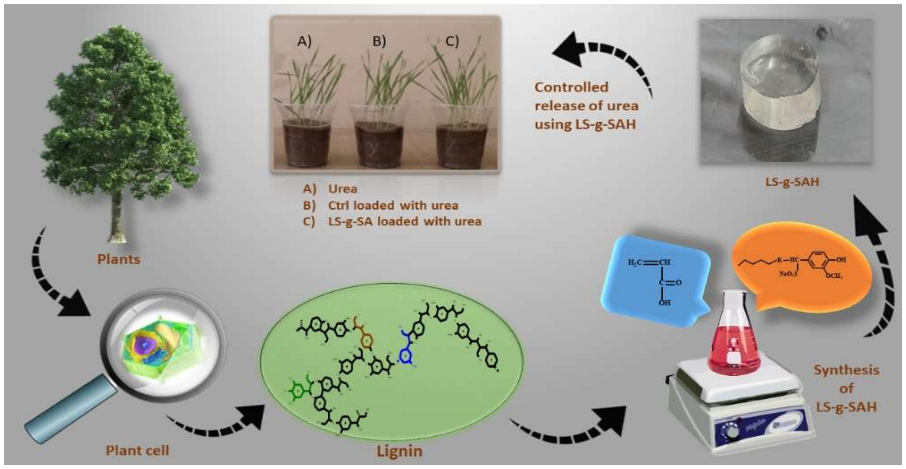
A)
B)
C)
A) Urea
B) Ctrl loaded with urea
C) LS-g-SA loaded with urea
Controlled release of urea using LS-g-SAH
LS-g-SAH
Plants
H₂C=CH
C=O
OH
R—HC
NaO₃S
OH
OCH₃
Synthesis of LS-g-SAH
Plant cell
Lignin

2.1 Introduction

Natural polymers-based hydrogels are of great interest to research community owing to their inherent characters of environment friendliness and biodegradability. Current work aims to synthesize lignosulfonate grafted sodium acrylate hydrogel (LS-g-SAH) and investigate its application in urea release behavior. The hydrogel was characterized by solid-state ^{13}C CP-MAS NMR, SEM, TGA, XRD, and Rheology. The release kinetics of was analyzed by using a UV-Visible spectrophotometer. The optimized composition of lignosulfonate, KPS, and N, N'-MBA showed the highest water absorbency of 560 $g{\cdot}g^{-1}$ in distilled water. The equilibrium swollen LS-g-SAH 12 hydrogel slowly released 60% of loaded urea in 24 hours and followed first-order release kinetics. Soil treatment with hydrogel has shown a significant effect in reducing the water evaporation rate. It also improved the seed germination and average height of wheatgrass. The synthesized LS-g-SAH is, thus, expected to have potential application in modern sustainable agriculture.

As the world's seventh largest country, India has approximately 157 million hectares of arable land, accounting for 53.2% of the total area. The land is continuously degraded by different means, thus reducing the total production potential to less than 20 percent. Therefore immediate attention is required in upgrading soil fertility, which caused less productivity due to low water retention capability, poor structure, high infiltration rate, low clay and humus content, and loss of agrochemicals through deep percolation or leaching [205].

A super absorbent crosslinked polymer known as hydrogel is a potential material to solve soil-fertility problems. Hydrogel is a 3D network structure composed of chemically or physically crosslinked polymers. It can hold a massive volume of water due to its swollen state's surface tension and capillary forces. The rate of water absorption by hydrogel is affected by the functional group and the density of the crosslinking network [206]. Natural biodegradable polymers should be used to develop economical agricultural water-absorbent materials. Nowadays, researchers are paying great attention to lignocellulosic polymeric material as a favorable, sustainable, and large-scale asset to be used as a chemical component in various syntheses. In this regard, lignin is a renewable feedstock readily available in an adequate amounts [207]. Lignin accounts for 16-33% of the biomass and is predominantly present in the secondary cell walls of terrestrial plants [69]. Lignin comprises three types of phenylpropane monomers known as monolignols. These monolignols are a) coniferyl alcohol, b) sinapyl alcohol, and c) p-coumaryl alcohol [208]. This inexpensive waste of pulp manufacturing process is the only scalable renewable raw material that consists of aromatic moieties [147]. It is also easily accessible, affordable, and underutilized today [209].

Also, a lignin hydrogel based study by Bukhard et al. showed that the synthesized hydrogels could degrade up to 14% in just 60 days compared with acrylamide-based hydrogels, indicating degradation of just 2% in 120 days [133]. Lignin has antimicrobial, antioxidant, and stabilizer properties [148]. It has also been used for metal elimination. For example, graphene hydrogel based on lignosulfonate, manufactured in a column system, rapidly eliminated $Pb^{2+}$from the aqueous solution. A free-standing lignin-based film with superior electrochemical performance was manufactured by using poly(N-vinyl imidazole)-co-poly(poly(ethylene glycol) methyl ether methacrylate) [147]. However, there has been little exploration of using lignin-based hydrogel for controlled-release applications in agriculture. Song et al. in 2020 synthesized novel lignin, konjac flour, and sodium alginate hydrogels, which proved to be efficient when tested for the growth of tobacco plants in drought-like conditions. They exhibited high water retention capacity and reduced soil nutrient leaching [99]. Urea is one of the most commonly used nitrogen fertilizers globally. But due to its leaching losses, its use efficiency is relatively low (on average 30-35%). It is a waste of resources that also results in the pollution of the environment. Slow-release urea through hydrogel is an effective way to address this issue [210]. In this work, Lignosulfonate grafted poly (sodium acrylate) hydrogels have been synthesized and used for agricultural applications. The sample LS-g-SAH 12 was selected for the detailed investigation, including i) solid-state ^{13}C CP-MAS NMR, Scanning electron microscopy (SEM), Fourier-transform infrared (FTIR) spectroscopy, X-ray diffraction (XRD), Thermo-gravimetric analysis (TGA) and Rheology, and ii) urea release kinetics. Additionally, a control with a composition comparable to LS-g-SAH 12 but lacking lignosulfonate was compared to the synthesized hydrogels.

2.2 Experimental

2.2.1 Materials

Lignosulfonic acid sodium salt (LS) (M wt. ~52,000) was purchased from Sigma Aldrich. Acrylic acid (AA) and N'N-methylenebisacrylamide (N, N'-MBA) were bought from CDH Pvt Ltd. Potassium persulfate (KPS) were purchased from SD fine –chem Ltd. Urea and NaOH were purchased from CDH Pvt Ltd, and Qualikems Fine Chem Pvt. Ltd. respectively. All necessary water-based polymerization solutions were prepared using distilled water.

2.2.2 Synthesis of LS-g-SAH

The free radical co-polymerization technique is used to synthesize LS-g-SAH, where KPS and NN-MBA were utilized as an initiator and crosslinker, respectively. At room temperature, NaOH was added to neutralize acrylic acid. The desired amount of LS, AA, NaOH, N,N'-MBA, and KPS was stirred for 2 hours continuously. The reaction product was heated in a water bath preset at 60°C for two hours. After co-polymerization, the hydrogel was cut into thin slices and immersed in distilled water for 24 hours to remove the unreacted chemicals, as shown in Figure 1. 1. The hydrogel was then oven-dried at 50°C until constant weight [211]. Table 2. 1 summarizes the different formulations of synthesized hydrogels.

Table 2.1: Various compositions used in synthesis with their swelling index.

Formulation	LS (g)	NaOH (mol/L)	AAA (mL)	KPS (g)	NN-MBA (g)	Swelling index ($g \cdot g^{-1}$)	Gel %
LS-g-SAH 1	0.1	8.07	7.1	0.1	0.05	190.3	62.11
LS-g-SAH 2	0.1	8.07	7.1	0.1	0.07	172.82	63.38
LS-g-SAH 3	0.1	8.07	7.1	0.1	0.1	111.6	73.26
LS-g-SAH 4	0.1	8.07	7.1	0.1	0.12	60.22	77.59
LS-g-SAH 5	0.1	8.07	7.1	0.1	0.15	39.68	92.16
LS-g-SAH 7	0.1	8.07	7.1	0.04	0.08	89.31	85.31
LS-g-SAH 8	0.1	8.07	7.1	0.05	0.08	172.92	92.73
LS-g-SAH 9	0.1	8.07	7.1	0.08	0.08	252.83	96.90
LS-g-SAH 10	0.1	8.07	7.1	0.12	0.08	120.92	92.50
LS-g-SAH 11	0.1	8.07	7.1	0.14	0.05	560.24	95.28
LS-g-SAH 12	0.2	8.07	7.1	0.14	0.05	397.22	91.20
LS-g-SAH 13	0.3	8.07	7.1	0.14	0.05	336.35	85.99
LS-g-SAH 14	0.4	8.07	7.1	0.14	0.05	320.63	75.33
LS-g-SAH 15	0.05	8.07	7.1	0.14	0.05	248.32	72.04
LS-g-SAH 16	0.08	8.07	7.1	0.14	0.05	461	89.36

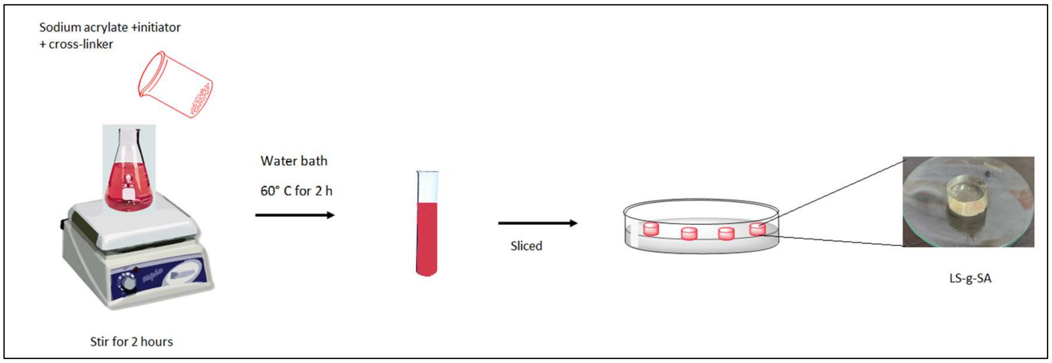

Figure 2. 1: Visual representation of the synthesis of LS-g-SAH.

2.2.3 Characterization of LS-g-SAH

The FTIR spectra in the range of 4000 to 650 cm^{-1} were recorded using Perkin Elmer 2000 FT-IR spectrometer. The solid-state ^{13}C-CPMAS NMR analysis of samples was done on a Bruker Ascend-400 spectrometer operating at 400 MHz. The surface morphology was determined through SEM on EVO 18 Research, Zeiss, instrument. TGA was conducted on Perkin Elmer, Thermogravimetric Analyzer, TGA 4000 in Nitrogen environment with a uniform heating rate of 10 °C/min. XRD measurements were recorded through RIGAKU with source CuK alpha performed at a voltage of 50 kV. The rheological analysis was carried out using Anton Par Rheometer (Model: Anton Par, Modular Compact Rheometer, MCR 302) with PP-25 parallel plate and 2.5mm inter-platen gap.

2.2.4 Swelling experiment

The swelling studies for LS-g-AA hydrogels were performed in pH 4.0, 7.0, and 9.2 buffer and distilled water at 37ºC. Dried hydrogel discs were weighed and placed in various pH media. These were removed after a fixed time interval and weighed. Filter paper has been used to remove additional surface water [211]. The samples were observed in triplicate. The swelling index (SI) ($g \cdot g^{-1}$) was calculated using the given equation 1:

$$SI = \frac{M_1 - M_2}{M_2} \tag{1}$$

Where, M_1 and M_2 represent the weight of equilibrium swollen hydrogel discs and wt. of dried hydrogel discs, respectively.

2.2.5 Gel content determination

The fraction of insoluble weight is known as gel content. The soluble part of the gel is extracted using the Soxhlet apparatus in boiling water for 24 hours to obtain the gel content. The swollen hydrogels were removed from the apparatus and oven dried at 50°C [212]. The gel content of hydrogel was determined from equation 2:

$$\text{Gel content (\%)} = = \frac{M_e}{M_i} * 100 \tag{2}$$

Where,

M_e and M_i are the respective weights of dry hydrogel before and after extraction.

2.2.6 Measurement of the highest water-retention capacity (WH%) of LS-g-SAH treated soil.

This study was carried out using the garden soil of DTU, Delhi. Up to 1% of the hydrogel was added to 50g of dry soil (less than 30 mesh size) and placed in a PVC tube (4.5 cm diameter). Its bottom was secured with a nylon cloth and weighed to obtain W_1. The treated soil samples were slowly saturated by adding tap water until they started to seep out from the bottom. The tubes were then re-weighed and marked W_2. A control experiment without LS-g-SAH was also conducted [213]. The largest water-retention capacity of treated soil was determined using equation 3:

$$\text{WH\%} = \frac{W_2 - W_1}{50} * 100 \qquad (3)$$

2.2.7 Water Evaporation rate of LS-g-SAH and soil.

A water evaporation test was used to investigate LS-g-SAH-treated soil's ability to retain water within its system structure for 55 days. Oven-dried soil (at 60°C for 48 hours) was used to prepare different sets of hydrogel-treated soil along with a control set. Each mixture was fed with 50 mL distilled water and weighed (marked as M_i). The total water, soil, and hydrogel weight is kept as 'M_T.' Then, these were placed at room temperature and weighed daily (M_t) [214]. Here, the effect of LS-g-SAH in different amounts on soil is studied by considering the water evaporation loss value from blank soil as a control. The water evaporation rate (WER) was determined using equation 4.

$$\text{WER} = \frac{M_i - M_t}{M_T} \times 100 \qquad (4)$$

2.2.8 Loading and release of urea by LS-g-SAH.

Urea was loaded onto the hydrogel by immersing a pre-weighed dry LS-g-SAH into a urea solution (0.034 mol·L^{-1}) for 24 h. After that, the swollen gels were removed from the water and dried till a constant weight was achieved.

The amount of urea released by LS-g-SAH was evaluated by soaking the dried urea-loaded samples in a beaker with 100 mL of distilled water at ambient temperature. Later, 1 ml water was drawn from the medium at fixed intervals to observe the released urea, and the same amount of distilled water was added to the beaker to keep the volume constant [215].

A standard method from The Specialized Standard of the People's Republic of China (SN/T 1004-2001) was used to determine the concentration of urea residue. At 430 nm, a spectrophotometer detected a complex compound of urea and p-dimethylamino benzaldehyde (DMAB). The general reaction showing the formation of chromogen that follows Beer-Lambert law and absorbs energy at 430 nm in the UV-Visible spectrum is shown below in scheme 1. 1. Then, the standard calibration curve was used to formulate the below-mentioned formula for the determination of urea concentration [210].

$$C\ (ppm) = \frac{A-0.1735}{0.0002} \tag{5}$$

Where, A is the UV absorbance of solution of unknown concentration.

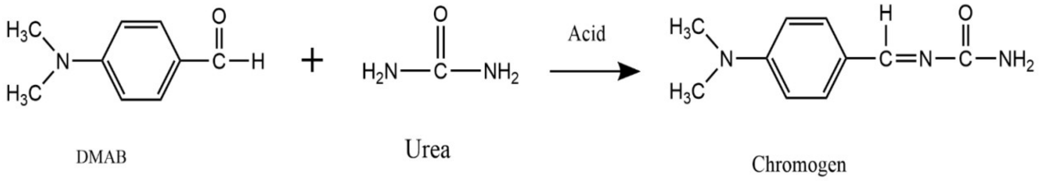

Scheme 1. 1: DMAB-urea reaction

2.2.9 Plant Growth Performance study.

Three sets of 300 grams of soil were placed in plastic pots with filter paper placed below with a small hole; (A) only urea, (B) control hydrogel-loaded urea, and (C) LS-g-SAH loaded with urea (at a depth of 5 cm). A plastic pot with direct urea in soil without hydrogel was kept as a check. Fifteen wheat seeds were sown in all three plastic pots with the same amount of hydrogel. Pots were exposed to environmental conditions, and irrigation was kept constant from day one for all containers. Growth profiles for all wheat grasses were observed at various time intervals. Germination was recorded by counting germinated seeds over two weeks. Just the appearance of the radicle was considered an indicator of seed germination. The plant shoots and roots were removed carefully from the soil. The shoot and root lengths and their fresh weight were recorded. The plant material was dried for 24 hours at 70°C to determine the dry mass [216].

2.3 Results and discussion

2.3.1 Mechanism of the formation of lignosulfonate-g-sodium acrylate hydrogels.

The KPS used as an initiator generated anion radicals which further helped to generate phenoxy radicals on LS. The active radicals also reacted with the vinyl groups of Sodium Acrylate, leading to the propagation of chain-forming poly sodium acrylate. This poly(sodium acrylate) propagated until crosslinked and terminated by MBA to form lignosulfonate-g-acrylic acid hydrogels, as shown in scheme 2. 2. The electrostatic repulsion created by the negatively charged carboxylate ions in the poly(sodium acrylate) polymer chains will lead to a network expansion. This will improve the hydrogel's capacity to absorb water [213].

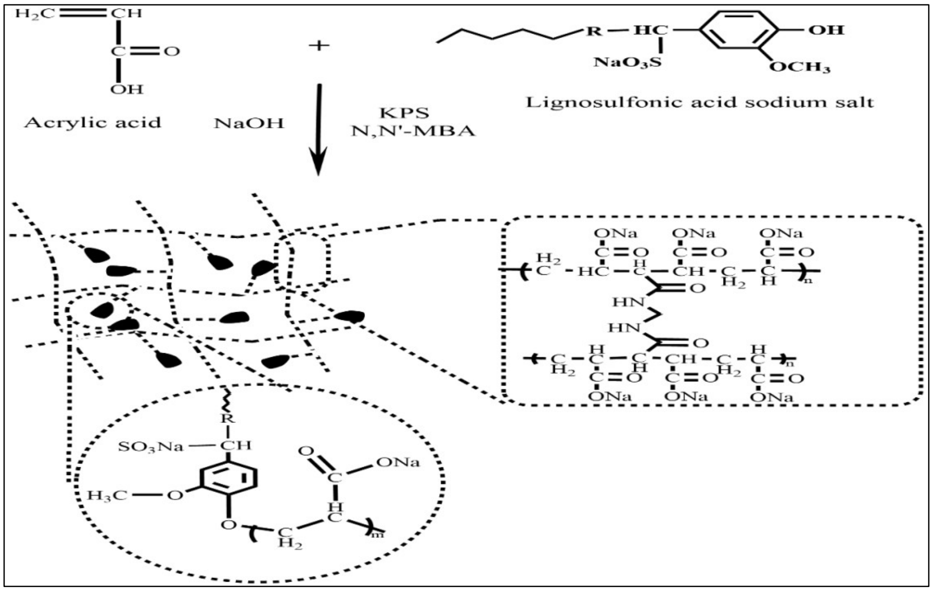
H₂C=CH
C=O
OH
Acrylic acid
+
NaOH
KPS
N,N'-MBA
R—HC
NaO₃S
OH
OCH₃
Lignosulfonic acid sodium salt
ONa
C=O
HN
HN
R
SO₃Na—CH
H₃C—O
ONa
m
n

Scheme 1. 2: Synthesis of LS-g-SAH.

2.3.2 Characterization of hydrogel.

2.3.2.1 Fourier-transform infrared (FTIR) spectroscopy

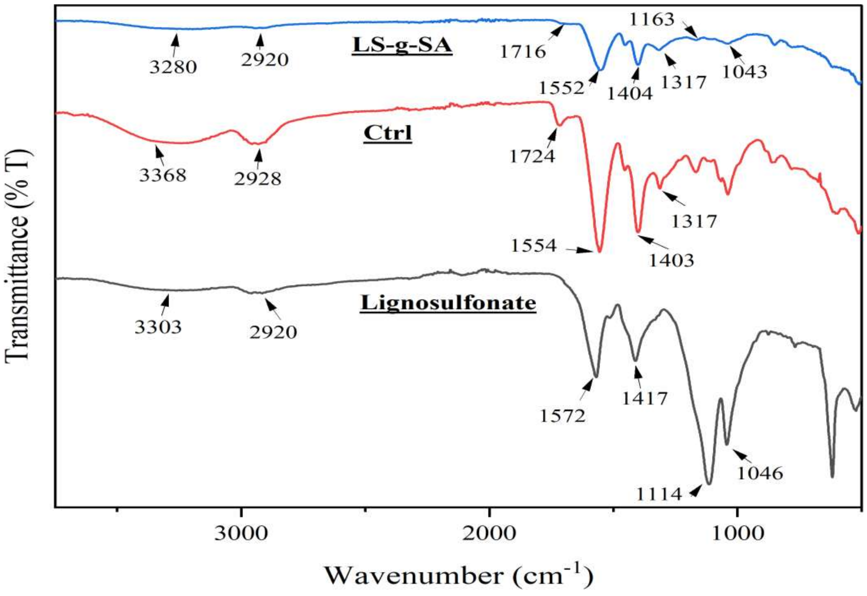

Figure 2.2: The FT-IR spectra of a) LS, b) Ctrl, and c) LS-g-SAH.

The FT-IR of LS, Ctrl and LS-g-SAH has been shown in Figure 2. 3. The -OH stretching vibration of LS is observed as a broad band around 3,303 cm^{-1}. LS, ctrl, and LS-g-SAH shows a peak around 2,920 cm^{-1} due to C–H stretching in –CH_2 or – CH_3 groups. The vibration of the aromatic skeleton is observed from the two firm peaks at 1,572 and 1,417 cm^{-1}. [69] The strong peak at 1,046 cm^{-1} arises due to C–O–S stretching vibration, and the peak at 1,114 cm^{-1} is assigned to O=S=O antisymmetric stretching vibration in the LS. [69] Both these characteristic peaks confirm the presence of LS in LS-g-SAH. Further, new peaks were found when LS was compared to LS-g-SAH. The strong bands at 1404 and 1554 cm^{-1} are due to the asymmetric stretching in the carboxylate anion. The broad band and a peak at 1317 cm^{-1} and 627 cm^{-1}, respectively, correspond to the C-N and O=C–N groups of N, N'-MBA [217].

2.3.2.2 SS ^{13}C CPMAS

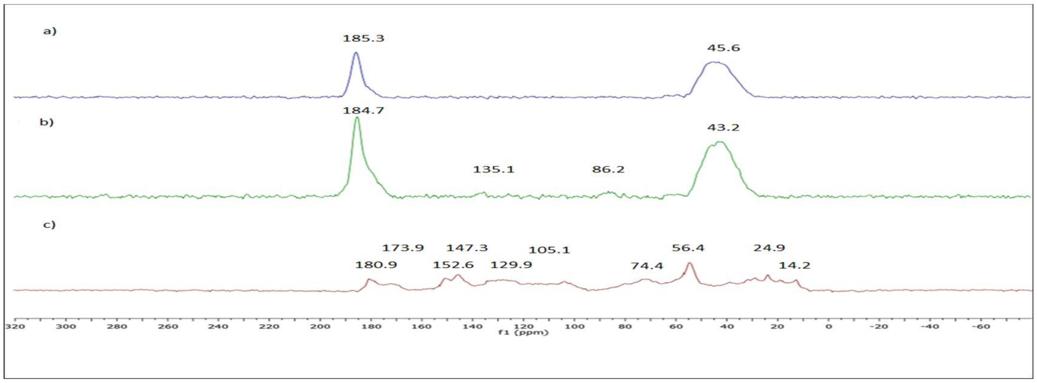

Figure 2. 3: SS ^{13}C CP-MAS NMR spectrum of a) ctrl, b) LS-g-SAH, and c) LS.

Solid state ^{13}C NMR spectroscopy is a powerful tool for the structural characterization of polymers. The spectra of LS, LS-g-SAH, and ctrl is presented in Figure 2. 3. Peaks around 45 ppm and 185 ppm of LS-g-SAH and ctrl were assigned to saturated aliphatic chains and C from carbonyl ester (COONa), COOH, respectively. Characteristic peaks of basic aromatic and aromatic rings with branched C-C bonds can be observed in the range of 140-110 ppm and 75-10 ppm. The appearance of signals around 50-10 ppm in LS represents aliphatic C chain [218, 219][220, 221]. Most of the peaks of LS merged inside LS-g-SAH due to their low intensity. However, the presence of peaks at 135.1 ppm and 86.2 ppm confirms the presence of LS in LS-g-SAH. The results support the observations of the FT-IR spectra. The presence of free COOH groups and crosslinks probably increased the intensity of the peak at 184.7 ppm.

2.3.2.3 Scanning electron microscopy (SEM)

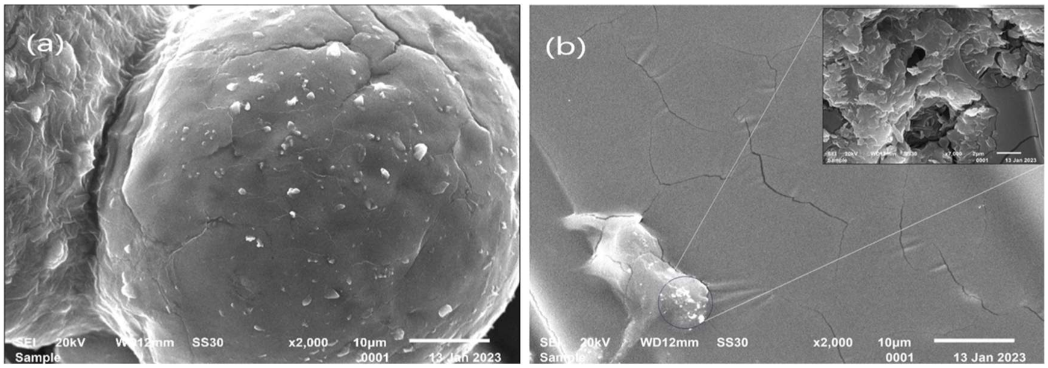
(a)
SEI 20kV WD12mm SS30 x2,000 10μm
Sample 0001 13 Jan 2023
(b)
SEI 20kV WD12mm SS30 x2,000 10μm
Sample 0001 13 Jan 2023

Figure 2.4: The SEM images of a) LS and b) LS-g-SAH.

The SEM images of the LS (a) and LS-g-SAH samples (b) at the different magnifications are presented in Figure 2. 4. The surface of LS is even and smooth in granular form. On the contrary, the LS-g-SAH is rough, uneven, and porous. This could be due to the grafting of LS onto poly(acrylate) chain, further facilitating the adsorption of more water.

2.3.2.4 Thermal analysis

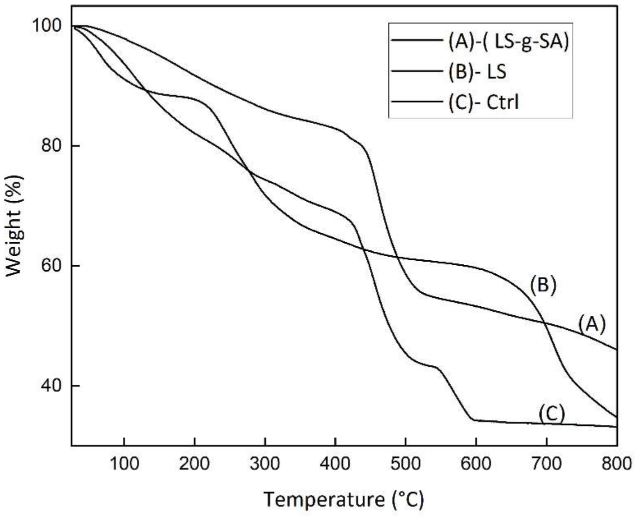

Figure 2. 5: TGA analysis a) LS-g-SAH, b) LS, and c) Ctrl.

As shown in Figure 2.5, both LS and LS-g-SAH samples have been observed in the range of 29-802 °C and have three weight loss ranges. The initial 16.3% weight loss at the stage (70°C -380 °C) in LS-g-SAH is due to moisture loss from the polymer. Between 436 -514°C, the weight loss percent of 23.4 is mainly due to the beginning of decomposition. The third stage, from 660°C -781°C, is the decomposition of the main polymeric backbone with a weight loss of 19.7% [147]. For the LS, up to 150 °C, the first decomposition is associated with removing volatile compounds and moisture, like acetaldehyde, acetone, and methanol. With the increase in temperature from 150°C to 250°C LS began to decompose, known as vitrification transformation. The primary decomposition occurred between 200 and 400°C. Weight loss of LS above 500 °C could be attributed to the CO from degrading C=O, C–O–C, and degeneration of aromatic rings [222][223]. The results from ^{13}C NMR and LS FTIR also support high amounts of C=O groups. Moreover, LS likely reacted with carbon from a sodium-containing salt that served as an activator for the dry pyrolysis process, further creating a mass loss between 650 and 800 °C [224]. The point of the highest rate change is found at approximately 500°C for LS-g-SAH, 450°C, and 270°C for ctrl and LS, respectively. LS-g-SAH had a higher residual weight of about 83% up to 400°C compared to 69% and 64% of ctrl and LS. Similarly, at 800°C, the LS-g-SAH resulted in more than 46% of residual mass when compared to just 34% and 33% of the residual mass of LS and ctrl hydrogels. This observation indicated that grafting of LS has improved the thermal stability of LS-g-SAH.

2.3.2.5 XRD

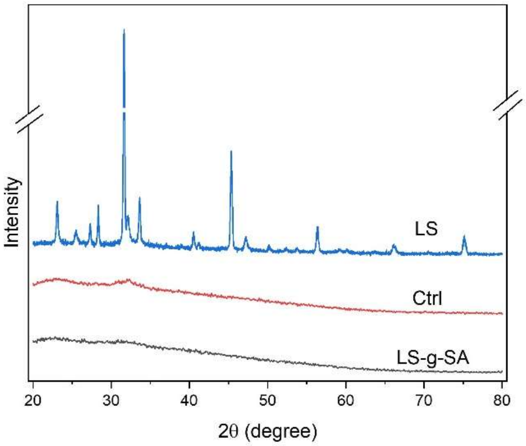

Figure 2. 6: XRD analysis of a) LS, b) Ctrl, and c) LS-g-SAH.

The XRD patterns (Figure 2. 6) in the 2θ range of 20°-80° of lignin showed several peaks at 23.12°, 25.52°, 27.32°, 28.34°, 31.64°, 33.60°, 40.48°, 45.34°, 56.36° and 75.16°. The LS-g-SAH and ctrl showed two broad complex peaks in the range with their maxima at 22° and 32°. The observed maxima are characteristic of an amorphous polymer structure [225]. The data revealed that lignin's crystallinity is destroyed after grafting onto poly(sodium acrylate). Such a similar result has been observed by grafting carboxymethyl cellulose on sodium acrylate [226].

2.3.2.6 Rheology

The knowledge of rheology can easily understand the relationship between chemical structure and the macroscopic behavior of hydrogels [227]. Rheological properties of LS-g-SAH are compared with ctrl to investigate the effect of the presence of lignin in the hydrogel, as shown in Figure 2. 7.

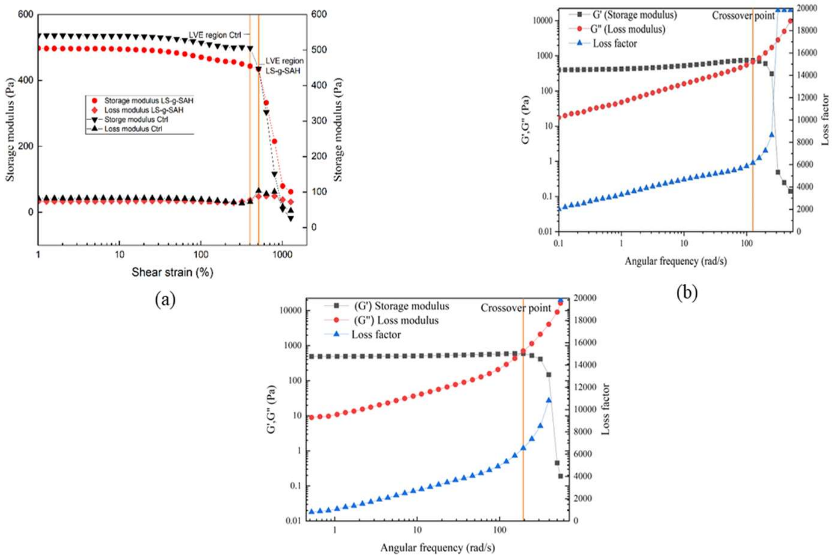

(a) (b) (c)

Figure 2.7: Rheological analysis a) amplitude sweep b) Frequency sweep of LS-g-SAH, and c) Frequency sweep of Ctrl hydrogel

During the amplitude sweep test, the shear stress amplitude was changed at a rate of 10rad/s. At low deformation, the loss modulus (G″) and storage modulus (G′) are consistent, indicating that the hydrogel structure remained unaffected. It is called a linear-viscoelastic region (LVE). The disruption of structure with decreased modulus suggests the termination of the LVE region. The ctrl and LS-g-SAH showed viscoelastic solid behavior up to a high strain of 402 and 511%, representing that LS-g-SAH may bear a higher shear strain than ctrl.

The frequency varied from 0.1 to 500 rad/s during the frequency sweep test while keeping the shear strain % within the LVE region constant. It was observed that the loss modulus was found to be prevalent at higher frequencies while the storage modulus was prevalent at lower frequencies representing the viscoelastic solid behavior. Tan θ (dimensionless) generally varies from 0 to 1 for viscoelastic solutions. For an ideal viscous behavior, tan θ is infinity, i.e., θ is 90° and for a perfect elastic behavior, tan θ is 0, i.e., θ is 0°. [228]

Table 2. 2: Frequency sweep data of LS-g-SAH and ctrl hydrogels

	Low frequency			Cross-over point	High frequency		
Sample	**Storage modulus G' (Pa)**	**Loss modulus G" (Pa)**	**Loss factor Tan θ**	**Angular frequency (rad/s)**	**Storage modulus G' (Pa)**	**Loss modulus G" (Pa)**	**Loss factor Tan θ**
LS-g-SAH	400	17.58	0.04	126	0.14	1722	infinite
Ctrl	491	8.89	0.018	194	0.19	2107	infinite

It was observed from Table 2. 2 that the cross-over point for LS-g-SAH falls in the low-frequency region (126 rad/s), indicating that its chain-chain interaction breaks at a lower frequency in comparison to ctrl. LS-g-SAH and ctrl had a loss factor of 0.04 and 0.018, representing the dominancy of elastic behavior at low frequency and viscous behavior at high frequency, which agrees with the previously reported literature [229]. However, ctrl hydrogel shows more elastic behavior at low frequencies.

2.3.3 Gel content (%)

The gel content percentage of LS-g-SAH present in table 1 was calculated using Eq. (2). The gel percentage of hydrogels varied according to the concentration of crosslinker, biopolymer, and initiator. The gel content reduced as the concentration of the crosslinker and biopolymer increased. In contrast, the initiator initially enhanced the gel content but decreased when added in amounts greater than 0.08g. Gel contents of synthesized hydrogels were found in the 64 - 97 % range.

2.3.4 Effect of variation of different parameters on the swelling index.

The relationship between various parameters and water absorbency was investigated by Flory, who concluded that hydrogel absorption depends on several parameters [230]. Therefore, the variables affecting the reaction, such as the concentration of biopolymer, initiator, and crosslinker, are studied to obtain the optimum reaction conditions.

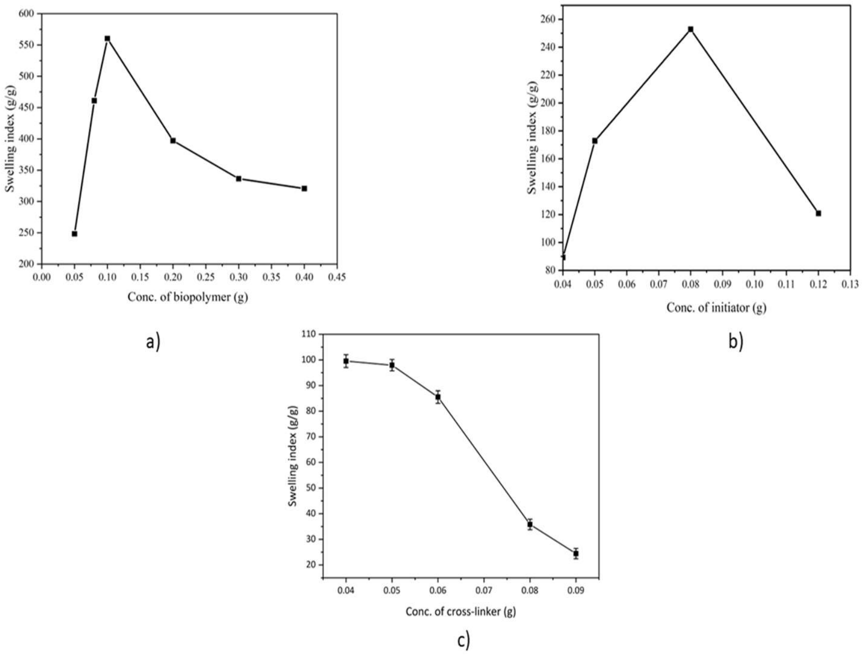

Figure 2.8: Effect of variation in a) biopolymer, b) initiator, and c) crosslinker on the swelling index of LS-g-SAH.

2.3.4.1 Effect of biopolymer

The concentration of hydrophilic biopolymer is one of the influencing factors of the swelling property of hydrogel. Figure 2. 8(a) shows that LS was varied from 0.05 g to 0.4 g in hydrogel to find the optimum concentration. Adding LS provided a more significant number of diverse hydrophilic groups to the hydrogel, resulting in an increment in the SI. After the LS content reached 0.1 g, the amount of ionic hydrophilic groups in the hydrogel, such as sulfonic acid and carboxyl groups, could have become higher than the non-ionic hydrophilic groups such as amide group and hydroxyl group, which further led to the declination of the SI. [231]

2.3.4.2 Effect of initiator

The reaction initiator creates active sites on the polymer. Thus, it plays a crucial role in the preparation of hydrogel. The SI of hydrogel increased with an increase in initiator concentration from 0.4 g to 0.08 g. Afterward, it decreased with the increasing amount of the initiator, according to Figure 2. 8(b). The maximum water absorbance was obtained at 0.08g of the initiator. An increase in the amount of initiator up to 0.08g generated more free radicals, resulting in larger chain ends in the network while shortening the average length of the kinetic chain. Accordingly, the SI would increase. However, an initiator concentration greater than 0.08 g may have increased the reaction velocity and decreased the network space of the polymer, which resulted in a decrease in the SI. [108]

2.3.4.3 Effect of concentration of crosslinker

It is evident from Figure 2. 8(c) that the SI sharply decreased with the increase in the crosslinker concentration of hydrogel. The graft reaction did not occur effectively with a concentration of MBA lower than 0.03g resulting in a jelly-like product with poor dimensional stability. Beyond this amount, adding more crosslinker to hydrogel resulted in more crosslink junctions in the polymeric chains. It increases the extent of crosslinking and reduces the free available volume inside the polymeric network [108, 232]. This results in a less swelling tendency of the hydrogel.

2.3.5 Swelling studies

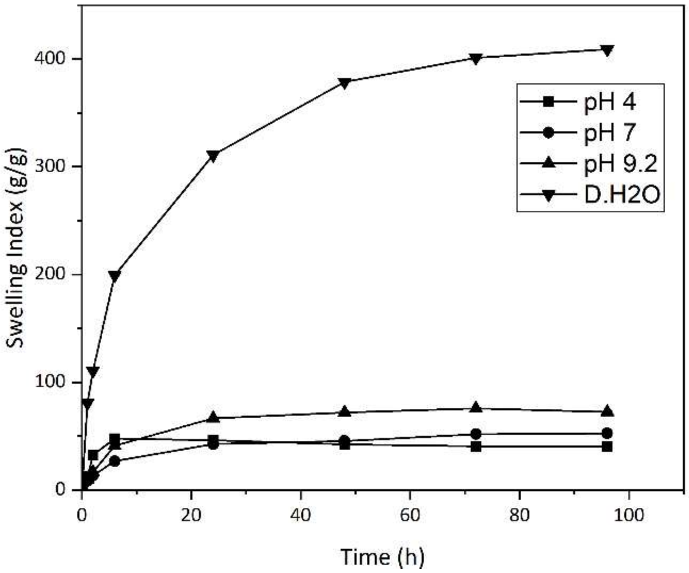

Figure 2.9: Swelling study of hydrogel

In general, the swelling index of different formulations in distilled water has been reported in Table 1. The swelling performance of L10 was investigated in various pH, i.e., pH 4.0, 7.0, and 9.2, and distilled water. Figure 2. 9 shows the enhancement in equilibrium SI from 51 to 73 with an increase in pH from 4, 7, and 9.2. Lower swelling of hydrogel in an acidic medium may be attributed to the improper ionization of the crosslinked network. Hence, at a lower pH, a collapsed state was observed. However, in alkaline conditions, electrostatic repulsions may have been produced by the carboxylate anions (COO^-). This might have caused a widening of space present in hydrogel networks, leading to an increase in the SI of the hydrogel [232, 233].

2.3.6 Agricultural applications of LS-g-SAH

2.3.6.1 Highest water retention capacity

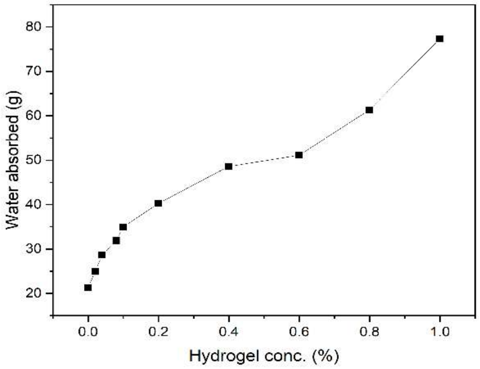

Figure 2.10: Water retention capacity plot of soil amended with LS-g-SAH.

Water availability in the soil is of utmost importance for better plant growth. As a result, the impact of LS-g- SA hydrogel on soil's maximum water retention capacity (WH%) was investigated. The amount of absorbed water and the corresponding concentration of incorporated hydrogel is shown in Figure 2. 10. It proved that the synthesized hydrogel exhibited excellent water-absorbing capacity and could be used to improve the soil water-retention capacity and reduce the frequent irrigation requirement.

2.3.6.2 Evaporation study

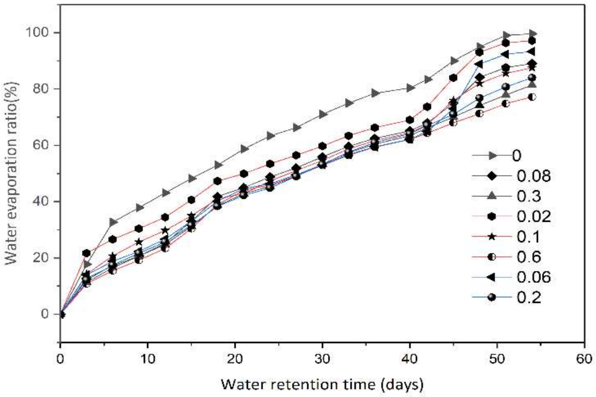

Figure 2.11: Water evaporation study of soil amended with different concentrations of LS-g-SAH.

Evaporation refers to the water loss from the soil directly to the atmosphere through water vapor. The water-holding capacity of soil affects the water evaporation rate of the soil. The control's water evaporation ratio from the study was higher than soil amended with LS-g-SAH, probably due to the interaction between water and polymer molecules and the macromolecular network hindrance [214]. Figure 2. 11 shows that adding just 0.6g LS-g-SAH to the soil reduced the evaporation rate from 99 to 76.69% of the total added water on the 54th day.

2.3.6.3 Release kinetics of urea

The power of law equation is used to understand the mechanism involved in releasing urea.

$$\frac{Mt}{M\infty} = k_{kP}t^{n} \tag{6}$$

where M_t and M_∞ Represents the urea released at time t and the equilibrium point, respectively. Whereas the ratio of M_t to M_∞ denotes the fraction of total urea released at the time 't', while 'k' is a polymer structure constant. The coefficient 'n' describes the type of diffusion involved. Only the section of the release curve where the ratio $\frac{M_t}{M_\infty} < 0 \cdot 6$ should be used to determine the exponent 'n' [234, 235].

Diffusion-controlled release is indicated by a Fickian diffusion mechanism with $n \geq 0.45$, whereas $0.45<n<0.89$ corresponds to non-Fickian transport, and $n=0.89$ corresponds to case-II relaxational transport, which specifies swelling-controlled release [235].

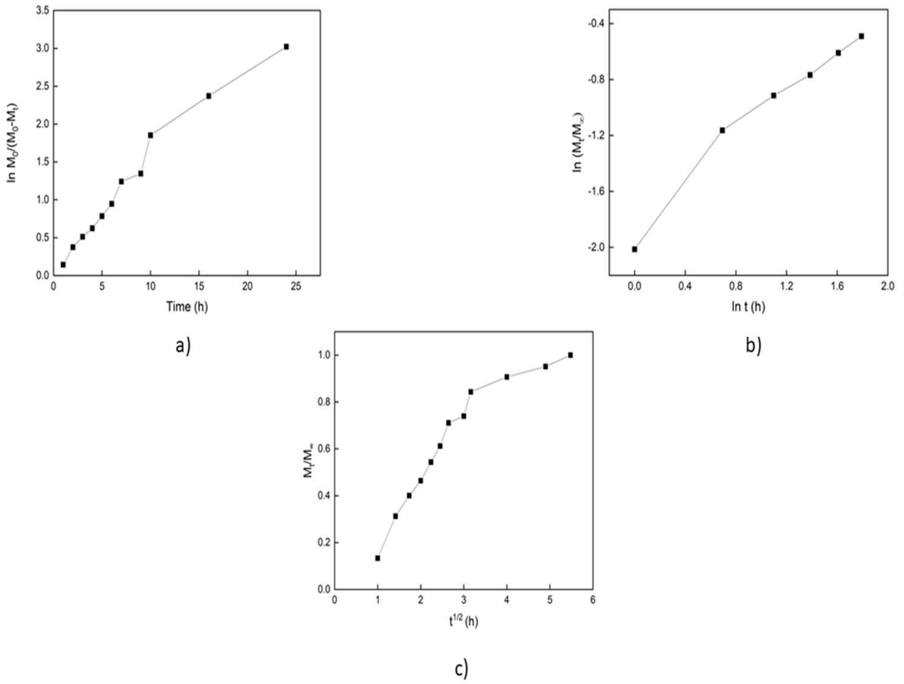

Figure 2.12: Urea release kinetics a) first order, b) Korsmeyer–Peppas, and c) Higuchi model in distilled water.

Table 2.3: Mathematical models used for the study of release kinetics from LS-g-SAH.

Mathematical models used for the study of release kinetics from LS-g-SAH.

Model	Equation	Parameter		R sq.
First-Order	$f = 100[1 - e^{-k_1 t}]$ f = amount of the released drug k_1 = rate constant, t = time	k_1	0.174	0.9932
Higuchi	$f = k_H t^{0.5}$ f = amount of the released drug k_H = Higuchi dissolution constant t = time	k_H	22.134	0.8242
Korsmeyer–Peppas	$f = k_{kp} t^n$ k_{KP} = constant depicting the experimental parameters f = amount of the drug released n = release exponent	k_{KP} n	0.4099 0.8193	0.9656

The slow-release process of urea through LS-g-SAH occurs in the following manner; firstly, the water tries to enter the hydrogel. Afterward, the hydrogel starts to swell by absorbing water until a dynamic exchange is developed between the free water of the hydrogel and the water present in the soil. Meanwhile, the urea in the hydrogel matrix continues to dissolve and diffuse. It gets released into the water due to the osmosis differences and dynamic exchange of free water [214].

From Table 2. 3. "n" is 0.8193, representing a non-Fickian diffusional release of urea from the synthesized hydrogel. The coefficient of determination values (R^2) showed its maximum value to be 0.9932 for the first-order kinetics (Figure 2. 12); hence, the release followed the First order kinetics model.

2.3.6.4 Plant Growth Performance

The plant growth performance study using the LS-g-SAH is shown in Figure 2. 13.

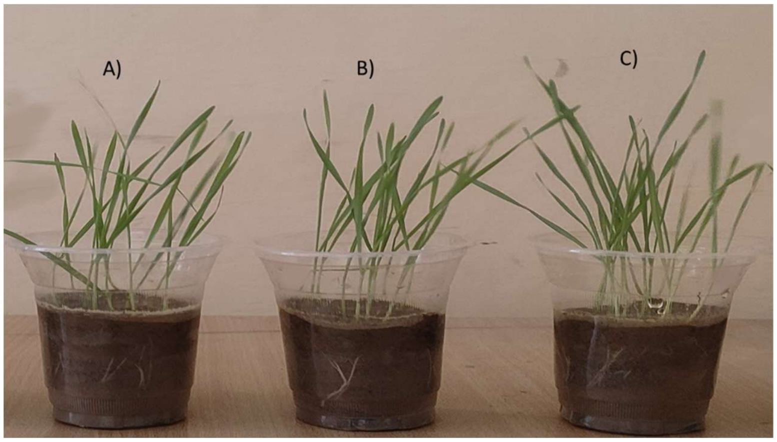

Figure 2. 13: Effect of hydrogel treatment on wheatgrass after 14 days. a) only urea, b) control hydrogel-loaded urea, and c) LS-g-SAH loaded with urea.

Table 2.4: Wheatgrass growth parameters on the 14th day. a) only urea, b) control hydrogel-loaded urea, and c) LS-g-SAH loaded with urea.

Sample	Total fresh weight of wheatgrass (Average) (g)	Total dry Weight of wheatgrass (Average) (g)	Average number of germinated seeds (per pot) at 14th day	Average wheatgrass height (cm) at 14th day	Average shoot height (cm) on the 14th day
a	0.7927	0.2860	13	17.2	12.4
b	0.8102	0.3002	12	17.7	12.8
c	0.8993	0.3004	15	19.7	14.4

The wheatgrass growth can be observed by the changed total dry and fresh weight, the average number of germinated seeds, the average wheatgrass height, and the average shoot height of all samples. All these are mentioned in Table 2. 4. The height of the plants increased with the advancing age of the crops. On the 14th day, significantly tallest grasses (the tallest grass was 27 cm) were recorded in LS-g-SAH, followed by sample B, i.e., ctrl, though the shortest plants were recorded under sample A. The germination and growth of seeds are known to be improved with the prolonged availability of urea. LS-g-SAH showed 100% germination followed by control hydrogel (86.6%), i.e., sample B and untreated soil (80%), respectively.

2.4 Conclusion

Novel LS-g-SAH was synthesized and loaded with urea using the gravitational equilibrium method. When observed in different media, the maximum water absorbency was 560 $g{\cdot}g^{-1}$ in distilled water. Using synthesized hydrogel remarkably raised the soil's water-holding capacity (WH%) from 21.27 to 77.3 g. Also, the water evaporation rate reduced from 99 to 76.69% of the total added water. The release kinetics study of urea in water revealed that LS-g-SAH showed a slow-release pattern with 60% release in 24 h following first-order release kinetics. The release pattern followed the Non-Fickian release mechanism. The increased height of wheatgrass also confirmed the beneficial effects of LS-g-SAH. Thus, the synthesized poly (sodium acrylate) hydrogel based on lignin can serve as a water retention agent and has the potential to be used for the gradual release of various agrochemicals.

CHAPTER-3

HUMIC ACID-INTEGRATED POLYMERIC HYDROGEL: A DUAL STRATEGY FOR SUSTAINED PESTICIDE DELIVERY AND SOIL WATER RETENTION

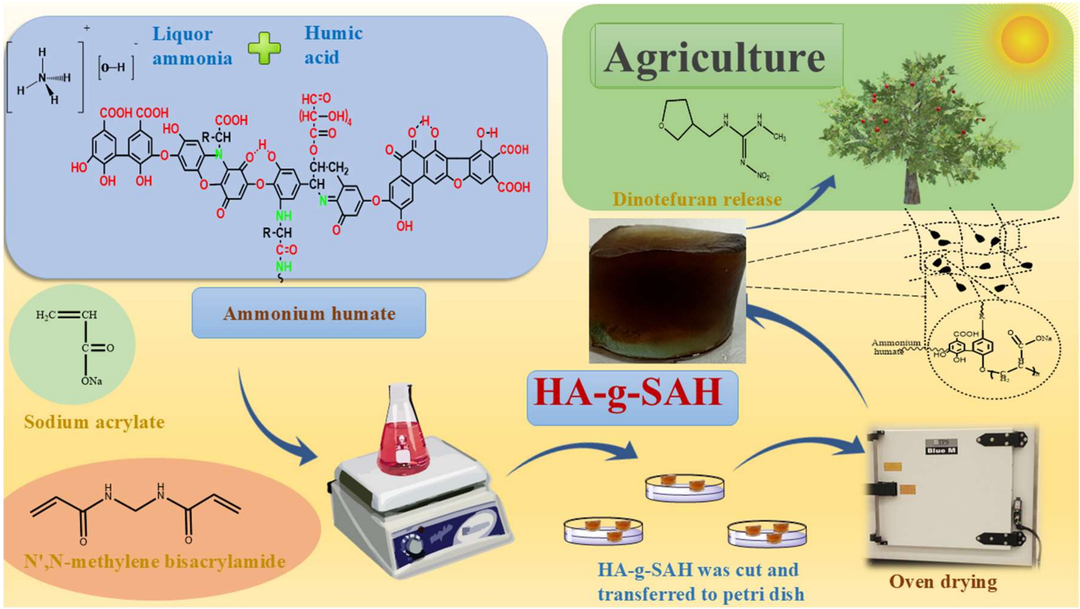
Liquor ammonia
Humic acid
Agriculture
Dinotefuran release
Ammonium humate
Sodium acrylate
HA-g-SAH
N',N-methylene bisacrylamide
HA-g-SAH was cut and transferred to petri dish
Oven drying

3.1 Introduction

The extensive use of neonicotinoid insecticides, particularly dinotefuran, poses risks of groundwater and soil contamination because of their persistence and high water solubility. This study developed a humic acid (as ammonium humate)-grafted poly(sodium acrylate) hydrogel (HA-g-SAH) via free-radical copolymerization to enable controlled pesticide release. The hydrogel was comprehensively characterized by ^{13}C CPMAS NMR, FT-IR, XRD, SEM, and TGA analyses to confirm its structural integrity and stability. Swelling performance was optimized using different formulations, revealing significant effects of biopolymer, initiator, and crosslinker concentrations, with HA-g-SAH achieving a maximum swelling index of 320.92 $g{\cdot}g^{-1}$ in comparison to 162.27 $g{\cdot}g^{-1}$ for the control (ctrl). Network parameters were also calculated. Dinotefuran loading efficiency reached 65.24%, exceeding that of the ctrl hydrogel (54.35%). Release experiments demonstrated a gradual and extended pesticide release, with HA-g-SAH releasing 78.45% of dinotefuran over 49 h, while the ctrl released 64.21% within 33 h. Kinetic modelling indicated that the release of dinotefuran followed non-Fickian diffusion mechanism, best described by the Korsmeyer–Peppas and Weibull models. Soil amendment studies further showed that HA-g-SAH significantly enhanced water retention capacity (79.46% at 1% hydrogel), outperforming the ctrl (58.49%). These findings highlight that grafting ammonium humate improves swelling and loading efficiency and provides extended pesticide release and superior soil moisture management. The proposed HA-g-SAH system thus offers a sustainable strategy for reducing pesticide leaching and enhancing agricultural productivity.

Since their introduction, pesticides have played an essential role in enhancing yield of crops to fulfil the food requirements of an increasing population. These have become essential tools in agriculture, helping to safeguard crops from the invasion of pests.[236] Approximately 2 million tons of pesticides are currently utilized in the agricultural sector. [237] According to the Environmental Protection Agency, pesticides are substances designed to eliminate or control harmful organisms, including weeds, plant diseases, and other species. They are also employed against various living threats such as nematodes, insects, arthropods, and even vertebrates.[238]

Among various pesticides, dinotefuran ((RS)-1-methyl-2-nitro-3-(tetrahydro-3-furyl methyl) guanidine), is classified as a 3rd generation neonicotinoid (Fig. 3.1). It is recognized as a highly effective insecticide due to its broad-spectrum activity against numerous pest species [239, 240]. It has been widely employed to manage insects such as aphids, beetles, and whiteflies. The physicochemical characteristics of dinotefuran include a molecular weight of 202.2 Da, high water solubility (39,830 $mg \cdot L^{-1}$ at 20 °C), low lipophilicity (log KOW = −0.55), moderate soil adsorption (log KOC = 1.41), soil persistence with a 50-100 days half-life, and rapid degradation in water via photolysis (half-life <2 days).[241, 242]

Pesticides can inadvertently reach the soil after application via spray drift or by being washed off plant surfaces through rainfall. Once in the soil, these compounds may undergo plant uptake, chemical or microbial transformation, or downward percolation, which can lead to leaching into groundwater. Traces of neonicotinoids have also been identified in both groundwater and drinking water, primarily as a consequence of surface runoff and leaching processes.[243] Thus, the contamination of groundwater by pesticides is of particular concern, as it often represents the primary source of potable water in many developing regions.

It is essential to develop an environmentally sustainable system that may address the challenges associated with applying pesticides. From the literature, it was found that dinotefuran can be applied to leaves, soil, and irrigation water through pricking-in-hole treatments, spraying, and drenching. [244] However, these methods cause the leaching out of pesticides into groundwater and soil.

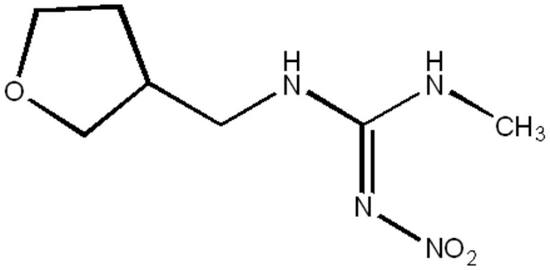

Figure 3. 1: Molecular structure of Dinotefuran

In recent years, hydrogels have gained attention as effective systems for the encapsulation and controlled delivery of agrochemicals.[245, 246] Among various hydrogel materials, polysodium acrylate hydrogels have garnered attention owing to their biocompatibility, tunable properties, and potential for controlled release.

This study introduces a novel strategy for synthesizing poly(sodium acrylate)-based hydrogels incorporating humic acid, designed for the controlled release of dinotefuran. Humic acid is generally acidic. As shown in fig. 3.2, it has several functional groups (carboxylic, hydroxyl, ketone, etc.). These results in a higher cation-exchange-capacity. Therefore, it could also act as an alternative material for N fertiliser carrier.[131] Ammonium humate as an N-carrier can extend supplementary benefits such as nutrient retention, carbon (C) sequestration, delivery of humic substances, reduction in greenhouse gases, etc.[247] The humic acid used in the present study has been treated with liquor ammonia to synthesize an ammonium salt of humic acid. Incorporating humic acid into polysodium acrylate hydrogel provides improved water retention and soil conditioning benefits. Here, HA-g-SAH and control (ctrl) are synthesized using the graft copolymerization method and characterized by ^{13}C CPMAS NMR, FT-IR, XRD, SEM, and TGA to understand their structural and thermal properties. A series of formulations were developed to systematically investigate the influence of key formulation variables—including biopolymer, crosslinker, and initiator's content on the swelling profile of the network of hydrogel. The entire experimental protocol was conducted in triplicate to ensure statistical robustness and data reliability. Furthermore, the release kinetics of dinotefuran is investigated through UV-vis spectrophotometry, shedding light on the controlled release capabilities of the hydrogel. It explores the potential of HA-g-SAH as versatile platforms for agricultural applications with enhanced environmental performance and sustainability.

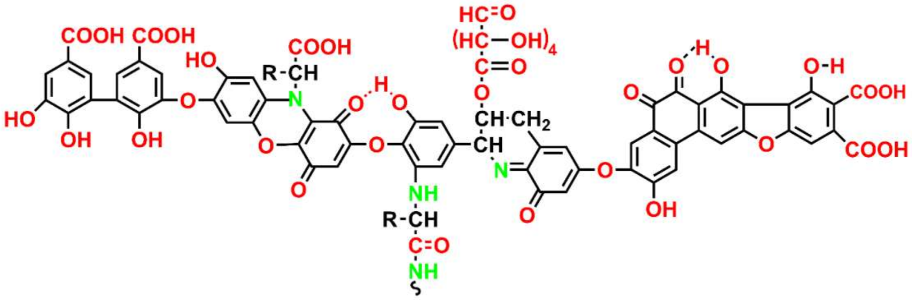

Figure 3. 2: Molecular structure of humic acid

3.2 Material and Methods

3.2.1 Materials

Humic acid, N',N-methylene bisacrylamide (MBA), and Acrylic acid (AA) were purchased from SD Fine chem Ltd., while Sodium Hydroxide (NaOH), Liquor ammonia, and Potassium persulfate (KPS), were sourced from CDH Pvt Ltd. Dinotefuran (96.5%) was generously provided by the Institute of Pesticide Formulation and Technology, Gurugram, India. Distilled water was utilized to prepare all water-based polymerization solutions.

3.2.2 Preparation of Ammonium Humate

Humic acid, being inherently water-insoluble, necessitated preparing its salt form as ammonium humate. Our previously developed method is used for the preparation of ammonium humate. [131] Briefly, given the solubility of humic acid in anhydrous ammonia solution, it was introduced into an ammonium hydroxide solution and subjected to stirring (600 rpm) for 24 hours at 27°C. The ammonium cations in the hydroxide state facilitated the displacement of protons within the humic acid molecules, leading to their dissolution and activation.

3.2.3 Ex situ preparation of HA-g-SAH

HA-g-SAH and ctrl hydrogels were synthesized using free radical polymerization.[128] The synthesis involved KPS and MBA as initiator and crosslinker, respectively. At ambient temperature, AA (neutralized with 8.07 $\mathrm{mol \cdot L^{-1}}$ NaOH) was combined with ammonium humate. Subsequently, KPS and MBA were introduced and stirred continuously for 2 hours. The homogenous solution was placed in a water bath set at

60°C for an hour to facilitate the copolymerization process. Post-synthesis, HA-g-SAH were cut into discs and put in distilled water for 24 hours to eliminate residual reactants, as shown in Scheme 3.1. Finally, HA-g-SAH was oven-drying at 60°C. [37, 38]

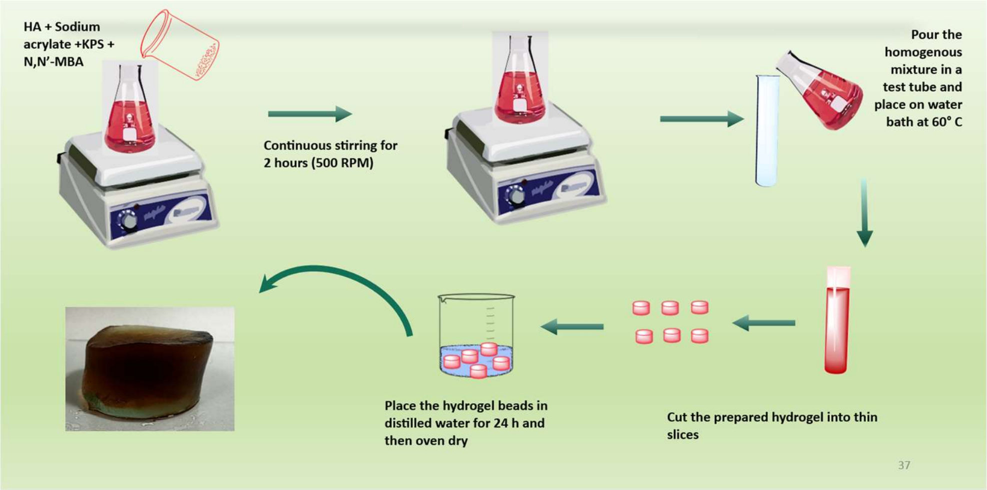
HA + Sodium acrylate +KPS + N,N'-MBA
Continuous stirring for 2 hours (500 RPM)
Pour the homogenous mixture in a test tube and place on water bath at 60° C
Cut the prepared hydrogel into thin slices
Place the hydrogel beads in distilled water for 24 h and then oven dry
37

Scheme 3. 1: Synthesis of HA-g-SAH using free radical polymerization

3.2.4 Characterization

3.2.4.1 ^{13}C CPMAS NMR

Solid-state ^{13}C CPMAS NMR spectra of samples were recorded on a Bruker Avance 400 spectrometer operating at 100 MHz for ^{13}C nuclei. The experimental parameters included a probe diameter of 4 mm, spinning rate of 10,000 kHz, contact time of 2000 µs, repetition time of 5 s, and a total of 10,000 scans.

3.2.4.2 FT-IR

FT-IR spectra of samples were obtained using a Perkin Elmer 2000 FT-IR spectrometer with a spectral resolution of 1 cm^{-1}. Solid samples for FT-IR analysis were prepared as pellets by homogenizing 5 mg of the samples with 100 mg dry KBr.

3.2.4.3 Wide-angle X-ray diffraction (XRD)

XRD measurements were analysed using a RIGAKU diffractometer with a Cu-Kα radiation source, operated at 50 kV with a step resolution of 0.04° (wavelength = 1.5406 Å).

3.2.4.4 Thermogravimetric analysis (TGA)

TGA was conducted on a Perkin Elmer, Thermogravimetric Analyser, TGA 4000 instrument, with samples heated under a nitrogen atmosphere at a rate of 10 $°C \cdot min^{-1}$.

3.2.4.5 Scanning electron microscopy (SEM)

SEM analysis was done using an EVO 18 Research, Zeiss, microscope. Before analysis, HA-g-SAH and ctrl samples were freeze-dried using Freezer Dryer, LabTech. A gold coating of samples followed the drying process.

3.2.5 Swelling study of HA-g-SAH in distilled water

The swelling studies for HA-g-SAH and ctrl were performed in distilled water. Discs of the hydrogels, which had been dried in an oven and weighed, were immersed in distilled water. At specific intervals, the discs were extracted from the distilled water, excess distilled water was blotted with tissue paper, and subsequent weight measurements were taken until a consistent weight was achieved. [6]

The swelling index (SI) ($g \cdot g^{-1}$) of HA-g-SAH and ctrl was calculated using the given Eq. (1).

$$SI(g \cdot g^{-1}) = \frac{W_2 - W_1}{W_1} \qquad (1)$$

W_2 represents to swollen hydrogel, while W_1 denotes to dried hydrogel.

3.2.6 Network parameters

3.2.6.1 Solvent Interaction Parameter (χ)

The solvent interaction parameter was determined to evaluate the molecular compatibility between the monomer/polymer components of the HA-g-SAH and ctrl hydrogels and the surrounding medium. It was determined using Eq. 2, which is based on the Flory–Huggins theory. [248]

$$\chi = \frac{ln(1-V_{2,s})+V_{2,s}}{V_{2,s}^2} \tag{2}$$

Where $V_{2,s}$ (mL·mol^{-1}) denotes the volume fraction of the HA-g-SAH, and ctrl in its equilibrium-swollen state.

3.2.6.2 Volume fraction ($V_{2,s}$)

The polymer volume fraction reflects the ability of the HA-g-SAH and ctrl network to permit solvent diffusion.[249] It was calculated using Eq. 3.

$$V_{2,s} = \left[1 + \frac{d_p}{d_s}\left(\frac{M_a}{M_b} - 1\right)\right]^{-1} \tag{3}$$

Where, d_s and d_p represent the densities (g·mL^{-1}) of solvent and HA-g-SAH and ctrl, respectively; M_a and M_b correspond to the weight (g) of the swollen and dry HA-g-SAH; and $V_{2,s}$ (mL·mol^{-1}) denotes the molar volume of the solvent within the HA-g-SAH at equilibrium swelling.

3.2.6.3 Molecular Weight between Crosslinks (M_c)

The Flory–Rehner theory was applied for estimatation of the average molecular weight between crosslinks in the interpenetrating polymeric networks of HA-g-SAH and ctrl, which reflects the degree of crosslinking within the hydrogel matrix. According to this model, Mc increases with an increase in the swelling ratio of the hydrogel. M_c was calculated using Eq. 4. [250]

$$M_c = \frac{d_p V_S (V_{2,s}^{\frac{1}{3}} - \frac{V_{2,s}}{2})}{ln(1-V_{2,s}) + V_{2,s} + xV_{2,s}^2} \tag{4}$$

3.2.6.4 Crosslinking density (ρ)

ρ is the density of crosslinking of the polymeric chains, which reflects the packing efficiency of the three-dimensional polymer network. It was calculated using Eq. (5).[251].

$$\rho = \frac{d_p}{M_c} \times N_A \tag{5}$$

where d_p is defined as the density of the swollen HA-g-SAH and ctrl and M_c as the molecular weight separating two crosslinks.

3.2.7 Release of Dinotefuran in water

3.2.7.1 Preparation of the dinotefuran standard curve

The dinotefuran standard curve was established using UV-vis spectrophotometry. Solutions of DNF were prepared in water to achieve concentrations varying from 4 to 20 μg·mL^{-1}, and their corresponding absorbances were recorded. A standard curve was generated using ORIGIN software, and the regression equation was derived.

Subsequently, the cumulative release of dinotefuran was measured via UV-vis spectrophotometer at 270.5 nm based on the standard curve in deionized water.

3.2.7.2 The loading efficiency and in vitro release of dinotefuran

Formulation HA-g-SAH 14 was used to assess the dinotefuran loading efficiency, selected based on its highest swelling capacity in distilled water. In this experiment, dinotefuran was incorporated into the hydrogel by immersing 0.1 g of HA-g-SAH in a 200 ppm dinotefuran solution for 24 h. The swollen HA-g-SAH were taken out and dried until a constant weight was obtained.

The difference in the total amount of dinotefuran loaded into HA-g-SAH and free dinotefuran in the respective supernatant was used to determine the amount of dinotefuran loaded in hydrogel formulations.[252] The analysis used a UV-vis spectrophotometer (Shimadzu UV-Spectrophotometer, UV-1800) at 254 nm. The standard calibration curve was subsequently employed to determine the concentration of dinotefuran from the measured absorbance values of the samples. The loading efficiency (LE) of dinotefuran was calculated using Eq. (6).[253]

$$LE\ (\%) = \frac{A_{total} - B_{free}}{A_{total}}\ X\ 100 \qquad (6)$$

A_{total} is the amount of dinotefuran used to prepare HA-g- SAH, and B_{free} is the amount of freely present dinotefuran in the supernatant.

The release of dinotefuran from HA-g-SAH was assessed by immersing the dried, dinotefuran-loaded HA-g-SAH in 100 mL of distilled water at room temperature. At fixed intervals, 1 mL aliquot of solution was withdrawn for analysis and immediately replaced with an 1 mL of distilled water to maintain a constant volume.[215] The concentration of dinotefuran in the collected supernatant was quantified by recording the absorbance at 254 nm using a UV–Vis spectrophotometer. [254] Also, the standard calibration curve was used to formulate the following Eq. (7) to determine dinotefuran concentration (C).

$$C\ (ppm) = \frac{A - 0.0069}{56.034} \tag{7}$$

where C represents the concentration of dinotefuran in the water sample, while A denotes the UV-vis absorbance of the solution with an unknown concentration.

3.2.7.3 Kinetics of Model Pesticide Release

To establish HA-g-SAH as a controlled-release system for pesticides, it is essential to understand the underlying release mechanisms and the factors affecting the release rate. Various mathematical models have been employed to better describe and predict the kinetics and behavior of pesticide release over time. The experimental release profiles were modelled using the Korsmeyer–Peppas and Weibull equations, and model fitting was carried out through linear regression analysis employing OriginPro and Microsoft Excel. Model fitting accuracy was assessed through the correlation coefficient (R^2), which indicates how much of the variability in the experimental results is explained by the model. Models with R^2 values approaching one were regarded as providing the best fit. The Akaike Information Criterion (AIC) was also employed to assess model adequacy further, particularly when comparing models of varying complexity. Lower AIC values indicated superior model performance and predictive efficiency. [255]

The release kinetics of Dinotefuran from HA-g-SAH were examined utilising the Korsmeyer-Peppas and Weibull models as outlined below, as Eq. (8-9) : [234, 256]

Korsmeyer -Peppas model: $\frac{M_t}{M_\infty} = k_{kp} t^n$ (8)

Weibull model: $R\ (t)= 1\text{-}e^{-\alpha t \beta}$ (9)

In these equations, 'M_t' represents the cumulative release of Dinotefuran at time 't' relative to the total loaded Dinotefuran. 'M_0' denotes the initial release amount, and 'k' signifies the kinetic constant governing the release process.

3.2.8 Water retention capacity (WRC)

Soil samples were air-dried under shaded conditions and passed through a 2 mm sieve. Portions of 100 g of the air-dried soil were placed in perforated plastic beakers lined with filter paper at the base. These beakers were then amended with varying amounts of dried HA-g-SAH, while unamended soil served as the control. The beakers were positioned in a water reservoir to allow capillary absorption for 24 hours. Afterward, the samples were removed, excess gravitational water was allowed to drain, and the soils were maintained at a constant temperature. The weight of the moistened soil in each beaker was recorded. The soil moisture-holding capacity (MHC) was calculated using the weight of the empty beaker and filter paper (W_{dry}), and final weight after water absorption (W_{wet}), according to Eq. (10).

$$\%\, WRC = \frac{W_{wet} - W_{dry}}{W_{dry}} \times 100 \tag{10}$$

3.2.9 Statistical Analysis

The experimental data in this study were processed and analyzed using OriginPro 2021, GraphPad Prism 10.2.3, ChemDraw 20.1.1, and Microsoft Excel. All data are shown as mean ± SEM, and significance was established at the 0.05 probability level with all analyses performed using a sample size of $n = 3$.

3.3. Results and Discussion

3.3.1 Synthesis of HA-g-SAH

The synthesis of water HA-g-SAH involves a complex chemical process. Initially, the reaction is believed to start with the thermal breakdown of APS, creating a sulfate anion radical. This radical then interacts with an alcoholic OH group in ammonium humate, forming a macro-radical. Subsequently, sodium acrylate and acrylic acid monomers act as receptors for these macro-radicals. The macro-radical generated from the initiator subsequently transfers free radicals to neighboring monomer molecules via chain propagation. This results in the grafting of ammonium humate onto the acrylic polymer chains, forming the graft copolymer. Polymerization concludes through the termination process, which occurs when two growing polymer chains combine, as illustrated in Scheme 2. Table 1 represents the various formulations for the synthesis of HA-g-SAH.

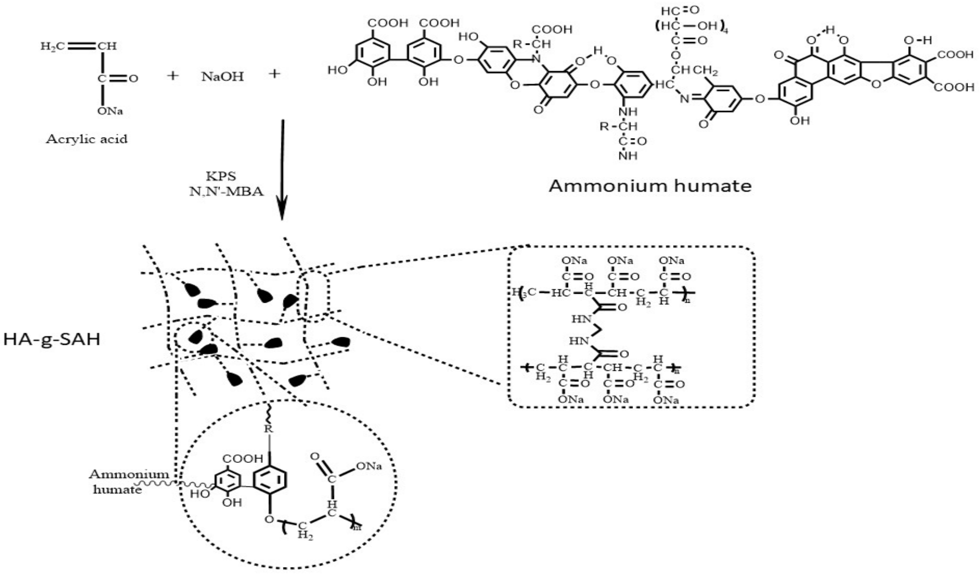
Acrylic acid
NaOH
KPS
N,N'-MBA
Ammonium humate
HA-g-SAH
Ammonium humate

Scheme 3.2: Mechanism of HA-g-SAH synthesis

Table 3.1: Various formulations of HA-g-SAH

Formulation	HA (g)	KPS (g)	MBA (g)	Swelling index ($g \cdot g^{-1}$)
HA-g-SAH 1	0.1	0.06	0.06	242.57
HA-g-SAH 2	0.1	0.06	0.08	239.18
HA-g-SAH 3	0.1	0.06	0.09	203.61
HA-g-SAH 4	0.1	0.06	0.1	187.42
HA-g-SAH 5	0.1	0.06	0.12	163.24
HA-g-SAH 6	0.1	0.06	0.14	203.24
HA-g-SAH 7	0.1	0.06	0.08	230.45
HA-g-SAH 8	0.1	0.08	0.08	243.67
HA-g-SAH 9	0.1	0.1	0.08	227.89
HA-g-SAH 10	0.1	0.12	0.08	212.82
HA-g-SAH 11	0.1	0.14	0.08	196.67
HA-g-SAH 12	0.05	0.06	0.1	201.34
HA-g-SAH 13	0.1	0.06	0.1	224.12
HA-g-SAH 14	0.2	0.06	0.1	249.45
HA-g-SAH 15	0.3	0.06	0.1	320.92
HA-g-SAH 16	0.4	0.06	0.1	293.82

3.3.2 Swelling Index and effect of parameters

The absorption of an aqueous solution is a crucial property of a hydrogel. During the swelling process, the elastic polymer chains undergo extension, whereas the crosslinking junctions prevent the complete dissolution of the polymer.[257] The swelling index of two hydrogels at equilibrium in distilled water was assessed at different time intervals. HA-g-SAH exhibited a swelling index of 320.92 $g \cdot g^{-1}$ in 35 hours, while Ctrl showed a swelling index of 162.27 $g \cdot g^{-1}$ in 31 hours. The analysis indicates that HA-g-SAH demonstrated greater swelling capacity and prolonged duration than ctrl. Thus, including ammonium humate enhanced the swelling efficiency of the synthesized hydrogel.

The variation in amount of experimental parameters employed in the preparation of the hydrogel series exerted a significant effect on both their structural and functional characteristics. To assess these influences, swelling behavior was evaluated in distilled water (pH 6.97). Furthermore, the roles of biopolymer concentration, i.e. HA, initiator level, i.e. KPS, and crosslinker, i.e. MBA content, in modulating the swelling capacity of the hydrogels were examined, with the corresponding results illustrated in Fig. 3.3.

3.3.2.1 Impact of Biopolymer on Swelling of Hydrogel

As the amount of HA increased, the swelling index showed a significant rise up to 0.3 g, as shown in Fig. 3.3a. This effect is mainly due to extra hydrophilic groups, including carboxyl and hydroxyl functionalities from humate, enhancing water absorption. However, at higher concentrations (0.4 g), a slight decrease in swelling was observed, likely due to excessive humate content leading to denser network formation and reduced chain mobility, which restricts water uptake.

3.3.2.2 Impact of Initiator on Swelling of Hydrogel

The effect of the initiator, KPS, revealed that the swelling index increased slightly as the initiator content was raised to 0.08 g, indicating efficient radical generation and a porous structure favorable for water absorption, as shown in Fig. 3.3b. Beyond this concentration, swelling decreased progressively, which may be explained by the formation of excessive radicals leading to chain termination and higher crosslinking density, thereby limiting swelling capacity.[258]

3.3.2.3 Impact of Crosslinker on Swelling of Hydrogel

In contrast, the influence of MBA, the crosslinking agent, showed an inverse relationship with swelling behavior, as shown in Fig. 3.3c. Increasing MBA content from 0.06 g to 0.14 g resulted in a sharp decrease in swelling index, as higher crosslinker concentration produces a more tightly crosslinked network that restricts polymer chain flexibility and reduces the free volume available for water penetration.[232]

Overall, the results demonstrate that swelling performance is governed by a balance between the hydrophilicity imparted by HA, the optimum initiator concentration of KPS for controlled network formation, and the crosslinking density dictated by MBA, where excess of either initiator or crosslinker significantly reduces the hydrogel's swelling ability.

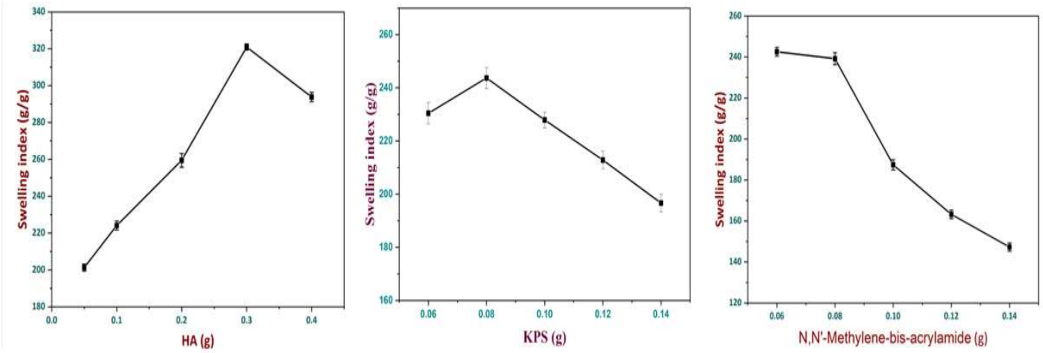

Figure 3.3: Effect of variation in amount of a) Biopolymer, b) Initiator, and c) Crosslinker on the swelling index of HA-g-SAH 14.

3.3.3 Characterization

3.3.3.1 ^{13}C CPMAS NMR

The structural characteristics of HA, HA-g-SAH, and ctrl were investigated using ^{13}C CPMAS NMR spectroscopy, as shown in Fig. 3.4. The spectrum of HA (Fig. 4a) exhibited broad and complex signals, reflecting its heterogeneous and multifunctional nature. Resonances were identified for aliphatic carbons in around 40-45 ppm region, a strong O-alkyl signal at 55–105 ppm corresponding to carbohydrate- and alkoxy-type carbons, aromatic/olefinic carbons between 110–160 ppm, and carboxyl/amide carbons in the 165–185 ppm region[218]. In contrast, the spectrum of the ctrl showed two well-resolved and sharp resonances, indicative of its more homogeneous chemical structure. A strong carbonyl resonance at ~180–183 ppm was assigned to the carboxylate groups of sodium polyacrylate, while the peak observed at ~40–50 ppm corresponded to the methine and methylene carbons of the saturated polymer backbone [259].

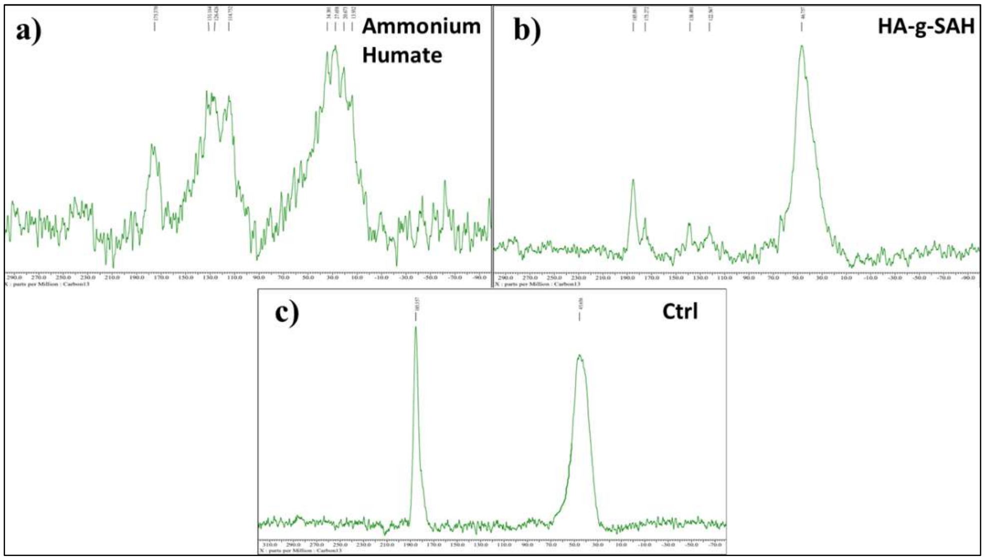

Figure 3.4: The plot of ^{13}C CPMAS NMR of a) ammonium humate, b) HA-g-SAH and c) ctrl

The spectrum of the HA-g-SAH (Fig. 4b) displayed features from both HA and ctrl, providing clear evidence of successful grafting. Prominent signals of ctrl (Fig. 4c) were observed, including the carbonyl resonance at ~180 ppm and the aliphatic backbone peak near ~40–50 ppm, while weaker and broadened signals corresponding to the humate backbone persisted in the O-alkyl (55–105 ppm) and aromatic (110–160 ppm) regions. Compared to native HA, the aromatic envelope was significantly attenuated, and the polyacrylate COO resonance dominated the carbonyl region.

Thus, the ^{13}C CPMAS NMR results confirm the successful HA grafting onto poly(sodium acrylate) chains. The grafted hydrogel combines the functional diversity of ammonium humate with the structural regularity of ctrl hydrogel.

3.3.3.2 FT-IR

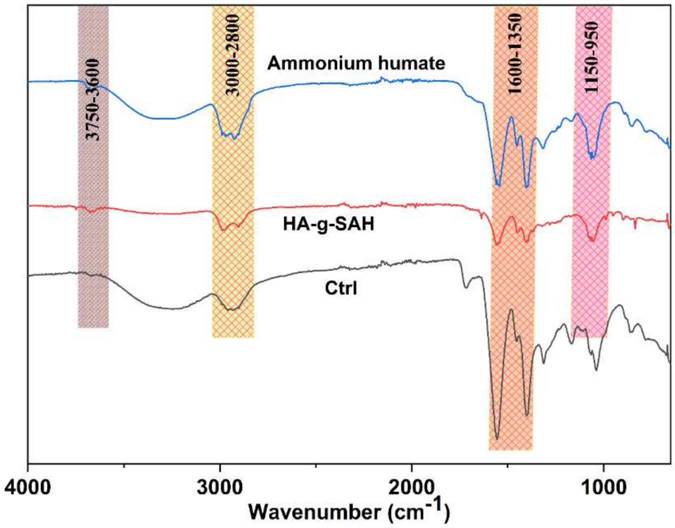

Figure 3.5: The plot of FT-IR of a) HA, b) HA-g-SAH and, c) ctrl

FT-IR spectroscopy was used to characterize the functional groups of HA, HA-g-SAH and ctrl hydrogel, as shown in Fig. 3.5. The HA spectrum revealed a broad band in the range of 3750–3000 cm^{-1}, which corresponds to overlapping –OH and –NH stretching vibrations associated with hydrogen bonding [260]. Peaks observed between 3000–2800 cm^{-1} were attributed to aliphatic C–H stretching[261]. Distinct absorptions within 1600–1350 cm^{-1} were linked to aromatic C=C and asymmetric COO^{-} vibrations, while a shoulder near 1720 cm^{-1} indicated the presence of carboxylic acid groups[262, 263]. Additional signals in the 1150–950 cm^{-1} region were assigned to C–O and C–O–C stretching modes of phenolic and polysaccharide structures, consistent with the complex chemical nature of humate.

The spectrum of ctrl showed fewer signals and was dominated by functional groups characteristic of acrylate salts. The most prominent features included symmetric and asymmetric COO^{-} stretching vibrations at ~1560 cm^{-1} and ~1410 cm^{-1}, respectively, along with strong C–O stretching bands in the 1200–1000 cm^{-1} range [264]. Notably, the absence of a carbonyl band around 1720 cm^{-1} confirmed that most carboxyl functionalities were present in their deprotonated (sodium carboxylate) form.

The HA-g-SAH spectrum displayed both HA and ctrl contributions, confirming the grafting process. The broad –OH band remained visible but with lower intensity, while the characteristic COO$^-$ absorptions of the acrylate chains became dominant. The carbonyl band near 1720 cm^{-1}, prominent in HA, was substantially reduced, suggesting conversion of COOH groups to COO$^-$ units during grafting. Moreover, the stronger C–O stretching bands at 1150–950 cm^{-1} and residual aromatic signals reflected the coexistence of humate and polyacrylate components within the copolymer. These changes in spectral features collectively demonstrate the successful incorporation of poly(sodium acrylate) chains into the humate framework, forming a hydrogel structure.

3.3.3.3 SEM

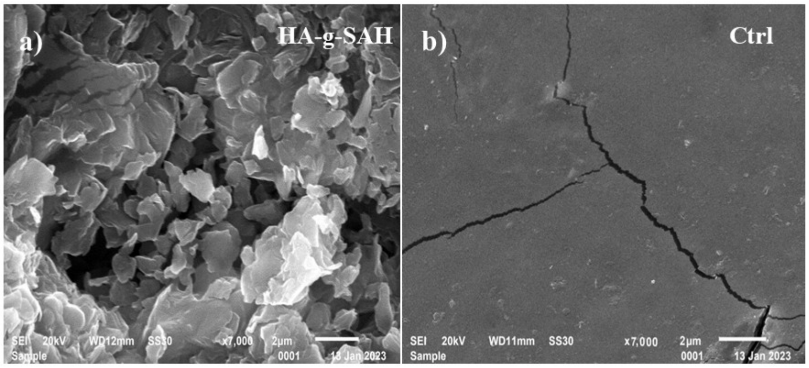
a)
HA-g-SAH
b)
Ctrl
SEI 20kV WD12mm SS30 x7,000 2μm 0001 13 Jan 2023 Sample
SEI 20kV WD11mm SS30 x7,000 2μm 0001 13 Jan 2023 Sample

Figure 3.6: SEM micrographs of a) HA-g-SAH and b) ctrl

SEM was employed to analyze the surface morphology of the hydrogels, allowing assessment of structural modifications resulting from the grafting of ammonium humate onto the poly(sodium acrylate) matrix, as depicted in Fig.3.6(a and b). The HA-g-SAH sample exhibited a heterogeneous surface with irregular, porous, and layered features, indicative of a more open and loosely packed network. Such a porous architecture is advantageous for water uptake and diffusion, supporting the hydrogel's improved swelling and retention capacity. Liu et al reported a similar porous and rough surface of CTS-g-PAA after introducing SH, resulting in CTS-g-PAA/SH superabsorbent.[265]

In contrast, the ctrl hydrogel showed a comparatively smooth and compact surface morphology, characterized by a dense structure with visible cracks but lacking significant porosity. The distinct morphological differences between the two samples confirm that incorporation of HA disrupts the compact structure of poly(sodium acrylate), introducing surface roughness and porosity that contribute to enhanced hydrogel performance.

3.3.3.4 XRD

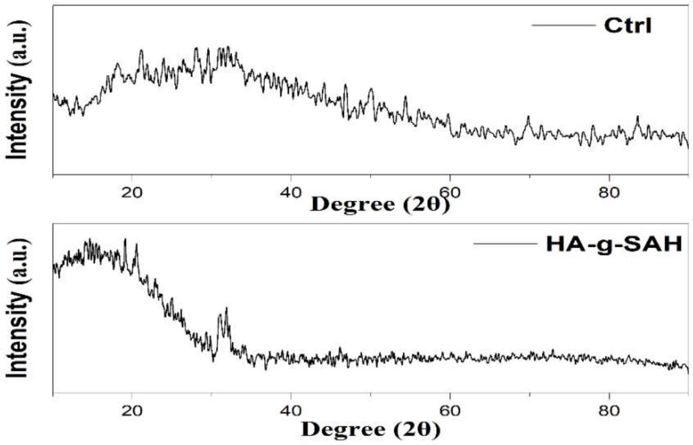

Figure 3.7: The plot of XRD of a) ctrl, and b) HA-g-SAH

XRD patterns were obtained for HA-g-SAH and ctrl hydrogels, as presented in Fig. 3.7, to investigate the influence of ammonium humate on microstructural arrangement. The XRD analysis showed that both HA-g-SAH and ctrl hydrogels exhibit broad diffraction halos within the 2θ range of 15–30°, indicative of an amorphous polymeric structure, consistent with previously reported findings.[225, 266] Similar results were reported by Bijendra Kumar et al., synthesized carboxymethylcellulose-g-poly(sodium acrylate)/$FeCl_3$ hydrogel beads, and observed broad peaks at 22.46° and 32.15°.[226]

The average molecular interchain spacing (<R>) was determined for HA-g-SAH and the ctrl sample from the strong diffraction peak at 31°, using Eq. (11-12).[267]

$$n\lambda = 2d\sin\theta \tag{11}$$

$$< R > = \frac{5}{8}\left(\frac{\lambda}{\sin\theta}\right) \tag{12}$$

The Ctrl hydrogel exhibited a spacing of 3.60 Å, while HA-g-SAH showed a much larger spacing of 7.66 Å. This significant increase in <R> demonstrates that grafting with ammonium humate expanded the network structure, likely due to steric hindrance from the bulky groups of ammonium humate, causing the molecular chains to spread apart. It resulted in higher average interchain spacing. Whereas, a lower value of <R> suggests a stronger intermolecular attraction and shorter interchain distances, which results in a more compact structure.[131]

3.3.3.5 TGA

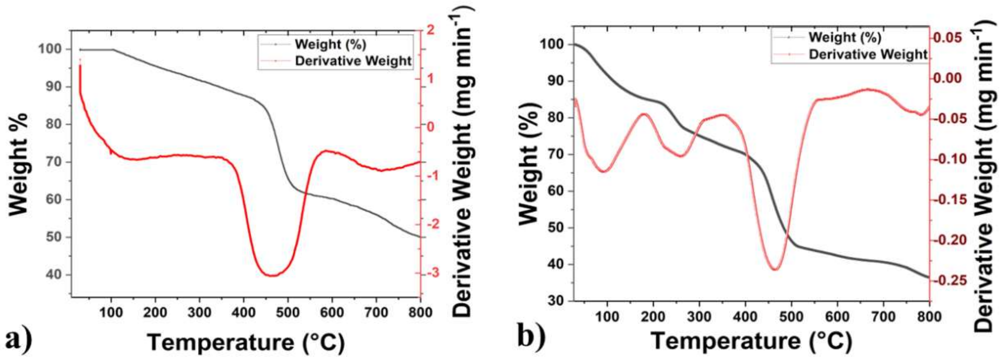

Figure 3.8: The plot of TGA of a) HA-g-SAH and b) ctrl

The thermal decomposition behavior of the hydrogels was evaluated using TGA and Differential thermogravimetry (DTG), as shown in Fig. 3.8 . Both the hydrogels exhibited a similar three-step degradation. DTG curves also showed multiple endothermic peaks for all samples.

The degradation process consisted of the following stages: initial weight loss up to 200 °C due to evaporation of moisture and decomposition of volatile compound; a second stage (200–400 °C) corresponding to poly(sodium acrylate) copolymer decomposition;[268] a third stage involving the breakdown of bonds between the polymeric backbone, grafting monomer, and crosslinker and weight loss in the 400–500 °C range associated with CO liberation from degrading C─O─C and C═O bonds, as well as aromatic ring degradation in HA-g-SAH.[222, 223] The residual mass per cent provides evidence of enhanced thermal stability due to the incorporation of lignite into hydrogels. HA-g-SAH and ctrl exhibited residual mass percentages of 50.26% and 34.4%, respectively, at 800°C. These distinctions demonstrated that the HA-g-SAH hydrogel has better thermal stability than the ctrl hydrogel.

3.3.4 Network Parameters

The synthesized hydrogel composite exhibited a brown colouration. The degree of crosslinking (ρ) was determined to be 2.536×10^{-16} and 5.47×10^{-20} mol·cm^{-3} for HA-g-SAH and ctrl, indicating a high crosslink density. Additional calculated parameters are summarized in Table 3.2.

Table 3. 2: Calculated value of network parameter.

Hydrogel	χ	$V_{2,s}$	$M_c \times 10^5$ (g·mol^{-1})	ρ (mol·cm^{-3})
HA-g-SAH	6.44	0.00627	1.163	2.536×10^{-16}
Ctrl	0.3172	0.00910	0.00735	5.47×10^{-20}

The network parameter analysis reveals that HA-g-SAH differs significantly from the ctrl hydrogel. The lower polymer volume fraction (V_2,s) of HA-g-SAH indicates greater swelling ability, while its much higher molecular weight between crosslinks (M_c) suggests a looser and more flexible network structure. Despite this, HA-g-SAH exhibits a higher crosslink density (ρ), likely due to additional interactions from humic acid functional groups that may have created localised crosslinking regions. The elevated χ value of HA-g-SAH reflects the reduced overall polymer–solvent affinity, yet the presence of hydrophilic groups in HA-g-SAH still promotes water uptake. Overall, grafting with ammonium humate in HA-g-SAH enhances swelling behavior and introduces a more heterogeneous, functionally interactive network than the ctrl.

3.3.5 Efficacy of loading efficiency (LE%)

The hydrogel formulation HA-g-SAH 14 exhibited a pesticide loading efficiency of 65.24%. However, LE% of ctrl was only calculated to be 54.35 %. The high loading capacity of HA-g-SAH can be ascribed to the hydrogen bonding and electrostatic interactions between the hydrogel matrix, functional groups of ammonium humate, and dinotefuran. Overall, the achieved loading of HA-g-SAH is considered adequate for pesticide delivery applications. Nevertheless, it may be further improved by optimizing the crosslinking density or increasing the initial pesticide concentration during loading.

3.3.6 *In vitro* release of pesticide

This study aimed to assess the performance of HA-g-SAH in agricultural fields. Thus, the in vitro pesticide release of dinotefuran loaded HA-g-SAH was performed in distilled water at 37 ˚C. The dinotefuran release was studied for up to 49 h using a UV–visible spectrophotometer, and it was observed that the pesticide release percentages individually for HA-g-SAH and ctrl were 78.45% and 64.21 %, respectively.

3.3.7 Pesticide release kinetics

The slow pesticide release process occurred sequentially through both formulations: initially, water enters the hydrogel and initiates swelling, establishing a dynamic equilibrium between the hydrogel's free water and the water surrounding the hydrogel. Concurrently, the hydrogel matrix swelled and facilitated the diffusion of the pesticide into the surrounding water, driven by osmotic gradients and the dynamic exchange of free water.[214] Moreover, for soluble agents present within a porous matrix, the rate of release is directly related to remaining concentration of the agent in the matrix, resulting in a gradual decline in the amount released over time.[269]

The release kinetics of dinotefuran from pesticide-loaded HA-g-SAH and ctrl hydrogels were evaluated using various kinetic models, as illustrated in Fig. 3.9. Table 3.3 summarizes the corresponding R^2 values for each model. Among the models tested, the Korsmeyer–Peppas model provided the best fit, indicating its suitability for describing the pesticide release mechanism from the hydrogels under ambient conditions. The model provides a detailed assessment of the release behavior, with the release exponent (n) determined as 0.876 for HA-g-SAH and 0.838 for the ctrl hydrogel. These n values indicate that non-Fickian diffusion is the dominant release mechanism, suggesting that both polymer chain relaxation and solute diffusion contribute to the release process. [58]. The higher 'n' value for HA-g-SAH suggests a more significant contribution of polymer relaxation/erosion in the release process, possibly due to ammonium humate grafting. The lower 'k' value for HA-g-SAH (0.368 for HA-g-SAH vs 0.3906 for ctrl) indicates a slower initial release rate.[270] This behavior aligns with the pesticide release profiles predicted by the Weibull model and its corresponding kinetic parameter, β'. The calculated values of 'β 'for HA-g-SAH and ctrl are 0.765 and 0.792. The calculated β values for HA-g-SAH and the ctrl hydrogel were 0.765 and 0.792, respectively. When the release exponent n falls between 0.5 and 1.0, the system exhibits non-Fickian behavior, indicating that the release mechanism involves a combination of polymer swelling and solute diffusion occurring at comparable rates.[271] The HA-g-SAH demonstrates maximum release in a duration of 49 h. In contrast, ctrl exhibits a relatively fast and less extended release over 33 h. Therefore, it can be concluded that introducing HA with poly(sodium acrylate) chains results in a slower release with an extended-release period.

This finding aligns with the study by Bajpai et al, which reported that CA/poly (SA) beads exhibit fair stability in their solvent medium, indicating a potential for extended release of the model drug.[272]

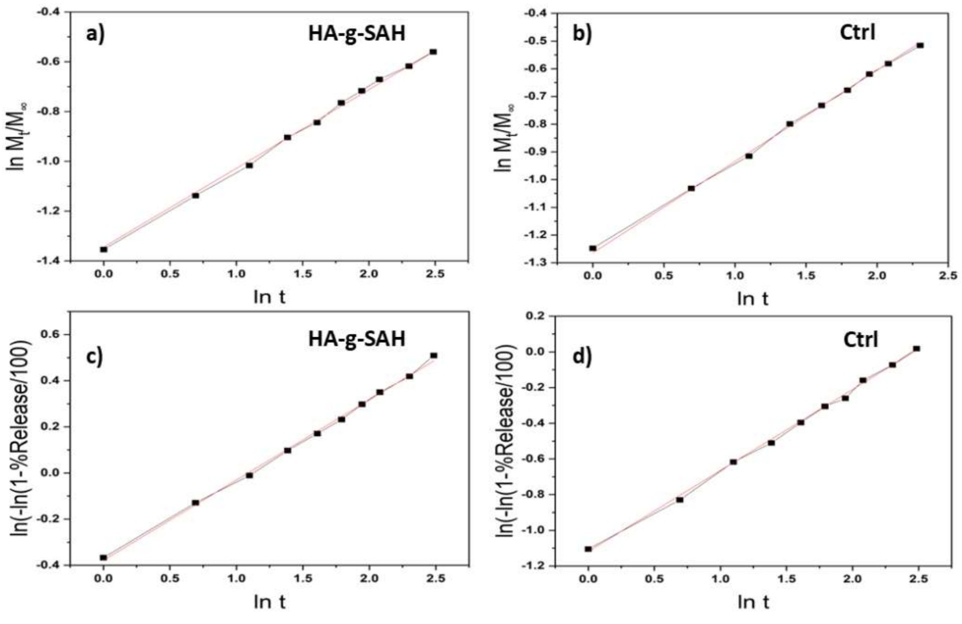

Figure 3.9: Kinetic modelling profiles: Korsmeyer Peppas model of a) HA-g-SAH, and b) ctrl; Weibull model of c) HA-g-SAH and d) Ctrl

3.3.8 Non-Fickian diffusion

When pesticides are encapsulated within hydrogels, their release into soil or water can occur through different mechanisms. In the case of Fickian diffusion, transport is primarily driven by concentration gradients. By contrast, non-Fickian (or anomalous) diffusion involves a combination of processes such as molecular diffusion, polymer relaxation, matrix swelling, and sometimes degradation of the hydrogel network [273, 274]. This anomalous behavior offers several advantages for agricultural applications. One of the key benefits is improved control over release profiles. Unlike purely Fickian diffusion, which may lead to an undesirable initial burst effect, non-Fickian systems achieve a more gradual and prolonged release due to the combined influence of diffusion and polymer matrix dynamics.[275] Such controlled release ensures steady pesticide availability, enhancing pest control efficacy over extended periods. Another significant advantage is the extension of release duration, as polymer relaxation and structural changes delay the overall release rate, reducing the need for frequent reapplications.[276] It also contributes to environmental protection, since slow and regulated release reduces leaching into groundwater and minimizes pesticide runoff, significant sources of ecological contamination. It improves effectiveness and reduces wastage, since pesticides are dispensed in response to real agricultural needs. A further advantage lies in the tunability of release kinetics: by adjusting the hydrogel's crosslinking density, polymer composition, or the addition of fillers such as bentonite, the release behavior can be fine-tuned. These findings suggest that non-Fickian diffusion provides a more efficient, sustainable, and environmentally responsible strategy for pesticide release than conventional Fickian diffusion.

Table 3.3: Release kinetics data of Dinotefuran from HA-g-SAH and ctrl using different mathematical models.

Model	Mathematical Equation	Parameter	Observation		R sq.	
			HA-g-SAH	Ctrl	HA-g-SAH	Ctrl
Korsmeyer–Peppas	$f = k_{kp}t^n$	k_{KP} = constant depicting the experimental parameters f = amount of the pesticide released n = release exponent	k_{KP} 0.3684 n 0.8761 AIC 20.461	k_{KP} 0.3906 n 0.8382 AIC 17.293	0.9796	0.9861
Weibull	$R(t)= 1-e^{-\alpha t^{\beta}}$	α= scale factor, β = shape factor	β 0.765	β 0.792	0.9842	0.9923

3.3.9 Water retention capacity

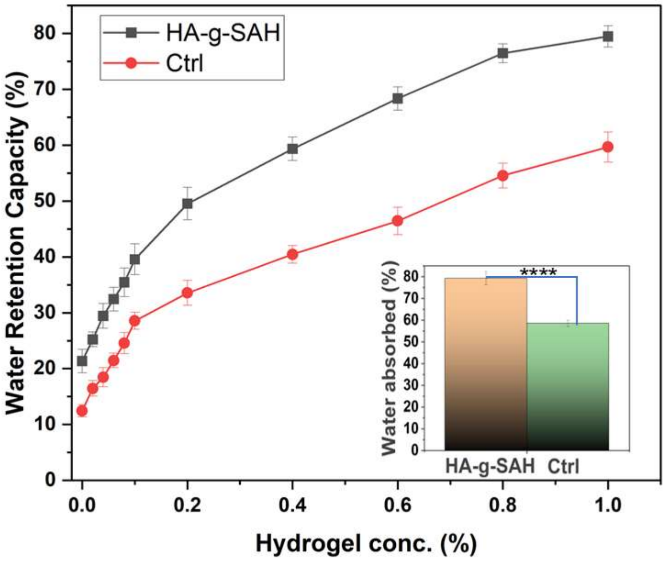

Figure 3.10: Water retention capacity plot of soil amended with HA-g-SAH and ctrl. Error bars represent standard deviation; ****$P < 0.0001$.

Table 3.4: ANOVA table for water retention capacity

Source	Sum of squares	DF	Mean square	F-Value	P-value
Water Retention Capacity	846.80	3	724.38	163.76	2.71×10^{-4}

The water retention capacity (WRC) of soils supplemented with HA-g-SAH and the ctrl was assessed over concentrations ranging from 0 to 1.0% (Fig. 3.10). Both amendments improved WRC relative to untreated soil; however, HA-g-SAH consistently outperformed the ctrl. At 1.0% loading, HA-g-SAH achieved 79.46 % WRC compared to 58.49 % for the ctrl, highlighting the superior efficiency of the grafted system. This enhancement is likely due to ammonium humate incorporation, which increases hydrophilicity and network porosity, as supported by SEM and XRD results. Collectively, these findings establish HA-g-SAH as a more effective hydrogel for improving soil moisture retention than ctrl.

The results of the ANOVA demonstrated statistically significant differences in water retention capacity, Dinotefuran release from hydrogels, between HA-g-SAH and the ctrl, as indicated by F-test p-values below 0.05, as shown in Table 4. A p-value of this magnitude implies less than a 5% probability of the null hypothesis being valid. Consequently, the observed variations can be attributed to the influence of the biopolymers employed in hydrogel synthesis rather than random experimental error.

3.4. Conclusion

This study presents HA-g-SAH as a slow-release system for controlled pesticide release and soil moisture enhancement. Structural characterisation using ^{13}C CPMAS NMR, FT-IR, SEM, XRD, and TGA confirmed successful grafting and network stability. Functionally, HA-g-SAH outperformed the ctrl hydrogel, exhibiting a markedly higher swelling capacity (320.92 $g \cdot g^{-1}$) and improved dinotefuran loading efficiency (65.24%), resulting in an extended and regulated release profile. Release kinetics indicated a non-Fickian mechanism driven by both diffusion and polymer relaxation. Soil amendment experiments further demonstrated substantial improvement in water retention, with values reaching 79.46% at 1% hydrogel incorporation, suggesting significant potential for mitigating drought-induced stress in crops. Conventional formulations promote rapid pesticide leaching. But the HA-g-SAH provides a sustainable approach to reduce environmental contamination while ensuring prolonged efficacy. By combining the nutrient-carrying capability of humic substances with a synthetic polymer scaffold, HA-g-SAH addresses two significant agricultural challenges—efficient pesticide delivery and improved water retention—within a single material platform. Thus, these findings highlight humate-based hydrogels as viable candidates for next-generation agrochemical systems to advance resource-efficient and sustainable farming.

3.5. Future Directions

Future research should focus on validating HA-g-SAH under real agricultural conditions across diverse soils, climates, and irrigation systems. Long-term studies on its biodegradability and ecological safety, including degradation products and soil-microbe interactions, are essential. Broadening the approach to other agrochemicals and developing multifunctional formulations that combine pesticides with nutrients could enhance system utility. Additionally, incorporating stimuli-responsive properties (e.g., pH, moisture) may enable more precise, on-demand release. Finally, scaling up production requires techno-economic and life-cycle assessments to ensure cost-effectiveness and sustainability at a commercial level.

CHAPTER-4

HARNESSING LIGNITE-BASED HYDROGEL FOR ENHANCED UV PROTECTION AND DELIVERY OF DINOTEFURAN IN AGRICULTURE

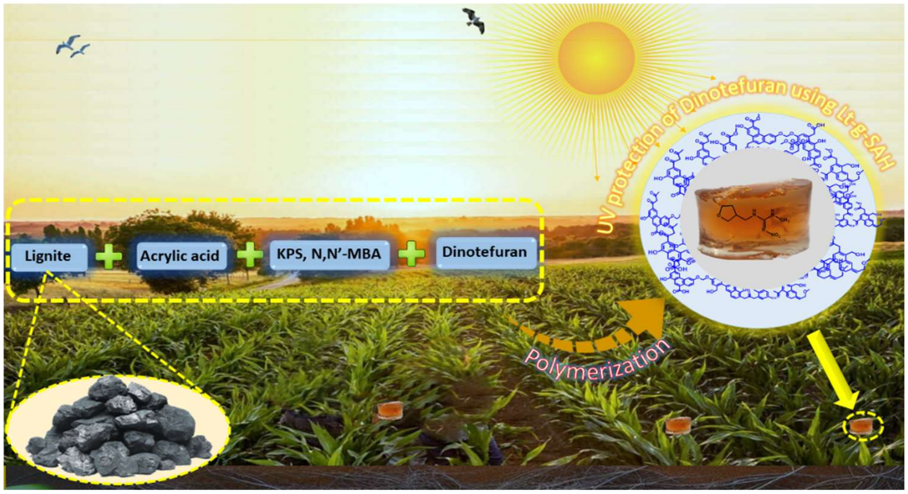
UV protection of Dinotefuran using Lt-g-SAH
Lignite
Acrylic acid
KPS, N,N'-MBA
Dinotefuran
Polymerization

4.1 Introduction

The agricultural sector relies heavily on pesticides to enhance productivity and ensure food security, but UV degradation often compromises their efficacy. The present study addresses this issue and introduces lignite-based poly sodium acrylate hydrogel as a protective shield against UV radiation for dinotefuran. The synthesis of lignite grafted poly(sodium acrylate) hydrogel (Lt-g-SAH) and control (ctrl) through graft co-polymerization method is detailed, with comprehensive characterization using ^{13}C CPMAS NMR, FT-IR, XRD, SEM, and TGA techniques. Additionally, the release kinetics of dinotefuran are investigated via UV-vis spectrophotometry to elucidate the controlled release. This study underscores the potential of lignite-based hydrogels as versatile platforms for sustainable agricultural practices, offering enhanced environmental performance in pesticide protection and delivery mechanisms. The incorporation of lignite not only enhances UV shielding but also improves water retention and offers potential as a nitrogen fertilizer carrier, addressing critical challenges in sustainable crop production. Through comprehensive evaluation, this study demonstrates the viability of lignite-based hydrogel as a cost-effective and eco-friendly solution for safeguarding pesticides and advancing agricultural sustainability.

The utilization of pesticides plays a pivotal role in boosting agricultural productivity and ensuring food security in modern agriculture [277]. Approximately 2 million tons of pesticides are currently applied to crops worldwide [237]. Among these pesticides, Dinotefuran ((RS)-1- methyl-2-nitro-3-(tetrahydro-3-furyl methyl) guanidine), a third-generation neonicotinoid (Figure 4. 1) stands out as a potent insecticide, acclaimed for its broad-spectrum efficacy against various pests, it is safe for crops, humans, and animals [239, 240, 278]. Dinotefuran has been used to manage a wide range of biting and sucking insects, including aphids (plant louse), whiteflies, and beetles. The chemical properties of dinotefuran are as follows: molecular mass (202.2 Da), water solubility (39,830 $mg{\cdot}L^{-}$

^{1}) @ 20 °C, Lipophilicity (log KOW) (−0.55), Soil Affinity (log KOC) value of 1.41, Soil Persistence (50–100 DT50 in days), Water Photolysis (<2 DT50 in days) [241, 242]. Dinotefuran can be applied on foliage, soil, nurseries, and paddy water through spraying, drenching, broadcasting, and pricking-in-hole treatments [244]. So, this study chose it as the model for the pesticides. However, Dinotefuran is easily photolyzed under sunlight, which leads to a low utilization rate and significantly reduces its effectiveness [279]. Photodegradation is a significant degradation pathway after spraying, directly impacting the sustainability of pesticides [280, 281]. As a result, improving Dinotefuan utilization and extending its anti-pest shelf life is critical for sustainable agricultural practice.

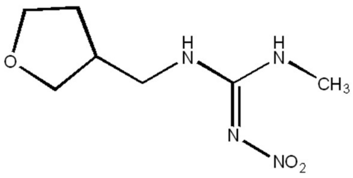

Figure 4.1: Molecular structure of Dinotefuran.

This degradation prevention is a challenge for the agricultural sector. To address this challenge, developing innovative formulations capable of protecting Dinotefuran from UV degradation is imperative. In recent years, hydrogels have emerged as promising candidates for efficiently encapsulating and delivering drugs[38, 39, 282–284] and agrochemicals [128, 245, 285–287]. Hydrogels are three-dimensional polymeric network having high water absorption [157]. Furthermore, crosslinking network chains within the hydrogel structure prevent dissolution and helps maintain its integrity.

Among various hydrogel materials, poly sodium acrylate hydrogels have garnered attention owing to their biocompatibility, tunable properties, and potential for controlled release.

This manuscript presents a novel approach utilizing Lt-g-SAH hydrogel as a protective matrix for dinotefuran against UV radiation. Lignite, a low-grade coal (Figure 4. 2) abundant in nature, offers an eco-friendly and cost-effective alternative for hydrogel synthesis. Lignite has high volatile content, chemical reactivity, and water content, low calorific value, and is easily weathered. Lignite accounts for about 40% of the total coal reserves in the world [288]. Electron paramagnetic resonance (EPR) spectroscopy confirmed that the lignite effectively screens UV irradiation, and no measurable effect of the irradiation on radical content was detected [289]. Another study by Jong Chan Ly states that introducing ether lignite lowered the UV transmittance of samples by approximately 20% [290]. Thus, incorporating lignite into Lt-g-SAH enhances its UV shielding properties. Incorporating lignite also provides additional benefits, such as improved water retention and soil conditioning. Lignite can also serve as a plant nutrition support mainly because of its high contents of humic substances, especially humic acids [289].

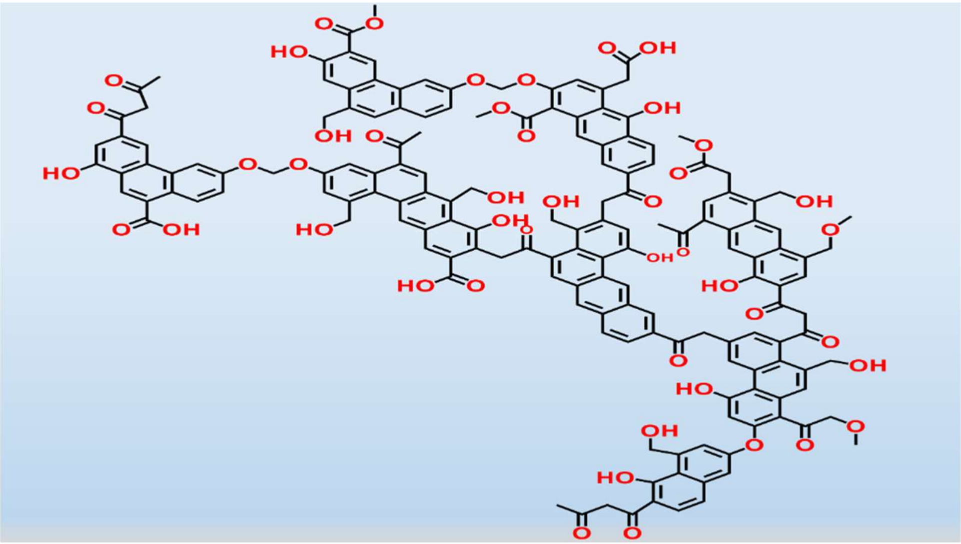

c

Figure 4.2: Molecular structure of lignite

Loss of Nitrogen (N) fertilizers is another critical challenge for sustainable crop production in modern agriculture. Lignite is generally acidic. It has more functional groups (hydroxyl, carboxylic, ketone, etc.), resulting in higher cation exchange capacity. The ammonium cations in the hydroxide state facilitated the displacement of protons within the Lignite molecules, leading to their dissolution and activation. Also, inherently water-insoluble lignite necessitated the preparation of its salt form as Ammonium lignite, which could be an alternative material for N fertilizer carriers. Thus, the lignite used in the present study has been treated with liquor ammonia to synthesize an ammonium salt of lignite [287]. Ammonium lignite as an N-carrier can extend supplementary benefits such as nutrient retention, carbon (C) sequestration, reduction in greenhouse gases and delivery of humic substances [247].

Lignite-based hydrogel as a novel pesticide UV protectant needs extensive exploration because the literature on this is either unavailable or very limited. Therefore, it was hypnotized that lignite as a pesticide UV protectant and slow-release pesticide carrier can produce a low-cost alternative to UV-protected chemical pesticides with improved environmental performance.

The manuscript aims to introduce a novel approach utilizing lignite-based poly sodium acrylate hydrogel to protect Dinotefuran from UV radiation while exploring its potential as a slow-release pesticide carrier. Here, lignite grafted poly(sodium acrylate) hydrogel (Lt-g-SAH) and control (ctrl) are synthesized using the graft co-polymerization method and characterized by FT-IR, XRD, SEM, and TGA to understand their structural and thermal properties. The effect of variation in parameters like initiator, biopolymer and crosslinker on the swelling index of hydrogels in distilled water is studied to optimize the synthesized hydrogels. Furthermore, the release kinetics of dinotefuran is investigated through UV-vis spectrophotometry, shedding light on the controlled release capabilities of the hydrogel.

By combining the UV shielding properties of lignite with the controlled release mechanisms of polysodium acrylate hydrogels, this study not only addresses the challenge of UV degradation in pesticides but also explores the potential of lignite-based hydrogels as versatile platforms for agricultural applications with enhanced environmental performance and sustainability.

4.2 Experimental

4.2.1 Materials

Lignite was procured from Neyvelli Pvt. Ltd Analytical grade reagents including acrylic acid (AA), sodium Hydroxide (NaOH), N' N-methylene bisacrylamide (MBA), liquor ammonia and potassium persulfate (KPS) were obtained from CDH Pvt Ltd. Dinotefuran (96.5%) was generously provided by the Institute of Pesticide Formulation and Technology, Gurugram, India. All the required water-based solutions were meticulously prepared with distilled water.

4.2.2 Preparation of Ammonium Lignite

Our previously developed method is used to prepare ammonium lignite [287]. Briefly, given the solubility of lignite in anhydrous ammonia solution, it was introduced into an ammonium hydroxide solution and subjected to stirring on a magnetic stirrer at 27 °C with a speed of 600 rpm for 24 hours.

4.2.3 *In situ* preparation of Dinotefuran loaded Lt-g-SAH

The hydrogels were synthesized following the methodology previously reported by our group [128]. The synthesis of Lt-g-SAH and ctrl variants involved utilizing the free radical co-polymerization method employing KPS as the initiator and MBA as the crosslinker. At ambient temperature, 7.2 g (AA) (neutralized with 8.07 mol·L^{-1} NaOH) was combined with 0.3 g of ammonium lignite. Subsequently, a determined amount of KPS and MBA were introduced and stirred continuously for 2 hours. It was followed by adding 10 mg·ml^{-1} of Dinotefuran solution in the resulting mixture. The solution was placed in a water bath set at 60°C for an additional two hours to facilitate the co-polymerization process. Post-synthesis, the hydrogel was sectioned into cylindrical pieces. Finally, the hydrogel underwent oven-drying at 50°C to achieve a constant weight [37, 38].

4.2.4 Gel content analysis

A 0.5 g dry Lt-g-SAH sample was immersed in 100 mL of distilled water overnight. Subsequently, the sample was soxhlet extracted using water for 2 hours to eliminate unreacted polymers and impurities. The resulting polymer was oven-dried at 60°C, followed by pulverization and storage in air-tight polyethylene containers for future experiments.

4.2.5 Pesticide Encapsulation efficiency (%) and Pesticide loading (%)

Tavakol et al. method was used to calculate the pesticide encapsulation efficiency (PEE%) and pesticide loading (PL%) with slight modifications [291]. 0.1 g of Lt-g-SAH and ctrl were immersed in 50 mL distilled water and swelled at room temperature for 24 h. Further, the swollen hydrogel was shattered, and centrifugation was carried out at 6000 rpm for 10 min. The amount of dinotefuran in the supernatant was monitored by a UV-vis spectrometer at 270.5 nm. The PEE % and PL % of Dinotefuran in the hydrogels were determined according to Eq. 1 and 2, respectively.

$$\text{PEE}\% = \frac{W_L}{W_T} \times 100 \tag{1}$$

$$\text{PL}\ \% = \frac{W_L}{W_H} \times 100 \tag{2}$$

In the context of the given parameters, W_L represents the weight of the dinotefuran present in the hydrogel, W_T denotes the theoretical amount of dinotefuran loaded into the hydrogel, and W_H is the weight of hydrogel beak taken into consideration.

4.2.6 Characterization

The structural and thermal characterization of the samples was performed using various analytical techniques. Solid-state ^{13}C Nuclear Magnetic Resonance Solid-state (^{13}C-NMR) spectroscopy was conducted on an ECX-400-II Jeol spectrometer equipped with a 9.38-T magnet and a 4 mm multinuclear solid-state probe at ambient temperature (25°C). Samples were packed into a 4 mm Magic Angle Spinning (MAS) probe, and spectra were recorded using the Cross-Polarization Magic Angle Spinning (CP-MAS) technique. Fourier Transform Infrared (FT-IR) spectroscopy was performed using a Perkin Elmer 2000 FT-IR spectrometer in Attenuated Total Reflectance (ATR) mode with a spectral resolution of 1 cm^{-1}. Scanning Electron Microscopy (SEM) was performed using an EVO 18 Research (Zeiss) microscope. Prior to SEM analysis, Lt-g-SAH and ctrl hydrogel samples were freeze-dried using a LabTech Freezer Dryer and subsequently gold-coated. Wide-angle X-ray diffraction (XRD) patterns were obtained using a RIGAKU instrument with Cu-Kα radiation ($\lambda = 1.5406$ Å) at 50 kV, with a resolution of 0.04 degrees. Thermogravimetric analysis (TGA) was carried out on a Perkin Elmer TGA 4000 instrument under a nitrogen atmosphere, with a heating rate of 10 °C min^{-1}.

4.2.7 Swelling of Lt-g-SAH and ctrl in distilled water

The swelling study for Lt-g-SAH and ctrl was performed by immersing oven-dried hydrogel discs in distilled water. At specific time intervals, the hydrogels were extracted from the swelling medium, excess water was blotted with filter paper, and subsequent weight measurements were taken until a consistent weight was achieved. The swelling index (SI) (g·g^{-1}) was determined with Eq. 3.

$$\mathrm{SI}\ (\mathrm{g{\cdot}g^{-1}}) = \frac{W_2 - W_1}{W_1} \tag{3}$$

Where, W_1 and W_2 are the weight of oven-dried and swollen hydrogel, respectively.

4.2.8 Agricultural applications of Lt-g-SAH

4.2.8.1 Maximum water-retention capacity (WH%) of soil treated with Lt-g-SAH and ctrl.

A study was conducted to assess the maximum water retention capacity of garden soil from Delhi Technological University. The experiment involved mixing various Lt-g-SAH and ctrl hydrogel concentrations with 50 g of dry soil (< 30 mesh size). These mixtures were placed in open-bottom PVC tubes (4.5 cm diameter) sealed with nylon cloth. Initial mass (W_1) was recorded. The samples were then saturated with distilled water until percolation occurred, and the final mass (W_2) was measured. A control experiment using soil without hydrogel was also performed. A control experiment with soil lacking hydrogel was also performed [213]. The hydrogel-treated soil's maximum water-retention capacity was calculated using Eq. 4. This method allowed for quantitative evaluation of hydrogel effects on soil water retention properties under controlled conditions.

$$\text{WH\%} = \frac{W_2 - W_1}{50} \times 100 \qquad (4)$$

4.2.8.2 UV protection of Dinotefuran

The UV protection of Dinotefuran by Lt-g-SAH and Ctrl hydrogel formulations were analyzed through a systematic UV exposure protocol. Prior to experimentation, all Dinotefuran-loaded hydrogel pellets from both groups were desiccated under dark conditions. The samples were then subjected to controlled UV irradiation in an ageing chamber equipped with three 6 W UV sources. To assess the progression of UV-induced degradation, samples were periodically extracted from the chamber at two-day intervals over a 30-day period. Quantification of non-degraded Dinotefuran in the hydrogel pellets was accomplished using UV spectroscopy. The analytical procedure involved immersing the extracted pellets in distilled water, followed by spectrophotometric measurement of the released Dinotefuran at an absorbance wavelength of 270.5 nm.[279]. To ensure statistical robustness and data reliability, the entire experimental protocol was conducted in triplicate.

4.2.8.3 Release study of dinotefuran in water

UV-visible spectrophotometry was used to generate the Dinotefuran standard curve. Dinotefuran concentrations, ranging from 4 to 20 $\mu g \cdot mL^{-1}$, were prepared in distilled water, and their corresponding absorbances were recorded at 270.5 nm. Origin

2021 software was used to generate a regression equation. Subsequently, the cumulative release of dinotefuran was also quantified via UV-vis spectroscopy based on the prepared standard curve.

Dinotefuran release kinetics were assessed by placing 100 mg of Lt-g-SAH and ctrl in 100 ml of distilled water. The beakers were subsequently agitated in a shaking bath at room temperature with a shaking rate of 80 rpm. At specified intervals, 1 mL of the supernatant was sampled from the system and replaced with equivalent fresh distilled water. The release kinetics of Dinotefuran from Lt-g-SAH were examined utilizing the First-order kinetics, Higuchi model, and Korsmeyer-Peppas models as outlined below: [234, 256]

First-order kinetics: $\log M_t = \log M_0 - (K_1 t/3.303)$

Higuchi model: $\frac{M_t}{M_\infty} = k_H t^{1/2}$

Korsmeyer -Peppas model: $\frac{M_t}{M_\infty} = k_{kp} t^n$

In these equations, M_t represents the cumulative release of Dinotefuran at the time 't' relative to the total loaded Dinotefuran. M_0 denotes the initial release amount, and k signifies the kinetic constant governing the release process.

4.2.8.4 Statistical analysis

All data were analyzed using OriginPro 2021, GraphPad Prism 10.2.3, ChemDraw 20.1.1, ImageJ and Microsoft Excel. The t-test was used to determine the statistical significance of the differences between the groups. Data are shown as means ± standard error of measurement. Statistical significance was defined using $P \leq 0.05$, $n = 3$.

4.3 Results and Discussion

4.3.1 Synthesis of Lt-g-SAH

The synthesis of Lt-g-SAH involves a complex chemical process. Initially, the reaction is believed to start with the thermal breakdown of APS, creating a sulfate anion radical. This radical interacts with an alcoholic OH group in ammonium lignite, forming a macro-radical. Subsequently, sodium acrylate and acrylic acid monomers act as receptors for these macro-radicals. The macro-radical-initiated monomers transfer free radicals to adjacent molecules through chain propagation. This process leads to the grafting of the lignite onto acrylic chains. The polymerization ends by joining two growing polymers by the crosslinker.

4.3.2 Characterization of hydrogels

4.3.2.1 ^{13}C CPMAS NMR

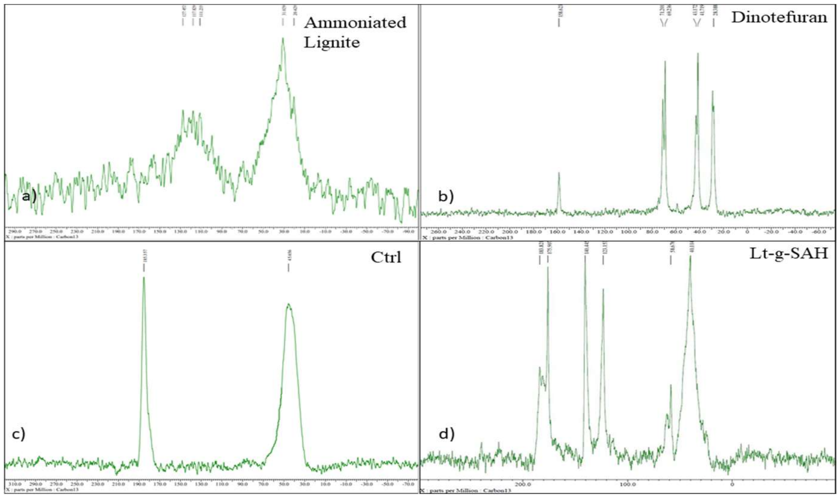

Figure 4.3: Solid-state ^{13}C-NMR of Ammoniated Lignite, b) Dinotefuran, c) Ctrl (without dinotefuran), and d) Lt-g-SAH.

Solid-state ^{13}C-NMR data were collected and processed using the Jeol Delta v6.0 program. This program uses ^{13}C CP/MAS-NMR at 100.52 MHz; a 2 ms contact time was applied when the acquisition time was 25.45 ms with a 3-second relaxation delay. The solid-state ^{13}C NMR spectra of lignite, dinotefuran and Lt-g-SAH are shown in Figure 4. 3, together with the solid-state spectrum of ctrl synthesized under the same conditions without lignite and dinotefuran. The carboxylate peak appears at approx. (183-185 ppm), methine and methylene resonances occur at about (40-49 ppm), representing the same chemical shifts in both spectra [37]. Despite the CP/MAS technique employed, the methine and methylene peaks in ctrl tend to overlap and could not be resolved entirely. Also, the methine and methylene of tetrahydrofuran in dinotefuran fall in between chemical shift values of 41-43 ppm, along with the peaks at aliphatic CH, CH_2 groups adjacent to NH in lignite at 36 ppm. The peak between 30-32 ppm arises due to the methyl group being closer to the carbonyl carbon. The peaks at 140.44 and 23.15 ppm in Lt-g-SAH are due to o-substituted aromatics, i.e. C-O, C-OH and C, CH from phenanthrene and anthracene of lignite, respectively [292].

4.3.2.2 FT-IR

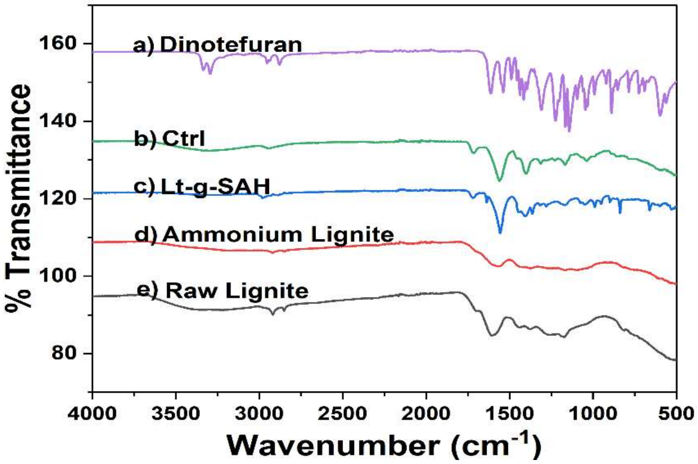

Figure 4.4: FT-IR spectra of a) Dinotefuran, b) Ctrl, c) Lt-g-SAH, d) Ammoniated Lignite, and e) Raw lignite.

Fourier Transform Infrared (FT-IR) spectroscopy analyzed Lt-g-SAH, ctrl, dinotefuran, ammoniated lignite, and raw lignite samples. As shown in Figure 4. 4, the spectra revealed characteristic peaks associated with various functional groups. A broad band at 3401 cm^{-1} was attributed to -OH stretching, while peaks at 2920 cm^{-1} and 2855 cm^{-1} corresponded to $-CH_2$ and $-CH_3$ stretching vibrations, respectively. The presence of free-COOH groups was indicated by a peak at 1710 cm^{-1}, suggesting incomplete neutralization in the initial synthesis. Carboxylate anionic peaks were observed at 1450 cm^{-1} and 1601 cm^{-1}, and an absorption peak at approximately 1590 cm^{-1} was assigned to aromatic ring C=C stretching [262, 263]. NH_4OH treatment of lignite resulted in the reduced intensity of the -COOH peak and a new peak at 1540 cm^{-1}, confirming ammoniated lignite salt formation [293]. Hydrogel spectra exhibited a broad peak in the 3300-3600 cm^{-1} range, indicating OH groups and aliphatic primary amines, with overlapping N-H stretching at 3308 cm^{-1} [260].

The hydrogel spectra (Lt-g-SAH and ctrl) exhibited a prominent band near 1535 cm^{-1}, attributed to the N-H moiety deformation of MBA [217]. Un-neutralized acrylic acid was identified by C=O stretching vibrations at 1710 cm^{-1}. Asymmetric stretching of carboxylate anions produced strong bands at 1404 cm^{-1} and 1554 cm^{-1}. The C-N group of MBA corresponded to a broad band and peak at 1323-1312 cm^{-1} [217]. The dinotefuran spectrum exhibited characteristic N-H stretching at approximately 3300 cm$^{-1,}$ and C-H stretches at 2880 and 2950 cm^{-1} [261]. These distinctive N-H and C-H peaks were also observed in dinotefuran-loaded Lt-g-SAH and ctrl samples, confirming successful incorporation into the hydrogels. Additional spectral features included a small peak at 1458 cm^{-1} (CH_2 deformation vibrations)[294], a strong peak at 1628 cm^{-1} (C=O stretching vibrations) [295], and a peak at ~1370 cm^{-1} (symmetric aliphatic C-H bending vibration of methyl groups, OCH_3). Notably, the band at ~1454 cm^{-1} showed higher intensity in Lt-g-SAH compared to ctrl, indicating the presence of lignite through symmetric aliphatic C-H vibrations of methylene (CH_2) and methoxyl (OCH_3) groups in the hydrogel.

4.3.2.3 SEM

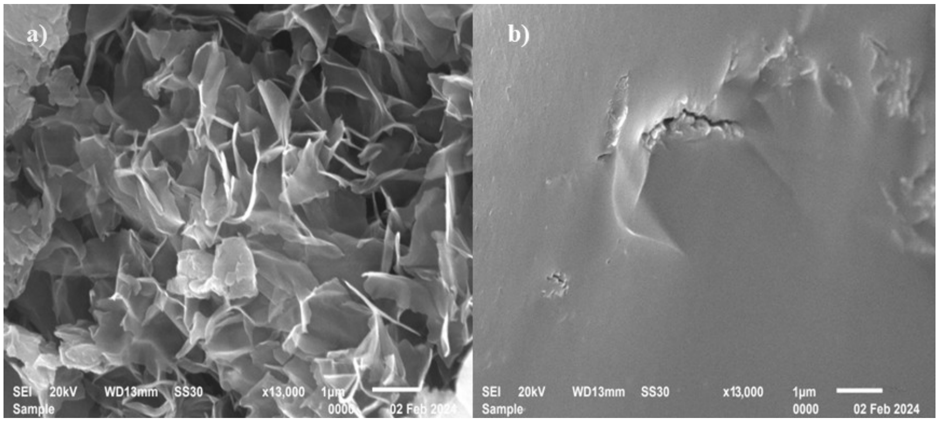
a)
b)
SEI 20kV WD13mm SS30 x13,000 1µm
Sample 0000 02 Feb 2024
SEI 20kV WD13mm SS30 x13,000 1µm
Sample 0000 02 Feb 2024

Figure 4. 5: SEM images of a) Lt-g-SAH and b) Ctrl

The surface morphology of Lt-g-SAH and Ctrl were observed using SEM at 13,000 X magnification. The grafting of lignite significantly impacts the morphology of Lt-g-SAH. Sample ctrl exhibits a smooth surface with few pores, as depicted in Figure 4. 5. In contrast, sample Lt-g-SAH displays a distinct porous and flaky structure. The pore diameter was calculated using ImageJ software and was found to be 0.95 µm. The surface observed is in alliance with some graphite-based products [296–298].

4.3.2.4 XRD

X-ray diffraction patterns were recorded for the synthesized Lt-g-SAH and Ctrl hydrogels. These XRD measurements were performed to analyze the effect of lignite presence on the microstructure arrangement. The XRD pattern of Lt-g-SAH and Ctrl shows a standard broad peak at $2\theta = 31.36°$ and 30.55°, respectively (Figure 4. 6c and 4. 6d). Kumar et al. synthesized carboxymethyl cellulose-g-poly (sodium acrylate)/$FeCl_3$ hydrogel beads where the hydrogel demonstrated broad peaks at 22.46° and 32.15° [226].

The XRD analysis of the coal sample from the Neyveli lignite field (Fig. 6a) indicates the dominance of clay minerals and carbonate phases. The principal mineral phases found in this coal are kaolinite, dolomite and siderite [299]. In the Lt-g-SAH, several minor peaks are present near 20°, which may be attributed to these lignite components. Significant peaks of dinotefuran and lignite are also present in the same region. After the *in-situ* loading, the peak of Dinotefuran at 10° (Figure 4. 6b) was shifted from higher to lower 2θ values in Lt-g-SAH and Ctrl, which indicates that dinotefuran is present in hydrogels, some amount of which is ionically crosslinked with polysodium acrylate chains.

The interplanar distance and average molecular interchain spacing (<R>) are calculated from the strong maximum at 31° in Lt-g-SAH and Ctrl using Eq. 5 and 6.

$$n\lambda = 2d\sin\theta \tag{5}$$

$$< R >= \frac{5}{8}\left(\frac{\lambda}{sin\theta}\right) \tag{6}$$

Table 4. 1: XRD data of Lt-g-SAH and ctrl

Sample	d (Å)	<R> (Å)
Lt-g-SAH	2.90	3.62
Crtl	2.88	3.54

The interplanar distances of Lt-g-SAH and ctrl hydrogels have been quantified as 2.90 and 2.88 Å, respectively, as shown in Table 4. 1. Additionally, the average molecular interchain spacing between polymeric chains in Lt-g-SAH and ctrl hydrogels has been determined to be 3.62 and 3.54 Å. A lower value of <R> suggests a stronger intermolecular attraction and shorter interchain distances, which results in a more compact structure. The presence of bulky groups of lignite on the polyacrylate chains leads to steric hindrance, causing the molecular chains to spread apart and resulting in a higher average interchain spacing and interplanar distance in the lignite-based hydrogel.

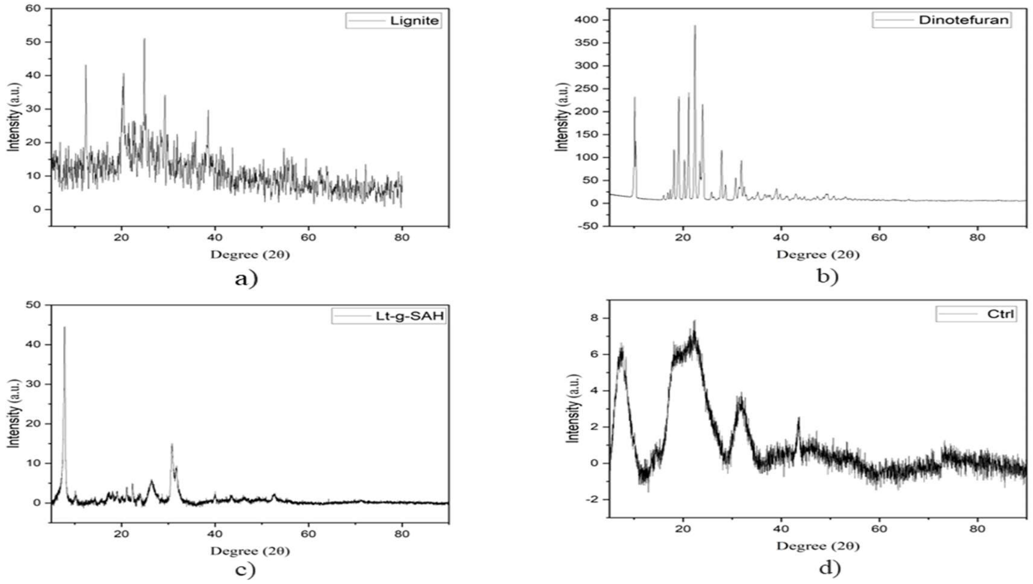

a) b) c) d)

Figure 4.6: X-ray diffraction (XRD) patterns of a) Ammoniated Lignite, b) Dinotefuran, c) Lt-g-SAH, and d) Ctrl.

4.3.2.5 TGA

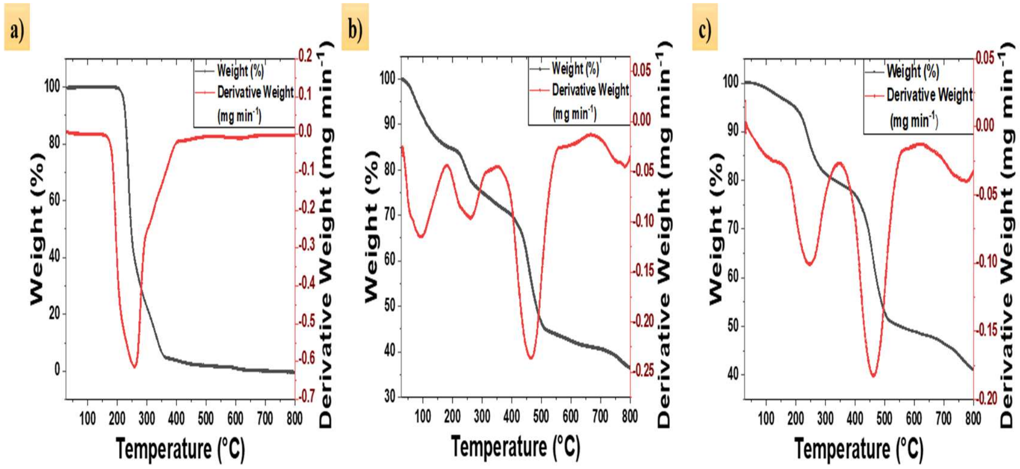

Figure 4.7: TGA plots of a) Dinotefuran, b) Ctrl, and c) Lt-g-SAH.

TGA was conducted to assess the thermal stability of dinotefuran, Ctrl, and Lt-g-SAH hydrogels, revealing multi-step degradation processes as illustrated in Figure 4. 7. Differential thermogravimetry (DTG) curves showed multiple endothermic peaks for all samples. The degradation process consisted of several stages: initial weight loss up to 200 °C due to moisture evaporation and volatile compound decomposition; a second stage (200-400 °C) corresponding to poly(sodium acrylate) copolymer decomposition [268], a third stage involving the breakdown of bonds between the polymeric backbone, grafting monomer, and crosslinker and weight loss in the 400-500 °C range associated with CO liberation from degrading C–O–C and C=O bonds, as well as lignite aromatic ring degradation in Lt-g-SAH [222, 223]. Dinotefuran exhibited a prominent rate change at approximately 250 °C [300]. This change point can also be observed in Ctrl and Lt-g-SAH, thereby supporting the presence of dinotefuran in both hydrogels.

The residual mass per cent provides evidence of enhanced thermal stability due to the incorporation of lignite into hydrogels. Notably, Lt-g-SAH and ctrl exhibited residual mass per cent of 41.01% and 36.39%, respectively, at 800 °C. Whereas dinotefuran completely degraded at 716.16°C. These distinctions demonstrated that the Lt-g-SAH hydrogel has better thermal stability than the ctrl hydrogel.

4.3.3 Swelling Index, (% PEF) and (% PL) of Lt-g-SAH and Ctrl in distilled water

The absorption of an aqueous solution is a crucial property of hydrogel. During the swelling process, the elastic polymer chains undergo extension, whereas the crosslinking junctions prevent the complete dissolution of the polymer [257]. The swelling index of two hydrogels at equilibrium in distilled water was assessed at different time intervals. Lt-g-SAH exhibited a swelling index of 187.1 $g \cdot g^{-1}$ at 35 hours, while Ctrl showed a 142.7 $g \cdot g^{-1}$ swelling index in 31 hours. The swelling study data analysis indicates that Lt-g-SAH demonstrated greater swelling capacity and prolonged duration than ctrl, suggesting that including lignite enhanced the synthesized hydrogel's swelling efficiency.

The encapsulation efficiency of Lt-g-SAH and ctrl hydrogel is 8.21% and 5.63%, respectively. ($p < 0.05$) The drug loading capacity increased from 64.36 % in ctrl to 70.12 % in Lt-g-SAH due to the incorporation of lignite. Compared to Lt-g-SAH beads, the encapsulation efficiency enhanced significantly ($p < 0.05$) by adding lignite. The enhancement of encapsulation efficiency indicates that the observed differences are associated with lignite's introduction during hydrogel synthesis and are not observed due to random errors. Lignite probably acted as a filler, increasing the crosslinking density of hydrogel and restricting the movement of SA chains, which hindered the exudation of dinotefuran from beads, resulting in improved drug loading efficiency [287, 301].

4.3.4 Effect of variation in concentration of different parameters on the swelling index of Lt-g-SAH

Flory researched the relationship between framework properties and water absorbency and concluded that a number of parameters determines solvent absorption by hydrogel. As a result, a systematic study was conducted to optimize hydrogel synthesis conditions focusing on key polymerization variables: biopolymer, initiator, and crosslinker concentrations.

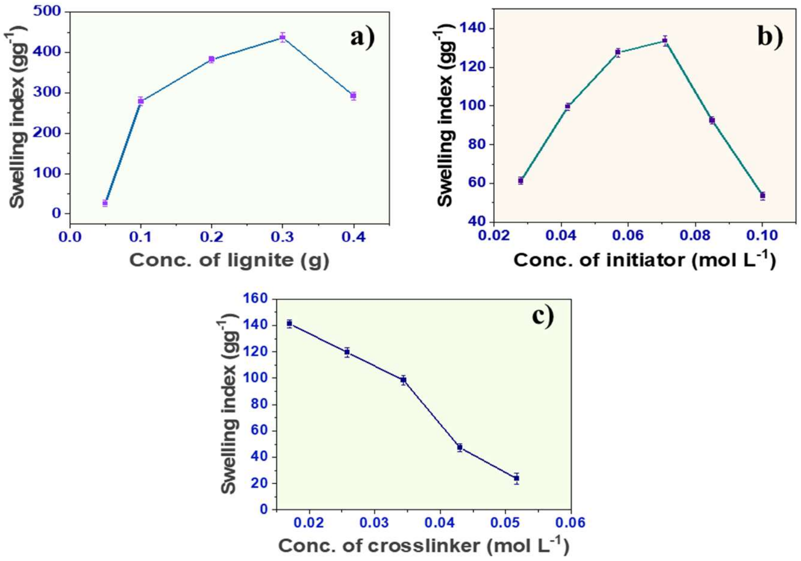

Figure 4. 8: Effect of variation in swelling index of Lt-g-SAH against: a) biopolymer, b) initiator, c) crosslinker. Error bars represent standard deviation.

4.3.5 Effect of variation in concentration of biopolymer on SI

The concentration of hydrophilic biopolymers is a critical parameter affecting the swelling characteristics of hydrogels. The impact of varying lignite content on hydrogel swelling behavior was studied with concentrations ranging from 0.05 g to 0.4 g (Figure 4. 8a). Incorporating lignite introduced a diverse array of hydrophilic moieties into the hydrogel matrix, resulting in an observed increase in the SI.

However, this trend was not monotonic. Upon reaching a lignite content of 0.3 g, a reversal was observed in the SI trend. This phenomenon may be attributed to a shift in the balance between the hydrogel structure's ionic and non-ionic hydrophilic groups. Specifically, at higher lignite concentrations, the proportion of ionic hydrophilic groups, such as carboxyl moieties, may have surpassed that of non-ionic hydrophilic groups like amide and hydroxyl functionalities [231]. This alteration in the hydrophilic group composition could explain the subsequent decrease in SI observed at lignite concentrations exceeding 0.3 g.

4.3.6 Effect of variation in concentration of initiator on SI

The reaction initiator plays a pivotal role in hydrogel synthesis by generating active sites on the polymer chains. This study investigated the influence of initiator concentration on the SI of the prepared hydrogels.

A biphasic relationship between initiator concentration and SI (Figure 4. 8b) was observed. As the initiator concentration increased from 0.02 to 0.10 mol·L^{-1}, SI rose correspondingly. However, this trend reversed at higher concentrations, with SI decreasing as initiator levels increased. The optimal distilled water absorption was achieved at an initiator concentration of 0.7 mol·L^{-1}.

This behavior can be explained by the interplay between free radical generation and network formation. The increasing amount of initiator likely produced more free radicals at lower concentrations (up to 0.07 mol·L^{-1}). It could lead to the formation of more chain ends within the network while simultaneously reducing the average kinetic chain length, potentially explaining the initial increase in SI.

Conversely, at initiator concentrations exceeding 0.07 mol·L^{-1} the reaction kinetics may have been altered significantly. The elevated initiator levels could have accelerated the polymerization rate, potentially resulting in a more compact network structure with reduced interstitial spaces. This structural change might account for the observed decrease in SI at higher initiator concentrations [108].

These findings highlight the critical importance of precisely controlling initiator concentration in hydrogel synthesis to achieve desired swelling properties, underscoring the complex relationship between reaction parameters and final hydrogel characteristics.

4.3.7 Effect of variation in concentration of crosslinker on SI

The study to analyze the effect of crosslinker concentration on hydrogel properties revealed a pronounced inverse relationship between the swelling index (SI) and crosslinker content, as illustrated in Figure 4. 8(c).

At crosslinker concentrations below 0.015 $mol \cdot L^{-1}$, insufficient graft polymerization was observed, resulting in the formation of a gelatinous substance lacking adequate structural integrity. This finding suggests a critical threshold of crosslinker concentration necessary for developing a stable hydrogel network.

As the concentration of MBA was increased beyond this threshold, we noted a marked decrease in SI. We attribute this phenomenon to additional crosslinking junctions within the polymer chains. The increased crosslinking density likely leads to a more constrained network structure characterized by reduced interstitial spaces and diminished free volume within the polymeric matrix [108, 232]. The observed relationship between crosslinker concentration and swelling behavior can be rationalized in terms of network topology and polymer chain mobility. Higher crosslinking densities typically result in more rigid structures with limited chain flexibility, impeding water uptake and subsequent hydrogel expansion.

These findings underscore the critical role of crosslinker concentration in modulating hydrogel swelling properties.

4.3.8 Agricultural application of Lt-g-SAH

4.3.8.1 Highest water retention capacity

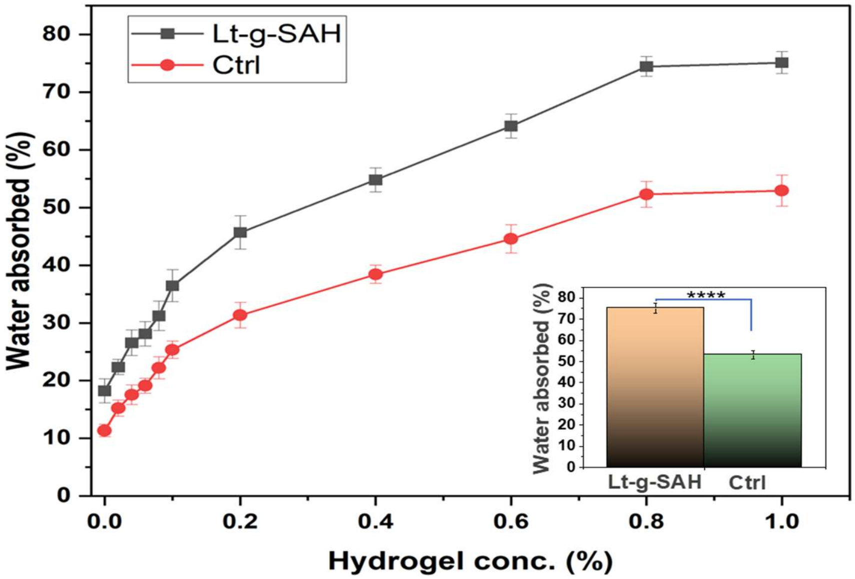

Figure 4.9: Water retention capacity plot of soil amended with Lt-g-SAH and Ctrl. Error bars represent standard deviation; ****P < 0.0001.

Water availability in soil is a critical factor influencing plant growth and development. This experiment evaluated the effect of Lt-g-SAH on water retention capacity (WH%) of soil, comparing it to a control soil sample. Figure 4. 9 illustrates the relationship between hydrogel concentration and water absorption in soil. Our findings demonstrate that incorporating Lt-g-SAH significantly enhanced the soil's water-retaining properties. Specifically, soil samples containing the synthesized Lt-g-SAH hydrogel exhibited a markedly higher water-absorbing capacity (75.12%) than the control soil (52.94%). This substantial improvement in water retention suggests that Lt-g-SAH could be an effective soil amendment for enhancing plant moisture availability. The hydrogel's ability to absorb and retain water may lead to several potential benefits in agricultural applications: Increased water use efficiency, reduced irrigation frequency, enhanced drought resilience, and improved nutrient retention.

4.3.8.2 UV protection of Dinotefuran by synthesized hydrogel

After exposure to ultraviolet light, the amounts of Dinotefuran released from Lt-g-SAH and Ctrl groups in distilled water were analyzed for 48 hours. Initial measurements revealed that Lt-g-SAH and Ctrl released 42.4 mg and 35.37 mg of Dinotefuran, respectively, in the absence of UV irradiation. Subsequent analysis after 30 days of continuous UV exposure demonstrated differential degradation patterns between the two groups. As shown in Figure 4. 10, the Lt-g-SAH group exhibited remarkable stability, with only a marginal decrease of 1.58% in Dinotefuran release, resulting in a final concentration of 41.73 mg.

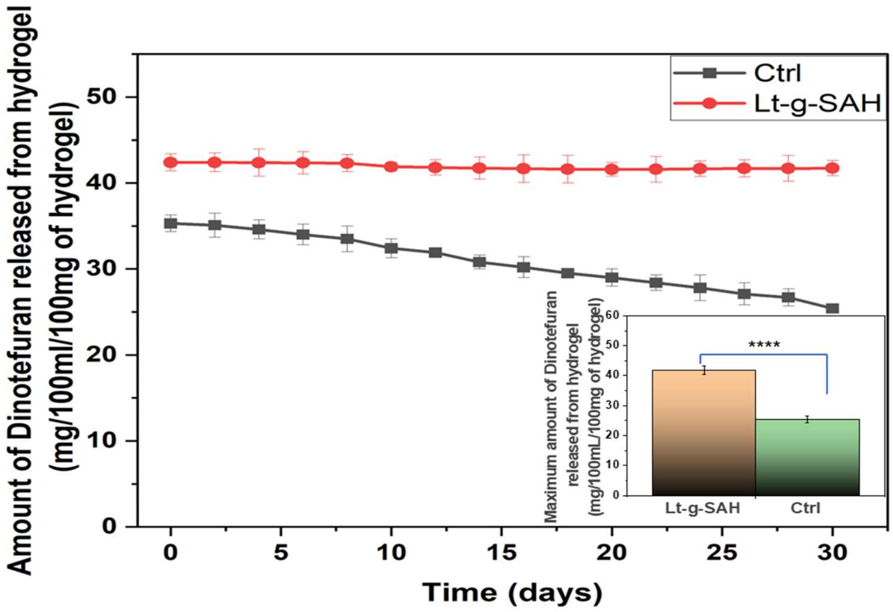

Figure 4.10: Amount of Dinotefuran released from Lt-g-SAH and Ctrl after UV irradiation. Error bars represent standard deviation; ****P < 0.0001.

In stark contrast, the Ctrl group experienced a substantial reduction of 28.11% in Dinotefuran release, with the final concentration diminishing to 25.42 mg. This marked disparity in pesticide release profiles can be attributed to the differential susceptibility of the formulations to UV-induced degradation over time. The results suggest that the

Lt-g-SAH formulation confers enhanced photostability to Dinotefuran, potentially offering improved efficacy and longevity in field applications where UV exposure is a significant factor.

The ANOVA results showed that the water retention capacity, Dinotefuran released from hydrogels and UV protection efficiency of Lt-g-SAH and ctrl is significant since the observed P-value (F-test) was smaller than 0.05, as shown in Table 4. 2. It indicates less than a 5% probability that the null hypothesis will be true. Thus, the observed changes are not due to the random errors associated with the measured parameter but rather to the change in the biopolymers used for hydrogel synthesis.

Table 4.2: ANOVA data of different studies.

Source	Sum of squares	DF	Mean square	F-Value	P-value
Water Retention Capacity	759.80	5	737.92	134.92	3.14×10^{-4}
Dino release study	343.28	5	227.92	7.90	4.82×10^{-2}
UV protection	431.19	5	394.47	7.70	2.80×10^{-3}

4.3.8.3 Release kinetics of Dinotefuran by Lt-g-SAH and Ctrl in distilled water

The release kinetics of Dinotefuran from Lt-g-SAH and control hydrogels were investigated in distilled water. As concluded from the swelling study, Lt-g-SAH exhibits better stability than ctrl in distilled water; hence, it is expected to release the entrapped pesticide over a long period. This finding aligns with the study by Bajpai et al., which reported that CA/poly (SA) beads exhibit fair stability in their solvent medium, indicating a potential for extended release of the model drug.[272]

The Lt-g-SAH demonstrates an almost 62.46% release in a duration of 39 h. In contrast, ctrl exhibits a relatively slower and less release (56.22%) extended over a time span of 33 h. In this way, it is clear that introducing lignite with poly(sodium acrylate) chains results in a slower release with an extended release period.

The process of slow pesticide release occurred through both formulations in a sequential manner: initially, water enters the hydrogel. The process initiates with water penetration into the hydrogel matrix, triggering swelling. It leads to a dynamic equilibrium between the free water within the hydrogel and the surrounding aqueous environment. Concurrently, the pesticide molecules entrapped within the hydrogel undergo dissolution and subsequent diffusion.

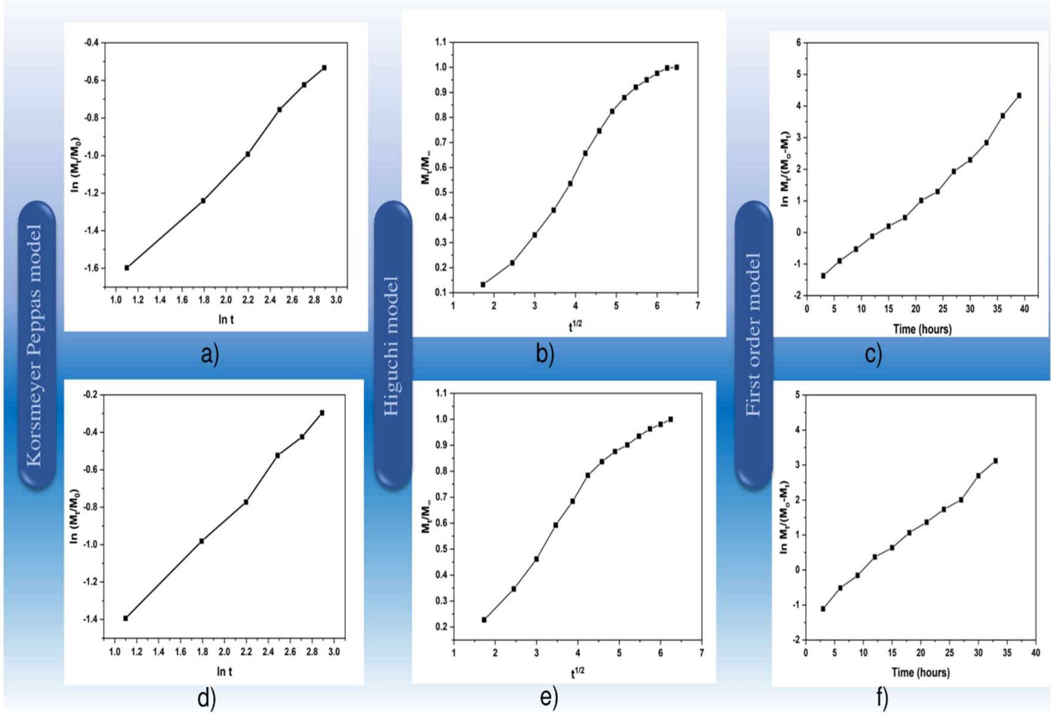

Figure 4. 11: a) Korsmeyer Peppas model of Lt-g-SAH, b) Higuchi model of Lt-g-SAH c) First order model of Lt-g-SAH d) Korsmeyer Peppas model of Ctrl e) Higuchi model of Ctrl f) First order model of Ctrl

The pesticide release into the surrounding water is driven by two primary factors: Osmotic gradients between the hydrogel interior and exterior and dynamic exchange of free water molecules [214]. The release mechanisms were analyzed using the Korsmeyer-Peppas model, Higuchi model, and First-order kinetics to understand the underlying processes involved in the release dynamics, as shown in Figure 4. 11.

Table 4.3: Release kinetics data of Dinotefuran using different mathematical models.

Model	Formulation	R^2	Parameter
Korsmeyer Peppas	Lt-g-SAH	0.9965	$n= 0.617$, $k_{KP}=12.060$ min^{-n}
	Ctrl	0.9931	$n=0.544$, $k_{KP}=15.164$ min^{-n}
Higuchi	Lt-g-SAH	0.9722	$k_H= 17.308$ $min^{-1/3}$
	Ctrl	0.9661	$k_H=16.378$ $min^{-1/3}$
First order	Lt-g-SAH	0.9904	$k_1=0.083$ min^{-1}
	Ctrl	0.9922	$k_1=0.091$ min^{-1}

From Table 4. 3, the Korsmeyer-Peppas and first-order models demonstrated the highest R^2 values (0.99) for both Lt-g-SAH and the control, indicating superior fit compared to the Higuchi model ($R^2 \approx 0.9722$ and 0.9661, respectively). It suggests that the Korsmeyer-Peppas and first-order models best describe the release kinetics. Notably, the Korsmeyer-Peppas model parameter 'n' exceeded 0.45 for both formulations, indicating a non-Fickian diffusional release mechanism. In non-Fickian or anomalous transport, pesticide release is influenced by diffusion and hydrogel swelling processes, with comparable rates for these phenomena. It results in time-dependent anomalous effects attributed to the gradual rearrangement of polymeric chains concurrent with diffusion [269]. The firm fit of the first-order release model further supports these time-dependent anomalous effects, as it assumes that the rate of concentration change is proportional to the concentration itself.

4.4 Conclusion

The study successfully synthesized and characterized Lt-g-SAH hydrogels for the controlled release of Dinotefuran, a pesticide. The hydrogels demonstrated an enhanced ability to swell and retain moisture compared to the control formulation. Through detailed release kinetics analysis, it was observed that Lt-g-SAH exhibited a more sustained and controlled release profile for Dinotefuran, aligning with the Korsmeyer-Peppas and First-order kinetic models, indicative of a non-Fickian diffusion mechanism. Incorporating lignite into the hydrogel matrix was crucial in achieving a slower and extended release, thus improving the hydrogel's efficacy in controlled pesticide delivery.

The study's findings also highlighted the superior stability of Lt-g-SAH in distilled water, suggesting its potential for long-term application in agricultural settings. The UV protection experiments further validated the hydrogels' effectiveness, as Lt-g-SAH showed significantly less Dinotefuran degradation under UV irradiation than Ctrl. It underscores the hydrogel's capability to safeguard the active ingredient, ensuring prolonged pest control activity.

In conclusion, the Lt-g-SAH hydrogel presents a promising advancement in controlled release systems for pesticides, offering a balanced approach to effective pest control and environmental sustainability. Future research should focus on field trials and evaluating the hydrogel's performance under various environmental conditions to fully realize its practical applications.

CHAPTER-5

NOVEL FORMULATIONS OF HUMIC ACID, LIGNIN, AND LIGNITE GRAFTED HYDROGELS FOR THE SLOW RELEASE OF THIAMETHOXAM.

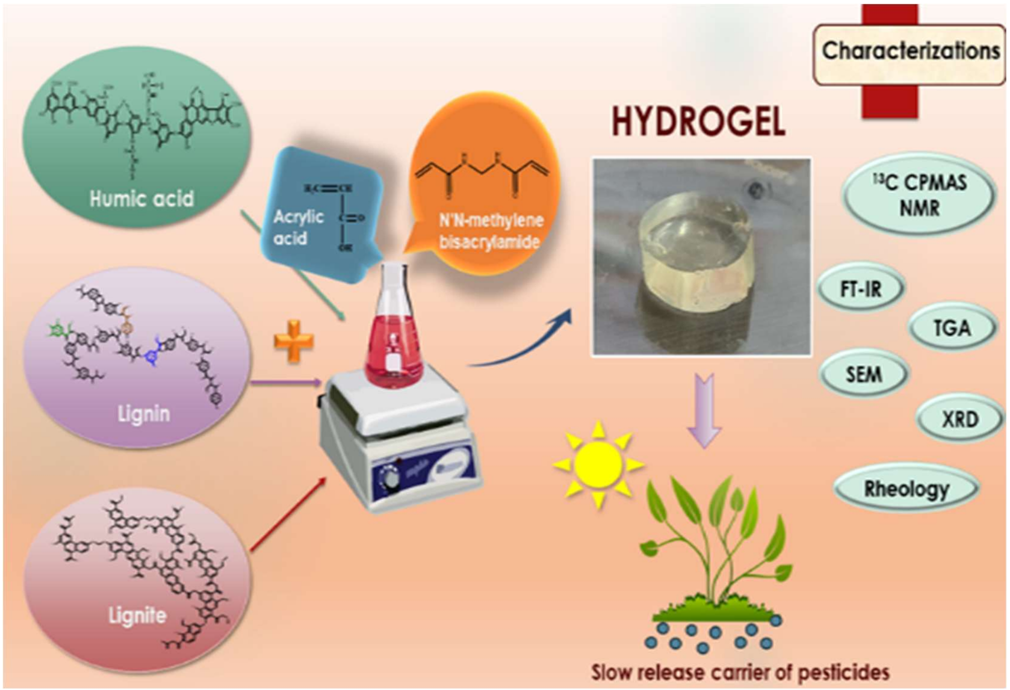
Humic acid
Lignin
Lignite
Acrylic acid
N'N-methylene bisacrylamide
HYDROGEL
Characterizations
^{13}C CPMAS NMR
FT-IR
TGA
SEM
XRD
Rheology
Slow release carrier of pesticides

5.1 Introduction

The objective of this study is to explore the novel use of natural polymers like Humic acid, Lignin, and Lignite based hydrogels for the formulation of pesticides and fertilizers that would reduce the residues in soil and run-off water that pose a threat to human health and the environment. We synthesized hydrogels by grafting Humic acid, lignin, and lignite onto acrylic acid with N'N-methylene bisacrylamide (MBA) for the ex-situ encapsulation of thiamethoxam, a common pesticide. Various characterization techniques including Fourier-transform infrared spectroscopy, Carbon-13 Solid-state Cross-Polarization Magic Angle Spinning Nuclear Magnetic Resonance, X-ray diffraction, Thermogravimetric Analysis, and Rheology were employed. The release kinetics of thiamethoxam in water from the developed formulations were analyzed using the Korsmeyer- Peppas model and the Weibull model. Humic acid and lignin-based hydrogels exhibited a long-sustained release for 49 hours, followed by lignite-based hydrogels (38 hours). According to ANOVA results, the change in biopolymer proved to be an effective factor in reducing the water evaporation rate, which decreased from 99% to 72.85% in the soil amended with synthesized hydrogels. In conclusion, the novel formulations of humic acid, lignin, and lignite exhibit potential as slow-release vehicles for pesticides and fertilizers. This study provides valuable insights for the research community, addressing the need to develop effective strategies for mitigating pesticide residues in soil and water bodies.

Today, pesticides have become the cornerstone of the predominant agricultural systems. These are important inputs for enhancing crop productivity and preventing major biological disasters. Worldwide, around 5 million tons of chemical pesticides are used every year, belonging to more than 100 classes with various modes of action.[302] However, more than 90% of conventional pesticide formulations run off into the environment and reside in agricultural products too. [303] Long-term exposure of pesticides to humans can cause reproductive complications, neurological disorders, immunological, and pulmonary diseases, and cancer. [304] Therefore, to increase the effectiveness of pesticide application and thereby reduce environmental risk, it is essential to develop innovative methods for pesticide formulation technologies. The controlled release of pesticides through hydrogel is a solution to the above problems. This means that the active components of the pesticide are released within a predetermined time and conditions via formulation with supporting materials.[305] Hydrogels are moist and flexible materials that possess a three-dimensional interlinked matrix, featuring remarkable water retention capabilities.[306] Hydrogels are classified as physically cross-linked [307], chemically cross-linked [308], or double-network [309] hydrogels based on the cross-linking techniques used. Secondary interactions result in the development of physically cross-linked hydrogels. On the other hand, several techniques such as water-soluble polymer cross-linking, radiation polymerization, free-radical polymerization, and polymer inter-transmission networks may be used for developing chemically cross-linked hydrogels.[310] Among these, the free radical polymerization technique is economical and gives higher swelling. Hydrogels have applications in biomedical [39], food and agriculture[282, 311], textile, cosmetics, water purification, remediation, and separation fields [312]. Economical controlled-release pesticide formulations should be developed using natural biodegradable polymers. Nowadays, researchers need to pay attention to the omnipresent- favorable, sustainable, and large-scale assets like humic acid, lignin and lignite to be used as a chemical component in various syntheses. The scale and importance of these “sleeping giants” is unimaginably large.[7]

The term Humic acid is used for the polymeric, brown-black, alkali-soluble acids found in soils, sea grasses, plants, sediments, fungi, and marine and terrestrial waters. It is the most active component of soil organic matter and a main fraction of humic substances.[313] Humic acids play multiple important roles in agriculture such as improving water holding capacity, soil structure, and texture, preventing microbial growth, increasing nutrient availability to soil, and transporting micronutrients to plants.[314]

Lignin is an aromatic hetero-polymer present as a constituent of the plant cell wall, along with cellulose and hemicellulose. Its functions include both defense against pathogens and mechanical support. The waste from the paper and bioethanol industries produces 100 million tonnes of this biopolymer annually. Lignin is estimated to make up 15–35% of lignocellulosic biomass.[315]

Often called brown coal, lignite is a soft, brown, combustible sedimentary rock that develops when peat naturally compresses.[316] It has poor thermal stability, the highest volatile content, and strong chemical reactions with low thermal safety.[317] The structures of Humic acid[4], Lignin[318], and Lignite[288] have been represented in Figure 5. 1.

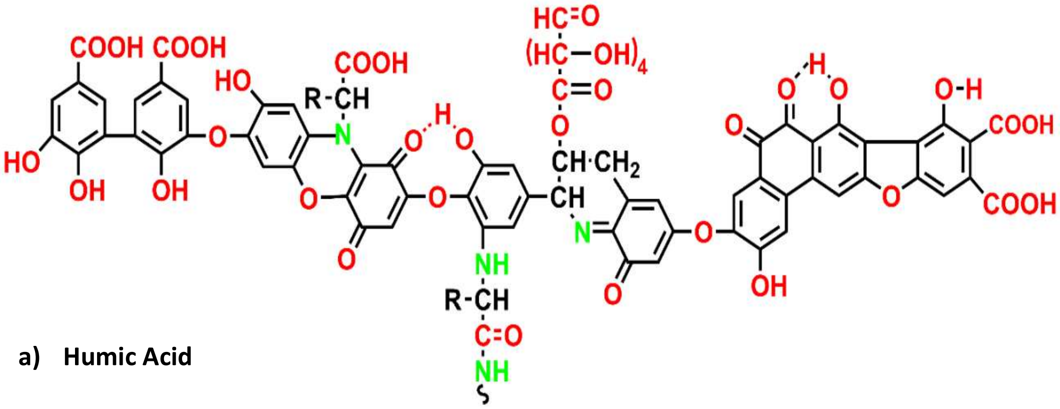

a) Humic Acid

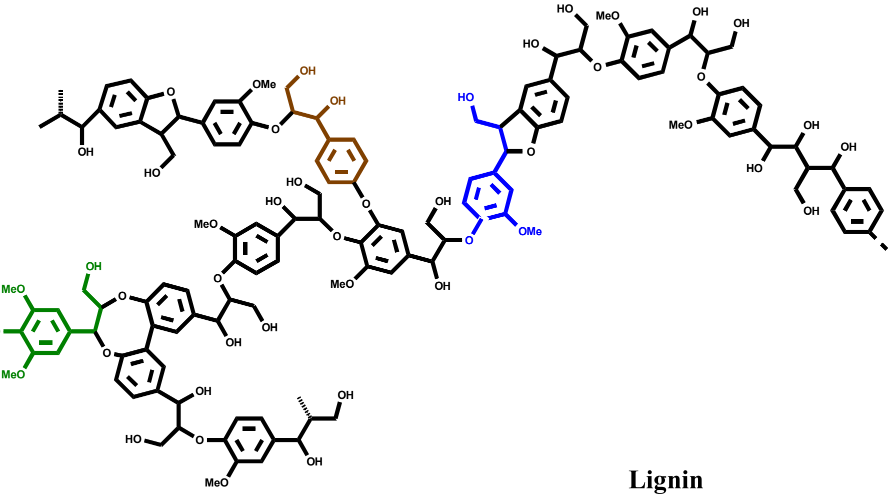

b) **Lignin**

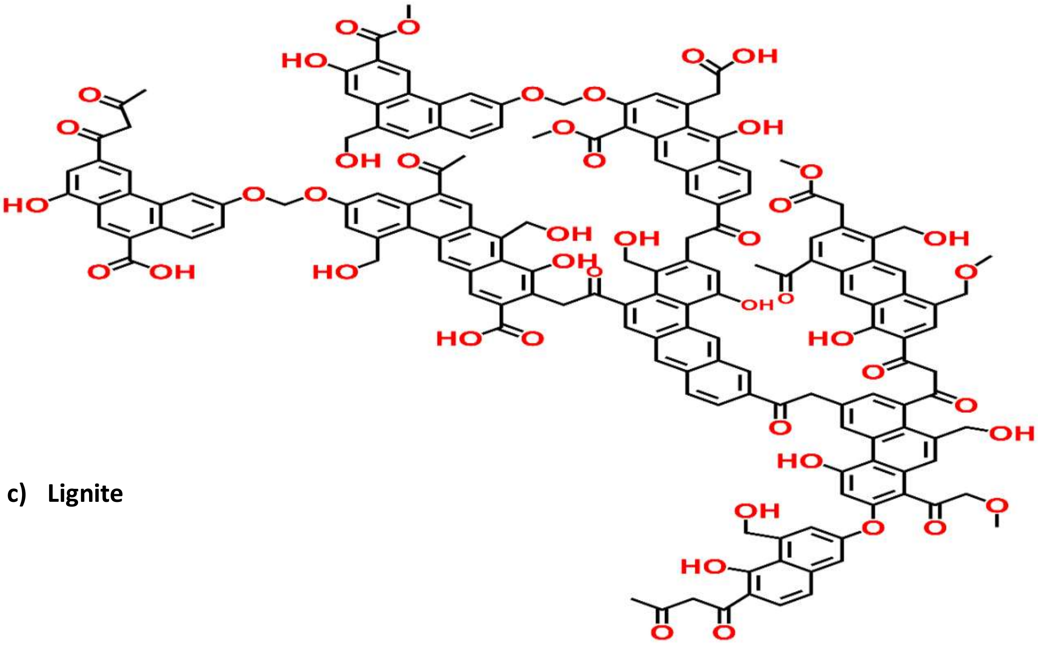

c) Lignite

Figure 5. 1: Chemical structures of a) Humic acid, b) Lignin, and c) Lignite.

Thiamethoxam (3-(2-chloro-1,3-thiazol-5-ylmethyl)-5-methyl-1,3,5-oxadiazinan4-ylidene(nitro) amine) has been chosen as the model insecticide in the present study due to its broad spectrum of activity against insects. The efficacy of this systematic pesticide for controlling several pests in different crops is very well established.[319]

Humic acid and lignite are well explored in geochemistry and agriculture [35, 320–326], it is just that in our opinion a polymer perspective on this relevant class of materials is missing. This leads to a pure chemical lab synthesis of ammonium humate and ammonium lignite and their utilization as an advanced polymer material like hydrogel.

In the present study, the above-mentioned natural polymers i.e. Humic acid, lignin (lignosulfonic acid sodium salt), and lignite are used to fabricate novel thiamethoxam loaded hydrogels. Humic acid grafted poly(sodium acrylate) hydrogel (HA-g-SAH), Lignosulfonic acid sodium salt grafted poly(sodium acrylate) hydrogel (LS-g-SAH), Lignite grafted poly(sodium acrylate) hydrogel (Lt-g-SAH) and control (ctrl) were synthesized by using the graft co-polymerization method. The synthesized hydrogels were characterized by FT-IR, XRD, SEM, and TGA. Their viscoelasticity has been studied using rheology. The release kinetics of thiamethoxam is studied through UV-vis spectrophotometry.

This work aims to synthesize formulations for thiamethoxam using Humic acid, lignin, and lignite-based hydrogels as a carrier. This will reduce the environmental influences of pesticide runoff into the water and contribute to the controlled release of the pesticides.

5.2 Experimental

5.2.1 Materials

Lignosulfonic acid sodium salt (LS) (M wt. ~52,000) was purchased from Sigma Aldrich. Humic acid, Acrylic acid (AA), Sodium Hydroxide (NaOH), and N'N-methylene bisacrylamide (MBA) were purchased from CDH Pvt Ltd. Lignite was obtained from Neyvelli Pvt. Ltd. Liquor ammonia and Potassium persulfate (KPS) were bought from SD Fine chem Ltd. Thiamethoxam (96.5 %) m/m was obtained through the courtesy of the Institute of Pesticide Formulation and Technology, Gurugram, India. All necessary water-based polymerization solutions were prepared using distilled water.

5.2.2 Preparation of Ammonium Humate and Ammonium Lignite

Humic acid and Lignite are water-insoluble. Thus, their salt in the form of Ammonium humate and Ammonium lignite was prepared. Since Humic Acid and Lignite are readily soluble in anhydrous ammonia solution (30%), these were put into ammonium hydroxide solution in a ratio of 1:15 by mass and stirred on a magnetic stirrer at 27°C and 600 rpm for 24 hours. This was followed by vacuum filtration and complete oven drying at 80°C. Ammonium cations in the hydroxide state were able to replace the protons into Humic acid and Lignite molecules resulting in their dissolution and activation.

5.2.3 Characterization of synthesized hydrogels

The FTIR spectra in the range of 4000 cm^{-1} to 650 cm^{-1} were recorded using Perkin Elmer 2000 FT-IR spectrometer at a resolution of 1 cm^{-1} to identify the present functional groups of synthesized hydrogels. The solid-state ^{13}C-NMR analysis of samples was carried out on a Bruker Ascend-400 spectrometer operating at 400 MHz. The surface morphology was determined through SEM on EVO 18 Research, Zeiss, instrument. TGA was conducted with a uniform heating rate of 10 °C/min on Perkin Elmer, Thermogravimetric Analyzer, TGA 4000 in the Nitrogen environment. The structure of hydrogels was described using XRD recorded through RIGAKU with source Cu-Kα performed at a voltage of 50 kV with a resolution of 0.04°. The rheological analysis was carried out using the Anton Par Rheometer (Model: Anton Par, Modular Compact Rheometer, MCR 302) with a PP-25 parallel plate and 2.5mm inter-platen gap.

5.2.4 Swelling experiment

The technique used to evaluate the swelling study of HA-g-SAH, LS-g-SAH, and Lt-g-SAH is well-established and has been documented in earlier research. In short, the samples under investigation were dried at 50 °C till complete moisture was removed, weighed, and then placed in distilled water at room temperature. The samples were weighed at predetermined intervals after being wiped using filter paper to eliminate extra water.[6] The swelling index was defined using equation 1:

$$\text{Swelling Index } (\text{g}\cdot\text{g}^{-1}) = \frac{W_O - W_d}{W_d} \quad (1)$$

in which W_d and W_0 are the dry and hydrated weight of the hydrogels, respectively.

5.2.5 Water evaporation study

A water evaporation test was used to investigate hydrogel-treated soil's ability to retain water within its system structure for 55 days. Oven-dried soil (at 60°C for 48 hours) was used to prepare different sets of hydrogel-treated soil along with a control set. Each mixture was fed with 50 ml of distilled water. The total weight of water, soil, and hydrogel is kept as 'M_i.' Then, these were placed at room temperature and weighed daily (M_t) [214]. Here, the effect of the addition of HA-g-SAH, LS-g-SAH, Lt-g-SAH, and ctrl on soil is studied by considering the water evaporation loss value from each hydrogel-treated soil samples as well as untreated soil (blank soil).[214] The water evaporation ratio (WER) was determined using equation 2. The evaluation of the results of WER was carried out using analysis of variance (ANOVA) which includes F-test and P-values.

$$\text{WER} = \frac{M_i - M_t}{50} \times 100 \tag{2}$$

Where, M_i is the initial total weight of water, soil, and hydrogel and M_t is the total weight of the mixture after a fix interval of time.

5.2.6 Determination of loading efficiency of thiamethoxam in the synthesized hydrogels

The difference in the total amount of thiamethoxam loaded into HA-g-SAH, LS-g-SAH, and Lt-g-SAH and the amount of free thiamethoxam in the respective supernatant was used to determine the amount of thiamethoxam loaded in hydrogel formulations [252]. The analysis was done using UV–Vis spectrophotometer (Shimadzu UV-Spectrophotometer, UV-1800) at 254 nm. Later, the standard curve was used to convert the absorbance of samples to the concentration of thiamethoxam. The loading efficiency (LE) of thiamethoxam was calculated using the following equation 3.

$$\text{LE (\%)} = \frac{A_{total} - B_{free}}{A_{total}} \times 100 \tag{3}$$

where A_{total} is the amount of thiamethoxam used to prepare HA-g-SAH, LS-g-SAH, and Lt-g-SAH, and B_{free} is the amount of freely present thiamethoxam in the supernatant.

5.2.7 *In vitro* loading and release of thiamethoxam by HA-g-SAH, LS-g-SAH, and Lt-g-SAH

Thiamethoxam was loaded onto the hydrogel by immersing a pre-weighed dry HA-g-SAH, LS-g-SAH, and Lt-g-SAH into a thiamethoxam solution (2000 ppm) for 24 h. After that, the swollen gels were removed from the water and dried till a constant weight was achieved.

The amount of thiamethoxam released by HA-g-SAH, LS-g-SAH, and Lt-g-SAH was evaluated by soaking the dried thiamethoxam-loaded samples in a beaker with 100 ml of distilled water at ambient temperature. Later, 1 ml of dissolved water was drawn from the medium at fixed intervals to observe the released thiamethoxam, and the same amount of distilled water was added to the beaker to keep the volume constant [215]. The analysis of thiamethoxam in the supernatant was done by measuring its absorbance at 254 nm using UV–vis spectrophotometer.[254] Also, the standard calibration curve was used to formulate the below-mentioned equation 4 for the determination of thiamethoxam concentration (C).

$$C\ (ppm) = \frac{A - 0.1735}{0.0002} \tag{4}$$

Where C is the concentration of thiamethoxam in the water sample and A is the UV-vis absorbance of the solution of unknown concentration.

5.3 Results and Discussion

5.3.1 Mechanism for the formation of HA-g-SAH, LS-g-SAH, and Lt-g-SAH

The KPS initiator generated anion radicals which further helped to produce phenoxy radicals on ammonium humate, lignosulphonate, and ammonium lignite. The active radicals also reacted with the vinyl groups of sodium acrylate, leading to the propagation of chain-forming poly sodium acrylate.[157, 232] Ganguly et al. reported that a divinylic monomer i.e. MBA generates interchain covalent crosslinking because of its multifunctional character.[327] Thus, poly(sodium acrylate) propagated until crosslinked and terminated by MBA to form HA-g-SAH, LS-g-SAH, and Lt-g-SAH. The electrostatic repulsion created by the negatively charged carboxylate ions in the poly(sodium acrylate) polymer chains will lead to a network expansion. This further improved the hydrogel's capacity to absorb water.[213]

5.3.2 Characterization of hydrogels

5.3.2.1 Fourier-transform infrared spectroscopy (FT-IR)

The FT-IR of all the formulations is shown in Figure 5. 2. Bands at 1586-1556 and 1402-1406 cm^{-1} are due to carboxylate group stretching of acrylate.[264, 328] The stretching vibration of associated -OH in all the hydrogels is observed between 3280-3303 cm^{-1} as a broadband. The peaks of free-OH groups present in Humic acid, Lignite, and Lignosulphonate sodium salt are observed at 3677 cm^{-1}.[329] Compared to IR peaks of ctrl a peak around 2966-2986 cm^{-1} is introduced in all the three HA-g-SAH, LS-g-SAH, and Lt-g-SAH hydrogels.[69] This is due to the gradual increase in C–H stretching because of the grafting of Humic acid, Lignosulphonate salt, and Lignite onto the hydrogel.[330] A peak at 1637 cm^{-1} in HA-g-SAH signifies the presence of conjugated C=C. The strong peak around 1058 cm^{-1} arises due to C–O–S stretching vibration and the peak at 1168 cm^{-1} is assigned to O=S=O antisymmetric stretching vibration in the LS-g-SAH.[69]. The strong bands at 1404 cm^{-1} and 1554 cm^{-1} are due to the asymmetric stretching in the carboxylate anion.[331] The broad band and a peak at 1323-1312 cm^{-1} correspond to the C-N group of MBA.[217] The peak around 3677 cm^{-1} is the characteristic peak of free O-H present in all three natural polymers, thereby confirming their presence in the hydrogels.

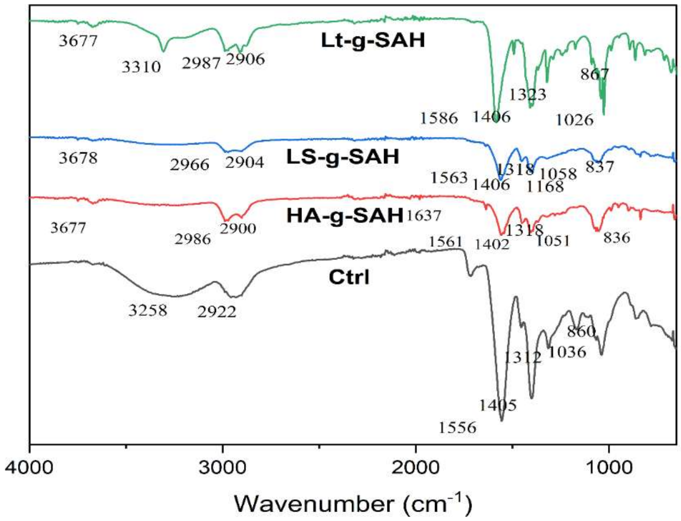

Figure 5. 2: FT-IR of a) HA-g-SAH, b) LS-g-SAH, c) Lt-g-SAH and, d) ctrl hydrogels.

5.3.2.2 ^{13}C Solid-state Cross-Polarization Magic Angle Spinning Nuclear Magnetic Resonance (^{13}C CPMAS NMR)

Solid state ^{13}C NMR spectroscopy is a powerful tool for the structural characterization of polymers. The spectra of synthesized HA-g-SAH, LS-g-SAH, LT-g-SAH, and ctrl were studied along with Ammonium Humate, Lignosulfonic acid sodium salt, and Ammonium Lignite as shown in Figure 5. 3. In the spectra, notable peaks at approximately 45 ppm and 185 ppm in HA-g-SAH, LS-g-SAH, LT-g-SAH, and ctrl were assigned to saturated aliphatic chains, and C from carbonyl ester (COONa), COOH, respectively. The prominent intensified peak at 185 ppm might be precisely attributed to the free COOH groups and crosslinks in the synthesized hydrogels.[332] The appearance of signals around 50-10 ppm indicated the aliphatic C chain.[218–221] The peaks between 54-56 ppm corresponded to methoxy, methyne, and quaternary C. Remarkably, Lt-g-SAH showcased distinctive peaks in this region depicting the presence of lignite in the hydrogel.[292] The bands between 110–165 ppm mainly corresponded to aromatic and olefinic carbons with HA-g-SAH revealing their presence, albeit at a lower intensity.[333] The presence of peaks at 135.1 ppm and 86.2 ppm verify the presence of Lignosulfonic acid in LS-g-SAH. Meanwhile, the majority of the peaks of natural polymers are integrated into their respective hydrogels.

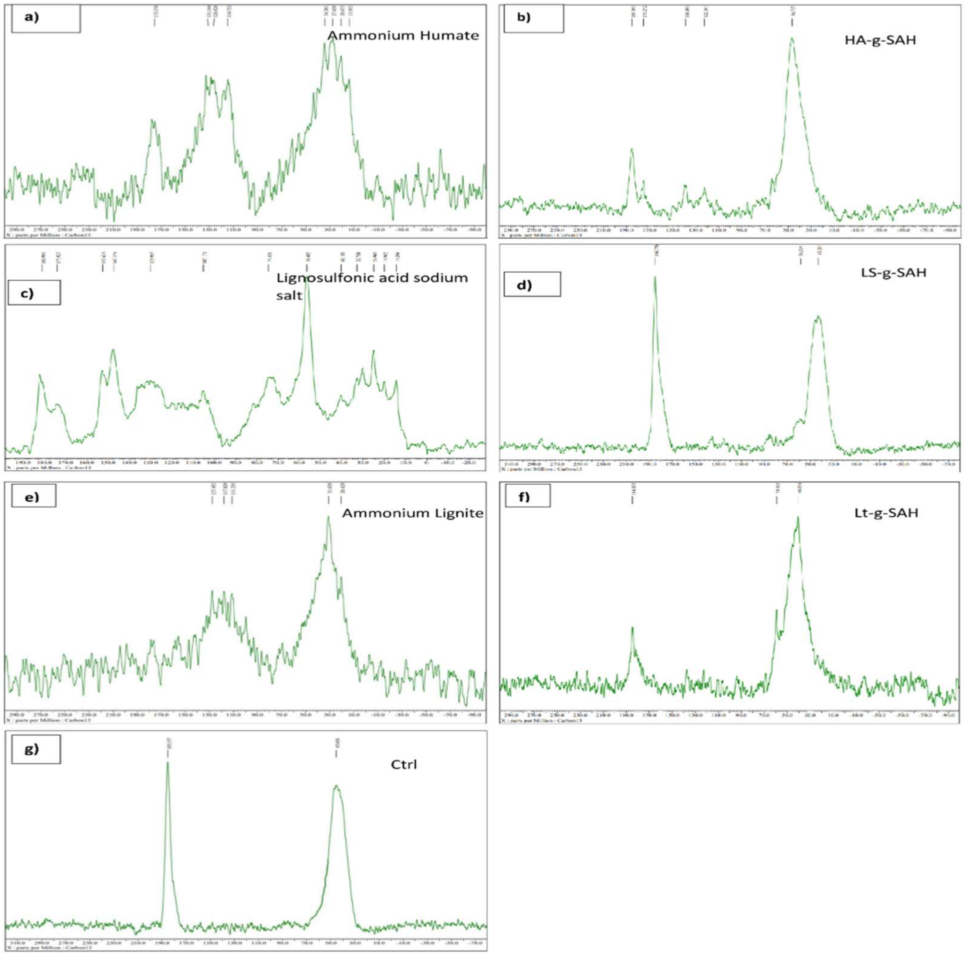

Figure 5. 3: SS ^{13}C CP-MAS NMR spectrum of a) Ammonium Humate, b) HA-g-SAH, c) Lignosulfonic acid sodium salt, d) LS-g-SAH, e) Ammonium Lignite, f) Lt-g-SAH and ag) Ctrl.

5.3.2.3 Scanning electron microscopy (SEM)

The SEM images of the a) HA-g-SAH, b) LS-g-SAH, and c) LT-g-SAH at the 7000X magnification are presented in Figure 5. 4. It was observed that all three natural polymer-based hydrogels have amorphous surfaces whereas ctrl was smooth and had some cracks in it. The pores present in hydrogels act as an interaction site for the hydrophilic groups of graft copolymers towards the external stimuli.[264] HA-g-SAH and LS-g-SAH showed some oval or spherical particles creating a porous structure. Haque et al. observed similar rough and discontinuous morphology for their cellulose-based hydrogels.[334] However, the lignite-based hydrogel is different as it showed the presence of irregularly shaped layered structures with jagged features. Lower porosity in conventionally formed hydrogel allows stronger intermolecular attraction and vice-versa.[267] This finding is also supported by the study of Kojima et al. The study demonstrated that lower porosity, achieved through higher crosslinking density, enhanced the intermolecular attraction due to the increased proximity of polymer chains, resulting in stronger bonding.[335]

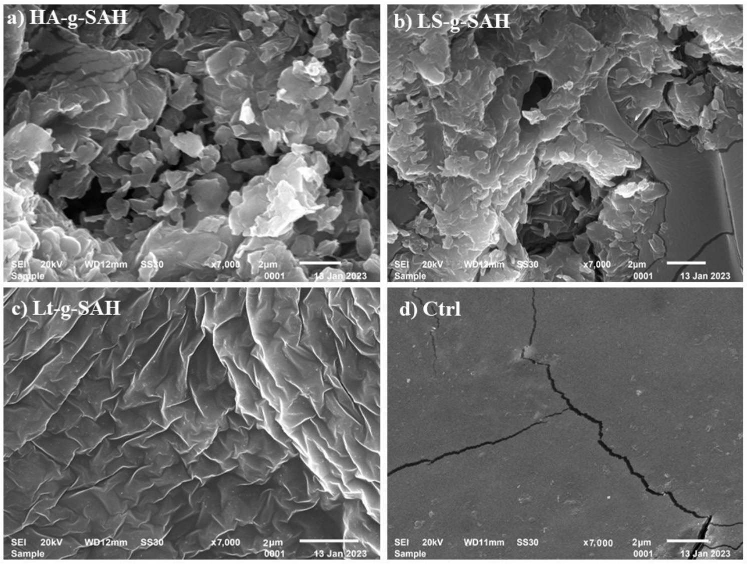
a) HA-g-SAH
b) LS-g-SAH
c) Lt-g-SAH
d) Ctrl
SEI 20kV WD12mm SS30 x7,000 2μm 0001 13 Jan 2023
Sample
SEI 20kV WD12mm SS30 x7,000 2μm 0001 13 Jan 2023
Sample
SEI 20kV WD12mm SS30 x7,000 2μm 0001 13 Jan 2023
Sample
SEI 20kV WD11mm SS30 x7,000 2μm 0001 13 Jan 2023
Sample

Figure 5.4: The SEM images of a) HA-g-SAH, b) LS-g-SAH, c) Lt-g-SAH and d) Ctrl

5.3.2.4 Thermal analysis

All of the hydrogels exhibited a similar three-step degradation as shown in Figure 5. 5. This aligns with the findings of Liu et al. [336] The initial weight loss at the first stage (up to 400 °C) is due to the entrapped moisture and decomposition of associated volatile compounds in hydrogels. Within the first stage, the increase in temperature from 150°C to 450°C marked the decomposition of LS, known as vitrification transformation in LS-g-SAH.[337] The decomposition of the sulfonic acid group in LS and small ungrafted molecular polymers of HA, LS, and Lignite took place in the range of 250-400°C [123]. The mass loss at 300 °C in HA-g-SAH probably corresponded to the decomposition of methylene groups, carboxylic groups, methyl groups, alcoholic groups, and carbohydrates present in the humic structure [338]. Weight loss in the second stage (400-500 °C) could be attributed to the liberation of CO from degrading C=O, C–O–C, and degeneration of aromatic rings present in HA, LS, and Lignite within HA-g-SAH, LS-g-SAH, and Lt-g-SAH.[222, 223]

The point of the highest rate change emerges prominently around 478°C, 479°C, and 470°C for HA-g-SAH, LS-g-SAH, and Lt-g-SAH respectively. This temperature was remarkably elevated in comparison to the control at 270°C. It highlights the enhanced thermal stability conferred by the grafting of three biopolymers to their respective hydrogels. Additionally, the third step of degradation is attributed to the breaking down of bonds between the polymeric backbone and grafting monomer and cross-linker present in the hydrogel network.[339] The residual mass percent provides evidence of enhanced thermal stability due to the incorporation of Humic Acid, Lignosulfonic acid sodium salt, and Lignite into hydrogels. Notably, HA-g-SAH, LS-g-SAH, Lt-g-SAH, and ctrl exhibited residual mass percent of 49.7%, 49.6%, 49.3%, and 33.1%, respectively at 800 °C.

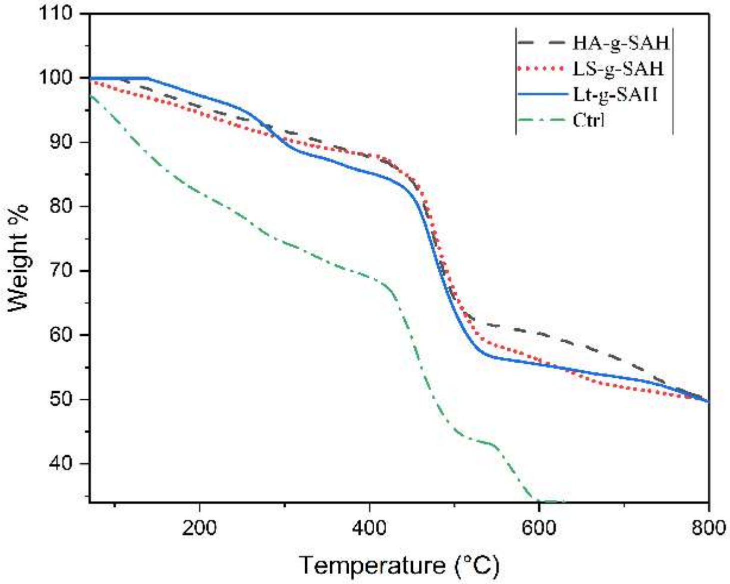

Figure 5.5: TGA analysis HA-g-SAH, LS-g-SAH, Lt-g-SAH, and Ctrl.

5.3.2.5 X-ray diffraction (XRD)

Two broad peaks were noticed in the XRD pattern of HA-g-SAH, LS-g-SAH, Lt-g-SAH, and ctrl hydrogels at 14° and 32° as shown in Figure 5. 6. The observed maxima are characteristic of an amorphous polymer structure and are found to agree with previous researches.[225, 266] Such a similar result has also been observed by grafting carboxymethyl cellulose on sodium acrylate [226]. The average molecular interchain spacing (<R>) was calculated from the strong maximum using the Bragg equation (equation 5).[267]

$$< R >= \frac{5}{8}(\frac{\lambda}{sin\theta}) \tag{5}$$

where, λ = the wavelength of radiation, and θ = diffraction maximum angle.

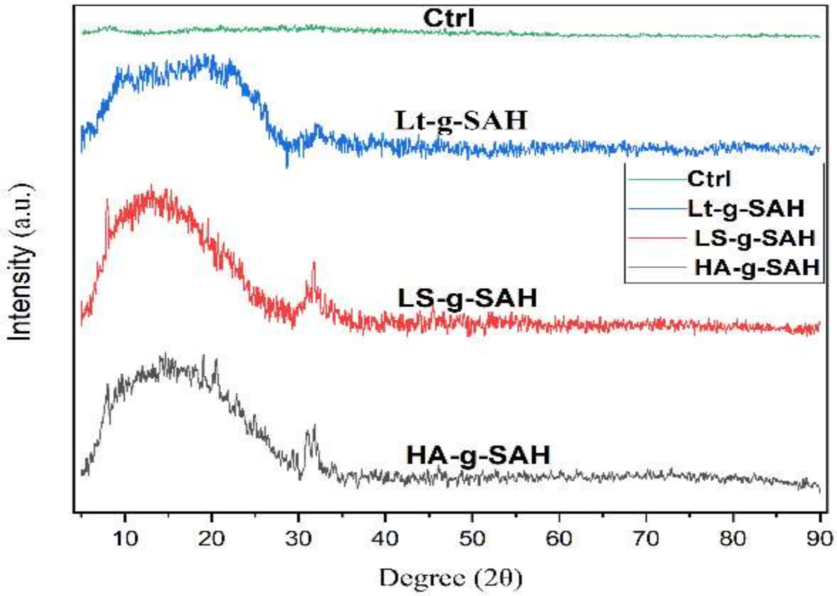

Figure 5. 6: XRD analysis of HA-g-SAH, LS-g-SAH, Lt-g-SAH, and ctrl.

The average molecular interchain spacing between chains in the HA-g-SAH, LS-g-SAH, and Lt-g-SAH and ctrl hydrogels is found to be 7.66 Å, 7.54 Å 7.13 Å and 3.60 Å. Low values of <R> represent a stronger intermolecular attraction and shorter interchain distances which further makes the structure more compact.

5.3.2.6 Rheology

The study of rheology helps to understand the relationship between the chemical structure and the macroscopic behavior of hydrogels.[227] The rheological properties of the synthesized hydrogels were compared with ctrl to investigate the effect of the presence of humic acid, lignin, and lignite in the hydrogels, as shown in Figures 5.7 and Figure 5. 8.

During the amplitude sweep test, the shear stress amplitude was changed at a rate of 10 rad/s. At low strain, the loss modulus (G″) and storage modulus (G′) are consistent, indicating that the hydrogel structure remained unaffected. This phase, recognized as linear-viscoelastic region (LVE), reflects the regime where the hydrogel structure remains undisturbed under applied deformation. However, the consistency between G″ and G′ decreased with a further increase in strain. This deviation from consistent modulus is an indication of the disruption of structure indicating the termination of the LVE region.

The frequency varied from 0.1 to 500 rad/s during the frequency sweep test while keeping the shear strain % within the LVE region constant. It was observed that the loss modulus was prevalent at higher frequencies while the storage modulus was prevalent at lower frequencies representing the viscoelastic solid behavior. Tan θ (dimensionless), a parameter denoting the ratio of storage modulus to loss modulus, generally varies from 0 to 1 for viscoelastic solutions. For an ideal viscous behavior, tan θ is infinity, i.e., θ is 90° and for a perfect elastic behavior, tan θ is 0, i.e., θ is 0°. [228]

It was observed from Table 5. 1 that the cross-over point for all the hydrogels falls in the low-frequency region (126-200 rad/s). Specifically, HA-g-SAH, LS-g-SAH, Lt-g-SAH, and ctrl had a loss factor of 0.026, 0.044, 0.081, and 0.018 representing the dominancy of elastic behavior at low frequency. The very high values of loss factor at high frequency represent the viscous behavior of hydrogels. This agrees with the previously reported literature. [229] However, HA-g-SAH was found to have the highest storage modulus of 1047.9 Pa and 0.504 Pa at both low and high angular frequencies, respectively. At low angular frequency, LS-g-SAH (400.3Pa) showed the lowest storage modulus whereas at high angular frequency, Lt-g-SAH takes the lead with the lowest storage modulus of 0.273 Pa.

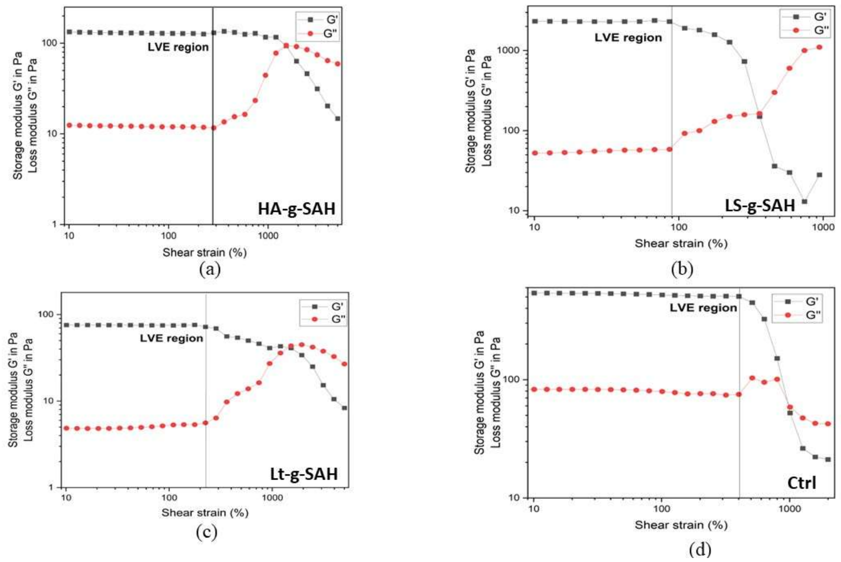

Figure 5.7: Rheological analysis - amplitude sweep of a) HA-g-SAH, b) LS-g-SAH, c) Lt-g-SAH, and d) ctrl.

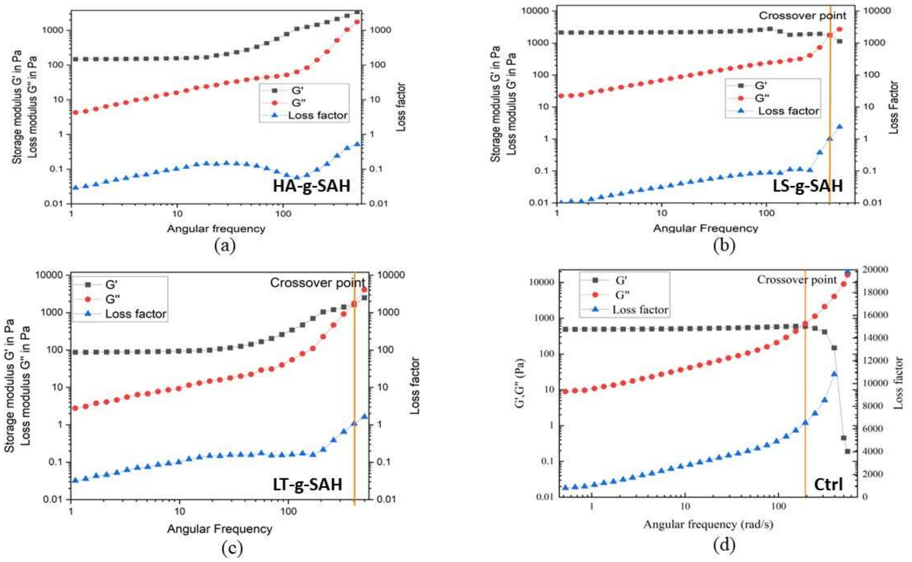

Figure 5. 8: Rheological analysis - frequency sweep of a) HA-g-SAH, b) LS-g-SAH, c) Lt-g-SAH, and d) ctrl.

Table 5.1: Frequency sweep rheological analysis data of HA-g-SAH, LS-g-SAH, Lt-g-SAH, and ctrl hydrogels.

Sample	Low frequency			Cross-over point	High frequency		
	Storage modulus G' (Pa)	Loss modulus G" (Pa)	Loss factor Tan θ	Angular frequency (rad/s)	Storage modulus G' (Pa)	Loss modulus G" (Pa)	Loss factor Tan θ
HA-g-SAH	1047.9	27.05	0.026	200	0.504	10080	20000
LS-g-SAH	400.03	17.58	0.044	126	0.490	9818.6	20000
Lt-g-SAH	671.91	54.73	0.081	200	0.273	5469.3	20000
Ctrl	491.08	8.89	0.018	194	0.453	9063.7	20000

5.3.3 Swelling study of HA-g-SAH, LS-g-SAH, Lt-g-SAH and ctrl

5.3.3.1 Swelling study

Table 5.2: Swelling study analysis of various compositions of HA-g-SAH, LS-g-SAH, Lt-g-SAH and ctrl hydrogels (KPS = 0.0098 mol·L^{-1}, MBA = 0.021 mol·L^{-1}).

Formulation	Ammonium Humate/Lignosulfonate/ Ammonium lignite (g)	SI (g.g^{-1})			
		HA-g-SAH	LS-g-SAH	Lt-g-SAH	Ctrl
1	0.0	-	-	-	142.58
2	0.05	136.66	121.78	95.64	-
3	0.1	201.45	170.56	113.87	-
4	0.2	267.56	258.33	159.22	-
5	0.3	280.92	230.45	187.4	-
6	0.4	228.12	187.34	152.72	-
7	0.5	173.45	136.45	135.65	-

Table 5.2 demonstrates the swelling behavior of the HA-g-SAH, LS-g-SAH, Lt-g-SAH and ctrl hydrogels studied in distilled water. The results indicate that the swelling Index is highly influenced by the concentration of biopolymers (Ammonium Humate/Lignosulfonate/ Ammonium lignite). HA-g-SAH hydrogel exhibited the highest swelling in distilled water (280.92 g·g^{-1}) in 47 hours. It was followed by LS-g-SAH (258.33 g·g^{-1}) in 37 hours and Lt-g-SAH (187.34 g·g^{-1}) in 34 hours. Ctrl hydrogel had the lowest SI of 142.58 g·g^{-1} in 31 hours. Thus, hydrogel formulation no's 5, 4, and 5 of Ammonium Humate, Lignosulfonate, and Ammonium lignite, respectively were

found to have the highest swelling and consequently used for the swelling and release experiments.

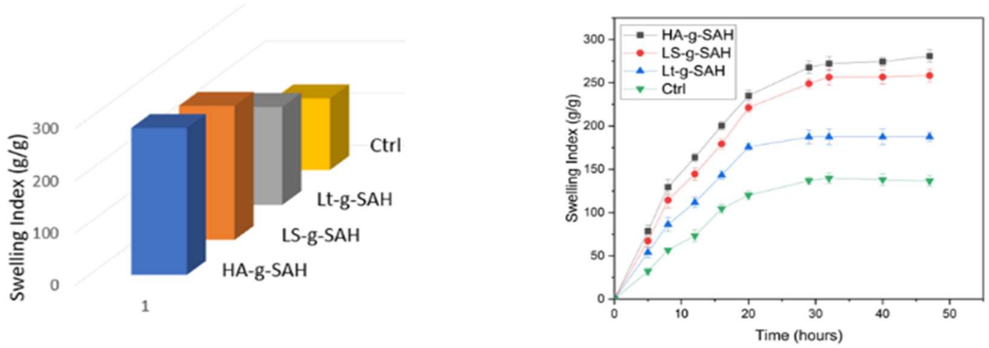

a) b)

Figure 5. 9: a) Comparative swelling, b) SI concerning time

Figure 5. 9(a and b), show the swelling index of all hydrogels in distilled water at various time intervals. It was observed that HA-g-SAH had an SI ($g{\cdot}g^{-1}$) of 280.9 ($g{\cdot}g^{-1}$) obtained in 47 hours. For others it was found to be - LS-g-SAH (258.33 $g{\cdot}g^{-1}$) in 37 hours, Lt-g-SAH (187.4 $g{\cdot}g^{-1}$) in 34 hours and control (142.58 $g{\cdot}g^{-1}$) in 31 hours. From the swelling study data, it can be concluded that HA-g-SAH had the highest swelling and it continued to swell up for the highest time among other hydrogels. All three natural polymer-based hydrogels i. e. HA-g-SAH, LS-g-SAH, and Lt-g-SAH had better swelling than control.

5.3.3.2 Loading efficiency of HA-g-SAH, LS-g-SAH, Lt-g-SAH, and ctrl

An ideal hydrogel used for release application should have good loading efficiency and allow for release over a longer duration of time. The loading efficiency of synthesized thiamethoxam-loaded hydrogels varied between 54% and 69%. Specifically, the LE (%) of HA-g-SAH, LS-g-SAH, Lt-g-SAH, and control hydrogels were determined to be 69.1%, 59.6%, 56.2%, and 54.5%, respectively.

5.3.4 Agricultural application of HA-g-SAH, LS-g-SAH, and Lt-g-SAH

5.3.4.1 Water evaporation study

The direct loss of water as water vapor from soil to the atmosphere is termed water evaporation. The rate of evaporation from the soil is influenced by the water-holding capacity of the soil. The application of hydrogels improved the water-holding capacity of the soil. Figure 10 shows that adding just 1 wt.% of the HA-g-SAH, LS-g-SAH, Lt-g-SAH, and control hydrogels to the soil (ISO 17556 standard soil) reduced the evaporation rate from 99% to 72.85%, 74.79%, 78.23%, and 85.23%, respectively of the total added water on the 54th day.

The ANOVA showed that the water evaporation ratio of HA-g-SAH, LS-g-SAH, Lt-g-SAH, and ctrl is significant since the observed P-value (F-test) was smaller than 0.05 as shown in Table 5. 3. This indicates that there is less than 5% probability of the null hypothesis to be true. Thus, the observed changes are not due to the random errors associated with the measured parameter but rather to the change in the biopolymers used for hydrogel synthesis, indeed.

This order of water evaporation ratio is also supported by the swelling study data where the highest swelling was obtained by HA-g-SAH followed by LS-g-SAH, Lt-g-SAH, and control hydrogels. The control's water evaporation ratio from the study was higher than soil amended with LS-g-SAH, probably due to the interaction between water and polymer molecules and the macromolecular network hindrance.[214] The extended time for water evaporation after applying hydrogel indicates the possibility for water to remain in the soil for a longer time, providing more time for the plant to absorb water and increase plant growth, especially during long dry spells and stress conditions.[340]

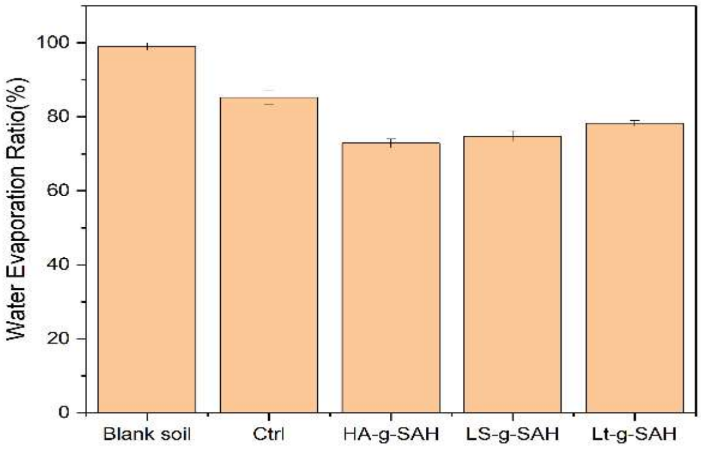

Figure 5.10: Water evaporation study of soil amended with HA-g-SAH, LS-g-SAH, Lt-g-SAH, and control hydrogels.

Table 5.3: ANOVA table for water evaporation ratio.

Source	Sum of squares	DF	Mean square	F-Value	P-value
Water Evaporation ratio	3842.729	3	1280.91	145.3515	2.57×10^{-7}

5.3.4.2 Release kinetics of Thiamethoxam

The release kinetics of thiamethoxam from HA-g-SAH, LS-g-SAH, Lt-g-SAH, and control hydrogels were observed in distilled water. It was found that hydrogels were capable of releasing thiamethoxam for 49 hours (HA-g-SAH and LS-g-SAH), 38 hours (Lt-g-SAH), and 32 hours (ctrl).

The Korsmeyer-Peppas model and Weibull model have been used to understand the mechanism involved in releasing thiamethoxam as shown in Figure 5. 11 and Figure 5. 12, respectively.

Korsmeyer-Peppas model is represented using equation 6.

$$\frac{M_t}{M_\infty} = k_{kp}t^n \tag{6}$$

where M_t and M_∞ represents the thiamethoxam released at time ‘t’ and the equilibrium point, respectively. The ratio of M_t to M_∞ denotes the fraction of total thiamethoxam released at the time 't', while 'k' is a polymer structure constant. In this model, the value of n characterizes the release mechanism. For cylindrical tablets, $0.45 \leq n$ corresponds to a Fickian diffusion mechanism, $0.45 < n < 0.89$ to non-Fickian transport, $n = 0.89$ to Case II (relaxational) transport, and $n > 0.89$ to super case II transport Only the section of the release curve where the ratio $\frac{M_t}{M_\infty} < 0 \cdot 6$ should be used to determine the exponent 'n'.[234, 235]

The Weibull model can be represented using equation 7.

$$\{log(-\ln(1-m)\} = \beta log(t - Ti) - log\alpha \tag{7}$$

Where, m is the amount of drug dissolved as a function of time t, β = shape parameter, α = scale parameter, Ti = Location parameter/ time lag usually zero, t = Time in hours. The α value in the Weibull model shows the time scale or apparent rate constant while the β value characterizes the shape of the curve.[341]

When it comes to polymeric matrices, the exponent β serves as a marker for the drug's method of transport across the matrix. In both fractal and Euclidian spaces, Fickian diffusion is linked to β values ≤ 0.75; on the other hand, β values in the range 0.75 < < 1 β are linked to a combined mechanism (Fick diffusion and swelling-controlled transport). For values of β higher than 1, it is demonstrated that the drug transport follows a complex release mechanism.[341, 342]

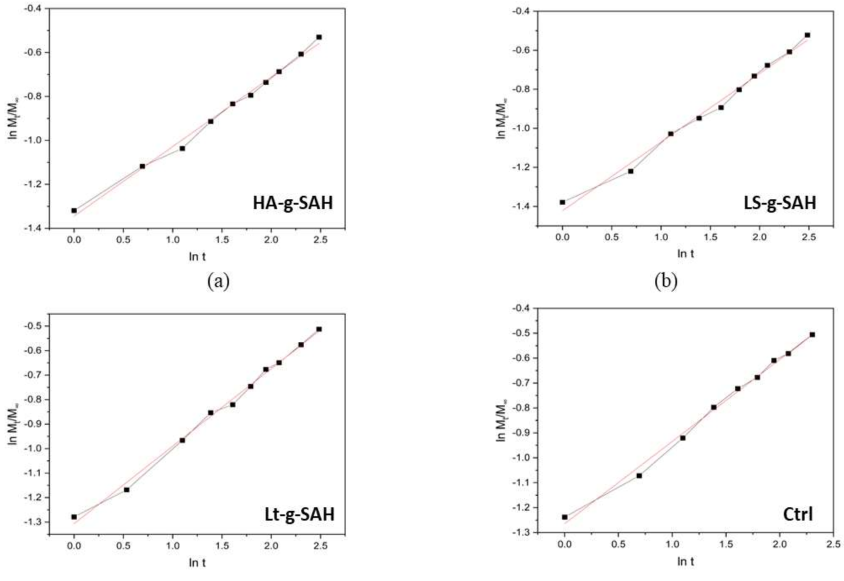

(a) (b)

(c) (d)

Figure 5. 11: Korsmeyer Peppas release kinetics of thiamethoxam from a) HA-g-SAH, b) LS-g-SAH, c) Lt-g-SAH, and d) ctrl.

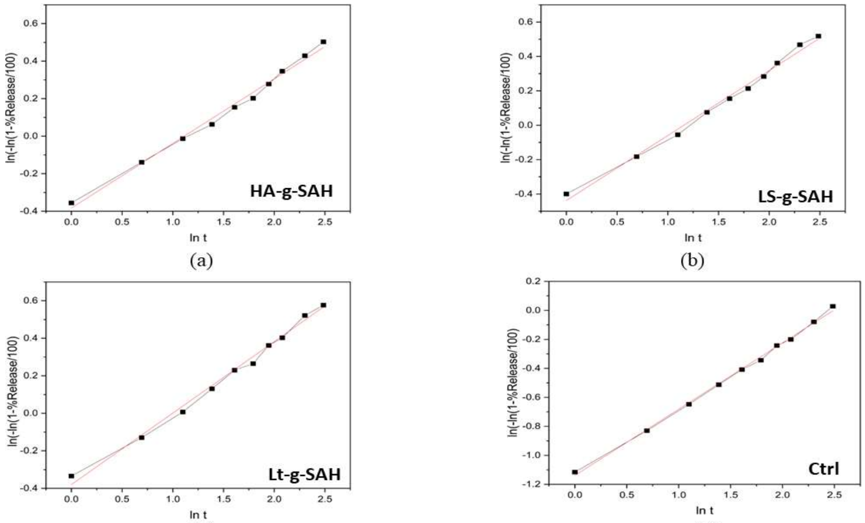

(a) (b)

(c) (d)

Figure 5. 12: Weibull release kinetics of thiamethoxam from a) HA-g-SAH, b) LS-g-SAH, c) Lt-g-SAH, and d) ctrl.

Table 5.4: Mathematical models used for the study of release kinetics of thiamethoxam.

Model	Equation	Formulation	R^2	Parameter	Diffusional mechanism
Korsmeyer Peppas	$f = k_{kp}t^n$ k_{KP} = constant depicting the experimental parameters f = amount of the drug released n = release exponent	HA-g-SAH	0.9940	n = 0.328	Fickian
		LS-g-SAH	0.9930	n = 0.366	Fickian
		Lt-g-SAH	0.9914	n = 0.329	Fickian
		Ctrl	0.9957	n = 0.334	Fickian
Weibull	$R(t)= 1-e^{-\alpha t^{\beta}}$ α= scale factor β = shape factor	HA-g-SAH	0.9934	β = 0.434	Fickian
		LS-g-SAH	0.9905	β = 0.482	Fickian
		Lt-g-SAH	0.9910	β = 0.445	Fickian
		Ctrl	0.9941	β = 0.455	Fickian

The slow-release process of thiamethoxam occurred through all the formulations in the following manner; firstly, the water tries to enter the hydrogel. Afterward, the hydrogel starts to swell by absorbing water until a dynamic exchange is developed between the free water of the hydrogel and the water present in the soil. Meanwhile, the thiamethoxam in the hydrogel matrix continues to dissolve and diffuse. It gets released into the water due to the osmosis differences and dynamic exchange of free water.[214]

From Table 5. 4, the coefficient of determination values (R^2) showed the maximum value to be 0.99 for the Korsmeyer -Peppas model and Weibull model indicating that the release followed both of them. The value of "n" is less than 0.45 in all the formulations for the Korsmeyer-Peppas model representing a Fickian diffusional release from the synthesized hydrogel. The exponent β is found to be less than 0.85 which also reports a Fickian diffusion from all the formulations. Thus, the Fickian diffusional mechanism observed from the Korsmeyer-Peppas model is also supported by the findings of the Weibull model.

5.4 Conclusion

In conclusion, this research successfully demonstrated the synthesis and characterization of novel hydrogels, namely HA-g-SAH, LS-g-SAH, and Lt-g-SAH, loaded with the pesticide- thiamethoxam. The synthesized hydrogels characterized using FT-IR and 13C NMR, coupled with the impressive water absorbency of 280.9 to 187.4 $g{\cdot}g^{-1}$ in distilled water, highlight the efficiency of these formulations. The swelling index revealed a distinct order, with HA-g-SAH exhibiting the highest absorbency, followed by LS-g-SAH, Lt-g-SAH, and the control group. Moreover, the synthesized hydrogels demonstrated a significant impact on reducing soil water evaporation rates from 99% to 72.85% (HA-g-SAH), 74.79% (LS-g-SAH), 78.23% (Lt-g-SAH), and 85.23% (ctrl) of the total added water on the 54th day. The slow release of thiamethoxam for 49 hours from the formulations suggests the possibility of using these novel hydrogels for the slow release of of pesticides and fertilizers. The release pattern followed the Fickian release mechanism as stated by the Korsmeyer-Peppas model and the Weibull model. This research article will bring humic acids, lignin, and lignite out of the traditional soil context by applying them in the modern field of sustainable agriculture. The hydrogel formulations presented in this study hold great potential for enhancing water retention in soil and optimizing the controlled release of agrochemicals. This research offers a promising foundation for more efficient and environmentally friendly farming practices.

CHAPTER- 6

COMPARATIVE ANALYSIS OF HUMIC ACID, LIGNIN AND LIGNITE-BASED HYDROGELS FOR METHYLENE BLUE DYE REMOVAL

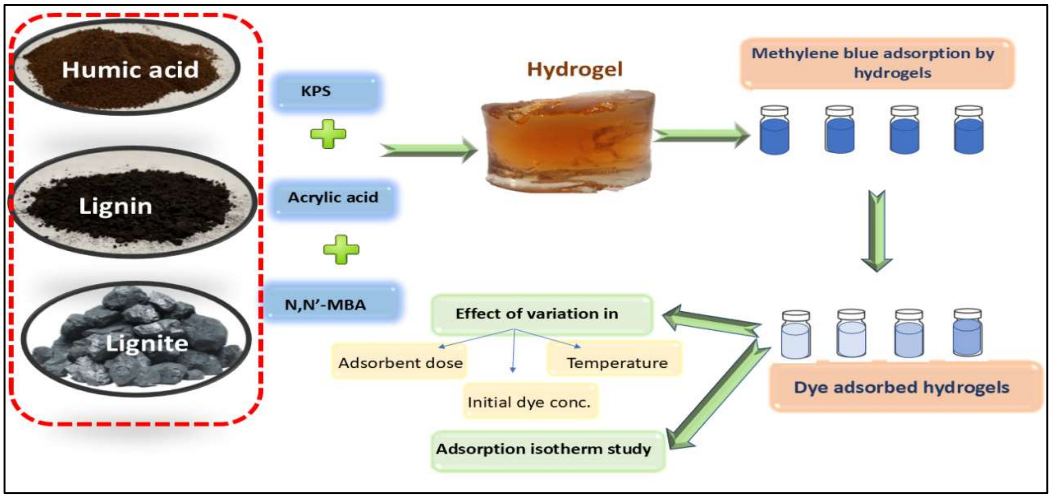
Humic acid
Lignin
Lignite
KPS
Acrylic acid
N,N'-MBA
Hydrogel
Methylene blue adsorption by hydrogels
Dye adsorbed hydrogels
Effect of variation in
Adsorbent dose
Temperature
Initial dye conc.
Adsorption isotherm study

6.1 Introduction

This study investigates the application of hydrogels incorporating natural polymers - ammonium humate, lignosulfonate, and ammonium lignite - for methylene blue (MB) dye removal from aqueous solutions. The hydrogels were synthesized via free radical polymerization and characterized using FTIR, ^{13}C-NMR, SEM, TGA, and XRD. The synthesized hydrogels demonstrated exceptional swelling capabilities. The influence of various parameters, including adsorbent dosage (0.1-0.4 g), temperature (293.15-323.15 K), and initial dye concentration (5-20 mg·L^{-1}) on MB removal efficiency was systematically evaluated using the Taguchi method. Under optimized conditions, HA-g-SAH achieved a maximum removal efficiency of 93.7% ±1.1% at 323.15 K, significantly outperforming LS-g-SAH (92.4% ±1.3%), Lt-g-SAH (82.4 ±1.4%), and the control (ctrl) hydrogel (67.9 ±0.9%). According to ANOVA results, the change of biopolymer proved to be an effective factor in the improved dye removal efficiency of hydrogels. Thermodynamic parameters- $\Delta G°$, $\Delta H°$, and $\Delta S°$ were also analyzed to understand the involved adsorption processes concerning temperature changes. The adsorption isotherm data was fitted to Langmuir and Freundlich models. These results demonstrate the potential of these natural polymer-based hydrogels as efficient and environmentally friendly adsorbents for dye removal from wastewater.

Synthetic dyes are used in various industries, including food production, textile processing, and pharmaceutical sector. Yet, approximately 80% of the dye-containing wastewater produced is often released untreated into waterways or used directly for irrigation, causing detrimental impacts on human health and ecosystems.[343] Synthetic dyes negatively impact all forms of life. The presence of sulphur, naphthol, vat dyes, nitrates, acetic acid, soaps, enzymes, chromium compounds and heavy metals like copper, arsenic, lead, cadmium, mercury, nickel, and cobalt and certain auxiliary chemicals all collectively make these effluents highly toxic. [344] The color associated with dyes not only causes aesthetic damage to the water bodies but also prevents light penetration through water, which reduces the rate of photosynthesis and dissolved oxygen levels, affecting the entire aquatic biota.[345] Also, the synthetic dyes are soluble organic compounds.

Methylene blue (MB), a widely used dye, contributes significantly to environmental pollution due to its toxicity. Its presence can interfere with photosynthesis and cause severe eye burns, potentially leading to permanent eye damage in both humans and animals.[346] Additionally, exposure to MB in humans can result in adverse effects such as tissue necrosis, cyanosis, jaundice, vomiting, increased heart rate, and other health complications.[347] Consequently, removing MB from industrial wastewater is a pressing ecological concern.

The high solubility of dye in water makes it difficult to remove them by conventional methods.[348]

However, nondestructive and destructive methods are effectively applied to remove dyes from wastewater. The nondestructive methods follow various techniques, such as ion exchange [349], chemical oxidation[350], ozone treatment [351], membrane separation [352], and coagulation [353] to remove dyes from industrial effluents. Noticeably, each technique has its advantages and limitations. The existing literature on wastewater remediation showed that the adsorption method is an auspicious technique for dye removal. [354]

Due to their inherent characteristics, polymeric materials have garnered significant attention as adsorbents for dye removal [157]. Hydrogel, a polymeric material, stands out for its exceptional hydrophilicity, mechanical properties, and high porosity, allowing it to absorb water a thousand times its original size.[128] Due to the characteristics of high water content, porosity and typical cell compatibility, hydrogels can be applied in drug release[38, 39, 282, 283, 355], pollution adsorption[157, 245], sensors [356, 357] and tissue engineering [358, 359] by regulating the chemical composition and structure of hydrogels. These have emerged as a promising solution for dye removal, especially for MB, owing to their crosslinked polymeric structure and chemically reactive functional groups. [245, 360–362]

Humic acid, lignin, and lignite are natural polymers that are highly suitable for constructing adsorbent hydrogels for water purification due to their abundance and biodegradable nature. Also, hydrogels reinforced with natural polymers possess excellent mechanical properties.[131] Humic acid is a large organic polymer found in soil and water. It has chelating properties and is important for soil and plant health. In literature, the direct utilization of this natural polymer for adsorption applications is extensively reported. Lignite, or brown coal, is well-known for its adsorptive properties. Several studies report lignite as an adsorbent for removing heavy metals, organic pollutants and dyes from wastewater.[363–366] Singh et al. synthesized a biodegradable hybrid hydrogel made from acrylic acid, sodium acrylate, acrylamide, and sodium humate for crystal violet and methylene blue adsorption. The swollen hydrogel exhibits higher adsorption capacity, whereas sodium humate (2.40 wt%) enhances swelling and adsorption efficiency. [367] Superabsorbent lignosulfonate-g-acrylic acid (LS-g-AA) hydrogels were developed by grafting acrylic acid (AA) onto the lignosulfonate (LS) backbone. Yu et al. reported that the equilibrium absorption of MB by (LS-g-AA) reached 2013 $mg \cdot g^{-1}$.[69]

All three natural polymers- humic acid, lignin and lignite- contain carboxylic acid and phenolic moieties that could enhance the cationic dye adsorption capability. Also, owing to their polyfunctionality, ammonium salts of humic acid and lignite along with lignosulfonate sodium salt can be grafted onto acrylic acid to synthesize hydrogels. Keeping this in view, the study focuses on the application of ammonium humate, lignosulfonate and ammonium lignite-based hydrogels (HA-g-SAH, LS-g-SAH, and Lt-g-SAH) for adsorption of MB from water. The effects of various optimization parameters including initial dye concentration, adsorbent dosage, and temperature, along with their contact time were studied to enhance the removal efficiency of MB dye in an aqueous solution. Taguchi experimental design was adopted for analyzing the adsorption factors having the most significant influence. The optimized swelling duration of all hydrogels from our previous study [131] has been employed as the contact time to obtain the best results. The adsorption isotherm study has also been carried out, where the dye removal efficiency of hydrogels is fitted to Langmuir and Freundlich models. As per the present literature, no such study has been conducted that employs these hydrogels together and presents a comparative analysis of hydrogels' dye removal efficiency, comparing them to non-grafted control hydrogel (ctrl). The results indicate that the synthesized hydrogel exhibits superior efficiency and effectiveness in removing MB from wastewater.

6.2 Experimental

6.2.1 Swelling Study

Swelling experiments were performed on varied biopolymer concentrations of HA-g-SAH, LS-g-SAH, Lt-g-SAH, and ctrl hydrogels at 37°C in distilled water to optimize the best compositions for the adsorption experiment. Initially, the weight of dried hydrogel discs was measured (W_d). At fix time intervals, the hydrogel discs were taken out of water. Excess surface water was removed using filter paper, and the hydrogel discs were reweighed (W_0). The swelling study was carried out in triplicate.

The swelling index (SI) was determined utilizing Eq. (1):

$$\text{SI (g·g}^{-1}\text{)} = \frac{W_o - W_d}{W_d} \tag{1}$$

6.2.2 MB Adsorption experiment mechanism

The experiments were designed using the Taguchi method with standard orthogonal array tables. The Taguchi methodology is an optimization technique that directs a small number of experiments to reduce interference from uncontrollable elements.[368] The L16 design aids in selecting the most effective set of control constraints, lowering the number of total experimental trials.[369]

The influence of the variation of adsorbent concentration (0.1-0.5g), temperature (293.13 - 323.15 K) and contact time (HA-g-SAH- 47 hours, LS-g-SAH 37 hours, Lt-g-SAH 34 hours, and ctrl 31 hours, based on their optimized swelling duration [131]) on the adsorption of MB were investigated at an initial dye concentration varying from 5 to 20 mg·L^{-1}. The unabsorbed MB content was determined by UV-vis absorption at 664 nm using a UV1800 Shimadzu spectrophotometer. To measure the UV absorbance of unabsorbed MB content, the mixture was immediately stirred, and 3 mL of suspension was taken out at specific [370]. The MB removal efficiency (% R) was calculated through Eq. (2):

$$\% \text{ R} = \frac{C_o - C_e}{C_o} \text{X } 100 \tag{2}$$

The adsorption capacity (q$_e$) (mg·g^{-1}) of HA-g-SAH, LS-g-SAH, Lt-g-SAH, and ctrl, hydrogels was calculated through Eq. (3):

$$q_e = \frac{C_0 - C_e}{m} V \tag{3}$$

C_0 and C_e are the initial and equilibrium dye concentrations (mg L^{-1}), respectively. V (L) represents the volume of the dye solution, and m (g) is the weight of HA-g-SAH, LS-g-SAH, Lt-g-SAH, and ctrl hydrogels.

6.3 Results and Discussion

Table 6. 1: Swelling study analysis of various compositions of HA-g-SAH, LS-g-SAH, Lt-g-SAH and ctrl hydrogels (KPS = 0.0098 mol·L^{-1}, MBA = 0.021 mol·L^{-1}).

Formulation	Ammonium Humate/Lignosulfonate/Ammonium lignite (g)	SI (g·g^{-1})			
		HA-g-SAH	LS-g-SAH	Lt-g-SAH	Ctrl
1	0.0	-	-	-	142.58
2	0.05	136.66	121.78	95.64	-
3	0.1	201.45	170.56	113.87	-
4	0.2	267.56	258.33	159.22	-
5	0.3	280.92	230.45	187.4	-
6	0.4	228.12	187.34	152.72	-
7	0.5	173.45	136.45	135.65	-

6.3.1 Swelling study

Table 6. 1 demonstrates the swelling behavior of the HA-g-SAH, LS-g-SAH, Lt-g-SAH and ctrl hydrogels studied in distilled water. The results indicate that the swelling Index is highly influenced by the concentration of biopolymers (Ammonium Humate/Lignosulfonate/Ammonium lignite). HA-g-SAH hydrogel exhibited the highest swelling in distilled water (280.92 g·g^{-1}) in 47 hours. It was followed by LS-g-SAH (258.33 g·g^{-1}) in 37 hours and Lt-g-SAH (187.4 g·g^{-1}) in 34 hours. Ctrl hydrogel had the lowest SI of 142.58 g·g^{-1} in 31 hours. Thus, hydrogel formulation no's 5, 4, and 5 of Ammonium Humate, Lignosulfonate, and Ammonium lignite, respectively were found to have the highest swelling and consequently used for the swelling and adsorption experiments.

6.3.2 MB adsorption and isotherm study

The %R of MB obtained from varying the adsorbent concentration (0.1-0.5g) temperature (293.13 - 323.15 K) on the adsorption of MB, investigated at an initial dye concentration varying from 5 to 20 mg·L^{-1} is reported in Table 6. 2. Figure 6. 1a represents the ANOVA box plots for Table 1, representing %R of MB dye with HA-g-SAH, LS-g-SAH, Lt-g-SAH and ctrl hydrogel. The ANOVA results indicated that the %R of HA-g-SAH, LS-g-SAH, Lt-g-SAH, and Ctrl were statistically significant, as the observed P-value (F-test) was less than 0.05. This suggests a probability of less than 5% for the null hypothesis to be valid. Consequently, the observed variations are attributed to the differences in the biopolymers used during hydrogel synthesis.

Table 6.2: Taguchi L16 design table for HA-g-SAH, LS-g-SAH, Lt-g-SAH and ctrl hydrogel.

Observations	Dosage (g)	Temperature (K)	Initial dye conc. (mg L^{-1})	HA-g-SAH	LS-g-SAH	Lt-g-SAH	Ctrl
Obs1	0.1	293.15	5	73.500	72.200	62.400	55.700
Obs2	0.1	303.15	10	75.000	74.000	64.000	56.000
Obs3	0.1	313.15	15	77.000	75.800	66.000	57.000
Obs4	0.1	323.15	20	79.000	77.000	69.500	59.000
Obs5	0.2	293.15	10	77.500	76.000	68.200	57.800
Obs6	0.2	303.15	5	76.400	75.000	67.600	57.100
Obs7	0.2	313.15	20	78.500	75.800	68.400	57.900
Obs8	0.2	323.15	15	80.900	78.200	70.100	58.800
Obs9	0.3	293.15	15	86.500	86.400	74.700	61.200
Obs10	0.3	303.15	20	91.600	87.300	79.400	66.500
Obs11	0.3	313.15	5	87.500	84.700	76.500	64.100
Obs12	0.3	323.15	10	92.500	90.400	82.300	69.800
Obs13	0.4	293.15	20	90.400	87.300	80.100	66.700
Obs14	0.4	303.15	15	90.000	87.100	79.200	65.200
Obs15	0.4	313.15	10	88.000	85.800	78.200	64.600
Obs16	0.4	323.15	5	89.500	85.100	79.400	64.900

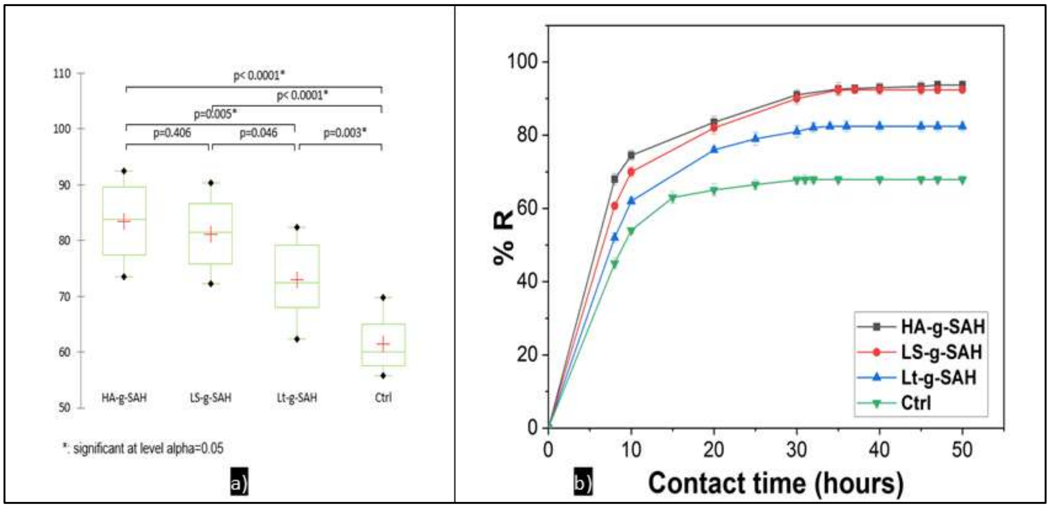

Figure 6.1: a) ANOVA box plots for Table 1, b) Effect of the contact time on %R by HA-g-SAH, LS-g-SAH, Lt-g-SAH, and Ctrl hydrogels at adsorbent conc.= 0.3 g, T= 323.15K, dye conc.= 20 mg·L^{-1}

6.3.2.1 Effect of variation in adsorbent dosage on %R of MB

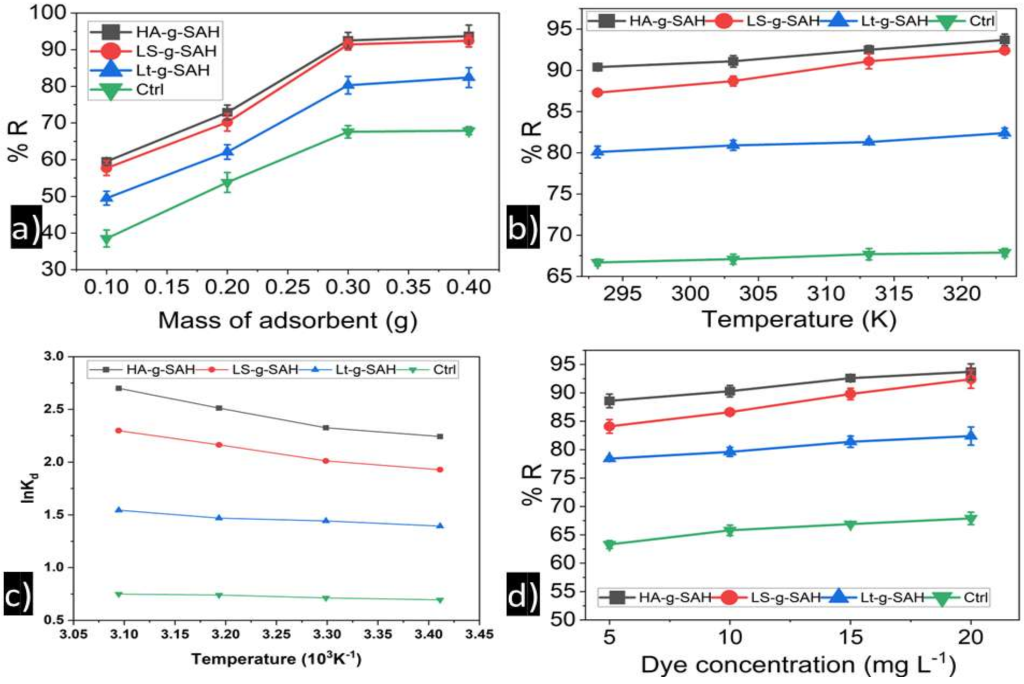

Figure 6.2: Effect of the variation in a) adsorbent dosage (T = 323.15 K, dye conc.= 20 mg·L^{-1}), b) temperature (adsorbent conc.= 0.3 g, dye conc.= 20 mg·L^{-1}), c) Van't Hoff plots of ln K$_d$ against 1/T and d) initial dye concentration (adsorbent conc.= 0.3 g, T= 323.15K), on %R by HA-g-SAH, LS-g-SAH, Lt-g-SAH, and Ctrl hydrogels

The amount of HA-g-SAH, LS-g-SAH, Lt-g-SAH and ctrl hydrogel used were 0.1 to 0.4 g per 100 ml of 20 $mg{\cdot}L^{-1}$MB dye at 323.15 K and their respective optimized contact time. From Figure 6. 2a it can be observed that the removal efficiency demonstrated a distinct sigmoidal pattern with increasing adsorbent dosage. At 0.1 g, HA-g-SAH achieved 59.5% ± 1.0% removal efficiency, with LS-g-SAH showing similar performance at 57.7% ± 2.0%. A significant enhancement occurred between 0.2 and 0.3 g, where HA-g-SAH and LS-g-SAH reached 92.5% ± 2.2% and 91.4% ± 1.5%, respectively. This sharp increase indicates a critical dosage threshold for optimal adsorption.

At 0.4 g, the systems approached equilibrium, with HA-g-SAH achieving maximum efficiency of 93.7% ± 3.0%, followed by LS-g-SAH (92.4% ± 1.6%), Lt-g-SAH (82.4% ± 2.7%), and ctrl hydrogel (67.9% ± 1.1%). The plateauing effect beyond 0.3 g suggests saturation conditions. The %R is found to be in the order HA-g-SAH > LS-g-SAH > Lt-g-SAH > Ctrl across all dosages representing intrinsic differences in adsorption capabilities, with HA-g-SAH's superior performance attributed to humic acid's abundant functional groups and favorable surface characteristics. This analysis identifies 0.3 g as the optimal adsorbent dosage, balancing maximum removal efficiency with material usage.

6.3.2.2 Effect of variation in temperature on %R of MB

Figure 6. 2b shows the adsorption of the dyes onto the HA-g-SAH, LS-g-SAH, Lt-g-SAH, and ctrl hydrogels from temperatures 293.15 K to 323.15 K. The free energy change (ΔG^0), enthalpy change (ΔH^0) and entropy change (ΔS^0) for dye adsorption were determined using Eq. (4-7). [370]:

$$K_d = \frac{C_0 - C_e}{C_e} \tag{4}$$

$$\Delta G^0 = RT \ln K_d \tag{5}$$

$$\Delta G^0 = \Delta H^0 - T\Delta S^0 \tag{6}$$

$$\ln (kd) = \frac{\Delta S^0}{R} - \frac{\Delta H^0}{RT} \tag{7}$$

K_d is the equilibrium constant, C_0 and C_e are the initial and equilibrium dye concentrations (mg·L^{-1}), R is the gas constant, and T is the temperature (K). Van't Hoff plots of ln K_d against 1/T shown as inset in Fig. 2c, and the ΔH^0 and ΔS^0 were calculated from the slope ($\frac{-\Delta H^0}{R}$) and intercept ($\frac{\Delta S^0}{R}$).

Table 6. 3: Thermodynamic parameters: ΔG°, ΔH°, and ΔS° of MB adsorbed on the HA-g-SAH, LS-g-SAH, Lt-g-SAH and ctrl.

Parameter	HA-g-SAH	LS-g-SAH	Lt-g-SAH	Ctrl
ΔG° (kJ·mol^{-1}) T=20	-6.0248	-5.17922	-3.74134	-1.86629
ΔG° (kJ·mol^{-1})T=30	-6.24894	-5.40425	-3.87828	-1.91482
ΔG° (kJ·mol^{-1}) T=40	-6.74973	-6.3499	-3.94839	-1.98819
ΔG° (kJ·mol^{-1}) T=50	-7.25279	-6.71124	-4.14737	-2.0128
ΔH° (kJ·mol^{-1})	12.13844	9.89366	3.7413	1.49652
ΔS° (J·K^{-1}·mol^{-1})	59.8608	49.63458	24.3844	10.8913

It can be observed from Figure 6. 2b that %R increases with temperature (293.15-323.15 K) for all adsorbents, with HA-g-SAH demonstrating superior performance (90.4 ±0.4% to 93.7±0.7%), followed by LS-g-SAH (87.3 ±0.4% to 92.4 ±0.4%), Lt-g-SAH (80.1±0.7% to 82.4 ±0.6%), and Ctrl (66.7 ±0.5% to 67.9 ±0.3%).

Table 6. 3 shows that the Gibbs free energy (ΔG°) values are negative and decrease with increasing temperature, indicating spontaneous adsorption with enhanced favorability at higher temperatures. The increasingly negative ΔG° values with temperature suggest that the adsorption process becomes more thermodynamically favorable at elevated temperatures.[371] The positive ΔH° values confirmed the endothermic nature of the adsorption process.[372] The positive entropy values (ΔS°) for all systems indicate increased randomness at the solid-solution interface during adsorption, suggesting the release of water molecules from hydrogels during adsorption.[373]The combination of positive ΔH° and ΔS° values, along with negative ΔG° values indicates that the adsorption process by hydrogels is driven by entropy.

6.3.2.3 Effect of variation in initial dye concentration on %R of MB

The concentration of the adsorbate solution also significantly influences the adsorption behaviour of the adsorbent.[374] Thus, the impact of initial MB dye concentration (5-20 mg·L^{-1}) on MB removal efficiency was investigated using HA-g-SAH, LS-g-SAH, Lt-g-SAH, and Ctrl hydrogel with 0.3g adsorbent dosage at 323.15 K. From Figure 6.2d, it can be concluded that %R increased with an increase in initial dye concentration for all the hydrogels. However, HA-g-SAH demonstrated exceptional performance, with %R rising from 88.58% ± 1.2% at 5 mg·L^{-1} to 93.7% ± 1.4% at 20 mg·L^{-1}, indicating optimal adsorbent-adsorbate interactions. LS-g-SAH showed similar behavior but slightly lower efficiency, improving from 84.1% ± 1.2% to 92.4% ± 1.6%. Lt-g-SAH displayed moderate performance, with efficiency increasing from 78.4% ± 0.3% to 82.4% ± 1.6%, while the ctrl hydrogel exhibited the lowest capacity, ranging from 63.3% ± 0.7% to 67.9% ± 1.1%. The consistent performance hierarchy (HA-g-SAH > LS-g-SAH > Lt-g-SAH > Ctrl) and minor standard deviations across all concentrations demonstrate the inherent differences in adsorption capabilities of all the hydrogels. Also, the gradual improvement in %R with increasing dye concentration suggests that HA-g-SAH, LS-g-SAH, and Lt-g-SAH hydrogels maintain effectiveness under varying pollutant loads, making them suitable for practical wastewater treatment applications.

6.3.2.4 Effect of variation in contact time on %R of MB

Analyzing contact time is crucial to assess the reaction extent during the adsorption process. Figure 6. 1b illustrates the influence of contact duration on MB adsorption by HA-g-SAH, LS-g-SAH, Lt-g-SAH, and ctrl hydrogels. This study revealed that the adsorption capacity of all hydrogels increased with time and a clear progression of MB dye adsorption is visible through three distinct kinetic phases. During the rapid initial phase spanning the first 10 hours, HA-g-SAH demonstrated the highest uptake at 74.5% ±1.4%, followed by LS-g-SAH at 70% ± 1.2%, Lt-g-SAH at 62% ± 0.9%, and the ctrl at 54% ±0.8%. The progressive phase from 10-30 hours showed HA-g-SAH and LS-g-SAH reaching approximately 90-91%, while Lt-g-SAH and the ctrl exhibited slower progression, achieving 79% ± 1.7% and 65% ±1.6%, respectively. In the final equilibrium phase, HA-g-SAH reached 93.7% ± 1.1% in 47 hours, while LS-g-SAH attained 92.4% ± 1.3% in 37 hours, Lt-g-SAH achieved 82.4% ± 1.4% in 34 hours, and the ctrl plateaued at 67.9% ± 0.9% in 31 hours. Throughout the study, the performance hierarchy remained consistent, with HA-g-SAH performing best, followed by LS-g-SAH, Lt-g-SAH, and the ctrl. Thus, the present biopolymers (ammonium humate, lignosulfonate sodium and ammonium lignite) significantly increase the adsorption of cationic dyes MB due to their ability to form strong electrostatic interactions with the positively charged dye molecules and through their negatively charged phenolic groups. Since all the modified hydrogels demonstrated superior adsorption properties compared to the ctrl, it may be concluded that the polyphenols act as an attractive surface for the cationic dye to bind to, enhancing the adsorption capacity of their respective hydrogels.

6.3.2.5 Adsorption Isotherms

Adsorption isotherms are valuable tools for understanding how adsorbate (MB dye) molecules are distributed between the solution phase at equilibrium and the adsorbent surface. By examining the interaction between adsorbate and adsorbent, adsorption isotherms provide insights into the adsorption capacity of the adsorbent [18]. Here, Langmuir and Freundlich models have been deployed.

The Langmuir isotherm model is well-suited for representing monolayer adsorption on a uniform surface. The Langmuir isotherm's linear form is represented by Eq. (8). [375]

$$\frac{q_e}{C_e} = \frac{1}{K_l q_{max}} + \frac{C_e}{q_{max}} \tag{8}$$

The parameters qe ($mg{\cdot}g^{-1}$), q_{max} ($mg{\cdot}g^{-1}$) and Ce ($mg{\cdot}L^{-1}$) represent the equilibrium adsorption capacity, maximum adsorption capacity, and equilibrium concentration of MB, respectively, while K_L(L mg^{-1}) denotes the Langmuir constant. These parameters can be determined by plotting a linear graph of C_e versus q_e/C_e and calculating the slope and intercept.

The dimensionless separation factor (R_L) is an indicator for evaluating the feasibility of a reaction. The R_L values may be interpreted as follows: favorable ($0 < R_L < 1$), or unfavorable ($R_L > 1$). It is calculated using Eq. (9).

$$R_L = \frac{1}{1+K_l C_i} \tag{9}$$

Where MB solution concentration is given in mg L^{-1} by C_i.

The Freundlich isotherm model proposes that adsorbent with heterogeneous surfaces experience multilayer adsorption. In the early stages, the more robust binding sites are mainly occupied, and the equilibrium concentration of the adsorbates largely influences the binding strength. The linear Equation for Freundlich isotherm is given by Eq. (10). [376]

$$\ln q_e = \ln K_f + \frac{1}{n} \ln C_e \tag{10}$$

where the Freundlich constant, K_f [$(mg \cdot g^{-1}) (L \cdot mg^{-1})$], gives an idea about binding energy, adsorption capacity, and quantity of adsorbate (MB) adsorbed at equilibrium[376]. The value of 1/n indicates the intensity of adsorption or the heterogeneity of the surface, while a value of n between 1 and 10 suggests that the adsorption process is favorable.

The regression coefficient (R^2) of isotherm plots can be used to evaluate the accuracy of the adsorption isotherm model by comparing experimental data to the theoretical equations. Fig. 3 and Fig. 4 depict the plots of Langmuir and Freundlich adsorption isotherms, and Tables 6.4 and 6.5 present the calculated parameters.

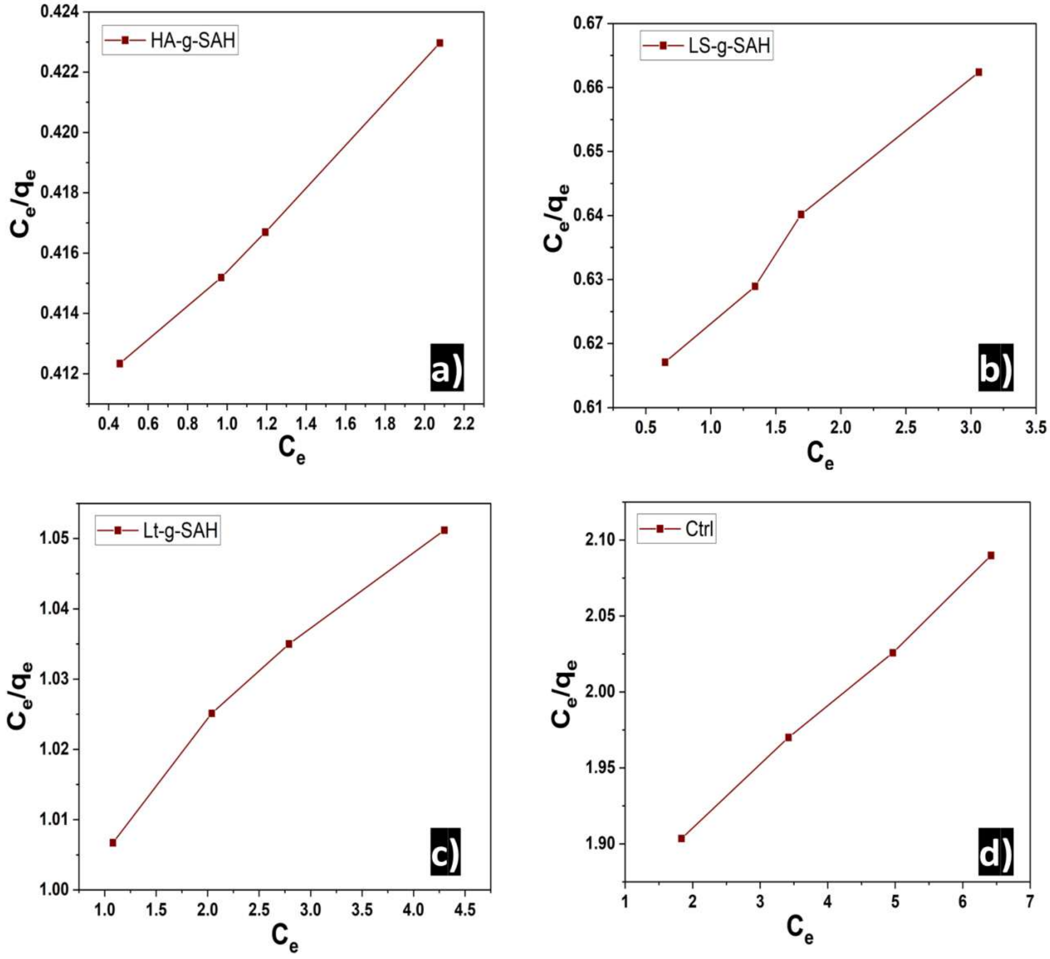

Figure 6.3: Langmuir Isotherm Graph of a) Ha-g-SAH, b) LS-g-SAH, c) Lt-g-SAH, and d) Ctrl.

Table 6.4: Isotherms data for Langmuir adsorption isotherm.

	R^2	b	R_L
HA-g-SAH	0.9751	0.038	0.37
LS-g-SAH	0.9786	0.024	0.62
Lt-g-SAH	0.9654	0.02	0.69
Ctrl	0.9168	0.015	0.76

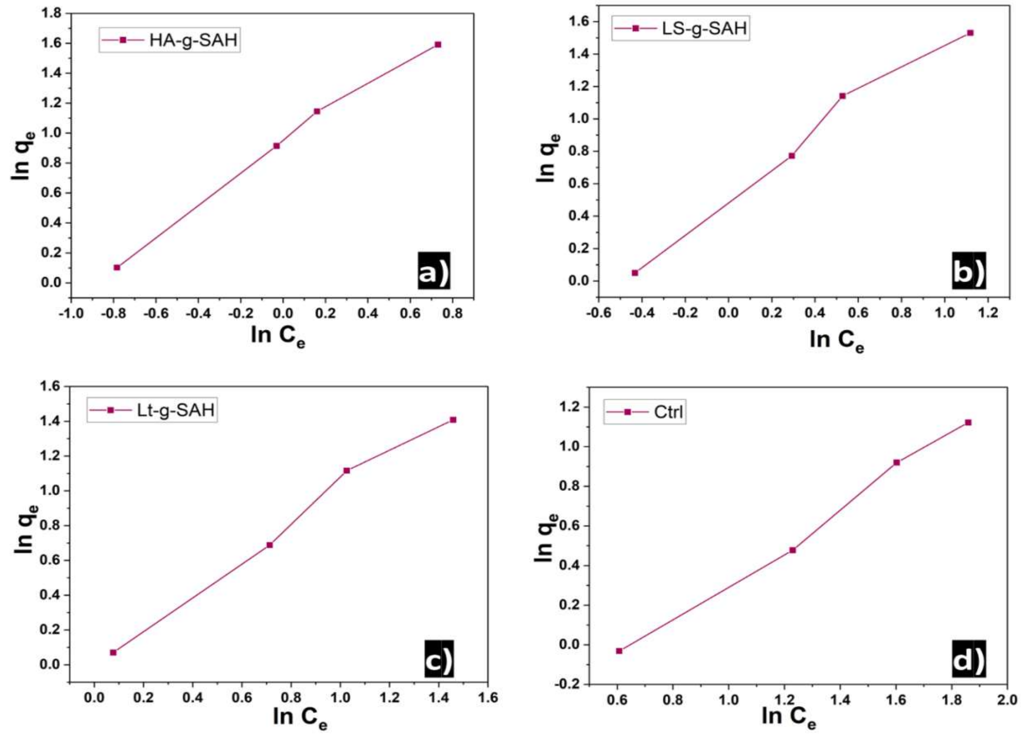

Figure 6. 4: Freundlich Isotherm Graph of a) Ha-g-SAH, b) LS-g-SAH, c) Lt-g-SAH, and d) Ctrl.

Table 6.5: Isotherms data for Freundlich adsorption isotherm

	R^2	**K_f**	**1/n**
HA-g-SAH	0.9854	2.84	0.31
LS-g-SAH	0.9685	2.52	0.36
Lt-g-SAH	0.9923	2.01	0.42
Ctrl	0.9962	1.65	0.58

The Langmuir and Freundlich isotherm models for adsorption of MB onto four different hydrogels—HA-g-SAH, LS-g-SAH, Lt-g-SAH, and a Ctrl hydrogel is shown in Figure 6.3 and Figure 6.4. The Langmuir model showed a good fit for all samples, with R^2 values ranging from 0.9168 for the ctrl to 0.9786. From Table 6.4, the Langmuir constant 'b', which reflects binding energy, was highest for HA-g-SAH (b=0.038), indicating the most substantial adsorption, while the ctrl hydrogel had the lowest b=0.015. The separation factor R_L values for all hydrogels fell within the range of 0 to 1, confirming favorable adsorption, with HA-g-SAH exhibiting the most favorable value (R_L=0.37) and the ctrl hydrogel the least favorable (R_L=0.76).

In the Freundlich model, the R^2 values indicated an excellent fit for all hydrogels. From Table 6.5, the Freundlich constant 'K_f', which signifies adsorption capacity, was highest for HA-g-SAH (K_f=2.84) and lowest for the ctrl (K_f=1.65), while the adsorption intensity parameter '1/n' ranged from 0.31 for HA-g-SAH to 0.58 for the ctrl, with lower values indicating more favorable adsorption. These results confirmed that HA-g-SAH is the most efficient adsorbent, demonstrating the highest adsorption capacity and most favorable intensity. LS-g-SAH and Lt-g-SAH also showed good adsorption performance, though slightly less effective than HA-g-SAH, while the ctrl hydrogel exhibited the weakest adsorption characteristics.

Overall, functionalized hydrogels (HA-g-SAH, LS-g-SAH, and Lt-g-SAH) outperformed the ctrl hydrogel, with HA-g-SAH emerging as the most effective adsorbent for MB dye removal due to its higher binding energy and superior adsorption capacity.

6.4 Conclusion

The research successfully demonstrated the application of efficient hydrogel systems incorporating natural polymers for MB dye removal from aqueous solutions. The comparative analysis revealed that HA-g-SAH exhibited superior performance with a maximum removal efficiency of 93.7 ±1.1% at 323.15 K and 0.3 g adsorbent dosage, followed by LS-g-SAH (92.4 ±1.3%) and Lt-g-SAH (82.4 ±1.1%), all significantly outperforming the ctrl hydrogel (67.9 ±0.9%). The adsorption process was found to be spontaneous and endothermic, as evidenced by the negative ΔG° values ranging from -7.25 to -1.86 kJ·mol^{-1} and positive ΔH° values (1.49 to 12.13 kJ·mol^{-1}). The Freundlich isotherm model provided the best fit (R^2 values: 0.9854-0.9962), indicating heterogeneous surface adsorption with favorable adsorption intensity parameters (1/n) ranging from 0.31 to 0.58. The enhanced performance of the functionalized hydrogels can be attributed to the presence of carboxylic and phenolic moieties from the natural polymers, which facilitate strong electrostatic interactions with the cationic dye molecules. The study establishes these natural polymer-based hydrogels as promising candidates for wastewater treatment applications, offering a sustainable solution for dye removal while maintaining high efficiency and environmental compatibility.

CHAPTER-7

CONCLUSION, FUTURE SCOPE AND SOCIAL IMPACT

7.1 Conclusion

The scientific community has focused more on renewable polymers made from various resources over the past few decades as a perfect and sustainable replacement for fossil fuels. Therefore, creating hydrogels using different kinds of natural polymers, such as Humic acid, lignin and lignite as a beginning material is of the utmost importance. All these natural polymers offer advantages that come with them by nature, such as reduced toxicity, affordability, and biodegradability.

7.2 Future Scope

According to the very favourable findings of this thesis, the hydrogels created using these polymers may have a wide range of applications in the fields of controlled release of pesticides, improving soil water retention, and treating dye pollution. However, Humic acid, lignin and lignite hydrogel-based formulations may further be explored for several new applications as discussed below:

- Development of sustainable, high-performance animal feed additives in the form of pellets and bypass proteins. - These hydrogels may be used to protect the fed amino acids while in the rumen of ruminants, allowing them to be digested within the small intestine. As a result, there will be an enhanced utilization of the essential amino acids, resulting in improved milk and meat production.
- Utilization in the development of various products for crop protection, including bio-based hydrogel dispersants, UV protectors, rheology modifiers, and binders.
- Synthesis of bio-based dyestuff dispersants in textile industries is also possible. Humic acid, lignin and lignite hydrogel with anionic derivative modification is

expected to enable them to adsorb onto dye particles and also interact through hydrogen bonding with the fibres to be dyed, providing colour fastness and excellent fibre staining properties.

- Although there is a growing corpus of studies on the potential of HA as an electrode in batteries and its high redox capabilities, its hydrogels have not yet been investigated as energy storage technologies.
- Hydrogel can function as a promising electrolyte, but its stable voltage window is constrained. Additionally, water, as a solvent, allows for a wide range of operational temperatures. Further investigation is required to overcome these shortcomings and improve hydrogels' mechanical stability and electrochemical properties.

Overall, this research focuses on the numerous fields in which HA, lignin and lignite-based hydrogels can be used, along with their future perspectives. Hopefully, this will shed new light on the employment of these biopolymers as the essential feedstock of a hydrogel.

7.3 Social Impact

This research contributes to society by offering renewable, affordable, and biodegradable alternatives to fossil fuel–based polymers. Hydrogels developed from humic acid, lignin, and lignite show promise in agriculture through improved soil water retention, controlled pesticide release, and sustainable livestock feed formulations that enhance productivity. Such innovations support food security, rural livelihoods, and reduced dependence on synthetic agrochemicals.

REFERENCES

1. Chen Y, Aviad T (2015) Effects of humic substances on plant growth. In: MacCarthy P, Clapp CE, Malcolm RL, Bloom PR (eds) Humic Substances in Soil and Crop Sciences: Selected Readings. Soil Science Society of America, Madison, WI, USA, pp 161–186

2. Mikkelsen RL (2005) Humic materials for agriculture. Better crop with plant food, Davis, California, USA, 89:6–10

3. Arif M, Alagawany M, Abd El-Hack ME, et al (2019) Humic acid as a feed additive in poultry diets: A review. Iran. J. Vet. Res. 20:167–172

4. Ouni Y, Ghnaya T, Montemurro F, et al (2014) The role of humic substances in mitigating the harmful effects of soil salinity and improve plant productivity. Int J Plant Prod 8:353–374

5. Qin S, Xu C, Xu Y, et al (2020) Molecular signatures of humic acids from different sources as revealed by ultrahigh resolution mass spectrometry. J Chem 2020:1–11. https://doi.org/10.1155/2020/7171582

6. Venezia V, Avallone PR, Vitiello G, et al (2022) Adding humic acids to gelatin hydrogels: A way to tune gelation. biomacromolecules 23:443–453. https://doi.org/10.1021/acs.biomac.1c01398

7. Yang F, Antonietti M (2020) The sleeping giant: A polymer view on humic matter in synthesis and applications. Prog Polym Sci 100:101182. https://doi.org/10.1016/j.progpolymsci.2019.101182

8. Rico-García D, Ruiz-Rubio L, Pérez-Alvarez L, et al (2020) Lignin-based hydrogels: synthesis and applications. Polymers (Basel) 12:81. https://doi.org/10.3390/polym12010081

9. Uraki Y, Koda K (2015) Lignin. In: Encyclopedia of polymeric nanomaterials. Springer Berlin Heidelberg, Berlin, Heidelberg, pp 1073–1080

10. Liu H, Xu T, Liu K, et al (2021) Lignin-based electrodes for energy storage application. Ind Crops Prod 165:113425. https://doi.org/10.1016/j.indcrop.2021.113425

11. Wasti S, Triggs E, Farag R, et al (2021) Influence of plasticizers on thermal and mechanical properties of biocomposite filaments made from lignin and polylactic acid for 3D printing. Compos Part B Eng 205:108483. https://doi.org/10.1016/j.compositesb.2020.108483

12. Chen M, Li Y, Liu H, et al (2023) High value valorization of lignin as environmental benign antimicrobial. Mater Today Bio 18:100520. https://doi.org/10.1016/j.mtbio.2022.100520

13. Hong S, Shen X, Yuan T-Q, et al (2023) Unlocking lignin's potential with innovative DES technology. Trends Chem. 11:827-839. https://doi.org/10. 1016 /j.trechm. 2023.08.006

14. da Costa Lopes AM, Silvestre AJD, Coutinho JAP (2023) On the path to improve lignin depolymerization and functionalization into bio-based platform chemicals: A short review. Curr Opin Green Sustain Chem 43:100850. https://doi.org/10.1016/j.cogsc.2023.100850

15. Cheah YW, Salam MA, Sebastian J, et al (2023) Upgrading of triglycerides, pyrolysis oil, and lignin over metal sulfide catalysts: A review on the reaction mechanism, kinetics, and catalyst deactivation. J Environ Chem Eng 11:109614. https://doi.org/10.1016/j.jece.2023.109614

16. Bajwa DS, Pourhashem G, Ullah AH, Bajwa SG (2019) A concise review of current lignin production, applications, products and their environmental impact. Ind Crops Prod 139:111526. https://doi.org/10.1016/j.indcrop .2019.111526

17. Wang Z, Deuss PJ (2023) The isolation of lignin with native-like structure. Biotechnol Adv 68:108230. https://doi.org/10.1016/j.biotechadv.2023.108230

18. Beaucamp A, Muddasar M, Amiinu IS, et al (2022) Lignin for energy applications – state of the art, life cycle, technoeconomic analysis and future trends. Green Chem 24:8193–8226. https://doi.org/10.1039/D2GC02724K

19. Yoo CG, Ragauskas AJ (2021) Opportunities and challenges of lignin utilization. In: Geun Yoo C, Ragauskas AJ (eds) lignin utilization strategies: from processing to applications. American Chemical Society, Washington DC, pp 1–12

20. Vasile C, Baican M (2023) Lignins as promising renewable biopolymers and bioactive compounds for high-performance materials. polymers (Basel) 15:3177. https://doi.org/10.3390/polym15153177

21. Stanisz M, Klapiszewski Ł, Collins MN, Jesionowski T (2022) Recent progress in biomedical and biotechnological applications of lignin-based spherical nano- and microstructures: a comprehensive review. Mater Today Chem 26:101198. https://doi.org/10.1016/j.mtchem.2022.101198

22. Sipponen MH, Österberg M (2019) Aqueous ammonia pre-treatment of wheat straw: process optimization and broad spectrum dye adsorption on nitrogen-containing lignin. Front Chem 7:545. https://doi.org/10.3389/fchem.2019.00545

23. Liang L, Wang Y-Y, Bhagia S, et al (2022) Chemical and morphological structure of transgenic switchgrass organosolv lignin extracted by ethanol, tetrahydrofuran, and γ-valerolactone pretreatments. ACS Sustain Chem Eng 10:9041–9052. https://doi.org/10.1021/acssuschemeng.2c00948

24. Meng X, Pu Y, Li M, Ragauskas AJ (2020) A biomass pretreatment using cellulose-derived solvent Cyrene. Green Chem 22:2862–2872. https://doi.org/10.1039/D0GC00661K

25. Liu Y, Deak N, Wang Z, et al (2021) Tunable and functional deep eutectic solvents for lignocellulose valorization. Nat Commun 12:5424. https://doi.org/10.1038/s41467-021-25117-1

26. Sarlaki E, Sharif Paghaleh A, Kianmehr MH, Asefpour Vakilian K (2021) Valorization of lignite wastes into humic acids: Process optimization, energy efficiency and structural features analysis. Renew Energy 163:105–122. https://doi.org/10.1016/j.renene.2020.08.096

27. Hoffmann K, Huculak-Maczka M (2012) The utilization possibility of waste lignite as a raw material in the process of obtaining humic acids preparations. Polish J Chem Technol 14:1–6. https://doi.org/10.2478/v10026-012-0093-2

28. Wang C-F, Fan X, Zhang F, et al (2017) Characterization of humic acids extracted from a lignite and interpretation for the mass spectra. RSC Adv 7:20677–20684. https://doi.org/10.1039/C7RA01497J

29. Tahir MM, Khurshid M, Khan MZ, et al (2011) Lignite-derived humic acid effect on growth of wheat plants in different soils. Pedosphere 21:124–131. https://doi.org/10.1016/S1002-0160(10)60087-2

30. Sarlaki E, Sharif Paghaleh A, Kianmehr MH, Asefpour Vakilian K (2019) Extraction and purification of humic acids from lignite wastes using alkaline treatment and membrane ultrafiltration. J Clean Prod 235:712–723. https://doi.org/10.1016/j.jclepro.2019.07.028

31. Khadem AF, Azman S, Plugge CM, et al (2017) Effect of humic acids on the activity of pure and mixed methanogenic cultures. Biomass and Bioenergy 99:21–30. https://doi.org/10.1016/j.biombioe.2017.02.012

32. Tripathi RC, Jain VK, Tripathi PSM (2009) Fungal biosolubilization of neyveli lignite into humic acid. Energy sources, Part A Recover Util Environ Eff 32:72–82. https://doi.org/10.1080/15567030802464354

33. Cheng G, Niu Z, Zhang C, et al (2019) Extraction of humic acid from lignite by KOH-hydrothermal method. Appl Sci 9:1356. https://doi.org/ 10.3390/app9 071356

34. Li Y, Yuan S (2021) Influence of addition of KOH on the yield and characteristics of humic acids extracted from lignite using NaOH. SN Appl Sci 3:47. https://doi.org/10.1007/s42452-020-04087-x

35. Huculak-Mączka M, Hoffmann J, Hoffmann K (2018) Evaluation of the possibilities of using humic acids obtained from lignite in the production of commercial fertilizers. J Soils Sediments 18:2868–2880. https://doi.org/10.1007/s11368-017-1907-x

36. Tanwar M, Gupta RK, Rani A (2024) Natural gums and their derivatives based hydrogels: in biomedical, environment, agriculture, and food industry. Crit Rev Biotechnol 44:275–301. https://doi.org/10.1080/073 88551.2022. 2157702

37. Tanwar M, Gupta RK, Rani A (2023) Carboxymethylated gum tragacanth crosslinked poly(sodium acrylate)hydrogel: Fabrication, characterization, rheology and drug-delivery application. Indian J Chem Technol 30:308–319. https://doi.org/10.56042/ijct.v30i3.70100

38. Tanwar M, Rani A, Gupta RK (2023) Synthesis and characterization of carboxymethylated locust bean gum- co -poly(SA)- cl -poly(MBA) pH responsive hydrogel for controlled drug delivery of metformin hydrochloride. ChemistrySelect 8:e202302525. https://doi.org/10.1002/ slct.202302525

39. Kumar J, Purwar R (2024) Self-Healing, Biocompatible injectable hydrogel based on multialdehyde moringa oleifera gum and carboxymethyl chitosan: a suitable platform for drug delivery in wound healing application. ChemistrySelect 9:e202400309. https://doi.org/10.1002/slct.202400309

40. Palem RR, Madhusudana Rao K, Kang TJ (2019) Self-healable and dual-functional guar gum-grafted-polyacrylamidoglycolic acid-based hydrogels with nano-silver for wound dressings. Carbohydr Polym 223:115074. https://doi.org/10.1016/j.carbpol.2019.115074

41. Singh B, Varshney L, Francis S, Rajneesh (2017) Synthesis and characterization of tragacanth gum based hydrogels by radiation method for use in wound dressing application. Radiat Phys Chem 135:94-105. https://doi.org/10.1016/j.radphyschem.2017.01.044

42. Zhang W, Wei Y, Wei Q, et al (2023) Cascade enzymatic preparation of carboxymethyl chitosan-based multifunctional hydrogels for promoting cutaneous wound healing. Int J Biol Macromol 248:125793. https://doi.org/10. 1016/j.ijbiomac.2023.125793

43. Toropitsyn E, Ščigalková I, Pravda M, et al (2023) Enzymatically cross-linked hyaluronic acid hydrogels as in situ forming carriers of platelet-rich plasma: Mechanical properties and bioactivity levels evaluation. J Mech Behav Biomed Mater 143:105916. https://doi.org/10.1016/j.jmbbm.2023.105916

44. Costa RR, Reis RL, Pashkuleva I (2024) Hydrogels formed by polyelectrolyte complexation. In: Oliveira M, Silva-Correia J, Reis RL (eds) Hydrogels for Tissue Engineering and Regenerative Medicine. Elsevier, pp 311–330

45. Xiao J-X, Wang L-H, Xu T-C, Huang G-Q (2019) Complex coacervation of carboxymethyl konjac glucomannan and chitosan and coacervate characterization. Int J Biol Macromol 123:436–445. https://doi.org/10.1016/j.ijbiomac.2018.11.086

46. Maiti S, Khillar PS, Mishra D, et al (2021) Physical and self–crosslinking mechanism and characterization of chitosan-gelatin-oxidized guar gum hydrogel. Polym Test 97:107155. https://doi.org/10.1016/j.polymertesting.2021.107155

47. Varaprasad K, Raghavendra GM, Jayaramudu T, et al (2017) A mini review on hydrogels classification and recent developments in miscellaneous applications. Mater. Sci. Eng. C 79:958–971

48. Wan L, Li P, Yan M, et al (2023) Strong, self-healing, shape memory PAA-PANI/PVA/PDA/AOP conductive hydrogels with interpenetrating network and hydrogen bond interaction. Eur Polym J 191:112034. https://doi.org/10.1016/j.eurpolymj.2023.112034

49. Cai Y, Liu C, Gong K, et al (2023) Mussel-inspired quaternary composite hydrogels with high strength and high tissue adhesion for transdermal drug delivery: Synergistic hydrogen bonding and drug release mechanism. Chem Eng J 465:142942. https://doi.org/10.1016/j.cej.2023.142942

50. Adelnia H, Ensandoost R, Shebbrin Moonshi S, et al (2022) Freeze/thawed polyvinyl alcohol hydrogels: Present, past and future. Eur Polym J 164:110974. https://doi.org/10.1016/J.EURPOLYMJ.2021.110974

51. Zhang K yan, Li D, Wang Y, Wang L jun (2023) Carboxymethyl chitosan/polyvinyl alcohol double network hydrogels prepared by freeze-thawing and calcium chloride cross-linking for efficient dye adsorption. Int J Biol Macromol 253:126897. https://doi.org/10.1016/J.IJBIOMAC.2023.126897

52. Huang Jin, Fu Shiyu, Gan Lin (2019) Lignin-modified materials and their applications. In: Lignin chemistry and applications. Elsevier, pp 181–210

53. Borisenkov MF, Karmanov AP, Kocheva LS, et al (2016) Adsorption of β - glucuronidase and estrogens on pectin/lignin hydrogel particles. Int J Polym Mater Polym Biomater 65:433–441. https://doi.org/10.1080/00914037.2015. 1129955

54. Dong Y, Paukkonen H, Fang W, et al (2018) Entangled and colloidally stable microcrystalline cellulose matrices in controlled drug release. Int J Pharm 548:113–119. https://doi.org/10.1016/j.ijpharm.2018.06.022

55. Yang W, Fortunati E, Bertoglio F, et al (2018) Polyvinyl alcohol/chitosan hydrogels with enhanced antioxidant and antibacterial properties induced by lignin nanoparticles. Carbohydr Polym 181:275–284. https://doi.org/10.1016/j. carbpol.2017.10.084

56. Spasojević D, Zmejkoski D, Glamočlija J, et al (2016) Lignin model compound in alginate hydrogel: a strong antimicrobial agent with high potential in wound treatment. Int J Antimicrob Agents 48:732–735. https://doi.org/10.1016/j.ijantimicag.2016.08.014

57. Venezia V, Verrillo M, Avallone PR, et al (2023) Waste to wealth approach: improved antimicrobial properties in bioactive hydrogels through humic substance−gelatin chemical conjugation. https://doi.org/10.1021/acs. biomac.3c00143

58. Yalman V, Laçin NT (2019) Development of humic acid and alginate-based wound dressing and evaluation on inflammation. Mater Technol 34:705–717. https://doi.org/10.1080/10667857.2019.1619961

59. Jin C, Song W, Liu T, et al (2018) Temperature and pH responsive hydrogels using methacrylated lignosulfonate cross-linker: synthesis, characterization, and properties. ACS Sustain Chem Eng 6:1763–1771. https://doi.org/10.1021/acssuschemeng.7b03158

60. Bromberg LE, Ron ES (1998) Temperature-responsive gels and thermogelling polymer matrices for protein and peptide delivery. Adv. Drug Deliv. Rev. 31:197–221

61. Kanmaz N, Saloglu D, Hizal J (2019) Humic acid embedded chitosan/poly (vinyl alcohol) pH-sensitive hydrogel: Synthesis, characterization, swelling kinetic and diffusion coefficient. Chem Eng Commun 206:1168–1180. https://doi.org/10.1080/00986445.2018.1550396

62. Kai D, Low ZW, Liow SS, et al (2015) Development of lignin supramolecular hydrogels with mechanically responsive and self-healing properties. ACS Sustain Chem Eng 3:2160–2169. https://doi.org/10.1021 /acssuschemeng.5b00405

63. Fei Y, Jiang Z, Zhou D, et al (2023) Preparation a highly sensitive and flexible textile supercapacitor based on lignin hydrogel and polyaniline@carbon cloth composites. J Energy Storage 73:108978. https://doi.org/10.1016/ j.est.2023.108978

64. Li F, Wang X, Sun R (2017) A metal-free and flexible supercapacitor based on redox-active lignosulfonate functionalized graphene hydrogels. J Mater Chem A 5:20643–20650. https://doi.org/10.1039/c7ta03789a

65. Han X, Su Y, Che G, et al (2023) Novel lignin hydrogel sensors with antiswelling, antifreezing, and anticreep properties. ACS Sustain Chem Eng 11:8255–8270. https://doi.org/10.1021/acssuschemeng.2c07727

66. Wan K, Xiao Y, Fan J, et al (2022) Preparation of high-capacity macroporous adsorbent using lignite-derived humic acid and its multifunctional binding chemistry for heavy metals in wastewater. J Clean Prod 363:132498. https://doi.org/10.1016/j.jclepro.2022.132498

67. Wang Y, Jiang W, Li J, et al (2023) Zinc-ion engineered plant-based multifunctional hydrogels for flexible wearable strain sensors, bio-electrodes and zinc-ion hybrid capacitors. Chem Eng J 465:142917. https://doi.org /10.1016/j.cej.2023.142917

68. Wang Y, Xiong Y, Wang J, Zhang X (2017) Ultrasonic-assisted fabrication of montmorillonite-lignin hybrid hydrogel: Highly efficient swelling behaviors and super-sorbent for dye removal from wastewater. Colloids Surfaces A Physicochem Eng Asp 520:903–913. https://doi.org/10.1016/j.colsurfa .2017.02.050

69. Yu C, Wang F, Zhang C, et al (2016) The synthesis and absorption dynamics of a lignin-based hydrogel for remediation of cationic dye-contaminated effluent. React Funct Polym 106:137–142. https://doi.org/10.1016/j. reactfunctpolym.2016.07.016

70. Tang Y, Zeng Y, Hu T, et al (2016) Preparation of lignin sulfonate-based mesoporous materials for adsorbing malachite green from aqueous solution. J Environ Chem Eng 4:2900–2910. https://doi.org/10.1016/j.jece.2016.05.040

71. Anirudhan TS, Suchithra PS, Radhakrishnan PG (2009) Synthesis and characterization of humic acid immobilized-polymer/bentonite composites and their ability to adsorb basic dyes from aqueous solutions. Appl Clay Sci 43:336–342. https://doi.org/10.1016/j.clay.2008.09.015

72. Zheng L, Seidi F, Wu W, et al (2023) Dual-functional lignin-based hydrogels for sustained release of agrochemicals and heavy metal ion complexation. Int J Biol Macromol 235:123701. https://doi.org/10.1016/j.ijbiomac.2023.123701

73. Hua B, Wei H, Hu C, et al (2024) Preparation of pH/temperature-responsive semi-IPN hydrogels based on sodium alginate and humic acid as slow-release and water-retention fertilizers. Polym Bull 81:4175–4198. https://doi.org/ 10.1007/s00289-023-04901-7

74. Sun Y, Ma Y, Fang G, et al (2016) Controlled pesticide release from porous composite hydrogels based on lignin and polyacrylic acid. BioResources 11:2361–2371. https://doi.org/10.15376/biores.11.1.2361-2371

75. Niu Y, Ke R, Yang T, Song J (2019) pH-responsively water-retaining controlled-release fertilizer using humic acid hydrogel and nano-silica aqueous dispersion. J Nanosci Nanotechnol 20:2286–2291. https://doi.org/ 10.1166/jnn.2020.17216

76. Huang J, Wan Y, Wang M, et al (2022) Lignin nanorods reinforced nanocomposite hydrogels with UV-shielding, anti-freezing and anti-drying applications. Ind Crops Prod 187:115324. https://doi.org/10.1016/j.indcrop. 2022.115324

77. Miao Y, Tang Z, Zhang Q, et al (2022) Biocompatible lignin-containing hydrogels with self-adhesion, conductivity, uv shielding, and antioxidant activity as wearable sensors. ACS Appl Polym Mater 4:1448–1456. https://doi.org/10.1021/acsapm.1c01817

78. Thakur S, Govender PP, Mamo MA, et al (2017) Progress in lignin hydrogels and nanocomposites for water purification: Future perspectives. Vacuum 146:342–355. https://doi.org/10.1016/j.vacuum.2017.08.011

79. Ghobashy MM (2019) The application of natural polymer-based hydrogels for agriculture. In: hydrogels based on natural polymers. Elsevier, pp 329–356

80. Kazanskii KS, Dubrovskii SA (1992) Chemistry and physics of "agricultural" hydrogels. pp 97–133

81. Miroshnichenko D, Lebedeva K, Cherkashina A, et al (2022) Study of hybrid modification with humic acids of environmentally safe biodegradable hydrogel films based on hydroxypropyl methylcellulose. C-Journal Carbon Res 8:71. https://doi.org/10.3390/c8040071

82. Baker H, Khalili F (2003) Comparative study of binding strengths and thermodynamic aspects of Cu(II) and Ni(II) with humic acid by Schubert's ion-exchange method. Anal Chim Acta 497:235–248. https://doi.org/10.1016/j.aca.2003.08.036

83. Shaker MA, Albishri HM (2014) Dynamics and thermodynamics of toxic metals adsorption onto soil-extracted humic acid. Chemosphere 111:587–595. https://doi.org/10.1016/j.chemosphere.2014.04.088

84. Klučáková M, Kalina M, Smilek J, Laštůvková M (2018) The transport of metal ions in hydrogels containing humic acids as active complexation agent. Colloids Surfaces A Physicochem Eng Asp 557:116–122. https://doi.org/10.1016/j.colsurfa.2018.02.042

85. Singh T, Singhal R (2012) Poly(acrylic acid/acrylamide/sodium humate) superabsorbent hydrogels for metal ion/dye adsorption: Effect of sodium humate concentration. J Appl Polym Sci 125:1267–1283. https://doi.org/10.1002/app.35435

86. Li H, Li Y, Li C (2013) Characterization of humic acids and fulvic acids derived from sewage sludge. Asian J Chem 25:10087–10091. https://doi.org/10.14233/ajchem.2013.15162

87. Miao Z, Li K, Liu P, et al (2018) Natural humic-acid-based phototheranostic agent. Adv Healthc Mater 7:1701202 . https://doi.org/10.1002/adhm.201701 202

88. Zhang Y, Mao J, Jiang W, et al (2021) Lignin sulfonate induced ultrafast polymerization of double network hydrogels with anti-freezing, high strength and conductivity and their sensing applications at extremely cold conditions. Compos Part B Eng 217:108879. https://doi.org/10.1016/j.compositesb. 2021.108879

89. Gan D, Xing W, Jiang L, et al (2019) Plant-inspired adhesive and tough hydrogel based on Ag-Lignin nanoparticles-triggered dynamic redox catechol chemistry. Nat Commun 10:1–10. https://doi.org/10.1038/s41467-019-09351-2

90. Afewerki S, Wang X, Ruiz-Esparza GU, et al (2020) Combined catalysis for engineering bioinspired, lignin-based, long-lasting, adhesive, self-mending, antimicrobial hydrogels. ACS Nano 14:17004–17017. https://doi.org/10.1021/acsnano.0c06346

91. Cui H, Jiang W, Wang C, et al (2021) Lignin nanofiller-reinforced composites hydrogels with long-lasting adhesiveness, toughness, excellent self-healing, conducting, ultraviolet-blocking and antibacterial properties. Compos Part B Eng 225:109316. https://doi.org/10.1016/j.compositesb.2021.109316

92. Parajuli D, Adhikari CR, Kuriyama M, et al (2006) Selective Recovery of gold by novel lignin-based adsorption gels. Ind Eng Chem Res 45:8–14. https://doi.org/10.1021/ie050532u

93. Kubo S, Kadla JF (2005) Hydrogen bonding in lignin: A fourier transform infrared model compound study. Biomacromolecules 6:2815–2821. https://doi.org/10.1021/bm050288q

94. Oveissi F, Naficy S, Le TYL, et al (2018) Tough and processable hydrogels based on lignin and hydrophilic polyurethane. ACS Appl Bio Mater 1:2073–2081. https://doi.org/10.1021/ACSABM.8B00546

95. Ravishankar K, Venkatesan M, Desingh RP, et al (2019) Biocompatible hydrogels of chitosan-alkali lignin for potential wound healing applications. Mater Sci Eng C 102:447–457. https://doi.org/10.1016/J.MSEC.2019.04.038

96. Huang S, Shuyi S, Gan H, et al (2019) Facile fabrication and characterization of highly stretchable lignin-based hydroxyethyl cellulose self-healing hydrogel. Carbohydr Polym 223:115080. https://doi.org/10.1016/j.carbpol. 2019.115080

97. Wang Q, Pan X, Lin C, et al (2020) Ultrafast gelling using sulfonated lignin-Fe3+ chelates to produce dynamic crosslinked hydrogel/coating with charming stretchable, conductive, self-healing, and ultraviolet-blocking properties. Chem Eng J 396:125341. https://doi.org/10.1016/J.CEJ.2020.125341

98. Mishra S, Thombare N, Ali M, Swami S (2018) Applications of biopolymeric gels in agricultural sector. pp 185–228

99. Song B, Liang H, Sun R, et al (2020) Hydrogel synthesis based on lignin/sodium alginate and application in agriculture. Int J Biol Macromol 144:. https://doi.org/10.1016/j.ijbiomac.2019.12.082

100. Li X, Pan X (2010) Hydrogels based on hemicellulose and lignin from lignocellulose biorefinery: a mini-review. J Biobased Mater Bioenergy 4:289-297. https://doi.org/10.1166/jbmb.2010.1107

101. Buchmann C (2018) The swelling of interparticulate hydrogels in soil and their contribution to soil structural stability and soil-water interactions. Landau, Germany, https://kola.opus.hbz-nrw.de/files/1672/Dissertation_Buchmann.pdf.

102. Meng Y, Liu X, Li C, et al (2019) Super-swelling lignin-based biopolymer hydrogels for soil water retention from paper industry waste. Int J Biol Macromol 135:815–820. https://doi.org/10.1016/j.ijbiomac.2019.05.195

103. Agnihotri S, Singhal R (2017) Effect of sodium humate on the swelling characteristics and agricultural application of superabsorbent hydrogels of poly (acrylic acid / sodium alginate / sodium humate). J Polym Mater 34:663–680

104. Shahid SA, Qidwai AA, Anwar F, et al (2012) Effects of a novel poly (AA-co-AAm)/AlZnFe 2O 4/ potassium humate superabsorbent hydrogel nanocomposite on water retention of sandy loam soil and wheat seedling growth. Molecules 17:12587–12602. https://doi.org/10.3390/molecules17 1112587

105. El-Sayed AE-R, Mohamed S (2017) Enhancing olive trees growth and productivity by using hydrogel and potassium humate under rain-fed condition in northern western coastal zone. Egypt J Desert Res 67:137–151. https://doi.org/10.21608/ejdr.2017.5849

106. Hua S, Wang A (2008) Preparation and properties of superabsorbent containing starch and sodium humate. Polym Adv Technol 19:1009–1014. https://doi.org/10.1002/pat.1068

107. Zheng Y, Wang A (2008) Study on superabsorbent composites. XVIII. Preparation, characterization, and property evaluation of poly(acrylic acid-co-acrylamide)/ organomontmorillonite/sodium humate superabsorbent composites. J Appl Polym Sci 108:211–219. https://doi.org/10.1002/app .27439

108. Li W, Wang J, Zou L, Zhu S (2008) Synthesis and characterization of potassium humate-acrylic acid-acrylamide hydrogel. J Polym Res 15:435–445. https://doi.org/10.1007/s10965-008-9189-z

109. Li A, Zhang J, Wang A (2007) Preparation and slow-release property of a poly(acrylic acid)/attapulgite/sodium humate superabsorbent composite. J Appl Polym Sci 103:37–45. https://doi.org/10.1002/app.23901

110. Mazloom N, Khorassani R, Zohuri GH, et al (2019) Development and characterization of lignin-based hydrogel for use in agricultural soils: preliminary evidence. CLEAN – Soil, Air, Water 47:1900101. https://doi.org /10.1002/ clen.201900101

111. Flory PJ, Rehner J (1943) Statistical mechanics of cross-linked polymer networks II. Swelling. J Chem Phys 11:521–526. https://doi.org/10.1063/ 1.1723792

112. Kabiri K, Omidian H, Hashemi SA, Zohuriaan-Mehr MJ (2003) Synthesis of fast-swelling superabsorbent hydrogels: effect of crosslinker type and concentration on porosity and absorption rate. Eur Polym J 39:1341-1348. https://doi.org/10.1016/S0014-3057(02)00391-9

113. Zohuriaan-Mehr MJ, Motazedi Z, Kabiri K, et al (2006) Gum arabic-acrylic superabsorbing hydrogel hybrids: Studies on swelling rate and environmental responsiveness. J Appl Polym Sci 102:5667–5674. https://doi.org/10.1002/app.25033

114. Wu L, Huang S, Zheng J, et al (2019) Synthesis and characterization of biomass lignin-based PVA super-absorbent hydrogel. Int J Biol Macromol 140:538–545. https://doi.org/10.1016/j.ijbiomac.2019.08.142

115. Dumitriu RP, Stoica I, Vasilescu DS, et al (2018) Alginate/lignosulfonate blends with photoprotective and antioxidant properties for active packaging applications. J Polym Environ 26:1100-1112. https://doi.org/10.1007/s10924-017-1018-1

116. Yang L, Yang Y, Chen Z, et al (2014) Influence of super absorbent polymer on soil water retention, seed germination and plant survivals for rocky slopes eco-engineering. Ecol Eng 62:27-32. https://doi.org/10.1016/j.ecoleng.2013 .10.019

117. Banedjschafie S, Durner W (2015) Water retention properties of a sandy soil with superabsorbent polymers as affected by aging and water quality. J Plant Nutr Soil Sci 178:796-806. https://doi.org/10.1002/jpln.201500128

118. Morales A, Labidi J, Gullón P (2020) Assessment of green approaches for the synthesis of physically crosslinked lignin hydrogels. J Ind Eng Chem 81:475–487. https://doi.org/10.1016/j.jiec.2019.09.037

119. Morales A, Labidi J, Gullón P (2020) Effect of the formulation parameters on the absorption capacity of smart lignin-hydrogels. Eur Polym J 129:109631. https://doi.org/10.1016/j.eurpolymj.2020.109631

120. Ciolacu D, Cazacu G (2017) New green hydrogels based on lignin. J Nanosci Nanotechnol 18:2811–2822. https://doi.org/10.1166/jnn.2018.14290

121. Mazloom N, Khorassani R, Zohury GH, et al (2020) Lignin-based hydrogel alleviates drought stress in maize. Environ Exp Bot 175:104055. https://doi.org/10.1016/j.envexpbot.2020.104055

122. Wang Y, Zhu Y, Liu Y, et al (2021) Research on preparation and properties of a multifunctional superabsorbent based on semicoke and humic acid. Eur Polym J 159:110750. https://doi.org/10.1016/j.eurpolymj.2021.110750

123. Yu X, Wang Z, Liu J, et al (2019) Preparation, swelling behaviors and fertilizer-release properties of sodium humate modified superabsorbent resin. Mater Today Commun 19:124–130. https://doi.org/10.1016/j.mtcomm .2018.12.015

124. Zhang J, Liu R, Li A, Wang A (2006) Preparation, swelling behaviors, and slow-release properties of a poly(acrylic acid-co-acrylamide)/sodium humate superabsorbent composite. Ind Eng Chem Res 45:48–53. https://doi.org/10. 1021/ie050745j

125. Wang W, Wang A (2009) Synthesis, swelling behaviors, and slow-release characteristics of a guar gum-g-poly(sodium acrylate)/sodium humate superabsorbent. J Appl Polym Sci 112:2102–2111. https://doi.org/10. 1002/app.29620

126. Peng Z, Chen F (2011) Synthesis and properties of lignin-based polyurethane hydrogels. Int J Polym Mater 60:674-683. https://doi.org/10.1080/0091 4037.2010 .551353

127. Ma Y, Wang R, Fang G, Li D (2012) Preparation and release performance of polyacrylic acid grafted alkali lignin-based iron fertilizer. Nongye Gongcheng Xuebao/Transactions Chinese Soc Agric Eng 28:208–214. https://doi.org/ 10.3969/j.issn.1002-6819.2012.18.030

128. Manu, Kumar D, Gupta RK (2023) Synthesis, characterization and application of Lignosulphonate-g- poly(sodium acrylate) hydrogel. Indian J Chem Technol 30:753–764. https://doi.org/10.56042/ijct.v30i6.1325

129. Chu M, Zhu SQ, Li HM, et al (2006) Synthesis of poly(acrylic acid)/sodium humate superabsorbent composite for agricultural use. J Appl Polym Sci 102:5137–5143. https://doi.org/10.1002/app.24661

130. Song J, Chen L, Niu Y, Ruan H (2022) Sustained urea release performance of humic acid hydrogel for green vegetable growth environment evaluation. J Porous Mater 29:1747–1758. https://doi.org/10.1007/s10934-022-01282-6

131. Manu, Kumar D, Gupta RK (2024) novel formulations of humic acid, lignin, and lignite grafted hydrogels for the slow release of thiamethoxam. ChemistrySelect 9:e202304939. https://doi.org/10.1002/slct. 202304939

132. Wei X, Chen H, Lin D, et al (2023) A field study of nano-FeS loaded lignin hydrogel application for Cd reduction, nutrient enhancement, and microbiological shift in a polluted paddy soil. Chem Eng J 451:138647. https://doi.org/10.1016/j.cej.2022.138647

133. Wilske B, Bai M, Lindenstruth B, et al (2014) Biodegradability of a polyacrylate superabsorbent in agricultural soil. Environ Sci Pollut Res 21:9453–9460. https://doi.org/10.1007/s11356-013-2103-1

134. Takigami H, Taniguchi N, Shimizu Y, Matsui S (1998) Toxicity assays and their evaluation on organic polymer flocculants used for municipal sludge dewatering. Water Sci Technol 38:207–215. https://doi.org/10.2166/wst. 1998.0294

135. Mai C, Schormann W, Majcherczyk A, H□ttermann A (2004) Degradation of acrylic copolymers by white-rot fungi. Appl Microbiol Biotechnol 65:479-487. https://doi.org/10.1007/s00253-004-1668-5

136. Liu C, Li Y, Zhuang J, et al (2022) Conductive hydrogels based on industrial lignin: opportunities and challenges. Polymers (Basel) 14:1–19. https://doi.org/10.3390/polym14183739

137. Yamamoto H, Amaike M, Saitoh H, Sano Y (1999) Gel formation of lignin and biodegradation of the lignin gels by microorganisms. Mater Sci Eng C 7:143–147. https://doi.org/10.1016/s0928-4931(99)00134-4

138. Yan A, Wang Y, Tan SN, et al (2020) Phytoremediation: A promising approach for revegetation of heavy metal-polluted land. Front. Plant Sci. 11. https://doi.org/10.3389/fpls.2020.00359.

139. Su X, Hu J, Zhang J, et al (2021) Investigating the adsorption behavior and mechanisms of insoluble Humic acid/starch composite microspheres for metal ions from water. Colloids Surfaces A Physicochem Eng Asp 610:125672. https://doi.org/10.1016/j.colsurfa.2020.125672

140. Sedláček P, Smilek J, Klučáková M (2013) How the interactions with humic acids affect the mobility of ionic dyes in hydrogels - Results from diffusion cells. React Funct Polym 73:1500–1509. https://doi.org/10.1016/j.reactfunctpolym.2013.07.008

141. Pérez AL, Anderson KA (2009) Soil-diffusive gradient in thin films partition coefficients estimate metal bioavailability to crops at fertilized field sites. Environ Toxicol Chem 28:2030–2037. https://doi.org/10.1897/08-637.1

142. Sagbas S, Kantar C, Sahiner N (2014) Preparation of poly(humic acid) particles and their use in toxic organo-phenolic compound removal from aqueous environments. Water Air Soil Pollut 225:1–10. https://doi.org/10. 1007/s11270-013-1809-5

143. Jada A, Ait Akbour R, Douch J (2006) Surface charge and adsorption from water onto quartz sand of humic acid. Chemosphere 64:1287–1295. https://doi.org/10.1016/j.chemosphere.2005.12.063

144. Zhou P, Yan H, Gu B (2005) Competitive complexation of metal ions with humic substances. Chemosphere 58:1327–1337. https://doi.org/10.1016 /j.chemosphere.2004.10.017

145. Sedláček P, Smilek J, Klučáková M (2014) How the interactions with humic acids affect the mobility of ionic dyes in hydrogels - 2. Non-stationary diffusion experiments. React Funct Polym 75:41–50. https://doi.org/10.1016/ j.reactfunctpolym.2013.12.002

146. Fernandes AN, Almeida CAP, Menezes CTB, et al (2007) Removal of methylene blue from aqueous solution by peat. J Hazard Mater 144:412–419. https://doi.org/10.1016/j.jhazmat.2006.10.053

147. Meng Y, Lu J, Cheng Y, et al (2019) Lignin-based hydrogels: A review of preparation, properties, and application. Int J Biol Macromol 135:1006–1019. https://doi.org/10.1016/j.ijbiomac.2019.05.198

148. Thakur VK, Thakur MK (2015) Recent advances in green hydrogels from lignin: A review. Int. J. Biol. Macromol. 72:834–847. https://doi.org/10. 1016/j.ijbiomac.2014.09.044

149. Yi JZ, Zhang LM (2008) Removal of methylene blue dye from aqueous solution by adsorption onto sodium humate/polyacrylamide/clay hybrid hydrogels. Bioresour Technol 99:2182–2186. https://doi.org/10.1016/j.biortech.2007.05.8

150. Wang H, Huang M, Li L, et al (2024) Highly efficient copper ions removal by sodium alginate/sodium humate@polyacrylamide: adsorption behavior and removal mechanism. Water, Air, Soil Pollut 235:250. https://doi.org/10.1007/s11270-024-07046-z

151. Feng Z, Zheng Y, Wang H, et al (2023) Sodium humate based double network hydrogel for Cu and Pb removal. Chemosphere 313:137558. https://doi.org/10.1016/j.chemosphere.2022.137558

152. Zhang X, Li Y, Zou W, et al (2024) Preparation of composite porous hydrogel montmorillonite/humic acid/polyvinyl alcohol@polypyrrole based on pickering emulsion template method for enhancing hexavalent chromium ions adsorption from aqueous solution. J Inorg Organomet Polym Mater 34:745–758. https://doi.org/10.1007/s10904-023-02857-9

153. Chen R, Zhang Y, Shen L, et al (2015) Lead(II) and methylene blue removal using a fully biodegradable hydrogel based on starch immobilized humic acid. Chem Eng J 268:348–355. https://doi.org/10.1016/j.cej.2015.01.081

154. Gong X, Sawut A, Simayi R, et al (2024) Preparation of modified humic acid/TiO 2 /P(AA- co -AM) nanocomposite hydrogels with enhanced dye adsorption and photocatalysis. Soft Matter 20:2937–2954. https://doi.org/10.1039/D3SM01749D

155. Ma J, Luo J, Liu Y, et al (2018) Pb(ii), Cu(ii) and Cd(ii) removal using a humic substance-based double network hydrogel in individual and multicomponent systems. J Mater Chem A 6:20110–20120. https://doi.org/10. 1039/c8ta07250g

156. Choe SR, Haldorai Y, Jang SC, et al (2018) Fabrication of alginate/humic acid/Fe-aminoclay hydrogel composed of a grafted-network for the efficient removal of strontium ions from aqueous solution. Environ Technol Innov 9:285–293. https://doi.org/10.1016/j.eti.2017.12.008

157. Akshita Srivastava, Manu, Gupta RK (2023) Xanthan gum and lignin grafted chemically crosslinked hydrogels for dye removal: synthesis, characterization and isotherms studies. Polym Sci Ser A 65:725–733. https://doi.org/10.1134/S0965545X23600552

158. Tahari N, de Hoyos-Martinez PL, Abderrabba M, et al (2020) Lignin - montmorillonite hydrogels as toluene adsorbent. Colloids Surfaces A Physicochem Eng Asp 602:125108. https://doi.org/10.1016/j.colsurfa.2020.125108

159. Li J, Li H, Yuan Z, et al (2019) Role of sulfonation in lignin-based material for adsorption removal of cationic dyes. Int J Biol Macromol 135:1171–1181. https://doi.org/10.1016/j.ijbiomac.2019.06.024

160. Luo H, Ren S, Ma Y, et al (2015) Preparation and properties of kraft lignin-n-isopropyl acrylamide hydrogel. BioResources 10:3507–3519. https://doi.org/10.15376/BIORES.10.2.

161. Wang C, Feng X, Shang S, et al (2023) Lignin/sodium alginate hydrogel for efficient removal of methylene blue. Int J Biol Macromol 237:124200. https://doi.org/10.1016/j.ijbiomac.2023.124200

162. Tian R, Liu Q, Zhang W, Zhang Y (2018) Preparation of lignin-based hydrogel and its adsorption on Cu^{2+} ions and Co^{2+} ions in wastewaters. J Inorg Organomet Polym Mater 28:2545–2553. https://doi.org/10.1007/s10904-018-0943-3

163. Yuan H, Peng J, Ren T, et al (2021) Novel fluorescent lignin-based hydrogel with cellulose nanofibers and carbon dots for highly efficient adsorption and detection of Cr(VI). Sci Total Environ 760:143395. https://doi.org/10.1016/j.scitotenv.2020.143395

164. Jiang S, Zhang Z, Zhou T, et al (2022) Lignin hydrogel-based solar-driven evaporator for cost-effective and highly efficient water purification. Desalination 531:115706. https://doi.org/10.1016/j.desal.2022.115706

165. Liu Y, Huang Y, Zhang C, et al (2020) Nano-FeS incorporated into stable lignin hydrogel: A novel strategy for cadmium removal from soil. Environ Pollut 264:114739. https://doi.org/10.1016/j.envpol.2020.114739

166. Sun X-F, Hao Y, Cao Y, Zeng Q (2019) Superadsorbent hydrogel based on lignin and montmorillonite for Cu(II) ions removal from aqueous solution. Int J Biol Macromol 127:511–519. https://doi.org/10.1016/j.ijbiomac.2019.01.058

167. Liu K, Du H, Zheng T, et al (2021) Recent advances in cellulose and its derivatives for oilfield applications. Carbohydr Polym 259:117740. https://doi.org/10.1016/J.CARBPOL.2021.117740

168. Landi G, La Notte L, Palma AL, Puglisi G (2022) Electrochemical performance of biopolymer-based hydrogel electrolyte for supercapacitors with eco-friendly binders. Polymers (Basel) 14:4445. https://doi.org/10.3390/ polym14204445

169. Ajjan FN, Mecerreyes D, Inganäs O (2019) Enhancing Energy Storage Devices with Biomacromolecules in Hybrid Electrodes. Biotechnol J 14:1900062. https://doi.org/10.1002/biot.201900062

170. Xu T, Liu K, Sheng N, et al (2022) Biopolymer-based hydrogel electrolytes for advanced energy storage/conversion devices: Properties, applications, and perspectives. Energy Storage Mater 48:244–262. https://doi.org/10.1016/j .ensm.2022.03.013

171. Zhang SS (2007) A review on the separators of liquid electrolyte Li-ion batteries. J Power Sources 164:351–364. https://doi.org/10.1016/j .jpowsour.2006.10.065

172. Li H, Han C, Huang Y, et al (2018) An extremely safe and wearable solid-state zinc ion battery based on a hierarchical structured polymer electrolyte. Energy Environ Sci 11:941–951. https://doi.org/10.1039/C7EE03232C

173. Lopez J, Sun Y, Mackanic DG, et al (2018) A dual-crosslinking design for resilient lithium-ion conductors. Adv Mater 30:1804142. https://doi.org/10.1002/ adma.201804142

174. Yin B-S, Zhang S-W, Ren Q-Q, et al (2017) Elastic soft hydrogel supercapacitor for energy storage. J Mater Chem A 5:24942–24950. https://doi.org/10.1039 /C7TA08152A

175. Powell C, Beall GW (2015) Graphene oxide and graphene from low grade coal: Synthesis, characterization and applications. Curr Opin Colloid Interface Sci 20:362–366. https://doi.org/10.1016/J.COCIS.2015.11.003

176. Li Y, Jia X, Li X, et al (2023) Study on the potential of sludge-derived humic acid as energy storage material. Waste Manag 162:55–62. https://doi.org/10.1016/J.WASMAN.2023.03.015

177. Beall GW, Duraia E-SM, Yu Q, Liu Z (2014) Single crystalline graphene synthesized by thermal annealing of humic acid over copper foils. Phys E Low-dimensional Syst Nanostructures 56:331–336. https://doi.org/10.1016/j.physe.2013.10.008

178. Wang C, Cheng T, Zhang D, Pan X (2023) Electrochemical properties of humic acid and its novel applications: A tip of the iceberg. Sci Total Environ 863:160755. https://doi.org/10.1016/j.scitotenv.2022.160755

179. Zhu H, Yin J, Zhao X, et al (2015) Humic acid as promising organic anodes for lithium/sodium ion batteries. Chem Commun 51:14708–14711. https://doi.org/10.1039/c5cc04772b

180. Duraia E-SM, Niu S, Beall GW, Rhodes CP (2018) Humic acid-derived graphene–SnO_2 nanocomposites for high capacity lithium-ion battery anodes. J Mater Sci Mater Electron 29:8456–8464. https://doi.org/10.1007/s10854-018-8858-x

181. Hekmat F, Shahi M, Shahrokhian S (2021) Direct fabrication of phosphorus-doped nickel sulfide and eco-friendly biomass-derived humic acid as efficient electrodes for energy storage applications. Sustain Energy Fuels 5:4869–4881. https://doi.org/10.1039/D1SE00905B

182. Wang H, Yang Y, Guo L (2017) Renewable-biomolecule-based electrochemical energy-storage materials. Adv Energy Mater 7:1700663. https://doi.org/10.1002/aenm.201700663

183. Xing B, Yuan R, Zhang C, et al (2017) Facile synthesis of graphene nanosheets from humic acid for supercapacitors. Fuel Process Technol 165:112–122. https://doi.org/10.1016/j.fuproc.2017.05.021

184. Zhu Y, Chen M, Li Q, et al (2017) High-yield humic acid-based hard carbons as promising anode materials for sodium-ion batteries. Carbon N Y 123:727–734. https://doi.org/10.1016/j.carbon.2017.08.030

185. Yin J, Zhang D, Zhao J, et al (2014) Meso- and micro- porous composite carbons derived from humic acid for supercapacitors. Electrochim Acta 136:504–512. https://doi.org/10.1016/j.electacta.2014.05.115

186. Huang G, Geng Q, Xing B, et al (2020) Manganous nitrate -assisted potassium hydroxide activation of humic acid to prepare oxygen-rich hierarchical porous carbon as high-performance supercapacitor electrodes. J Power Sources 449:227506. https://doi.org/10.1016/j.jpowsour.2019.227506

187. Zhang H-B, Yang Z, Qiao K, et al (2022) Green preparation of N-doped hierarchical porous carbon composites from humic acid extraction residue of lignite as anodes for lithium/sodium-ion batteries. Colloids Surfaces A Physicochem Eng Asp 648:129400. https://doi.org/10.1016/j.colsurfa. 2022.129400

188. Liu X, Whitacre JF, Mauter MS (2018) Mechanisms of humic acid fouling on capacitive and insertion electrodes for electrochemical desalination. Environ Sci Technol 52:12633–12641. https://doi.org/10.1021/acs.est .8b03261

189. Budnyak TM, Slabon A, Sipponen MH (2020) Lignin–Inorganic interfaces: chemistry and applications from adsorbents to catalysts and energy storage materials. ChemSusChem 13:4344–4355. https://doi.org/10.1002/cssc.20 2000216

190. Liu C, Li Y, Zhuang J, et al (2022) Conductive hydrogels based on industrial lignin: opportunities and challenges. Polymers (Basel) 14:3739. https://doi.org/10.3390/polym14183739

191. Wang D, Lee SH, Kim J, Park CB (2020) “Waste to Wealth”: Lignin as a renewable building block for energy harvesting/storage and environmental remediation. ChemSusChem 13:2807–2827. https://doi.org/10.1002/cssc .202000394

192. Cui L, An Y, Xu H, et al (2021) An all-lignin-based flexible supercapacitor based on a nitrogen-doped carbon dot functionalized graphene hydrogel. New J Chem 45:21692–21700. https://doi.org/10.1039/D1NJ04054E

193. Peng Z, Wang C, Zhang Z, Zhong W (2019) Synthesis and enhancement of electroactive biomass/polypyrrole hydrogels for high performance flexible all-solid-state supercapacitors. Adv Mater Interfaces 6:1901393. https://doi.org/10.1002/admi.201901393

194. Wang Q, Zhang H, Pan X, et al (2019) Adhesive, transparent tannic acid@ sulfonated lignin-pam ionic conductive hydrogel electrode with anti-UV, antibacterial and mild antioxidant function. Materials (Basel) 12:4135. https://doi.org/10.3390/MA12244135

195. Liu T, Ren X, Zhang J, et al (2020) Highly compressible lignin hydrogel electrolytes via double-crosslinked strategy for superior foldable supercapacitors. J Power Sources 449:227532. https://doi.org/10.1016/j. jpowsour. 2019.227532

196. Hong R, Zhang Z, Pan S, et al (2023) Construction of PVA-lignosulfonate hydrogels for improved mechanical performances and all-in-one flexible supercapacitors. Int J Biol Macromol 225:1494–1504. https://doi.org/10.1016/j.ijbiomac.2022.11.206

197. Qiu F, Huang Y, He G, et al (2020) A lignocellulose-based neutral hydrogel electrolyte for high-voltage supercapacitors with overlong cyclic stability. Electrochim Acta 363:137241. https://doi.org/10.1016/j.electacta.2020.137241

198. Mondal AK, Xu D, Wu S, et al (2022) High lignin containing hydrogels with excellent conducting, self-healing, antibacterial, dye adsorbing, sensing, moist-induced power generating and supercapacitance properties. Int J Biol Macromol 207:48–61. https://doi.org/10.1016/j.ijbiomac.2022.02.144

199. Mondal AK, Wu S, Xu D, et al (2021) Preparation of lignosulfonate ionic hydrogels for supercapacitors, sensors and dye adsorbent applications. Int J Biol Macromol 187:189–199. https://doi.org/10.1016/j.ijbiomac.2021.07.021

200. Peng Z, Zou Y, Xu S, et al (2018) High-performance biomass-based flexible solid-state supercapacitor constructed of pressure-sensitive lignin-based and cellulose hydrogels. ACS Appl Mater Interfaces 10:22190–22200. https://doi.org/10.1021/acsami.8b05171

201. Zhang Z, Yu C, Peng Z, Zhong W (2021) Mechanically stiff and high-areal-performance integrated all-in-wood supercapacitors with electroactive biomass-based hydrogel. Cellulose 28:389–404. https://doi.org/10.1007/s 10570-020-03509-8

202. Park JH, Rana HH, Lee JY, Park HS (2019) Renewable flexible supercapacitors based on all-lignin-based hydrogel electrolytes and nanofiber electrodes. J Mater Chem A 7:16962–16968. https://doi.org/10.1039/c 9ta03519b

203. Wang D, Yang F, Cong L, et al (2022) Lignin-containing hydrogel matrices with enhanced adhesion and toughness for all-hydrogel supercapacitors. Chem Eng J 450:138025. https://doi.org/10.1016/j.cej.2022.138025

204. Wang J, Gao C, Hou P, et al (2023) All-bio-based, adhesive and low-temperature resistant hydrogel electrolytes for flexible supercapacitors. Chem Eng J 455:140952. https://doi.org/10.1016/j.cej.2022.140952

205. Rajakumar R, Sankar J (2016) Hydrogel: novel soil conditioner and safer delivery vehicle for fertilizers and agrochemicals-A Review. Int J Appl Pure Sci Agric 2:163-172

206. Wang Q, Guo J, Lu X, et al (2021) Wearable lignin-based hydrogel electronics: A mini-review. Int. J. Biol. Macromol. 181:45–50. https://doi.org/ 10.1016/j.ijbiomac.2021.03.079.

207. Mandlekar N, Cayla A, Rault F, et al (2018) An Overview on the Use of lignin and its derivatives in fire retardant polymer systems. In: Poletto M (ed) Lignin - Trends and Applications. InTech, pp 207–231

208. Ludmila H, Michal J, Andrea Š, Aleš H (2015) Lignin, potential products and their market value. Wood Res 60:973–986

209. Fernández-Pérez M, Flores-Céspedes F, Daza-Fernández I, et al (2014) Lignin and lignosulfonate-based formulations to protect pyrethrins against photodegradation and volatilization. Ind Eng Chem Res 53:13557–13564. htt ps://doi.org/10.1021/ie500186e

210. Zheng T, Liang Y, Ye S, He Z (2009) Superabsorbent hydrogels as carriers for the controlled-release of urea: Experiments and a mathematical model describing the release rate. Biosyst Eng 102:44–50. https://doi.org/10.1016/j.biosystemseng.2008.09.027

211. Gupta AP, Warkar SG (2015) Synthesis, characterization and swelling properties of poly (acrylamide-cl-carboxymethylguargum) hydrogels. Int J Pharma Bio Sci 6:P516–P529.

212. Akalin GO, Pulat M (2020) Controlled release behavior of zinc-loaded carboxymethyl cellulose and carrageenan hydrogels and their effects on wheatgrass growth. J Polym Res 27:6. https://doi.org/10.1007/s10965-019-1950-y

213. Ni B, Liu M, Lü S (2009) Multifunctional slow-release urea fertilizer from ethylcellulose and superabsorbent coated formulations. Chem Eng J 155:892–898. https://doi.org/10.1016/j.cej.2009.08.025

214. Rabat NE, Hashim S, Majid RA (2016) Effect of different monomers on water retention properties of slow release fertilizer hydrogel. Procedia Eng 148:201–207. https://doi.org/10.1016/j.proeng.2016.06.573

215. Raafat AI, Eid M, El-Arnaouty MB (2012) Radiation synthesis of superabsorbent CMC based hydrogels for agriculture applications. Nucl Instruments Methods Phys Res Sect B Beam Interact with Mater Atoms 283:71–76. https://doi.org/10.1016/j.nimb.2012.04.011

216. Akhter J, Mahmood K, Malik KA , Mardan A, Ahmad M (2004) Effects of hydrogel amendment on water storage of sandy loam and loam soils and seedling growth of barley, wheat and chickpea. Plant Soil Environ 10:463–469. https://doi.org/10.17221/4059-PSE

217. Reddy BV, Rao GR (2008) Vibrational spectra and modified valence force field for N,N’-methylenebisacrylamide. Indian J Pure Appl Phys 46:611–616

218. Sun Y, Ma Y, Fang G, et al (2016) Synthesis of acid hydrolysis lignin-g-poly-(acrylic acid) hydrogel superabsorbent composites and adsorption of lead ions. BioResources 11:5731–5742. https://doi.org/10.15376/biores.11.3.5731-5742

219. Ma Y, Sun Y, Fu Y, et al (2016) Swelling behaviors of porous lignin based poly (acrylic acid). Chemosphere 163:610–619. https://doi.org/10.1016/j.chemosphere.2016.08.035

220. Tomar RS, Gupta I, Singhal R, Nagpal AK (2007) Synthesis of poly (Acrylamide-co-acrylic acid) based superaborbent hydrogels: Study of network parameters and swelling behaviour. Polym - Plast Technol Eng 46:481–488. https://doi.org/10.1080/03602550701297095

221. Mali KK, Dhawale SC, Dias RJ (2017) Synthesis and characterization of hydrogel films of carboxymethyl tamarind gum using citric acid. Int J Biol Macromol 105:463–470. https://doi.org/10.1016/j.ijbiomac.2017.07.058

222. He M-K, He Y-L, Li Z-Q, et al (2022) Structural characterization of lignin and lignin-carbohydrate complex (LCC) of sesame hull. Int J Biol Macromol 209:258–267. https://doi.org/10.1016/J.IJBIOMAC.2022.04.009

223. Hemmilä V, Hosseinpourpia R, Adamopoulos S, Eceiza A (2020) Characterization of wood-based industrial biorefinery lignosulfonates and supercritical water hydrolysis lignin. Waste and Biomass Valorization 11:5835–5845. https://doi.org/10.1007/s12649-019-00878-5

224. Zhang Jishi, Zhao Lei, Yu Fei, Zang Lihua (2019) Comparison of sodium lignosulfonate and derived biochar for influencing methane bioevolution. Energy & Fuels 33:8812–8820. https://doi.org/10.1021/acs.energyfuels.9b00522

225. Adnadjevic B, Jovanovic J (2008) Novel approach in investigation of the poly(acrylic acid) hydrogel swelling kinetics in water. J Appl Polym Sci 107:3579–3587. https://doi.org/10.1002/app.27451

226. Kumar B, Priyadarshi R, Sauraj, et al (2020) Nanoporous sodium carboxymethyl cellulose-g-poly (sodium acrylate)/fecl3 hydrogel beads: synthesis and characterization. Gels 6:49. https://doi.org/10.3390/gels6040049

227. Stojkov G, Niyazov Z, Picchioni F, Bose RK (2021) Relationship between structure and rheology of hydrogels for various applications. Gels 7:255. https://doi.org/10.3390/gels7040255

228. Yadav R, Purwar R (2021) Influence of metal oxide nanoparticles on morphological, structural, rheological and conductive properties of mulberry silk fibroin nanocomposite solutions. Polym Test 93:106916. https://doi.org/10.1016/j.polymertesting.2020.106916

229. Sani Mamman I, Teo YY, Misran M (2021) Synthesis, characterization and rheological study of Arabic gum-grafted-poly (methacrylic acid) hydrogels. Polym Bull 78:3399–3423. https://doi.org/10.1007/s00289-020-03267-4

230. Mark HF, Atlas SH (1965) Principles of polymer stability. Polym Eng Sci 5:204–207. https://doi.org/10.1002/pen.760050321

231. Wang X, Wang Y, He S, et al (2018) Ultrasonic-assisted synthesis of superabsorbent hydrogels based on sodium lignosulfonate and their adsorption properties for Ni^{2+}. Ultrason Sonochem 40:221–229. https://doi.org/10.1016/j.ultsonch.2017.07.011

232. Khushbu, Warkar SG, Kumar A (2019) Synthesis and assessment of carboxymethyl tamarind kernel gum based novel superabsorbent hydrogels for agricultural applications. Polymer (Guildf) 182:121823. https://doi.org/10.1016/j.polymer.2019.121823

233. Singh B, Sharma V (2016) Designing galacturonic acid /arabinogalactan crosslinked poly(vinyl pyrrolidone)- co-poly(2-acrylamido-2-methylpropane sulfonic acid) polymers: Synthesis, characterization and drug delivery application. Polymer (Guildf) 91:50–61. https://doi.org/10.1016/j.polymer. 2016.03.037

234. Costa P, Sousa Lobo JM (2003) Evaluation of Mathematical Models Describing Drug Release from Estradiol Transdermal Systems. Drug Dev Ind Pharm 29:89–97. https://doi.org/10.1081/DDC-120016687

235. Alam MA, Takafuji M, Ihara H (2014) Silica nanoparticle-crosslinked thermosensitive hybrid hydrogels as potential drug-release carriers. Polym J 46:293–300. https://doi.org/10.1038/pj.2014.2

236. Yang Y, Wang X, Wang Y, et al (2024) Pesticide contamination remediation by biochar-immobilized microorganisms: a review. Int J Environ Sci Technol 21:2225–2238. https://doi.org/10.1007/s13762-023-05204-0

237. Leskovac A, Petrović S (2023) Pesticide Use and Degradation Strategies: Food Safety, Challenges and Perspectives. Foods 12:2709. https://doi.org/10.3390/foods12142709

238. Zhou W, Li M, Achal V (2025) A comprehensive review on environmental and human health impacts of chemical pesticide usage. Emerg Contam 11:100410. https://doi.org/10.1016/j.emcon.2024.100410

239. Wakita T (2011) Molecular Design of Dinotefuran with Unique Insecticidal Properties. J Agric Food Chem 59:2938–2942. https://doi.org/10.1021/ jf1030778

240. Kurwadkar ST, Dewinne D, Wheat R, et al (2013) Time dependent sorption behavior of dinotefuran, imidacloprid and thiamethoxam. J Environ Sci Heal Part B 48:237–242. https://doi.org/10.1080/03601234.2013.742412

241. Okeke ES, Olisah C, Malloum A, et al (2024) Ecotoxicological impact of dinotefuran insecticide and its metabolites on non-targets in agroecosystem: Harnessing nanotechnology- and bio-based management strategies to reduce its impact on non-target ecosystems. Environ Res 243:117870. https://doi.org/10.1016/j.envres.2023.117870

242. Liu X, Zhou Y, Ma Y, et al (2021) Photocatalytic degradation of dinotefuran by layered phosphorus-doped carbon nitride and its mechanism. J Photochem Photobiol A Chem 414:113287. https://doi.org/10.1016/j.jphotochem.2021.113287

243. Alford AM, Krupke CH (2019) Movement of the neonicotinoid seed treatment clothianidin into groundwater, aquatic plants, and insect herbivores. Environ Sci Technol 53:14368–14376. https://doi.org/10.1021/ acs.est.9b05025

244. Ham HJ, Choi JY, Jo YJ, et al (2022) Residues and uptake of soil-applied dinotefuran by lettuce (Lactuca sativa L.) and celery (Apium graveolens L.). Agriculture 12:1443. https://doi.org/10.3390/agriculture12091443

245. Manu, Kumar D, Gupta RK (2024) Natural polymers-humic acid and lignin based hydrogels: In agriculture, environment and energy storage. Ind Crops Prod 219:119029. https://doi.org/10.1016/j.indcrop.2024.119029

246. Nandal M, Kumar D, Gupta RK (2025) Harnessing lignite-based hydrogel for enhanced uv protection and delivery of dinotefuran in agriculture. ChemistrySelect 10:e05884. https://doi.org/10.1002/slct.202405884

247. Rashid M, Hussain Q, Hayat R, et al (2023) Lignite scaffolding as slow-release N-fertilizer extended the SN retention and inhibited N Losses in alkaline calcareous soils. ACS Omega 8:22732–22741. https://doi.org/10.1021/acsomega.3c01611

248. Mudassir J, Ranjha NM (2008) Dynamic and equilibrium swelling studies: crosslinked pH sensitive methyl methacrylate-co-itaconic acid (MMA-co-IA) hydrogels. J Polym Res 15:195–203. https://doi.org/10.1007/s10965-007-9159-x

249. Bukhari SMH, Khan S, Rehanullah M, Ranjha NM (2015) Synthesis and Characterization of chemically cross-linked acrylic acid/gelatin hydrogels: effect of ph and composition on swelling and drug release. Int J Polym Sci 2015:1–15. https://doi.org/10.1155/2015/187961

250. Shah S, Ranjha NM, Javaid Z (2013) Development and evaluation of pH-dependent interpenetrating network of acrylic acid/polyvinyl alcohol. Iran Polym J 22:811–820. https://doi.org/10.1007/s13726-013-0180-0

251. Larrañeta E, Imízcoz M, Toh JX, et al (2018) Synthesis and characterization of lignin hydrogels for potential applications as drug eluting antimicrobial coatings for medical materials. ACS Sustain Chem Eng 6:9037–9046. https://doi.org/10.1021/acssuschemeng.8b01371

252. Dharmalingam K, Anandalakshmi R (2019) Fabrication, characterization and drug loading efficiency of citric acid crosslinked NaCMC-HPMC hydrogel films for wound healing drug delivery applications. Int J Biol Macromol 134:815–829. https://doi.org/10.1016/j.ijbiomac.2019.05.027

253. J. Penn M, Hennessy MG (2022) Optimal loading of hydrogel-based drug-delivery systems. Appl Math Model 112:649–668. https://doi.org/10.1016/j.apm.2022.08.008

254. Elabasy A, Shoaib A, Waqas M, et al (2020) Cellulose nanocrystals loaded with thiamethoxam: Fabrication, characterization, and evaluation of insecticidal activity against phenacoccus solenopsis tinsley (hemiptera: Pseudococcidae). Nanomaterials 10:5–7. https://doi.org/10.3390/nano10040788

255. Heredia NS, Vizuete K, Flores-Calero M, et al (2022) Comparative statistical analysis of the release kinetics models for nanoprecipitated drug delivery systems based on poly(lactic-co-glycolic acid). PLoS One 17:e0264825. https://doi.org/10.1371/journal.pone.0264825

256. Bayer IS (2023) Controlled drug release from nanoengineered polysaccharides. Pharmaceutics 15:1364. https://doi.org/10.3390/pharmaceutics15051364

257. Arens L, Barther D, Landsgesell J, et al (2019) Poly(sodium acrylate) hydrogels: synthesis of various network architectures, local molecular dynamics, salt partitioning, desalination and simulation. Soft Matter 15:9949–9964. https://doi.org/10.1039/C9SM01468C

258. Sennakesavan G, Mostakhdemin M, Dkhar LK, et al (2020) Acrylic acid/acrylamide based hydrogels and its properties - A review. Polym Degrad Stab 180:109308. https://doi.org/10.1016/j.polymdegradstab.2020.109308

259. Prashar V, Nandal M, Gupta RK, Tyagi YK (2024) Novel synthesis, and application of carboxymethylated cassia fistula -based hydrogel for extended-release of dinotefuran. ChemistrySelect 9:e202403421. https://doi.org/10.1002/slct.202403421

260. Fatima N, Jamal A, Huang Z, et al (2021) Extraction and chemical characterization of humic acid from nitric acid treated lignite and bituminous coal samples. Sustainability 13:8969. https://doi.org/10. 3390/su13168969

261. Abdel-Ghany MF, Hussein LA, El Azab NF (2017) Novel potentiometric sensors for the determination of the dinotefuran insecticide residue levels in cucumber and soil samples. Talanta 164:518–528. https://doi.org/10. 1016/j.talanta.2016.12.019

262. Liu X, Tu Y, Liu S, et al (2021) Adsorption of ammonia nitrogen and phenol onto the lignite surface: An experimental and molecular dynamics simulation study. J Hazard Mater 416:125966. https://doi.org/10.1016/j.jhazmat.2021.125966

263. Cepus V, Borth M, Seitz M (2016) IR spectroscopic characterization of lignite as a tool to predict the product range of catalytic decomposition. Int J Clean Coal Energy 05:13–22. https://doi.org/10.4236/ijcce.2016.51002

264. Astrini N, Anah L, Haryono A (2017) Water absorbency of chitosan grafted acrylic acid hydrogels. IOP Conf Ser Mater Sci Eng 223:012045. https://doi.org/10.1088/1757-899X/223/1/012045

265. Liu J, Wang Q, Wang A (2007) Synthesis and characterization of chitosan-g-poly(acrylic acid)/sodium humate superabsorbent. Carbohydr Polym 70:166–173. https://doi.org/10.1016/j.carbpol.2007.03.015

266. Rop K, Mbui D, Karuku GN, et al (2020) Characterization of water hyacinth cellulose-g-poly(ammonium acrylate-co-acrylic acid)/nano-hydroxyapatite polymer hydrogel composite for potential agricultural application. Results Chem 2:100020. https://doi.org/10.1016/j.rechem.2019.100020

267. Erceg T, Cakić S, Cvetinov M, et al (2020) The properties of conventionally and microwave synthesized poly(acrylamide-co-acrylic acid) hydrogels. Polym Bull 77:2089–2110. https://doi.org/10.1007/s00289-019-02840-w

268. Wang X, Wang Y, Hou H, et al (2017) Ultrasonic method to synthesize glucan-g -poly(acrylic acid)/sodium lignosulfonate hydrogels and studies of their adsorption of cu^{2+} from aqueous solution. ACS Sustain Chem Eng 5:6438–6446. https://doi.org/10.1021/acssuschemeng.7b00332

269. Bruschi ML (2015) Mathematical models of drug release. In: strategies to modify the drug release from pharmaceutical systems. Elsevier, pp 63–86

270. Nandal M, Prashar V, Bansiwal M, et al (2025) Novel molasses-grafted poly(sodium acrylate) hydrogel: A sustainable solution for water retention and controlled dinotefuran release. Indian J Chem Technol 32:161–175. https://doi.org/10.56042/ijct.v32i2.15397

271. Martín-Camacho U de J, Rodríguez-Barajas N, Sánchez-Burgos JA, Pérez-Larios A (2023) Weibull β value for the discernment of drug release mechanism of PLGA particles. Int J Pharm 640:123017. https://doi.org /10.1016/j.ijpharm.2023.123017

272. Bajpai SK, Kirar N (2016) Swelling and drug release behavior of calcium alginate/poly (sodium acrylate) hydrogel beads. Des Monomers Polym 19:89–98. https://doi.org/10.1080/15685551.2015.1092016

273. Peppas NA, Sahlin JJ (1989) A simple equation for the description of solute release. III. Coupling of diffusion and relaxation. Int J Pharm 57:169–172. https://doi.org/10.1016/0378-5173(89)90306-2

274. Ritger PL, Peppas NA (1987) A simple equation for description of solute release I. Fickian and non-fickian release from non-swellable devices in the form of slabs, spheres, cylinders or discs. J Control Release 5:23–36. https://doi.org/10.1016/0168-3659(87)90034-4

275. Ahmad F, de Moura MR, Capparelli Mattoso LH (2011) Biodegradable hydrogel as delivery vehicle for the controlled release of pesticide. in: pesticides - formulations, effects, fate. InTech. https://doi.org/10.5772/14139

276. Flores-Céspedes F, Villafranca-Sánchez M, Fernández-Pérez M (2023) Alginate-Bentonite-based hydrogels designed to obtain controlled-release formulations of dodecyl acetate. Gels 9:388. https://doi.org/10.3390/ gels9050388

277. Lakshmipathy K, Sindhu S, Singh A, et al (2024) A review on pesticides degradation by using ultraviolet light treatment in agricultural commodities. eFood 5:1–17. https://doi.org/10.1002/efd2.129

278. Kobashi K, Harada T, Adachi Y, et al (2017) Comparative ecotoxicity of imidacloprid and dinotefuran to aquatic insects in rice mesocosms. Ecotoxicol Environ Saf 138:122–129. https://doi.org/10.1016/j.ecoenv.2016.12.025

279. Feng P, Chen J, Fan C, et al (2020) An eco-friendly MIL-101@CMCS double-coated dinotefuran for long-acting active release and sustainable pest control. J Clean Prod 265:121851. https://doi.org/10.1016/j.jclepro.2020.121851

280. Liang R, Tang F, Wang J, Yue Y (2019) Photo-degradation dynamics of five neonicotinoids: Bamboo vinegar as a synergistic agent for improved functional duration. PLoS One 14:e0223708. https://doi.org/10.1371/journal.pone.0223708

281. Rop K, Mbui D, Njomo N, et al (2019) Biodegradable water hyacinth cellulose-graft-poly(ammonium acrylate-co-acrylic acid) polymer hydrogel for potential agricultural application. Heliyon 5:e01416. https://doi.org/10.1016/j.heliyon.2019.e01416

282. Tanwar M, Gupta RK, Rani A (2024) Natural gums and their derivatives based hydrogels: in biomedical, environment, agriculture, and food industry. Crit Rev Biotechnol 44:275–301. https://doi.org/10.1080/07388551.2022. 2157702

283. Kumar J, Purwar R (2024) Injectable mesquite gum and carboxymethyl chitosan hydrogel using schiff base crosslinks: a versatile platform for drug delivery in wound care. Macromol Res 32:1237–1254. https://doi.org/10. 1007/s13233-024-00300-7

284. Kumar J, Purwar R (2024) Biodegradable, biocompatible, and self-healing, injectable hydrogel based on oxidized Azadirachta indica gum and carboxymethyl chitosan through dynamic imine-linkage for biomedical application. Iran Polym J. 34:465–483. https://doi.org/10.1007/s13726-024-01386-7

285. Guo T, Wang W, Song J, et al (2021) Dual-responsive carboxymethyl cellulose/dopamine/cystamine hydrogels driven by dynamic metal-ligand and redox linkages for controllable release of agrochemical. Carbohydr Polym 253:117188. https://doi.org/10.1016/j.carbpol.2020.117188

286. Saruchi, Kumar V, Mittal H, Alhassan SM (2019) Biodegradable hydrogels of tragacanth gum polysaccharide to improve water retention capacity of soil and environment-friendly controlled release of agrochemicals. Int J Biol Macromol 132: 1252-1261. https://doi.org/10.1016/j.ijbiomac.2019.04.023

287. Manu, Kumar D, Gupta RK (2024) Synthesis and characterization of natural polymers- humic acid, lignin, and lignite-g-poly(sodium acrylate) hydrogels for slow release of thiamethoxam. Chem Sel 9: e202304939. https://doi.org/10.1002/slct.202304939

288. Cheng G, Li Z, Cao Y, Jiang Z (2020) Research progress in lignite flotation intensification. Int. J. Coal Prep. Util. 40:59–76. https://doi.org/10.1080/19392699.2018.1541894

289. Pekař M, Sýkorová I, Koutník I (2009) Progressive and efficient non-energy applications of lignite. Brno, Czech Republic 6:11-15.

290. Ly JC (2008) Ultraviolet disinfection system for constructed wetlands. Humbolt State University, Cal Poly Humboldt theses and projects. 1276. https://digitalcommons.humboldt.edu/etd/1276

291. Tavakol M, Vasheghani-Farahani E, Dolatabadi-Farahani T, Hashemi-Najafabadi S (2009) Sulfasalazine release from alginate-N,O-carboxymethyl chitosan gel beads coated by chitosan. Carbohydr Polym 77:326–330. https://doi.org/10.1016/j.carbpol.2009.01.005

292. He Q, Yeasmin H, Hoadley A, Qi Y (2022) Physical and chemical changes in lignite during mechanical and thermal dewatering process and associated changes in the organic compounds in the wastewater. Int J Coal Prep Util 42:1040–1054. https://doi.org/10.1080/19392699.2019.1682563

293. Wang Y, Yamamoto Y, Kiyono H, Shimada S (2008) Highly ordered boron nitride nanotube arrays with controllable texture from ammonia borane by template-aided vapor-phase pyrolysis. J Nanomater 2008:1–7. https://doi.org/10.1155/2008/606283

294. Qi R, Jones DL, Liu Q, et al (2021) Field test on the biodegradation of poly(butylene adipate-co-terephthalate) based mulch films in soil. Polym Test 93:107009. https://doi.org/10.1016/j.polymertesting.2020.107009

295. Wang W-B, Huang D-J, Kang Y-R, Wang A-Q (2013) One-step in situ fabrication of a granular semi-IPN hydrogel based on chitosan and gelatin for fast and efficient adsorption of Cu2+ ion. Colloids Surfaces B Biointerfaces 106:51–59. https://doi.org/10.1016/j.colsurfb.2013.01.030

296. Smausz T, Kondász B, Gera T, et al (2017) Determination of UV–visible–NIR absorption coefficient of graphite bulk using direct and indirect methods. Appl Phys A 123:633. https://doi.org/10.1007/s00339-017-1249-y

297. Chai H, Peng X, Liu T, et al (2017) High-performance supercapacitors based on conductive graphene combined with $Ni(OH)_2$ nanoflakes. RSC Adv 7:36617–36622. https://doi.org/10.1039/C7RA04986B

298. Cilento F, Curcio C, Martone A, et al (2022) Effect of graphite nanoplatelets content and distribution on the electromagnetic shielding attenuation mechanisms in 2d nanocomposites. J Compos Sci 6:257. https://doi.org/10.3390/jcs6090257

299. Prakash S (2012) Mode of occurence of trace elements in coal. National Institute of Technology Rourkela. http://hdl.handle.net/2080/2060.

300. Li X, Zhang W, Li X, et al (2023) Purity assessment of dinotefuran using mass balance and quantitative nuclear magnetic resonance. Molecules 28:3884. https://doi.org/10.3390/molecules28093884

301. Niu B, Jia J, Wang H, et al (2019) In vitro and in vivo release of diclofenac sodium-loaded sodium alginate/carboxymethyl chitosan-ZnO hydrogel beads. Int J Biol Macromol 141:1191–1198. https://doi.org/10.1016/j.ijbiomac.2019.09.059

302. Panico SC, van Gestel CAM, Verweij RA, et al (2022) Field mixtures of currently used pesticides in agricultural soil pose a risk to soil invertebrates. Environ Pollut 305:119290. https://doi.org/10.1016/j.envpol.2022.119290

303. Zhao X, Cui H, Wang Y, et al (2018) Development strategies and prospects of nano-based smart pesticide formulation. J Agric Food Chem 66:6504–6512. https://doi.org/10.1021/acs.jafc.7b02004

304. Roy A, Roy M, Alghamdi S, et al (2022) Role of microbes and nanomaterials in the removal of pesticides from wastewater. Int J Photoenergy 2022:1–12. https://doi.org/10.1155/2022/2131583

305. Huang Y, Hu Q, Cui G, et al (2020) Release-controlled microcapsules of thiamethoxam encapsulated in beeswax and their application in field. J Environ Sci Heal Part B 55:342–354. https://doi.org/10.1080/03601 234.2019.1697588

306. Hong F, Qiu P, Wang Y, et al (2024) Chitosan-based hydrogels: From preparation to applications, a review. Food Chem X 21:101095. https://doi.org/10.1016/j.fochx.2023.101095

307. Shang M, Jiang H, Li J, et al (2023) A dual physical crosslinking starch-based hydrogel exhibiting high strength, fatigue resistance, excellent biocompatibility, and biodegradability. Food Chem X 18:100728. https://doi.org/10.1016/j.fochx.2023.100728

308. Lin Y, Chen S, Liu Y, et al (2023) A composite hydrogel scaffold based on collagen and carboxymethyl chitosan for cartilage regeneration through one-step chemical crosslinking. Int J Biol Macromol 226:706–715. https://doi.org/10.1016/j.ijbiomac.2022.12.083

309. Wang P, Liao Q, Zhang H (2023) Polysaccharide-based double-network hydrogels: polysaccharide effect, strengthening mechanisms, and applications. biomacromolecules 24:5479–5510. https://doi.org/10.1021/ acs.biomac.3c00765

310. Patel DK, Jung E, Priya S, et al (2024) Recent advances in biopolymer-based hydrogels and their potential biomedical applications. Carbohydr Polym 323:121408. https://doi.org/10.1016/j.carbpol.2023.121408

311. Das SK, Ghosh GK (2022) Hydrogel-biochar composite for agricultural applications and controlled release fertilizer: A step towards pollution free environment. Energy 242:122977. https://doi.org/10.1016/j.energy.2021.122977

312. Thakur S, Chaudhary J, Thakur A, et al (2022) Highly efficient poly(acrylic acid-co-aniline) grafted itaconic acid hydrogel: Application in water retention and adsorption of rhodamine B dye for a sustainable environment. Chemosphere 303:134917. https://doi.org/10.1016/j.chemosphere.2022.134917

313. Duary S (2020) Humic acid-A critical review. Int J Curr Microbiol Appl Sci 9:2236–2241. https://doi.org/10.20546/ijcmas.2020.910.270

314. Ampong K, Thilakaranthna MS, Gorim LY (2022) Understanding the role of humic acids on crop performance and soil health. Front Agron 4:848621. https://doi.org/10.3389/fagro.2022.848621

315. Chelliah R, Wei S, Vijayalakshmi S, et al (2023) A comprehensive mini-review on lignin-based nanomaterials for food applications: systemic advancement and future trends. Molecules 28:6470. https://doi.org/10.3390/ molecules28186470

316. Di Gianfrancesco A (2017) The fossil fuel power plants technology. In: materials for ultra-supercritical and advanced ultra-supercritical power plants. Elsevier, pp 1–49. https://doi.org/10.1016/B978-0-08-100552-1.000014

317. Yu J, Sha D (2022) Study on combustion kinetic characteristics of lignite and semi-coking dust. ACS Omega 7:33097–33106. https://doi.org/10.1021/acsomega.2c03199

318. Mandlekar N, Cayla A, Rault F, et al (2018) An overview on the use of lignin and its derivatives in fire retardant polymer systems. In: Poletto M (ed) Lignin - Trends and Applications. InTech, pp 207–231

319. Sarkar DJ, Kumar J, Shakil NA, Walia S (2012) Release kinetics of controlled release formulations of thiamethoxam employing nano-ranged amphiphilic PEG and diacid based block polymers in soil. J Environ Sci Heal Part A 47:1701–1712. https://doi.org/10.1080/10934529.2012.687294

320. Abdel-Baset S, Abdelrazik E, Shehata A (2020) Potentials of potassium humate, ammonium humate, and vermicompost tea in controlling root-knot nematode, Meloidogyne arenaria and improving biochemical components in eggplant. African J Biol Sci 16:119–134. https://doi.org/10.21608/ajbs. 2020.126615

321. Kirdey TA, Veselov AP (2017) Phytoprotective effect of ammonium humate at high copper concentrations in the environment. Biol Bull 44:1284–1288. https://doi.org/10.1134/S1062359017100065

322. Lyons G, Genc Y (2016) Commercial humates in agriculture: real substance or smoke and mirrors? Agronomy 6:50. https://doi.org/10.3390/agrono my6040050

323. Ciarkowska K, Sołek-Podwika K, Filipek-Mazur B, Tabak M (2017) Comparative effects of lignite-derived humic acids and FYM on soil properties and vegetable yield. Geoderma 303:85–92. https://doi.org/10. 1016/j.geoderma.2017.05.022

324. Chokejaroenrat C, Watcharenwong A, Sakulthaew C, Rittirat A (2020) Immobilization of atrazine using oxidized lignite amendments in agricultural soils. Water, Air, Soil Pollut 231:249. https://doi.org/10. 1007/s11270-020-04608-9

325. Munir MAM, Irshad S, Yousaf B, et al (2021) Interactive assessment of lignite and bamboo-biochar for geochemical speciation, modulation and uptake of Cu and other heavy metals in the copper mine tailing. Sci Total Environ 779:146536. https://doi.org/10.1016/j.scitotenv.2021.146536

326. Singh VP, Singh BD, Mathews RP, et al (2021) Petrographical-geochemical characteristics and floral-faunal compositions of the Valia lignite deposits from Cambay Basin (Gujarat), western India. Int J Coal Geol 248:103866. https://doi.org/10.1016/j.coal.2021.103866

327. Ganguly S, Mondal S, Das P, et al (2018) Design of psyllium-g-poly(acrylic acid-co-sodium acrylate)/cloisite 10A semi-IPN nanocomposite hydrogel and its mechanical, rheological and controlled drug release behaviour. Int J Biol Macromol 111:983–998. https://doi.org/10.1016/j.ijbiomac.2018.01.100

328. Magalhães ASG, Almeida Neto MP, Bezerra MN, et al (2012) Application of ftir in the determination of acrylate content in poly(sodium acrylate-co-acrylamide) superabsorbent hydrogels. Quim Nova 35:1464–1467. https://doi.org/10.1590/S0100-40422012000700030

329. Zhang W, Jiang S, Wang K, et al (2015) Thermogravimetric dynamics and ftir analysis on oxidation properties of low-rank coal at low and moderate temperatures. Int J Coal Prep Util 35:39–50. https://doi.org/10. 1080/19392699.2013.873421

330. Liu C, Yuan B, Guo M, et al (2021) Effect of sodium lignosulfonate on bonding strength and chemical structure of a lignosulfonate/chitosan-glutaraldehyde medium-density fiberboard adhesive. Adv Compos Hybrid Mater 4:1176–1184. https://doi.org/10.1007/s42114-021-00351-9

331. Temel S, Gokmen FO, Yaman E (2020) Antibacterial activity of ZnO nanoflowers deposited on biodegradable acrylic acid hydrogel by chemical bath deposition. Bull Mater Sci 43:18. https://doi.org/10.1007/s12034-019-1967-1

332. Neppel A, Eaton DR, Hunkeler D, Hamielec AE (1988) Effect of crosslinking on the 13C nuclear magnetic resonance spectra of superabsorbent poly(sodium acrylates). Polymer (Guildf) 29:1338–1342. https://doi.org/10.1016/0032-3861(88)90067-5

333. Al-Faiyz YSS (2017) CPMAS 13 C NMR characterization of humic acids from composted agricultural Saudi waste. Arab J Chem 10:S839–S853. https://doi.org/10.1016/j.arabjc.2012.12.018

334. Haque MO, Mondal MIH (2016) Synthesis and characterization of cellulose-based eco-friendly hydrogels. Rajshahi Univ J Sci Eng 44:45–53. https://doi.org/10.3329/rujse.v44i0.30386

335. Chavda H, Patel C (2011) Effect of crosslinker concentration on characteristics of superporous hydrogel. Int J Pharm Investig 1:17. https://doi.org/10.4103/2230-973X.76724

336. Liu Y, Zhu Y, Mu B, et al (2024) One-step green construction of granular composite hydrogels for ammonia nitrogen recovery from wastewater for crop growth promotion. Environ Technol Innov 33:103465. https://doi.org/10.1016/j.eti.2023.103465

337. Mayr SA, Wagner S, Nagl R, et al (2023) Physicochemical insights into enzymatic polymerization of lignosulfonates. ACS Sustain Chem Eng 11:17739–17751. https://doi.org/10.1021/acssuschemeng.3c05521

338. Santos A, Bertoli A, Borges AC, et al (2018) New organomineral complex from humic substances extracted from poultry wastes: synthesis, characterization and controlled release study. J Braz Chem Soc 29:140–150. https://doi.org/10.21577/0103-5053.20170122

339. Bora A, Karak N (2022) Starch and itaconic acid-based superabsorbent hydrogels for agricultural application. Eur Polym J 176:111430. https://doi.org/10.1016/j.eurpolymj.2022.111430

340. Rajanna GA, Manna S, Singh A, et al (2022) Biopolymeric superabsorbent hydrogels enhance crop and water productivity of soybean–wheat system in Indo-Gangetic plains of India. Sci Rep 12:11955. https://doi.org/10.1038/s4 1598-022-16049-x

341. Ekenna IC, Abali SO (2022) Comparison of the use of kinetic model plots and dd solver software to evaluate the drug release from griseofulvin tablets. J Drug Deliv Ther 12:5–13. https://doi.org/10.22270/jddt.v12i2-S.5402

342. Paolino D, Tudose A, Celia C, et al (2019) Mathematical models as tools to predict the release kinetic of fluorescein from lyotropic colloidal liquid crystals. Materials (Basel) 12:693. https://doi.org/10.3390/ma12050693

343. Lin J, Ye W, Xie M, et al (2023) Environmental impacts and remediation of dye-containing wastewater. Nat Rev Earth Environ 4:785–803. https://doi.org/10.1038/s43017-023-00489-8

344. Kant R (2012) Textile dyeing industry an environmental hazard. Nat Sci 04:22–26. https://doi.org/10.4236/ns.2012.41004

345. Lellis B, Fávaro-Polonio CZ, Pamphile JA, Polonio JC (2019) Effects of textile dyes on health and the environment and bioremediation potential of living organisms. Biotechnol Res Innov 3:275–290. https://doi.org/10.1016/j.biori.2019.09.001

346. Tan IAW, Ahmad AL, Hameed BH (2008) Adsorption of basic dye using activated carbon prepared from oil palm shell: batch and fixed bed studies. Desalination 225:13–28. https://doi.org/10.1016/j.desal.2007.07.005

347. Vadivelan V, Kumar KV (2005) Equilibrium, kinetics, mechanism, and process design for the sorption of methylene blue onto rice husk. J Colloid Interface Sci 286:90–100. https://doi.org/10.1016/j.jcis.2005.01.007

348. Hassan MM, Carr CM (2018) A critical review on recent advancements of the removal of reactive dyes from dyehouse effluent by ion-exchange adsorbents. Chemosphere 209:201–219. https://doi.org/10.1016/j.chemosphere.2018.06.043

349. Joseph J, Radhakrishnan RC, Johnson JK, et al (2020) Ion-exchange mediated removal of cationic dye-stuffs from water using ammonium phosphomolybdate. Mater Chem Phys 242:122488. https://doi.org/10.1016/j.matchemphys.2019.122488

350. Dutta S, Gupta B, Srivastava SK, Gupta AK (2021) Recent advances on the removal of dyes from wastewater using various adsorbents: a critical review. Mater Adv 2:4497–4531. https://doi.org/10.1039/D1MA00354B

351. Augustowski D, Gala M, Kwaśnicki P, Rysz J (2021) Efficiency boost in dye-sensitized solar cells by post- annealing uv-ozone treatment of TiO_2 mesoporous layer. Materials (Basel) 14:4698. https://doi.org/10.3390 /ma14164698

352. Jirankova H, Mrazek J, Dolecek P, Cakl J (2010) Organic dye removal by combined adsorption—membrane separation process. Desalin Water Treat 20:96–101. https://doi.org/10.5004/dwt.2010.1170

353. Jargalsaikhan M, Lee J, Jang A, Jeong S (2021) Efficient removal of azo dye from wastewater using the non-toxic potassium ferrate oxidation–coagulation process. Appl Sci 11:6825. https://doi.org/10.3390/app11156825

354. Sivakumar R, Lee NY (2022) Adsorptive removal of organic pollutant methylene blue using polysaccharide-based composite hydrogels. Chemosphere 286:131890. https://doi.org/10.1016/j.chemosphere.2021.131890

355. Kumar J, Purwar R (2024) A Schiff base hydrogel of oxidized okra gum and carboxymethylated chitosan: a biocompatible and biodegradable injectable system for drug delivery in wound care. Colloid Polym Sci 302:1923–1938. https://doi.org/10.1007/s00396-024-05316-0

356. Ma J, Zhong J, Sun F, et al (2024) Hydrogel sensors for biomedical electronics. Chem Eng J 481:148317. https://doi.org/10.1016/j.cej.2023.148317

357. Li H, Dai C, Hu Y (2024) Hydrogels for chemical sensing and biosensing. Macromol Rapid Commun 45:2300474. https://doi.org/10.1002/marc.202300474

358. Khan MUA, Stojanović GM, Abdullah MF Bin, et al (2024) Fundamental properties of smart hydrogels for tissue engineering applications: A review. Int J Biol Macromol 254:127882. https://doi.org/10.1016/j.ijbiomac.2023.127882

359. Radulescu D-M, Neacsu IA, Grumezescu A-M, Andronescu E (2022) New insights of scaffolds based on hydrogels in tissue engineering. Polymers (Basel) 14:799. https://doi.org/10.3390/polym14040799

360. Zamani-Babgohari F, Irannejad A, Kalantari Pour M, Khayati GR (2024) Synthesis of carboxymethyl starch co (polyacrylamide/ polyacrylic acid) hydrogel for removing methylene blue dye from aqueous solution. Int J Biol Macromol 269:132053. https://doi.org/10.1016/j.ijbiomac.2024.132053

361. Seera SDK, Kundu D, Gami P, et al (2021) Synthesis and characterization of xylan-gelatin cross-linked reusable hydrogel for the adsorption of methylene blue. Carbohydr Polym 256:117520. https://doi.org/10.1016/j.carbpol.2020.117520

362. Tang Z, Hu X, Ding H, et al (2021) Villi-like poly(acrylic acid) based hydrogel adsorbent with fast and highly efficient methylene blue removing ability. J Colloid Interface Sci 594:54–63. https://doi.org/10.1016/j.jcis.2021.02.124

363. PEHLIVAN E, ARSLAN G (2006) Comparison of adsorption capacity of young brown coals and humic acids prepared from different coal mines in Anatolia. J Hazard Mater 138:401–408. https://doi.org/10.1016/j.jhazmat.2006.05.063

364. Havelcová M, Mizera J, Sýkorová I, Pekař M (2009) Sorption of metal ions on lignite and the derived humic substances. J Hazard Mater 161:559–564. https://doi.org/10.1016/j.jhazmat.2008.03.136

365. Zherebtsov SI, Malyshenko N V., Votolin KS, Ismagilov ZR (2020) Sorption of metal cations by lignite and humic acids. Coke Chem 63:142–148. https://doi.org/10.3103/S1068364X20030096

366. Klučáková M, Pavlíková M (2017) Lignitic humic acids as environmentally-friendly adsorbent for heavy metals. J Chem 2017:1–5. https://doi.org/10.1155/2017/7169019

367. Singh T, Singhal R (2015) Kinetics and thermodynamics of cationic dye adsorption onto dry and swollen hydrogels poly(acrylic acid-sodium acrylate-acrylamide) sodium humate. Desalin Water Treat 53:3668–3680. https://doi.org/10.1080/19443994.2013.871342

368. Vijayan JG, Prabhu TN, Pal K (2023) Poly(N-isopropyl acrylamide)-co-poly(sodium acrylate) hydrogel for the adsorption of cationic dyes from aqueous solution. Eur Phys J E 46:11. https://doi.org/10.1140/epje/s10189-023-00266-x

369. Osuchukwu OA, Salihi A, Abdullahi I, Obada DO (2022) Taguchi grey relational optimization of sol–gel derived hydroxyapatite from a novel mix of two natural biowastes for biomedical applications. Sci Rep 12:17968. https://doi.org/10.1038/s41598-022-22888-5

370. Yuan Z, Wang J, Wang Y, et al (2019) Preparation of a poly(acrylic acid) based hydrogel with fast adsorption rate and high adsorption capacity for the removal of cationic dyes. RSC Adv 9:21075–21085. https://doi.org/10. 1039/c9ra03077h

371. Can M (2016) Investigation of the factors affecting acid blue 256 adsorption from aqueous solutions onto red pine sawdust: equilibrium, kinetics, process design, and spectroscopic analysis. Desalin Water Treat 57:5636–5653. https://doi.org/10.1080/19443994.2014.1003974

372. Ashmawy A, Mahmoud A, Ali A, et al (2023) Novel kappa-carrageenan− poly (vinyl alcohol) − modified pumice Hydrogel composite for the adsorption of cationic dye. Egypt J Chem 66:21–35. https://doi.org/10.21608/ ejchem.2023.176082.7210

373. Aljeboree AM, Alkaim AF (2024) Studying removal of anionic dye by prepared highly adsorbent surface hydrogel nanocomposite as an applicable for aqueous solution. Sci Rep 14:9102. https://doi.org/10.1038/s41598-024-59545-y

374. Pathak J, Singh P (2023) Adsorptive removal of congo red using organically modified zinc–copper–nickel ternary metal hydroxide: kinetics, isotherms and adsorption studies. J Polym Environ 31:327–344. https://doi.org/10.1007/s10924-022-02612-0

375. Duran S, Şolpan D, Güven O (1999) Synthesis and characterization of acrylamide–acrylic acid hydrogels and adsorption of some textile dyes. Nucl Instruments Methods Phys Res Sect B Beam Interact with Mater Atoms 151:196–199. https://doi.org/10.1016/S0168-583X(99)00151-2

376. Pandey S, Do JY, Kim J, Kang M (2020) Fast and highly efficient removal of dye from aqueous solution using natural locust bean gum based hydrogels as adsorbent. Int J Biol Macromol 143:60–75. https://doi.org/10.1016/j.ijbiomac.2019.12.002

LIST OF PUBLICATIONS

1. Manu, Kumar D, Gupta RK (2024) Natural polymers-humic acid and lignin-based hydrogels: In agriculture, environment and energy storage. Ind Crops Prod 219:119029. https://doi.org/10.1016/j.indcrop.2024.119029. (IF=6.2)
2. Manu, Kumar D, Gupta RK (2024) Novel formulations of humic acid, lignin, and lignite grafted hydrogels for the slow release of thiamethoxam. ChemistrySelect 9:e202304939. https://doi.org/10.1002/slct.202304939. (IF=2)
3. Manu, Kumar D, Gupta RK (2023) Synthesis, characterization and application of Lignosulphonate-g-poly(sodium acrylate) hydrogel. Indian J Chem Technol 30:753–764. https://doi.org/10.56042/ijct.v30i6.1325. (IF=1)
4. Manu, Kumar D, Gupta RK (2025) Harnessing lignite-based hydrogel for enhanced UV protection and delivery of dinotefuran in agriculture. ChemistrySelect 10:e05884. https://doi.org/ 10.1002/slct.202405884. (IF=2)
5. Manu, Kumar D, Gupta RK, Comparative Analysis of Humic Acid, Lignin and Lignite-Based Hydrogels for Methylene Blue Dye Removal. Indian J Chem Technol (under review). (IF=1)
6. Manu, Kumar D, Gupta RK (2025) Humic acid-Integrated Polymeric Hydrogel: A Dual Strategy for Sustained Pesticide Delivery and Soil Water Retention. (submitted)

Industrial Crops & Products 219 (2024) 119029

Contents lists available at ScienceDirect

Industrial Crops & Products

journal homepage: www.elsevier.com/locate/indcrop

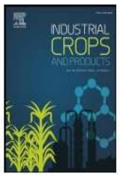

Natural polymers-humic acid and lignin based hydrogels: In agriculture, environment and energy storage

Manu, Devendra Kumar, Rajinder K. Gupta*

Department of Applied Chemistry, Delhi Technological University, Delhi, India

ARTICLE INFO

Keywords:
Natural polymers
Humic acid
Lignin
Hydrogels
Agriculture
Environment
Energy storage

ABSTRACT

The gradual depletion of fossil resources has intensified the search for sustainable alternatives to petroleum-based polymers. Among the remarkable natural polymers, humic acid (HA) and lignin stand out due to their versatile applications. Yet, a comprehensive review of hydrogels derived from these nature-derived polymers, specifically focused on agriculture, environment, and energy storage, remains conspicuously absent. This review article addresses this gap by systematically exploring the roles of HA and lignin-based hydrogels in these fields. In agriculture, these hydrogels exhibit immense potential to enhance soil structure, water retention, nutrient delivery, and the capacity to mitigate soil erosion and promote plant growth. Furthermore, these hydrogels showcase remarkable adsorption capabilities for various pollutants, positioning them as valuable assets in environmental applications. The research evaluates their adsorption mechanism and effectiveness in removing organic contaminants, heavy metals, and emerging pollutants from water sources, highlighting their crucial role in water purification and environmental protection. Additionally, these hydrogels demonstrate great promise as electrode materials and supercapacitors in energy storage. Their ability to efficiently store and release energy and eco-friendly attributes position them as viable candidates for sustainable energy storage solutions. This review article underscores the multifaceted potential of HA and lignin-based hydrogels and addresses the pressing need for a deeper understanding of their effects on agriculture, environmental sustainability, and energy storage. By harnessing the intrinsic properties of these natural polymers, these hydrogels are poised to revolutionize sectors and contribute significantly to a greener and more sustainable future.

1. Introduction

The constant rise in the world's population and gradual depletion of fossil resources has increased the interest of the research community towards the development of natural polymers as an alternative to petroleum-based polymers. Among the significant available natural resources are HA and lignin, which have high added values owing to their wide range of applicability. As far as we know, a comprehensive overview focusing on these nature-derived polymer-based hydrogels for agriculture, environment, and energy storage applications is still absent.

1.1. *Humic acid*

Most organic matter in soil is made up of humic compounds (humic and fulvic acids), which is frequently used interchangeably with soil organic matter (Chen and Aviad, 2015). The presence of carboxyl groups and the mild acidity of the phenolic groups in humic compounds contribute to their ability to exchange ions and form complexes. Due to their high pH-dependent charge, the filling of cation exchange sites, primarily with hydrogen (H) ions, makes the material an acid; called Humic Acid (HA). The dominance of cations other than H on the exchange sites makes it a salt of HA, technically termed humate (Mikkelsen, 2005).

HA is readily soluble under alkaline conditions; but insoluble in strong acids and has a pH below 2. The molecular weight of HA spans from 5000 to 100,000 Da, and these substances have a medium molecular size. Oxygen makes up 33–36 % of the total mass in this material, whereas nitrogen makes up 4 % (Arif et al., 2019). Fig. 1 shows HA's elemental composition, which typically contains carboxylic, phenolic, alcoholic, and carbonyl fractions (Ouni et al., 2014). The main sources of HA are soil, water, and leonardite (Qin et al., 2020).

The molecular structure of HA is made up of intricate organic combinations that are randomly connected to form incredibly complex substances. According to the widely accepted view, HAs are made up of

---

* Correspondence to: Department of Applied Chemistry, Delhi Technological University, India.
E-mail address: rkg67ap@yahoo.com (R.K. Gupta).

https://doi.org/10.1016/j.indcrop.2024.119029
Received 29 September 2023; Received in revised form 11 June 2024; Accepted 16 June 2024
0926-6690/© 2024 Elsevier B.V. All rights are reserved, including those for text and data mining, AI training, and similar technologies.

Indian Journal of Chemical Technology
Vol. 30, November 2023, pp. 753-764
DOI: 10.56042/ijct.v30i6.1325

Synthesis, characterization and application of Lignosulphonate-g-poly(sodium acrylate) hydrogel

Manu, Rajinder K. Gupta* & Devendra Kumar
Department of Applied Chemistry, Delhi Technological University, Delhi, India
*E-mail: rkg67ap@yahoo.com

Received 9 May 2023; accepted 9 September 2023

Natural polymer-based hydrogels are of great interest to research community owing to their inherent characters of environment friendliness and biodegradability. Current work aims to synthesize lignosulfonate grafted sodium acrylate hydrogel (LS-g-SAH) and investigate its application in urea release behaviour. The hydrogel has been characterized by different techniques. The release kinetics has been analyzed by using a UV-visible spectrophotometer. The optimized composition of lignosulfonate, KPS, and N,N'-MBA has shown the highest water absorbency of 560 g g^{-1} in distilled water. The equilibrium swollen LS-g-SAH 12 hydrogel has slowly released 60% of loaded urea in 24 h and followed first-order release kinetics. Soil treatment with hydrogel has shown a significant effect in reducing the water evaporation rate. It also improved the seed germination and average height of wheatgrass. The synthesized LS-g-SAH is, thus, expected to have potential application in modern sustainable agriculture.

Keywords: Hydrogel, Lignosulphonate, Release kinetics, Sustainable agriculture, Urea release

As world's seventh largest country, India has approximately 157 million hectares of arable land, accounting for 53.2% of the total area. The land is continuously degraded by different means, thus reducing the total production potential to less than 20 percent. Therefore immediate attention is required in upgrading soil fertility, which caused less productivity due to low water retention capability, poor structure, high infiltration rate, low clay and humus content, and loss of agrochemicals through deep percolation or leaching[1].

A super absorbent crosslinked polymer known as hydrogel is a potential material to solve soil-fertility problems. Hydrogel is a 3D network structure composed of chemically or physically crosslinked polymers. It can hold a massive volume of water due to its swollen state's surface tension and capillary forces. The rate of water absorption by hydrogel is affected by the functional group and the density of the crosslinking network[2]. Natural biodegradable polymers should be used to develop economical agricultural water-absorbent materials. Nowadays, researchers are paying great attention to lignocellulosic polymeric material as a favourable, sustainable, and large-scale asset to be used as a chemical component in various syntheses. In this regard, lignin is a renewable feedstock readily available in an adequate amounts[3]. Lignin accounts for 16-33% of the biomass and is predominantly present in the secondary cell walls of terrestrial plants[4]. Lignin comprises three types of phenylpropane monomers known as monolignols. These monolignols are a) coniferyl alcohol, b) sinapyl alcohol, and c) p-coumaryl alcohol[5]. This inexpensive waste of pulp manufacturing process is the only scalable renewable raw material that consists of aromatic moieties[6]. It is also easily accessible, affordable, and underutilized today [7].

Also, a lignin hydrogel based study by Bukhard et al. showed that the synthesized hydrogels could degrade up to 14% in just 60 days as compared with acrylamide-based hydrogels, indicating degradation of just 2% in 120 days[8]. Lignin has antimicrobial, antioxidant, and stabilizer properties[9]. It has also been used for metal elimination. For example, graphene hydrogel based on lignosulfonate, manufactured in a column system, rapidly eliminated Pb^{2+} from the aqueous solution (Thakur et al., 2017). A free-standing lignin-based film with superior electrochemical performance was manufactured by using poly(N-vinyl imidazole)-co-poly(poly(ethylene glycol) methyl ether methacrylate)[6]. However, there has been little exploration of using lignin-based hydrogel for controlled-release applications in

Check for updates

ChemistrySelect

Research Article
doi.org/10.1002/slct.202405884

Chemistry Europe
European Chemical Societies Publishing

www.chemistryselect.org

Harnessing Lignite-Based Hydrogel for Enhanced UV Protection and Delivery of Dinotefuran in Agriculture

Manu Nandal,[a] Devendra Kumar,[a] and Rajinder K. Gupta*[a]

The agricultural sector relies heavily on pesticides to enhance productivity and ensure food security, but UV degradation often compromises their efficacy. The present study addresses this issue and introduces dinotefuran-loaded, lignite-based polysodium acrylate hydrogel (Lt-g-SAH) as a protective shield against UV radiation for dinotefuran. The synthesis of Lt-g-SAH and control hydrogel (ctrl) through the graft co-polymerization method is detailed, with comprehensive characterization using ^{13}C CPMAS NMR, FT-IR, XRD, SEM, and TGA techniques. The release kinetics of dinotefuran are investigated via UV–vis spectrophotometry to elucidate the controlled release. This study highlights the potential of lignite-based hydrogels as versatile platforms in pesticide protection, where dinotefuran was found to have a marginal decrease of 1.58% in Lt-g-SAH compared to a 28.11% decrease in ctrl hydrogel and delivery mechanisms, with the Lt-g-SAH demonstrating 62.46% pesticide release in 39 h in contrast to 56.22% release from ctrl in 33 h. The pesticide loading increased from 64.36% in ctrl to 70.12% in Lt-g-SAH. Incorporating lignite in Lt-g-SAH also improves the soil's water retention capacity and offers potential as a nitrogen fertilizer carrier. Through comprehensive evaluation, this study demonstrates the viability of lignite-based hydrogel as a cost-effective and eco-friendly solution for safeguarding pesticides for agricultural sustainability.

1. Introduction

The utilization of pesticides plays a pivotal role in boosting agricultural productivity and ensuring food security in modern agriculture.[1] Approximately 2 million tons of pesticides are currently applied to crops worldwide.[2] Among these pesticides, dinotefuran ((RS)-1-methyl-2-nitro-3-(tetrahydro-3-furyl methyl)guanidine), a third-generation neonicotinoid (Figure 1), stands out as a potent insecticide, acclaimed for its broad-spectrum efficacy against various pests.[3–5] Dinotefuran has been used to manage a wide range of biting and sucking insects, including aphids (plant louse), whiteflies, and beetles. The chemical properties of dinotefuran are as follows: molecular mass (202.2 Da), water solubility (39830 mg L^{-1}) @ 20 °C, lipophilicity (log KOW) (−0.55), soil affinity (log KOC) value of 1.41, soil persistence (50–100 DT50 in days), and water photolysis (<2 DT50 in days).[6,7] Dinotefuran can be applied on foliage, soil, nurseries, and paddy water through spraying, drenching, broadcasting, and pricking-in-hole treatments.[8] While dinotefuran has been widely used due to its efficacy and concerns remain regarding its chronic effects on nontarget organisms.[6] Therefore, employing controlled-release systems offers a promising strategy to minimize environmental exposure and potential ecological risks. So, this study chose it as the model for the pesticides. However, dinotefuran is easily photolyzed under sunlight, which leads to a low utilization rate and significantly reduces its effectiveness.[9] Photodegradation is a significant degradation pathway after spraying, directly impacting the sustainability of pesticides.[10,11]

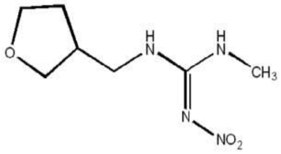

Figure 1. Molecular structure of dinotefuran.

As a result, improving dinotefuran utilization and extending its anti-pest shelf life is critical for sustainable agricultural practice.

This degradation prevention is a challenge for the agricultural sector. To address this challenge, developing innovative formulations capable of protecting dinotefuran from UV degradation is imperative. In recent years, hydrogels have emerged as promising candidates for efficiently encapsulating and delivering drugs[12–16] and agrochemicals.[17–21] Hydrogels are 3D polymeric networks with high water absorption.[22] Furthermore, crosslinking network chains within the hydrogel structure prevents dissolution and helps maintain its integrity.

Among various hydrogel materials, poly sodium acrylate hydrogels have garnered attention owing to their biocompatibility, tunable properties, and potential for controlled release.

Lignite, a low-grade coal (Figure 2) abundant in nature, offers an eco-friendly and cost-effective alternative for hydrogel synthesis. Lignite has high volatile content, chemical reactivity, and water content; low calorific value; and is easily weathered. Lignite accounts for about 40% of the total coal reserves in the world.[23] Electron paramagnetic resonance (EPR) spectroscopy confirmed that the lignite effectively screens UV irradiation, and

---

[a] M. Nandal, Prof. D. Kumar, Prof. R. K. Gupta
Department of Applied Chemistry, Delhi Technological University, Bawana Road, Shahbad Daulatpur, Delhi, Delhi 110042, India
E-mail: rkg67ap@yahoo.com

© 2025 Wiley-VCH GmbH

Check for updates

ChemistrySelect

Research Article
doi.org/10.1002/slct.202304939

Chemistry Europe
European Chemical Societies Publishing

www.chemistryselect.org

Novel Formulations of Humic acid, Lignin, and Lignite Grafted Hydrogels for the Slow Release of Thiamethoxam

Manu,[a] Devendra Kumar,[a] and Rajinder K. Gupta*[a]

The objective of this study is to explore the novel use of natural polymers like Humic acid, Lignin, and Lignite based hydrogels for the formulation of pesticides and fertilizers that would reduce the residues in soil and run-off water that pose a threat to human health and the environment. We synthesized hydrogels by grafting Humic acid, lignin, and lignite onto acrylic acid with N'N-methylene bisacrylamide (MBA) for the ex-situ encapsulation of thiamethoxam, a common pesticide. Various characterization techniques including Fourier-transform infrared spectroscopy, Carbon-13 Solid-state Cross-Polarization Magic Angle Spinning Nuclear Magnetic Resonance, X-ray diffraction, Thermogravimetric Analysis, and Rheology were employed. The release kinetics of thiamethoxam in water from the developed formulations were analyzed using the Korsmeyer- Peppas model and the Weibull model. Humic acid and lignin-based hydrogels exhibited a long-sustained release for 49 hours, followed by lignite-based hydrogels (38 hours). According to ANOVA results, the change of biopolymer proved to be an effective factor in reducing the water evaporation rate, which decreased from 99% to 72.85% in the soil amended with synthesized hydrogels. In conclusion, the novel formulations of humic acid, lignin, and lignite exhibit potential as slow-release vehicles for pesticides and fertilizers. This study provides valuable insights for the research community, addressing the need to develop effective strategies for mitigating pesticide residues in soil and water bodies.

Introduction

Today, pesticides have become the cornerstone of the predominant agricultural systems. These are important inputs for enhancing crop productivity and preventing major biological disasters. Worldwide, around 5 million tons of chemical pesticides are used every year, belonging to more than 100 classes with various modes of action.[1] However, more than 90% of conventional pesticide formulations run off into the environment and reside in agricultural products too.[2] Long-term exposure of pesticides to humans can cause reproductive complications, neurological disorders, immunological, and pulmonary diseases, and cancer.[3] Therefore, to increase the effectiveness of pesticide application and thereby reduce environmental risk, it is essential to develop innovative methods for pesticide formulation technologies. The controlled release of pesticides through hydrogel is a solution to the above problems. This means that the active components of the pesticide are released within a predetermined time and conditions via formulation with supporting materials.[4] Hydrogels are moist and flexible materials that possess a three-dimensional interlinked matrix, featuring remarkable water retention capabilities.[5] Hydrogels are classified as physically cross-linked,[6] chemically cross-linked,[7] or double-network[8] hydrogels based on the cross-linking techniques used. Secondary interactions result in the development of physically cross-linked hydrogels. On the other hand, several techniques such as water-soluble polymer cross-linking, radiation polymerization, free-radical polymerization, and polymer inter-transmission networks may be used for developing chemically cross-linked hydrogels.[9] Among these, the free radical polymerization technique is economical and gives higher swelling. Hydrogels have applications in biomedical,[10] food and agriculture,[11,12] textile, cosmetics, water purification, remediation, and separation fields.[13] Economical controlled-release pesticide formulations should be developed using natural biodegradable polymers. Nowadays, researchers need to pay attention to the omnipresent- favorable, sustainable, and large-scale assets like humic acid, lignin and lignite to be used as a chemical component in various syntheses. The scale and importance of these "sleeping giants" is unimaginably large.[14]

The term Humic acid is used for the polymeric, brown-black, alkali-soluble acids found in soils, sea grasses, plants, sediments, fungi, and marine and terrestrial waters. It is the most active component of soil organic matter and a main fraction of humic substances.[15] Humic acids play multiple important roles in agriculture such as improving water holding capacity, soil structure, and texture, preventing microbial growth, increasing nutrient availability to soil, and transporting micronutrients to plants.[16]

Lignin is an aromatic hetero-polymer present as a constituent of the plant cell wall, along with cellulose and hemicellulose. Its functions include both defense against pathogens and mechanical support. The waste from the paper and bioethanol industries produces 100 million tonnes of this biopolymer annually. Lignin is estimated to make up 15–35% of lignocellulosic biomass.[17]

Often called brown coal, lignite is a soft, brown, combustible sedimentary rock that develops when peat naturally compresses.[18] It has poor thermal stability, the highest volatile

---

[a] *Manu, Prof. D. Kumar, Prof. R. K. Gupta*
Department of Applied Chemistry
Delhi Technological University
PIN-110042, Delhi, India
E-mail: rkg67ap@yahoo.com

© 2024 Wiley-VCH GmbH

DELHI TECHNOLOGICAL UNIVERSITY

(Formerly Delhi College of Engineering)
Shahbad Daulatpur, Main Bawana Road, Delhi-42

PLAGIARISM VERIFICATION

Title of the Thesis **Synthesis And Application of Natural Polymer Based Hydrogels** Total Pages **258** Name of the Scholar **Ms. Manu**

Supervisor (s)

(1) **Prof. D. Kumar**

(2) **Prof. Rajinder K. Gupta**

Department **Applied Chemistry**

This is to report that the above thesis was scanned for similarity detection. Process and outcome is given below:

Software used: **Turnitin** Similarity Index: **9%**, Total Word Count: **40,428**.

Date: ____________

CURRICULUM VITAE

Name: Ms. Manu

Email: manu.nandal29@gmail.com | Phone: 7988680533

Address: A4/224 Sector-17, Rohini, Delhi – 110085

Date of Birth: 29th June 1995

Languages: English, Hindi

Career Objective

To contribute to the advancement of sustainable materials through innovative research in polymer chemistry, with a particular emphasis on the development of bio-based hydrogels for applications in agriculture, environmental protection, and energy storage.

Research Interests

Polymer Chemistry: Synthesis and characterization of natural polymer-based hydrogels.

Sustainable Materials: Development of renewable polymer-based solutions (lignin, humic acid, xanthan gum).

Agricultural Applications: Hydrogels for controlled-release fertilizers, pesticides, and soil water management.

Environmental Applications: Hydrogels for dye removal, wastewater treatment, and UV protection.

Energy Storage: Lignite-based hydrogels for energy and environmental protection.

Technical Skills

Material Characterization: NMR, FT-IR, XRD, SEM, TGA, DSC, UV-Vis, Rheology, BET.

Academic Background

Ph.D. (Chemistry) – Pursuing, Delhi Technological University, Delhi. Thesis Title: "Synthesis and Application of Natural Polymer-Based Hydrogels."

M.Sc. (Chemistry) – DCRUST, Murthal, Haryana (2016–2018) – First Division.

B.Sc. (PCM) – Maharishi Dayanand University, Rohtak, Haryana (2013–2016) – First Division.

Achievements & Awards

Commendable Research Award for excellence in research, Delhi Technological University (Sept 2024).

Qualified CSIR-NET JRF (Chemical Sciences) – Dec 2023, All India Rank 41.

Publications

- Manu, D. Kumar, R.K. Gupta (2025). Harnessing lignite-based hydrogel for enhanced UV protection and delivery of dinotefuran in agriculture. ChemistrySelect, 10, e05884.
- Manu, I. Kapoor, M. Bansiwal, T. Kansal, R.K. Gupta (2025). Molasses-grafted poly(sodium acrylate) hydrogel: A sustainable solution for water retention and pesticide delivery. Indian Journal of Chemical Technology, 32, 161–175.
- V. Parashar, Manu, Y.K. Tyagi, R.K. Gupta (2024). Carboxymethylated Cassia fistula-based hydrogel for extended release of dinotefuran. ChemistrySelect, 9, e202403421.
- Kumar, R.K. Gupta (2024). Natural polymers-humic acid and lignin based hydrogels: In agriculture, environment and energy storage. Industrial Crops and Products, 219, 119029.
- Manu, D. Kumar, R.K. Gupta (2024). Novel Formulations of Humic acid, Lignin, and Lignite Grafted Hydrogels for the Slow Release of Thiamethoxam. ChemistrySelect, 9(26), e202304939.
- Manu, D. Kumar, R.K. Gupta (2023). Synthesis, characterization and application of Lignosulphonate-g-poly (sodium acrylate) hydrogel. Indian Journal of Chemical Technology, 39(6), 753–764.
- Srivastava, Manu, R.K. Gupta (2023). Xanthan Gum and Lignin Grafted Chemically Crosslinked Hydrogels for Dye Removal. Polymer Science, Series A, 65(6), 725–733.

- R. Yadav, Ayush, Manu, A. Rani (2023). Xanthan gum and CMC sodium salt hydrogels for agricultural application. Bulgarian Chemical Communications, 55(Special Issue A), 131–137.
- Manu, Kumar D, Gupta RK (2025) Comparative Analysis of Humic Acid, Lignin and Lignite-Based Hydrogels for Methylene Blue Dye Removal. Indian J Chem Technol (under review).
- Manu, Kumar D, Gupta RK (2025) Humic acid-Integrated Polymeric Hydrogel: A Dual Strategy for Sustained Pesticide Delivery and Soil Water Retention. ChemistrySelect (under review)

Conferences

- Inulin based crosslinked superabsorbent hydrogel: Synthesis and characterization – SPSI-MACRO 2023, IIT Guwahati (Poster).
- Natural Polymer-Based Hydrogel in Agriculture – RTCSSE-2023, NIT Delhi (Oral).

Workshops

DST-STUTI Workshop, BITS Pilani, Rajasthan (Oct 2022).

Annual Information Literacy Workshop on e-Resources (7th Edition), Sept 2023.

References

Prof. Devendra Kumar, Professor, Delhi Technological University – dkumar@dce.ac.in

Prof. Rajinder K. Gupta, Professor, Delhi Technological University – rkg67ap@yahoo.com

Declaration

I hereby declare that the information furnished above is true to the best of my knowledge.

Place: Rohini, Delhi Date:

Signature: